

**Effect of Overturning Restraint on the Performance of Fully Sheathed  
and Perforated Timber Framed Shear Walls**

by  
Christian P. Heine

Thesis submitted to the Faculty of the  
Virginia Polytechnic Institute and State University  
In partial fulfillment of the requirements for the degree of

**MASTER OF SCIENCE**

in  
Wood Science and Forest Products

APPROVED:

---

J. Daniel Dolan

---

Joseph R. Loferski

---

Maurice W. White

December, 1997  
Blacksburg, Virginia

# **Effect of Overturning Restraint on the Performance of Fully Sheathed and Perforated Timber Framed Shear Walls**

By

Christian P. Heine

Committee Chairman: Dr. James D. Dolan

Wood Science and Forest Products

## **(Abstract)**

This study investigates the monotonic and cyclic response of light-frame wood shear walls with and without openings. Effects of overturning restraint in the form of tie-down anchors and corner segments on light-frame shear walls with and without door and window openings were quantified. While the results are useful to refine a design methodology for shear walls containing openings, they also provide important knowledge that is needed to accurately quantify anchorage requirements for shear wall design, and assess remaining load and ductility capacity of wood frame buildings after earthquakes or hurricanes.

Sixteen full-scale wall specimens were tested using monotonic and sequential phased displacement (SPD) patterns. A total of five different wall configurations, five anchorage, and two loading conditions were used. All walls were eight feet (2.4m) high. Straight wall specimens were forty feet (12.2m) long, whereas corner walls measured twelve feet (3.7m) in length. The analysis includes data from a previous investigation in order to further expand the scope of this study. Results reveal that ultimate capacity and stiffness increase with increasing overturning restraint. A shift in failure mode was observed when overturning restraints were omitted. Accumulated damage experienced by the wall specimens tested cyclically was fairly uniform, regardless of the amount of overturning restraint or size of openings present

## **Acknowledgements**

I wish to express my deep appreciation to Dr. J. Daniel Dolan for chairing my advisor committee, providing guidance, unending support and friendship. I consider it a privilege to have been associated and worked with him.

I am also particularly grateful to Drs. Joseph R. Loferski and Maurice W. White for their assistance, many helpful insights and valuable suggestions throughout the project.

My special thanks are extended to the National Association of Homebuilders for the financial assistance provided, and in particular to Jay H. Crandell for his time and expertise.

I am equally indebted to my friend and colleague Alexander Salenikovich who has helped me punch in tens of thousands of nails and whose enthusiasm and commitment was an important source of inspiration.

My warmest thanks are reserved for my parents, Barbara and Peter Heine, whose love and incredible support made this degree possible. Thanks to both of you for being such great teachers of children. I am truly blessed to have such wonderful parents.

Finally, I dedicate this thesis to my grandfather, Erich Heine. A proud and wise man who always believed in me and taught me the importance of commitment and accomplishment.

# Table of Contents

<b>INTRODUCTION .....</b>	<b>1</b>
1.1 PROBLEM OVERVIEW .....	1
1.2 OBJECTIVES AND SCOPE .....	3
1.3 THESIS OVERVIEW .....	4
<b>BACKGROUND.....</b>	<b>6</b>
2.1 GENERAL.....	6
2.2 TEST METHODS .....	7
2.3 NAILED TIMBER CONNECTIONS.....	8
2.3.1 <i>Characteristics of Nailed Joints</i> .....	9
2.4 LIGHT-FRAME SHEAR WALLS.....	10
2.4.1 <i>Principal Shear Wall Action</i> .....	10
2.4.2 <i>Parameters Influencing Shear Capacity</i> .....	12
2.4.2 <i>Experimental Shear Wall Studies</i> .....	14
2.4.3 <i>Analytical Modeling</i> .....	17
2.5 SUMMARY .....	21
<b>TEST WALLS AND PROCEDURES .....</b>	<b>23</b>
3.1 GENERAL.....	23
3.2 DESCRIPTION OF TEST WALLS.....	25
3.2.1 <i>Design and Construction of Straight Test Walls</i> .....	25
3.2.2 <i>Attachment to Test Frame and Instrumentation of Straight Walls</i> .....	29
3.2.3 <i>Design and Construction of Corner Walls</i> .....	35
3.2.4 <i>Attachment to the Test Frame and Instrumentation of Corner Walls</i> .....	36
3.2.5 <i>Precision of Instruments</i> .....	41
3.3 TESTING PROCEDURES .....	41
3.3.1 <i>Monotonic Loading</i> .....	41
3.3.2 <i>Sequential Phased Displacement Loading</i> .....	42
3.4 SUMMARY .....	45
<b>PROPERTY DEFINITIONS.....</b>	<b>47</b>
4.1 GENERAL.....	47
4.2 PERFORATED SHEAR WALL METHOD.....	47

4.2.1 Sheathing Area Ratio .....	47
4.2.2 Shear Load Ratio .....	49
4.3 SUGIYAMA'S EMPIRICAL EQUATIONS .....	49
4.4 CAPACITY AND FAILURE .....	50
4.4.1 Wall Capacity.....	50
4.4.2 Failure .....	51
4.5 EQUIVALENT ENERGY ELASTIC-PLASTIC PARAMETERS .....	51
4.5.1 Elastic Stiffness .....	52
4.5.2 Yield Strength and Yield Displacement.....	53
4.5.3 Ductility .....	53
4.6 EARTHQUAKE PERFORMANCE INDICATORS .....	54
4.6.1 Damping.....	54
4.6.2 Cyclic Stiffness.....	56
4.7 CONCLUDING REMARKS .....	56
<b>MONOTONIC TEST RESULTS OF STRAIGHT WALLS AND DISCUSSION .....</b>	<b>58</b>
5.1 GENERAL.....	58
5.2 LOAD-DRIFT RELATIONSHIP.....	58
5.3 DUCTILITY.....	62
5.4 PERFORATED SHEAR WALL METHOD.....	63
5.5 SUGIYAMA'S EQUATIONS .....	65
5.6 OVERALL WALL RESPONSE.....	67
5.6.1 Tie-down Tension Bolts.....	67
5.6.2 End Stud Uplift Displacement.....	72
5.6.3 Sheathing Displacement.....	74
5.7 GENERAL OBSERVATIONS .....	79
5.8 SUMMARY .....	80
<b>SPD TEST RESULTS OF STRAIGHT WALLS AND DISCUSSION.....</b>	<b>82</b>
6.1 GENERAL.....	82
6.2 LOAD-DRIFT RELATIONSHIP.....	82
6.3 DUCTILITY.....	88
6.4 PERFORATED SHEAR WALL METHOD.....	89
6.5 SUGIYAMA'S EQUATIONS .....	91
6.6 EARTHQUAKE PERFORMANCE .....	94
6.6.1 Equivalent Viscous Damping.....	94

6.6.2 Cyclic Stiffness.....	100
6.7 OVERALL WALL RESPONSE.....	103
6.7.1 Tie-down Tension Bolts.....	103
6.7.2 End Stud Uplift Displacement.....	108
6.7.3 Sheathing Displacement.....	109
6.7.4 General Observations.....	120
6.8 SUMMARY.....	121
<b>SPD TEST RESULTS OF WALLS WITH CORNERS AND DISCUSSION.....</b>	<b>123</b>
7.1 GENERAL.....	123
7.2 LOAD-DRIFT RELATIONSHIP.....	123
7.3 DUCTILITY.....	126
7.4 EARTHQUAKE PERFORMANCE.....	127
7.4.1 Equivalent Viscous Damping.....	127
7.4.2 Cyclic Stiffness.....	130
7.4 OVERALL WALL RESPONSE.....	132
7.4.1 Tension bolts.....	132
7.4.2 End Stud Displacement.....	137
7.4.3 Sheathing Displacement.....	138
7.4.4 General Observations.....	144
7.5 SUMMARY.....	144
<b>COMPARISONS BETWEEN TESTS.....</b>	<b>146</b>
8.1 GENERAL.....	146
8.2 MONOTONIC VS. SPD PERFORMANCE OF STRAIGHT WALLS.....	147
8.2.1 Strength.....	147
8.2.2 Equivalent Energy Elastic-Plastic Parameters.....	152
8.3 EFFECT OF CORNER FRAMING.....	155
8.3.1 Capacity.....	155
8.3.2 Equivalent Energy Elastic Plastic Parameters.....	157
8.4 SUMMARY.....	159
<b>SUMMARY, CONCLUSIONS, AND RECOMMENDATIONS.....</b>	<b>160</b>
9.1 SUMMARY.....	160
9.2 CONCLUSIONS.....	160
9.2.1 Overturning Restraint.....	160

9.2.2 <i>Testing Procedures</i> .....	161
9.2.3 <i>Perforated Shear Wall Design Method</i> .....	162
9.2.4 <i>Other Conclusions and Observations</i> .....	163
9.2 RECOMMENDATIONS FOR FUTURE RESEARCH .....	163
<b>BIBLIOGRAPHY</b> .....	<b>164</b>
<b>APPENDIX</b> .....	<b>170</b>
<b>VITA</b> .....	<b>211</b>

## List of Tables

TABLE 3.1: SPECIMEN CONFIGURATIONS .....	24
TABLE 3.2: OPENING SIZES FOR WALL CONFIGURATIONS .....	25
TABLE 3.3: WALL MATERIALS AND CONSTRUCTION DATA.....	29
TABLE 3.4: SPD PROTOCOL OF THE FIRST EIGHT PHASES .....	45
TABLE 5.1: LOAD-DISPLACEMENT DATA .....	61
TABLE 5.2: RELATIVE CAPACITIES BASED ON ENGINEERED CONSTRUCTION. ....	61
TABLE 5.3: CAPACITIES AND ACTUAL AND PREDICTED SHEAR STRENGTH RATIOS .....	64
TABLE 5.4: ACTUAL AND PREDICTED SHEAR STRENGTH RATIOS AT VARIOUS INTERSTORY DRIFTS .....	66
TABLE 5.5: FORCE RESISTED BY TENSION BOLT AT OR NEAR WALL CAPACITY .....	69
TABLE 5.6: VERTICAL END STUD DISPLACEMENT AT WALL CAPACITY .....	73
TABLE 6.1: INITIAL CYCLIC AND STABILIZED CYCLIC LOAD RESISTANCE DATA .....	86
TABLE 6.2: RELATIVE CAPACITIES BASED ON ENGINEERED CONSTRUCTION. ....	87
TABLE 6.3: INITIAL CYCLIC AND STABILIZED CYCLIC DUCTILITY .....	89
TABLE 6.4: COMPARISON OF ACTUAL INITIAL CAPACITY WITH THEORETICAL PREDICTED CAPACITY.....	90
TABLE 6.5: INITIAL CYCLIC AND STABILIZED CYCLIC LOAD RESISTANCE DATA .....	93
TABLE 6.6: EVDR MODE AND ITS RELATIVE FREQUENCY.....	99
TABLE 6.7: EVDR FROM THE FIRST THREE PHASES OF SPD LOADING (ELASTIC RANGE).....	99
TABLE 6.8: FORCE RESISTED BY TENSION BOLT AT OR NEAR WALL CAPACITY .....	108
TABLE 6.9: END STUD DISPLACEMENT BETWEEN POSITIVE AND NEGATIVE PEAK DRIFTS DURING INITIAL CYCLE OF $\Delta_{PEAK\ LOAD}$ .....	109
TABLE 7.1: INITIAL CYCLIC AND STABILIZED CYCLIC LOAD RESISTANCE DATA .....	125
TABLE 7.2: CORNER WALL DUCTILITY .....	127
TABLE 7.3: EVDR FROM THE FIRST THREE PHASES OF SPD LOADING (ELASTIC RANGE).....	130
TABLE 7.4: END STUD DISPLACEMENT BETWEEN POSITIVE AND NEGATIVE PEAK DRIFTS DURING INITIAL CYCLE OF $\Delta_{PEAK\ LOAD}$ AND $\Delta_{FAILURE}$ .....	137
TABLE 8.1: CAPACITIES OF MONOTONIC AND SPD TESTED STRAIGHT WALLS.....	152
TABLE 8.2: EQUIVALENT ENERGY ELASTIC-PLASTIC PARAMETERS .....	154
TABLE 8.3: MONOTONIC AND INITIAL CYCLIC INTERSTORY DRIFTS AT YIELD, CAPACITY AND FAILURE .....	155

TABLE 8.4: CYCLIC CAPACITIES AND UNIT SHEAR VALUES OF WALLS WITH CORNER FRAMING AND LONG STRAIGHT WALLS WITH AND WITHOUT TIE-DOWN ANCHORS.....	156
TABLE 8.5: EQUIVALENT ENERGY ELASTIC-PLASTIC CURVE PARAMETERS .....	158
TABLE A.1: INITIAL CYCLIC DATA OF WALL A (NO ANCHORS, $r = 1.0$ ).....	171
TABLE A.2: STABILIZED CYCLIC DATA OF WALL A (NO ANCHORS, $r = 1.0$ ).....	172
TABLE A.3: INITIAL CYCLIC DATA OF WALL D (NO ANCHORS, $r = 0.48$ ).....	175
TABLE A.4: STABILIZED CYCLIC DATA OF WALL D (NO ANCHORS, $r = 0.48$ ).....	176
TABLE A.5: INITIAL CYCLIC DATA OF WALL E (NO ANCHORS, $r = 0.30$ ).....	179
TABLE A.6: STABILIZED CYCLIC DATA OF WALL E (NO ANCHORS, $r = 0.30$ ) .....	180
TABLE A.7: INITIAL CYCLIC DATA OF WALL A (MAX. ANCHORS, $r = 1.0$ ).....	183
TABLE A.8: STABILIZED CYCLIC DATA OF WALL A (MAX. ANCHORS, $r = 1.0$ ).....	184
TABLE A.9: INITIAL CYCLIC DATA OF WALL D (MAX. ANCHORS, $r = 0.48$ ).....	187
TABLE A.10: STABILIZED CYCLIC DATA OF WALL D (MAX. ANCHORS, $r = 0.48$ ).....	188
TABLE A.11: INITIAL CYCLIC DATA OF WALL E (MAX. ANCHORS, $r = 0.30$ ) .....	191
TABLE A.12: STABILIZED CYCLIC DATA OF WALL E (MAX. ANCHORS, $r = 0.30$ ) .....	192
TABLE A.13: INITIAL CYCLIC DATA OF WALL 2.1 (2 FT CORNER SEGMENTS).....	195
TABLE A.14: STABILIZED CYCLIC DATA OF WALL 2.1 (2 FT CORNER SEGMENTS).....	196
TABLE A.15: INITIAL CYCLIC DATA OF WALL 2.2 (2 FT CORNER SEGMENTS).....	199
TABLE A.16: STABILIZED CYCLIC DATA OF WALL 2.1 (2 FT CORNER SEGMENTS).....	200
TABLE A.17: INITIAL CYCLIC DATA OF WALL 4.1 (4 FT CORNER SEGMENTS).....	203
TABLE A.18: STABILIZED CYCLIC DATA OF WALL 4.1 (4 FT CORNER SEGMENTS).....	204
TABLE A.19: INITIAL CYCLIC DATA OF WALL 4.2 (4 FT CORNER SEGMENTS).....	207
TABLE A.20: STABILIZED CYCLIC DATA OF WALL 4.2 (4 FT CORNER SEGMENTS).....	208

## List of Figures

FIGURE 1.1: FORCES ACTING ON A SHEAR WALL SEGMENT ACCORDING TO THE SIMPLE DIAPHRAGM THEORY (SIMPLIFICATION), WHERE $B$ STANDS FOR WALL WIDTH AND $H$ INDICATES WALL HEIGHT (FROM STEWART 1987).....	2
FIGURE 1.2: A) SHEAR WALL COMPOSED OF TRADITIONAL SHEAR WALL SEGMENTS. B) PERFORATED SHEAR WALL CONTAINING UNRESTRAINED SEGMENTS.....	2
FIGURE 2.1: FAILURE MODES OF A NAIL JOINT IN SINGLE SHEAR (AFTER STEWART, 1987) .....	9
FIGURE 2.2: FAILURE OF JOINTS WITH RELATIVELY THIN SHEATHING (AFTER STEWART, 1987) .....	10
FIGURE 2.3: TYPICAL STRUCTURAL BEHAVIOR OF A SHEAR WALL UNIT (AFTER ALMSARKER, 1995).....	11
FIGURE 3.1: WALL ASSEMBLY .....	27
FIGURE 3.2: WALL CONSTRUCTION.....	27
FIGURE 3.3: STRAIGHT WALL ORIENTATION AND TEST SET-UP.....	31
FIGURE 3.4: GEOMETRY OF LVDT FIXTURE TO MEASURE STUD UPLIFT.....	32
FIGURE 3.5: INTERIOR INSTRUMENTATION OF STRAIGHT WALL SPECIMENS .....	34
FIGURE 3.6: CONSTRUCTION DETAIL CORNER .....	35
FIGURE 3.7: TEST SET UP FOR CORNER WALLS .....	38
FIGURE 3.8: CORNER WALL INSTRUMENTATION.....	39
FIGURE 3.9: MEASUREMENT AMPLIFICATION OF THE LVDT FIXTURE .....	40
FIGURE 3.10: INTERIOR INSTRUMENTATION OF CORNER WALLS.....	41
FIGURE 3.11: DISPLACEMENT PATTERN OF MONOTONIC AND SPD LOADING.....	43
FIGURE 4.1: SHEATHING AREA RATIO VARIABLES .....	48
FIGURE 4.2: TYPICAL HYSTERESIS LOOPS OF A SHEAR WALL UNDER SPD LOADING .....	50
FIGURE 4.3: EQUIVALENT ELASTIC PLASTIC CURVE AND LOAD-INTERSTORY DRIFT (ENVELOPE) CURVE .....	52
FIGURE 4.4: TYPICAL INITIAL OR STABILIZED HYSTERESIS LOOP PLOTTED TO DETERMINE CYCLIC STIFFNESS AND POTENTIAL ENERGY.....	56
FIGURE 5.1: LOAD VS. INTERSTORY DRIFT CURVES OF WALL CONFIGURATION A.....	59
FIGURE 5.2: LOAD VS. INTERSTORY DRIFT CURVES OF WALL CONFIGURATION D.....	60
FIGURE 5.3: LOAD VS. INTERSTORY DRIFT CURVES OF WALL CONFIGURATION E.....	60
FIGURE 5.4: SHEAR STRENGTH RATIOS AT CAPACITY (EQ. 4.4).....	65

FIGURE 5.5: PREDICTED SHEAR STRENGTH RATIO AT CAPACITY USING EQUATION 4.6 .....	67
FIGURE 5.6: RESISTED LOAD BY TENSION BOLTS OF WALLS A, D, E, RESPECTIVELY, NOT RESTRAINED AGAINST UPLIFT, ALONG WITH THE CORRESPONDING LOAD ENVELOPE CURVES .....	70
FIGURE 5.7: RESISTED LOAD BY TENSION BOLTS OF WALLS A, D, E, RESPECTIVELY, WITH MAXIMUM UPLIFT RESTRAINTS, ALONG WITH THE CORRESPONDING LOAD ENVELOPE CURVES .....	71
FIGURE 5.8: FALSE UPLIFT DISPLACEMENT MEASURED IF WALL IS ONLY RACKING (NO ANCHORS) .....	73
FIGURE 5.9: MIDPOINT MOVEMENT OSB PANEL 5, WALL D, MAXIMUM AMOUNT OF ANCHORS .....	75
FIGURE 5.10: MIDPOINT MOVEMENT OSB PANEL 7, WALL D, MAXIMUM AMOUNT OF ANCHORS .....	75
FIGURE 5.11: GENERAL SHEATHING ROTATION RELATIVE TO THE FRAMING .....	77
FIGURE 5.12: ROTATION OF OSB PANEL 5, WALL D, MAXIMUM AMOUNT OF ANCHORS .....	77
FIGURE 5.13: ROTATION OF OSB PANEL 7, WALL D, MAXIMUM AMOUNT OF ANCHORS .....	78
FIGURE 6.1: LOAD VS. INTERSTORY DRIFT ENVELOPE CURVES OF WALL CONFIGURATION A .....	83
FIGURE 6.2: LOAD VS. INTERSTORY DRIFT ENVELOPE CURVES OF WALL CONFIGURATION D .....	84
FIGURE 6.3: LOAD VS. INTERSTORY DRIFT ENVELOPE CURVES OF WALL CONFIGURATION E.....	85
FIGURE 6.4: SHEAR STRENGTH RATIOS AT CAPACITY (EQ. 4.4) AS A FUNCTION OF SHEATHING AREA RATIO	91
FIGURE 6.5: SHEAR STRENGTH RATIO AT CAPACITY USING EQUATION 4.6.....	94
FIGURE 6.6: INITIAL EVDR VS. INTERSTORY DRIFT OF WALL CONFIGURATIONS A, D, AND E.....	96
FIGURE 6.7: STABILIZED EVDR VS. INTERSTORY DRIFT OF WALL CONFIGURATIONS A, D, AND E.....	97
FIGURE 6.8: INITIAL CYCLIC STIFFNESS VS. INTERSTORY DRIFT OF WALL CONFIGURATIONS A, D, AND E..	101
FIGURE 6.9: STABILIZED CYCLIC STIFFNESS VS. INTERSTORY DRIFT OF WALL CONFIGURATIONS A, D, E...	102
FIGURE 6.10: RESISTED LOAD BY TENSION BOLTS OF WALLS A, D, AND E, RESPECTIVELY, NOT RESTRAINED AGAINST UPLIFT, ALONG WITH THE CORRESPONDING INITIAL LOAD ENVELOPE CURVES.....	104
FIGURE 6.11: RESISTED LOAD BY TENSION BOLTS OF WALLS A, D, AND E, RESPECTIVELY, WITH MAXIMUM UPLIFT RESTRAINTS, ALONG WITH THE CORRESPONDING INITIAL LOAD ENVELOPE CURVES .....	105
FIGURE 6.12: ROTATION AND MIDPOINT MOVEMENT OF OSB PANEL 2, WALL A, NO ANCHORS .....	111
FIGURE 6.13: ROTATION AND MIDPOINT MOVEMENT OF OSB PANEL 4, WALL A, NO ANCHORS .....	112
FIGURE 6.14: ROTATION AND MIDPOINT MOVEMENT OF OSB PANEL 2, WALL A, MAXIMUM AMOUNT OF ANCHORS .....	113
FIGURE 6.15 ROTATION AND MIDPOINT MOVEMENT OF OSB PANEL 4, WALL A, MAXIMUM AMOUNT OF ANCHORS .....	114
FIGURE 6.16: ROTATION AND MIDPOINT MOVEMENT OF OSB PANEL 5, WALL D, MAXIMUM AMOUNT OF ANCHORS .....	115
FIGURE 6.17: ROTATION AND MIDPOINT MOVEMENT OF OSB PANEL 7, WALL D, MAXIMUM AMOUNT OF ANCHORS .....	116

FIGURE 6.18: ROTATION AND MIDPOINT MOVEMENT OF OSB PANEL 1, WALL E, MAXIMUM AMOUNT OF ANCHORS .....	117
FIGURE 6.19: GENERAL SHEATHING ROTATION RELATIVE TO THE FRAMING, CYCLIC LOADING .....	119
FIGURE 7.1: INITIAL LOAD VS. INTERSTORY DRIFT ENVELOPE CURVES OF ALL CORNER WALLS .....	124
FIGURE 7.2: INITIAL AND STABILIZED EVDR VS. INTERSTORY DRIFT OF ALL CORNER WALLS.....	129
FIGURE 7.3: INITIAL AND STABILIZED CYCLIC STIFFNESS OF ALL CORNER WALLS .....	131
FIGURE 7.4: RESISTED LOAD BY TENSION BOLTS OF WALL 2.1 WITH 2 FOOT CORNER FRAMING ALONG WITH THE CORRESPONDING INITIAL LOAD ENVELOPE CURVE.....	133
FIGURE 7.5: RESISTED LOAD BY TENSION BOLTS OF WALL 2.2 WITH 2 FOOT CORNER FRAMING ALONG WITH THE CORRESPONDING INITIAL LOAD ENVELOPE CURVE.....	134
FIGURE 7.6: RESISTED LOAD BY TENSION BOLTS OF WALL 4.1 WITH 4 FOOT CORNER FRAMING ALONG WITH THE CORRESPONDING INITIAL LOAD ENVELOPE CURVE. LEADS TO ONE BOLT WERE DEFECTIVE. ....	135
FIGURE 7.7: RESISTED LOAD BY TENSION BOLTS OF WALL 4.2 WITH 4 FOOT CORNER FRAMING ALONG WITH THE CORRESPONDING INITIAL LOAD ENVELOPE CURVE.....	136
FIGURE 7.8: ROTATION AND MIDPOINT TRANSLATION OF THE MID OSB PANEL, WALL 2.1 .....	139
FIGURE 7.9: ROTATION AND MIDPOINT TRANSLATION OF THE MID OSB PANEL, WALL 2.2 .....	140
FIGURE 7.10: ROTATION AND MIDPOINT TRANSLATION OF THE MID OSB PANEL, WALL 4.1 .....	141
FIGURE 7.11: ROTATION AND MIDPOINT TRANSLATION OF THE MID OSB PANEL, WALL 4.2 .....	142
FIGURE 7.12: SHEATHING ROTATION RELATIVE TO THE FRAMING WHEN UPLIFT IS CONSIDERED .....	143
FIGURE 8.1: MONOTONIC LOAD VS. DRIFT CURVES, INITIAL ENVELOPE, AND STABILIZED ENVELOPE CURVES FOR WALL CONFIGURATION A.....	149
FIGURE 8.2: MONOTONIC LOAD VS. DRIFT CURVES, INITIAL ENVELOPE, AND STABILIZED ENVELOPE CURVES FOR WALL CONFIGURATION D.....	150
FIGURE 8.3: MONOTONIC LOAD VS. DRIFT CURVES, INITIAL ENVELOPE, AND STABILIZED ENVELOPE CURVES FOR WALL CONFIGURATION E .....	151
FIGURE 8.4: UNIT SHEAR AT ULTIMATE CAPACITY OF WALLS WITH NO TIE-DOWN ANCHORS, TIE-DOWN ANCHORS AT THE END AND 2FT AND 4FT CORNER SEGMENTS, RESPECTIVELY .....	157
FIGURE A.1: HYSTERESIS LOOPS OF WALL A (NO ANCHORS) .....	173
FIGURE A.2: INITIAL HYSTERESIS LOOPS OF WALL A (NO ANCHORS) TOGETHER WITH HYST. AND POT. ENERGY FOR COMPARISON.....	174
FIGURE A.3: HYSTERESIS LOOPS OF WALL D (NO ANCHORS) .....	177

FIGURE A.4: INITIAL HYSTERESIS LOOPS OF WALL D (NO ANCHORS) TOGETHER WITH HYST. AND POT. ENERGY FOR COMPARISON .....	178
FIGURE A.5: HYSTERESIS LOOPS OF WALL E (NO ANCHORS) .....	181
FIGURE A.6: INITIAL HYSTERESIS LOOPS OF WALL E (NO ANCHORS) TOGETHER WITH HYST. AND POT. ENERGY FOR COMPARISON .....	182
FIGURE A.7: HYSTERESIS LOOPS OF WALL A (MAX. ANCHORS) .....	185
FIGURE A.8: INITIAL HYSTERESIS LOOPS OF WALL A (MAX. ANCHORS) TOGETHER WITH HYST. AND POT. ENERGY FOR COMPARISON .....	186
FIGURE A.9: HYSTERESIS LOOPS OF WALL D (MAX ANCHORS).....	189
FIGURE A.10: INITIAL HYSTERESIS LOOPS OF WALL D (MAX. ANCHORS) TOGETHER WITH HYST. AND POT. ENERGY FOR COMPARISON .....	190
FIGURE A.11: HYSTERESIS LOOPS OF WALL E (MAX. ANCHORS).....	193
FIGURE A.12: INITIAL HYSTERESIS LOOPS OF WALL E (MAX. ANCHORS) TOGETHER WITH HYST. AND POT. ENERGY FOR COMPARISON .....	194
FIGURE A.13: HYSTERESIS LOOPS OF WALL 2.1 (2 FT CORNER SEGMENTS).....	197
FIGURE A.14: INITIAL HYSTERESIS LOOPS OF WALL 2.1 (2 FT CORNER SEGMENTS) TOGETHER WITH HYST. AND POT. ENERGY FOR COMPARISON .....	198
FIGURE A.15: HYSTERESIS LOOPS OF WALL 2.2 (2 FT CORNER SEGMENTS).....	201
FIGURE A.16: INITIAL HYSTERESIS LOOPS OF WALL 2.2 (2 FT CORNER SEGMENTS) TOGETHER WITH HYST. AND POT. ENERGY FOR COMPARISON .....	202
FIGURE A.17: HYSTERESIS LOOPS OF WALL 4.1 (4 FT CORNER SEGMENTS).....	205
FIGURE A.18: INITIAL HYSTERESIS LOOPS OF WALL 4.1 (4 FT CORNER SEGMENTS) TOGETHER WITH HYST. AND POT. ENERGY FOR COMPARISON .....	206
FIGURE A.19: HYSTERESIS LOOPS OF WALL 4.2 (4 FT CORNER SEGMENTS).....	209
FIGURE A.20: INITIAL HYSTERESIS LOOPS OF WALL 4.2 (4 FT CORNER SEGMENTS) TOGETHER WITH HYST. AND POT. ENERGY FOR COMPARISON .....	210

# Chapter 1

## Introduction

### 1.1 Problem Overview

A typical light-frame structure resists lateral wind or earthquake forces by transferring the load to the side walls which are then primarily loaded in shear. Such walls are commonly referred to as shear walls. It is assumed that the wall's structural sheathing resists the entire shear and transfers it to the foundation. Today, oriented strandboard (OSB) or plywood sheathing usually provide the shear resistance in light-frame walls.

Established engineered design of exterior shear walls containing wall and door openings involves the use of multiple, fully-sheathed shear wall segments. In engineered design one assumes that a shear wall segment acts as a cantilevered beam and overturning forces are calculated using principle structural theory (Figure 1.1). An individual segment is typically restrained against overturning forces at both ends, and the design capacity of an entire shear wall is simply the sum of the capacities for each wall segment. Contribution to design capacity of segments above and below openings is usually not accounted for to keep the procedure simple. However, it is obvious that segments above and below openings must affect the overall behavior of the shear wall.

An alternate empirical-based approach to the design of shear walls with openings is the perforated shear wall method which was adopted by the *Standard Building Code 1994 Revised Edition* (SBC 1994) and the *Wood Frame Construction Manual for One- and Two-Family Dwellings – 1995 High Wind Edition* (WFCM 1995). The perforated shear wall method consists of a combination of prescriptive provisions and empirical adjustments to design walls containing openings. Tabulated adjustment factors are used to reduce the theoretical strength of a fully-sheathed shear wall segment to compensate for the presence of openings. The method requires mechanical tie-down devices at each end of the entire wall rather than at the end of each fully sheathed segment. Accordingly, the number of tie-downs required for shear walls containing openings is reduced compared to traditional engineered design (Figure 1.2).

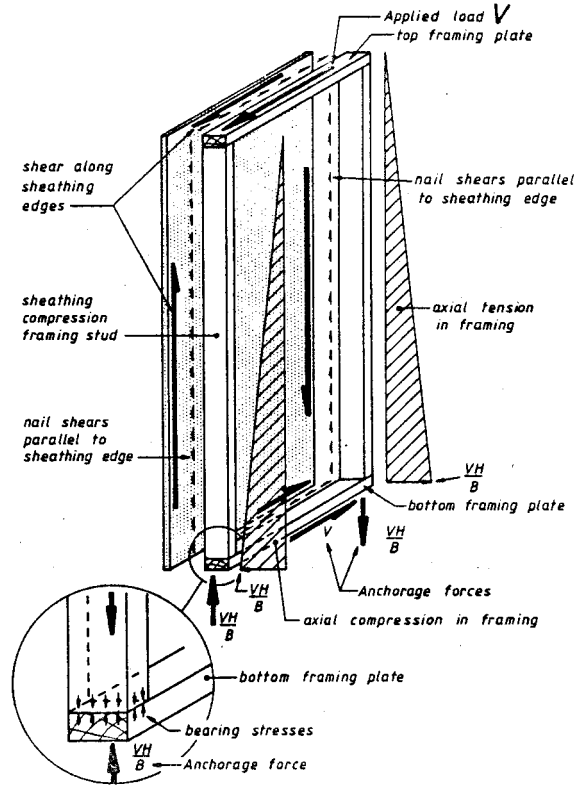


Figure 1.1: Forces acting on a shear wall segment according to the simple diaphragm theory (simplification), where  $B$  stands for wall width and  $H$  indicates wall height (from Stewart 1987)

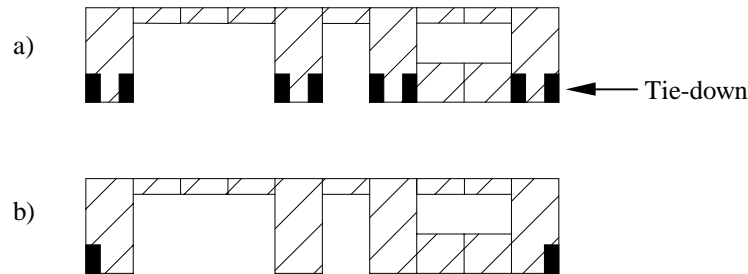


Figure 1.2: a) Shear wall composed of traditional shear wall segments. b) perforated shear wall containing unrestrained segments

Under low to moderate seismic conditions, overturning restraint may not be required at all. Especially if one considers that two mutually perpendicular walls intersecting in the corners of a building provide some hold-down capacity to each other.

A remarkable body of literature exists concerning the lateral resistance of sheathed light-frame walls. However, most of those walls were tested using a monotonic (one-directional) testing procedure and overturning restraints at the ends that essentially eliminate the overturning failure mode (separation of sheathing and studs from bottom plate). A synthesis of all previous work on testing of timber framed shear walls is virtually impossible, due to different test objectives, lack of test standards, and thousands of material combinations and test configurations possible (Foliente and Zacher 1994). The writer is not aware of any investigations that quantify the capacities of monotonically and reversed cyclically loaded full-scale shear walls without overturning restraint, with perforated shear wall method restraint, and fully restrained according to engineered design.

## **1.2 Objectives and Scope**

The purpose of this study is to quantify the effects of overturning restraint on the performance of light-frame shear walls. Other objectives that supplement the main purpose are to:

- Quantify the effect of tie-down anchors on full-size wood frame shear walls with and without openings loaded reversed cyclically and monotonically.
- Compare and evaluate the results of the monotonic and reversed cyclic testing procedure.
- Determine the applicability of the empirical, perforated shear wall design approach to conventionally built walls without considering overturning restraint provided by tie-down devices or gravity loads.
- Quantify the effects of transverse walls on uplift restraint of light-frame wood shear walls tested reversed cyclically

Apart from the walls with corner framing, each wall configuration was tested only once due to the high costs and time required to test full-scale specimens. Therefore, no statistical analysis is included. Furthermore, to reduce the total number of specimens, only five different wall configurations were tested. It must be noted that inherent to the property variation of wood, the results presented are part of a distribution of values one would obtain if a number of replications greater than one were used. However, due to the nails being the controlling failure mechanism and the large number of nails in each specimen, the performance should tend toward the mean value and the distribution of property values for wall specimens will have a small variance. Therefore, a large number of replicates is not necessary in most shear wall tests.

The framing lumber contained in all specimens was spruce-pine-fir. Since shear wall racking performance is influenced by the specific gravity of the framing material, the results presented have to be adjusted accordingly if compared with results from shear walls tested using different framing species.

Results of the walls including perpendicular segments are to be viewed as preliminary results only. Comparisons made between corner walls and walls containing tie-down anchors and the trends presented are to be confirmed with additional tests since there was a significant difference in length between the specimens.

### **1.3 Thesis Overview**

Based on published research conducted in the past, Chapter 2 presents a brief review of general shear wall performance, testing procedures and proposed models that predict shear wall response. Chapter 3 describes test organization and set-up as well as construction of the wall specimens, and elaborates on the testing protocols and loading histories used in this study. Chapter 4 defines how performance indicators are determined. Results and discussion of the monotonic and reversed cyclic tests of walls without corner framing are presented in Chapters 5 and 6, respectively, and the results of the reversed cyclic test of the walls with corner segments attached are discussed in Chapter 7. Chapter 8 draws comparisons between monotonic and cyclic tests and

elaborates on the effect of corner framing. The conclusions, which address the objectives, are presented in Chapter 9.

## Chapter 2

### Background

#### 2.1 General

A typical wood-framed shear wall consists of softwood framing which is composed of studs, spaced at a regular interval, bottom and top plates, some kind of sheathing that braces the wall and provides the shear resistance, and metal connectors that fasten the components together. In North America, the shear resistance in modern light-framed walls is frequently provided by oriented strandboard (OSB) or plywood sheathing, typically applied on one side of the wall. Interior sheathing generally consists of gypsum wallboard. The fasteners are usually smooth shanked nails of different length and diameter, depending on which elements are connected. Screws and glue are less frequently used since the structures exhibit rather brittle failure when these types of connections are incorporated (Foschi 1990).

A vast body of literature is available on the structural performance of shear walls. However, the behavior of shear walls during earthquakes or high wind events is still not completely understood. In fact, researchers point out that to this date, there still exists a large lack of knowledge and understanding, which may result in billions of dollars wasted on unnecessary components or in leaving out needed elements (Diekmann 1994). This is partly attributed to the fact that previous experimental studies of shear walls are difficult to compare due to different test objectives and lack of test standards (Foliente and Zacher 1994). Experimental studies are still of the essence today as they closely monitor structural behavior under loading and provide useful information to develop analytical models.

This chapter summarizes current test methods and highlights important findings on shear wall and connection behavior.

## 2.2 Test Methods

Until recently, the most commonly used testing procedure to evaluate mechanical properties of wood structural systems and connections has been the static-monotonic procedure, standardized by the American Society of Testing and Materials (ASTM 1997). The first standard to evaluate shear walls was published in 1977 under ASTM E 72-77. The main purpose of this test is to compare the performance of sheathing types. Although the load is applied in four “cycles” with increasing amplitude and constant rate until failure, it is still considered to be a monotonic test since the load is only one directional and each loading stage is applied separately. The procedure has been criticized as it stipulates a steel tie-down rod tying the top plate to a rigid base to prevent uplift at one end of the wall where the load is applied. Griffiths (1984) pointed out that the tie-down mechanisms over restrained the panel which resulted in unrealistic failure values. In order to overcome this problem the ASTM E 72-77 standard has been displaced by the ASTM E 564-76 standard, which uses uplift anchors connecting the end studs to the rigid base to resist the overturning moment. The specifications for the static, monotonic procedure to evaluate timber connections are published under ASTM D1761. The advantage of static monotonic procedures is the ease of set-up and performance and associated lower expense. Nevertheless, researchers have agreed that results do not provide sufficient information to evaluate earthquake performance of timber structures (Foliente 1996, Skaggs and Rose 1996).

The following test methods all try to quantify the reversed cyclic behavior of shear walls. However, a standardized procedure to serve as a common basis for research and design efforts has not yet been adopted. A relatively simple and feasible procedure, also employed in this study, is the quasi-static procedure. Quasi-static testing is commonly referred to as cyclic testing with slow rates of loading eliminating inertia effects. Today, quasi-static procedures are the most widely used procedures in structural earthquake engineering (Foliente 1996). Many quasi-static procedures follow displacement patterns where the amplitude increases over time at constant frequency until failure. Thus, the rate of loading is not constant.

A more versatile, but also more cost intensive, testing method is pseudodynamic testing. As the term “dynamic” indicates, the procedure uses higher rates of loading usually taken from earthquake records. Since inertia effects are included in the wall response, tests results are often difficult to interpret.

In contrast to the procedures discussed above where the load is applied uniformly along the top plate of the wall specimens, a different procedure, referred to as shake table testing, does not directly apply the load. Instead, the wall is attached with the sill plate and additional tie-down devices to the table and an inertial mass is mounted onto the top plate. The table simulates the ground motion during an earthquake, and is therefore closest to reality regarding load application. However, shake table testing is very costly and the forces created in the wall can only be determined indirectly by measuring accelerations. In addition, shake table sizes often limit the width of the wall specimens.

### **2.3 Nailed Timber Connections**

It is well established that the behavior of metal fasteners determines the response characteristics of light-framed shear walls subjected to cyclic or monotonic loading (Tuomi and McCutcheon 1977, Foschi 1982, Falk and Itani 1989). Nails are the most commonly used fasteners in structural components such as wooden shear walls. Dowrick (1986), Stewart (1987) and Dolan (1989) observed that the nailed sheathing-to-stud connection governs the static and dynamic performance of light-framed shear walls. Light-framed wood shear walls of that kind are able to sustain loads close to capacity over a relatively large displacement, and exhibit good energy dissipation characteristics, due to plastic deformations in the metal connectors. As a result, the characteristics of nailed joints are presented in some detail here.

Even though the first reversed-cyclic load tests on nailed timber joints were conducted almost forty years ago (Kaneta 1958), a standardized testing procedure has not been developed to date. Dolan (1993) proposed a modification of the Sequential Phased Displacement Procedure (Porter 1987) as standard test method to be adopted by the American Society of Testing and Materials. The procedure is still in review process.

### 2.3.1 Characteristics of Nailed Joints

Stewart (1987) discussed in great detail the factors influencing nail joint behavior. Based on a summary of the past literature he identified fastener slenderness and timber density, joint moisture content, grain direction, timber thickness, loading rate, relaxation, and the number of nails per joint as the major parameters that influence joint behavior.

In shear wall assemblies, nail joints are primarily loaded in single shear. Johansen (1949) first developed equations to predict the ultimate strength of a dowel type joint. Johansen's equations have later been verified experimentally by many researchers including Möller (1951), Larsen (1973), Aune and Patton-Mallory (1986), and Hilson et al. (1990). For fasteners in single shear, Johansen identified four modes of failure (Figure 2.1). Johansen's yield theory has been adopted by the *Eurocode 5*, the European code for the design of timber structures (ENV 1995-1-1 and 1995-1-2), and the *National Design Specification for Wood Construction* (AF&PA, 1991).

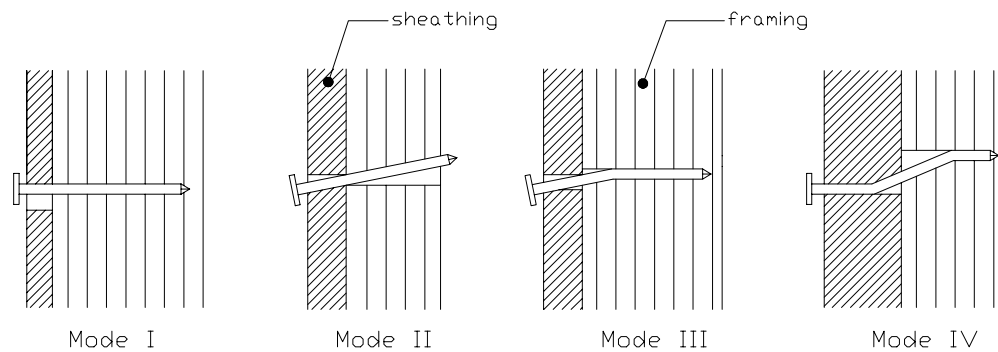


Figure 2.1: Failure modes of a nail joint in single shear (after Stewart, 1987)

The load-slip relationship of a nailed joint in single shear subjected to static loading does not exhibit linear elastic behavior or distinct yield point. Stewart (1987) tested nailed sheathing-to-timber joints under reversed cyclic loading to investigate failure modes. As noted by Thurston in 1984, Stewart obtained the typical “pinched” load-slip hysteresis loops due to a progressive degradation of lateral stiffness for each successive loading cycle. He also observed that the resisted load decreased between two

successive cycles at the same displacement level. Stewart further noted that depending on sheathing thickness the nail either partially withdrew from the framing or the nail head pulled through the sheathing at larger displacements. Nails penetrating thinner sheathing failed in fatigue as a result of a developed “plastic hinge” (Mode III) and the corresponding high reverse curvature demands on the nail shanks.

Dean (1988) found that a nailed sheathing-to-timber connection exhibits the highest ductility at a high sheathing thickness-to-nail-length ratio. In this case, the clamping force of the sheathing is greater than that of the framing and induces sufficient axial tension to incrementally withdraw the nail from the framing. As a result a single plastic hinge is less likely to develop and nails don't fail in fatigue at lower displacement levels. In addition, the withdrawn nail head does not damage the sheathing surface as do nails penetrating thinner sheathing which eventually pull through the sheathing (Figure 2.2).

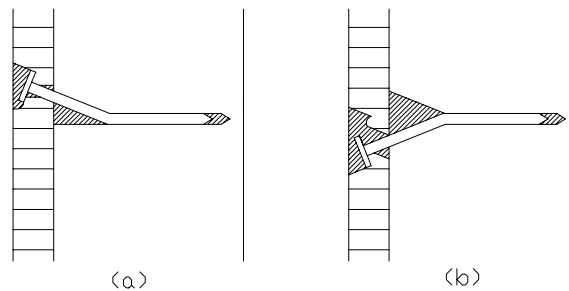


Figure 2.2: Failure of joints with relatively thin sheathing (after Stewart, 1987)

## 2.4 Light-frame Shear Walls

### 2.4.1 Principal Shear Wall Action

Figure 2.3 shows a typical shear wall unit and its distortion when subjected to lateral load. Frame joints can be regarded as being pinned. An induced shear load,  $H$ , at the top of the wall causes the framing to distort. Considering that the studs are attached to the plates by the sheathing and metal fasteners, the shear displacement of the timber frame is then resisted by the sheathing and the nails connecting it to the frame. Due to

the rigidity of the sheathing panel, it rotates less than the framing and slips over it because the nails deform and crush the wood fibers. Neglecting uplift, the total wall distortion,  $\gamma$ , is then a function of nail slip and shear distortion of the sheathing. However, the latter is relatively small compared to nail slip and is often neglected. Fasteners located at the corners resist the highest load because the largest displacement of the sheathing relative to the frame occurs in that area. Interior framing studs prevent the sheathing from buckling and support gravity loads (Stewart, 1987). Nails fastening the sheathing to the intermediate studs generally contribute little to wall strength.

Shear load induces tension and compression forces, respectively, along the vertical edges of the sheathing panel which are transferred to the end studs by the sheathing nails. The depicted shear wall action according to the simple diaphragm theory in Figure 1.1 is a strong simplification to facilitate the computation of uplift forces. In reality, due to the sheathing rotation as indicated in Figure 2.3 the end stud where the load is applied experiences tension at the bottom and compression at the top. The end stud away from the load application is under compression at the bottom and tension at the top. Both tension and compression forces reach their maximum at the bottom plate. The tension force causes the wall to separate from the bottom plate when the framing is not restrained against uplift.

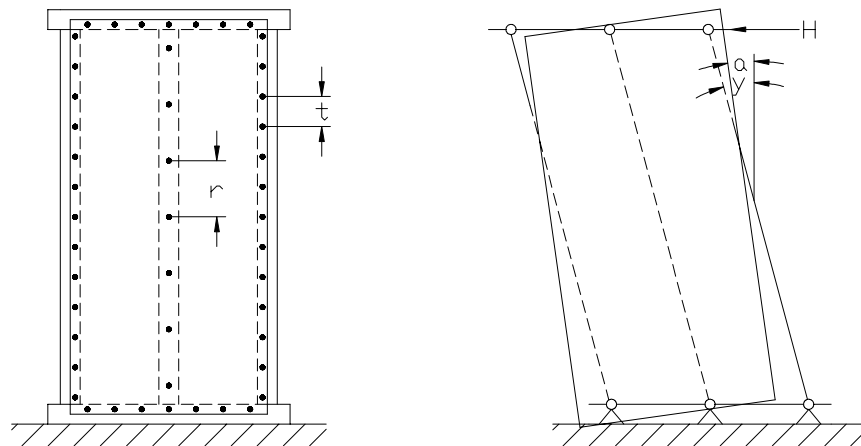


Figure 2.3: Typical structural behavior of a shear wall unit (after Almsarker, 1995)

A rather simple method may be used to calculate the shear capacity of a shear wall segment. Let  $t$  denote the distance between the fasteners along the perimeter of one sheathing panel, and let  $b$  stand for the panel width then the load carrying capacity of one shear wall panel can be determined using the simple equation (Eurocode 5 1995)

$$F_d = F_{f,d} \cdot \frac{b}{t} \quad (1.1)$$

where  $F_{f,d}$  is the design capacity of an individual fastener. This equation, however, does not account for concentrated forces at the corners of the panel and may not be used if uplift is important.

## 2.4.2 Parameters Influencing Shear Capacity

### 2.4.2.1 Uplift Restraints and Gravity Loads

Different testing standards diverge when it comes to the type and degree of overturning restraint required. For instance, Australian testing organizations do not require any uplift restraints (Reardon 1980). However, Stewart (1987) concluded from his shear wall tests that anchorage connections have a large influence on capacity and stiffness of shear walls. Dolan (1989) found that the overturning anchor connection fastening the end studs of his test walls to the foundation greatly enhanced wall performance. The anchor prevented the walls from rotating as a rigid body and averted separation from the bottom plate.

If the wall in Figure 2.3 were not restrained against uplift, the total horizontal deflection would be the sum of frame distortion and rigid body rotation of the wall unit. It is obvious that this will influence the stiffness of the system since it is safe to assume that the force required to rotate the wall unit about one edge is smaller than the force needed to distort it (note that this assumption is only valid for narrow wall units). The result is that a higher displacement with less force is achieved, thus the stiffness of the system is lower.

The higher the aspect ratio (height/length) of a given shear wall, the more it will act like a cantilevered beam and tie-down anchors will obviously improve the strength

when loaded in shear. However, for walls with relatively small aspect ratios (i.e. walls with lengths being several times the height) it is hard to believe that the wall would behave under lateral load as a cantilevered beam. Many engineers doubt that wood shear walls with low aspect ratios will overturn during earthquakes and questions have been raised whether this kind of anchorage is required (Diekmann 1994). The anchorage effect on such walls has yet to be quantified and is a major objective in this study.

Gravity loads reduce, or sometimes eliminate, panel uplift forces due to lateral loading and work similar to a tie-down device. During earthquakes, gravity loads may increase the stiffness of the shear wall. However, during high wind events uplift forces can exceed gravity loads and add to uplift forces caused by the overturning moment.

#### *2.4.2.2 Effect of Window and Door Openings*

Size and location of openings in shear walls generally affect wall capacity and stiffness. Ge (1991) found in a parametric study that openings significantly reduce racking stiffness of shear walls at low load levels. Johnson (1997) observed during sequential phased displacement tests of walls containing various openings that the fully-sheathed segments performed in a racking manner, whereas segments above and below openings more or less rotated as rigid bodies.

Many design procedures neglect the contribution to shear strength of sheathing segments below and above openings. Design capacity is assumed to be the sum of the shear capacities of each fully sheathed segment. However, Tissel and Rose (1988) noted that the sheathed area below or above large openings contributed significantly to the overall wall strength and stiffness.

#### *2.4.2.3 Other Parameters*

Fastener strength and spacing, and shear strength of the sheathing are other important parameters influencing the lateral load resisting capacity of shear walls. Ge (1991) reported that the sheathing stiffness influences the wall stiffness significantly at lower load levels only. At higher load levels and associated higher displacements sheathing stiffness becomes less important and the nail load-slip characteristic governs

wall performance. More parameters are covered in the following summary of experimental work on shear walls that has been conducted in the past.

#### **2.4.2 Experimental Shear Wall Studies**

Price and Gromala (1980) used ASTM E 72-77 to compare ultimate strength and stiffness of 8 feet (2.4 m) square panels sheathed with different structural flakeboards and plywoods. The authors reported the most common monotonic failure mode to be bending of the nail shank and withdrawal from the framing material. Results revealed that plywood sheathed panels reached slightly higher ultimate strength values than structural flakeboard

Wolfe (1983) used ASTM E 564-76 and evaluated the contribution of gypsum wallboard, wall length, and windbracing to racking performance of shear walls. A total of thirty, full scale walls were tested with aspect ratios ranging from 1 to 1/3. Wolfe found that gypsum wallboard in general contributed significantly to monotonic wall racking performance. He also observed that taped joints transferred load between individual boards, and contributed to stiffness and ultimate strength as the boards act together as a continuous diaphragm. Walls with gypsum boards oriented horizontally were up to 40 percent stronger than walls containing vertical oriented gypsum boards. The study concludes that for walls with gypsum board sheathing and windbracing, the sum of the stiffness for each individual component approximately equals the overall stiffness of the tested system.

Griffiths (1984) summarized the results of monotonic shear wall tests with different sheathing and framing materials, conducted at the University of Surrey in Guildford, England. Due to major disadvantages of the ASTM E 72-77 procedure, in the early 1970s the Princes Risborough Laboratories in England introduced a different monotonic testing procedure, the so-called standard PRL/Uofs test. Rather than restraining the wall panels from uplift using tie-down anchors, the English method incorporates vertical load applied to the panels using jacks. Stiffness and ultimate strength tests of 8 feet (2,4 m) square walls were conducted at different vertical load levels. Griffiths pointed out that a zero vertical load level represented a 'lower bound

case' accounting for light-weight structures subjected to 'hurricane type uplift conditions'. Most walls tested sustained 90 percent of the maximum load over a reasonably large displacement. Walls sheathed with plywood showed a 13 percent increase in racking strength when the frame species was changed from Spruce-Pine-Fir to Hem-Fir. Griffiths indicated that the modes of failure vary with board types, nail size, vertical loading and frame timber.

In 1984 Patton Mallory et. al. addressed the need for data on racking strength of timber shear walls longer than 8 feet (2.4 m), i.e. with an aspect ratio smaller than unity. Subsequently, Patton Mallory et. al. (1984 and 1985) published two articles about two static-monotonic test series conducted on small- and full-scale shear walls with aspect ratios ranging from 1 to 1/4. For both, small- and full-scale walls, ultimate shear strength was linearly proportional to wall length, but stiffness was not. Small-scale tests were found to be a good alternative to full-scale walls in terms of evaluating sheathing differences and composite action. The authors observed a shift in failure mode from an approximately symmetrical to a rather unsymmetrical pattern in longer walls. Consequently, longer walls with an aspect ratio smaller than one did not exhibit sheathing rotation about a geometric centroid during racking. This was contradictory to the belief that sheathing displacement would not change with increasing wall length. The tests also supported the hypothesis stated by Wolfe earlier in 1983, namely the sum of the strengths and stiffnesses of two walls sheathed on one side is equal to the total strength and stiffness of a wall sheathed on both sides, neglecting the contribution of the frame. Altogether eleven full-size walls were tested where 4 walls, 24 feet (7.3 m) in length, contained window and door openings. Based on values obtained from the tests, Patton-Mallory et al. suggested to estimate the racking strength of shear walls with openings by dividing the effective length (length with full-height sheathing) by the total length of the wall. This effective length ratio was then multiplied with the racking strength of a fully sheathed wall.

In Japan, Sugiyama (1981) proposed an empirical equation for shear walls containing openings without intermediate tie-down devices. The so-called perforated

shear wall design method which was adopted by the *Standard Building Code 1994 Revised Edition* (SBC 1994) is based on Sugiyama's equation. Yasumara and Sugiyama (1983) noted a significant strength reduction for shear wall assemblies subjected to reversed cyclic loads when compared to static monotonic loading. One year later Yasumara and Sugiyama (1984) studied the influence of openings in shear walls on stiffness and capacity employing static monotonic tests. They developed a design method that is based on a "shear strength ratio". The shear strength ratio indicates the capacity reduction of a wall containing openings when compared to a fully sheathed wall with the same dimensions. In 1994, Sugiyama and Matsumoto introduced three empirically derived equations to calculate shear strength reduction at shear deformation angles of 1/60, 1/100, and 1/300 radian. The shear strength ratio as well as the three equations are used in this study and are further discussed in Chapter 4. Johnson (1997) verified Sugiyama's empirical equations through full-scale shear wall tests and concluded that the method predicts overly conservative values for walls with large openings.

At the University of British Columbia, Canada, Dolan (1989) tested a total of 22 plywood and 20 waferboard sheathed, 8 feet (2.4 m) square wall panels in order to validate his proposed finite element model. He used five different test methods (only four are described here) with the intent to obtain more information about actual shear wall performance in earthquakes. The first specimens were tested in accordance with the ASTM E 72-77 procedure, with the exception that similar tie-down mechanisms, as described in ASTM E 564-76, were used. The panels sheathed with waferboard had slightly higher stiffness values than the plywood sheathed walls. However, differences in racking strength were statistically insignificant. Intending to make inference about the hysteretic behavior of shear walls Dolan carried through a quasi-static cyclic test with increasing displacement amplitudes. The essence of his results was that the peaks of the hysteretic curves appeared to coincide with the curve obtained in the monotonic test. In addition, the load capacity of the walls tested decreased as the number of cycles with constant displacement amplitudes increased. The shapes of the load deflection curves for all specimens tested, whether tested monotonically or cyclically, resembled curves

obtained from connection tests with nails, which led to the conclusion that racking and cyclic behavior of shear walls is mainly a function of fastener behavior. Wall stiffness increased with a more dense nailing schedule of the sheathing. Consequently walls containing more fasteners experience higher loads in earthquakes due to higher stiffness properties. Free vibration tests enabled Dolan to measure the natural frequencies of the walls before and after dynamic tests. Since the natural frequency of a whole assembly is different than that of a single panel the researcher modeled the missing structure by subjecting each panel to a respective dead load. Results showed that the fundamental frequency changed significantly as the walls were strained, which confirmed the ductile characteristic of nailed shear walls. Dolan summarized that there was no appreciable difference in the performance of walls sheathed with waferboard or plywood. Furthermore walls with sheathing oriented horizontally and fully blocked showed no difference in performance.

### **2.4.3 Analytical Modeling**

Analytical modeling is a complimentary part to experimental analysis for understanding the behavior of structural systems. There are essentially two types of analytical models, the finite element model and the closed form equation. Empirical equations are considered as method rather than model since they are limited to testing procedures and configuration used to derive them.

#### *2.4.3.1 Finite Element Models*

In the last twenty years the finite element analysis gained popularity and became, thanks to improving computer technology, a useful tool to model almost any type of structural problem. However, the finite element method is reasonably comprehensive and time consuming. Since the number of computations exponentially increases with the number of equations, the lack of sufficient computer speed remains the reason why there has yet to be proposed a general and easy-to-use finite element program suitable for detailed analysis of shear wall buildings. Thus, the current formulations are for research purposes rather than everyday design.

Foschi (1977) introduced a general finite element model for the monotonic analysis of wood diaphragms modeling a shear wall as a composite of four structural elements. The model addressed nonlinear load-deformation relationship by employing an exponential function and allowed the analysis of wood diaphragms by a computer program. Foschi estimated the parameters used to describe the exponential load-slip relationship by employing nail withdrawal data and methods published earlier in the literature. Nevertheless, the results of 20 feet (6 m) by 60 feet (18.2 m) diaphragms correlated well with analytical values.

A relatively similar finite element formulation was proposed by Itani and Cheung (1984). Connections between sheathing and frame were modeled as joint elements consisting of mutually perpendicular spring pairs. One joint element represented a single line of fasteners. For larger diaphragms, any sheathing arrangements, load applications, or diaphragm geometry could be analyzed and modeled with this method. The problem, however, was that with larger diaphragms the number of degrees-of-freedom increased to a great extent. Subsequently, Falk and Itani (1989) developed a super element that models a sheathing element together with all the fasteners connecting it to the framing. In other words the element represents multiple lines of fasteners as opposed to a single line as presented in the earlier model. Consequently, the number of degrees-of-freedom could be reduced by as much as 40 percent. The authors used the model to investigate the effect of nail spacing on overall stiffness of diaphragms. A decrease in nail spacing of perimeter nails resulted in a significant increase of diaphragm stiffness whereas various spacing between field nails had only a secondary effect on stiffness.

None of the models mentioned above accounted for cyclic or dynamic response of shear walls. Thus, all those models were validated through data of test walls subjected to one-directional, monotonic loading only.

In 1987 Stewart developed a single-degree-of-freedom method that simulated the response of timber shear walls subjected to dynamic loading. The advantage of a single-degree-of-freedom model is that it is less elaborate and uses less computation time. On the other hand, such a model is only capable of examining the overall wall response.

Furthermore, since necessary parameters are taken out of experimental results, single-degree-of-freedom models lose accuracy as the wall configuration changes.

Unlike the formulations discussed above, Dolan (1989) proposed a more general finite element model that allows a time-step dynamic analysis of shear walls until failure. Dolan extended and improved the model presented by Foschi in 1977. He modeled each sheathing-to-framing connector using three non-linear spring elements. In addition, three dimensional buckling of sheathing panels and bearing elements between sheathing panels were incorporated in the formulation. The result was a computer program capable of predicting the time-history of dynamic displacements of timber shear walls without limitations to wall configurations. In 1995, White and Dolan successfully included the feature of calculating forces and stresses in the program and reduced the analysis time.

#### *2.4.3.2 Closed Form Models*

Efforts in the past have been made to find a less elaborate analysis such as a so called closed-form equation. These are, on the basis of global assumptions, simplified straight forward equations, which are relatively easy to solve. Many of these models that have been proposed in the past correlate fairly well with experimental results. The downside, however, is that the equations are less versatile than finite element models. They are often tied to a certain wall configuration.

At the Forest Product Laboratory in Madison (WI) Tuomi and McCutcheon (1977) developed an equation to predict the static racking strength of wood stud shear walls sheathed on one side. The equation was derived by equating the energy of the racking load with the summation of the energy absorbed by each fastener. Potential energy of the system was assumed to be zero. The deformation of a single fastener with respect to racking load was determined by presuming that the diagonals of the deformed wood frame coincide with the diagonals of the sheathing. Initially, the two researchers neglected the shear deformation of the sheathing and assumed a linear load-slip behavior of the fasteners. Robertson (1980) indicated that experimental results had revealed that the unit racking strength does not remain constant as the total number of sheathing panels

changes. The developed equation, however, was based on a constant unit racking strength.

Itani et. al. (1982) extended the approach of Tuomi and McCutcheon such that they modeled the system ‘sheathing plus fasteners’ with two diagonal, linear-elastic springs. The result was a relatively simple method capable of determining the stiffness of continuous walls with and without openings. Panels below and above openings were neglected. However, at total wall displacements of 0.1 inch (2.54mm) the model deviated up to 18 percent from test values. In addition, the fact that the actual nail load-slip relationship is highly nonlinear severely limited the application of this method.

Based on observations of corrugated metal shear diaphragms (Easley, 1977) Easley et. al. (1982) derived a closed-form equation to calculate the stiffness of continuous wood shear wall panels sheathed on one side and subjected to static one-directional loading. The equation is essentially derived from a moment equilibrium formula for a particular sheathing panel. The method assumes a sheathing movement relative to the frame that differs from the movement pattern proposed by Tuomi and McCutcheon (1977). Easley et. al. proposed that the sheathing only distorts relative to sill and top plate whereas the studs remain parallel to the sheathing edges as the wall deforms. The researchers also assumed a certain nail force distribution and nail-slip pattern. Pertaining to this approach Gupta and Kuo (1985) stressed the fact that ‘the model has dual assumption’ and tends to underestimate the overall stiffness. Nevertheless, experimental results of 8 feet (2.4 m) high and 12 feet (3.7 m) wide walls, exposed to one directional, static load, matched predicted values fairly well.

Gupta and Kuo (1985) saw a need for a model that is not as elaborate as finite element models but more accurate than closed-form equations. Higher accuracy obtained through less assumptions implies more unknown variables or degrees-of-freedom. Consequently, the method offered an iterative solution only. The boundary conditions for the model were no uplift movements, no openings, and one-sided sheathing. Otherwise, there was no particular deformation pattern of the sheathing assumed, and there was no limitation regarding the length of the wall panel. The model also used an energy

approach, but as opposed to the method of Tuomi et. al. (1977) Gupta and Kuo acknowledged potential energy in terms of elastic bending and shear energy of studs and sheathing. It was found that the bending stiffness of studs and the shear stiffness of the sheathing do not contribute significantly to the load-deformation properties of shear walls.

McCutcheon (1985) revised the racking resistance equation introduced in 1977. He fit a simple power function to the test data of small-scale walls to account for nonlinear nail load-slip behavior. The deformation of the sheathing was also considered. Below design loads predicted racking displacements correlated well with experimental results of gypsum or plywood sheathed, 8 ft (2.4 m) high and up to 24 ft (7.3 m) wide walls.

Patton-Mallory and McCutcheon (1987) applied four types of curves to describe the nonlinear load-slip of nails in shear walls and substituted each one in the previously developed racking resistance equation. The study concluded that an asymptotic equation best describes fastener behavior until maximum capacity. Experimental results of 200 walls 22 inches (559 mm) high and up to 8 feet (2.4 m) wide proved that it is possible to predict racking performance of walls sheathed on both sides with different materials by applying the equation to each side. The drawback of the model first developed by Tuomi and McCutcheon (1977), however, is that it does not account for uplift movements of the sheathing. Further, the model has not been verified through long full-scale shear walls and reversed cyclic loading.

Two years after they had presented their model, Gupta and Kuo (1987) published a model that uses the same approach as the first one but takes stud and sheathing uplift into account. The model was applied to test data from the literature. The two authors found that vertical load and uplift constrains significantly increase the overall stiffness of shear walls.

## **2.5 Summary**

Based on the preceding literature review the following conclusions can be made.

- Shear wall response is influenced by nail density, sheathing thickness and loading rate.
- The nailed sheathing-to-stud connection governs the overall response of timber-framed shear walls. Nail slip is the main cause of wall distortion when subjected to lateral load.
- Ultimate shear strength is linearly proportional to wall length.
- Peaks of hysteretic curves obtained through cyclic testing appear to coincide with the load deflection curve from monotonic tests.
- Stiffness of sheathing does not influence shear wall capacity.
- Gypsum wallboard contributes significantly to wall racking performance.
- Wind uplift forces can exceed dead loads. In case of light-weight structures such as residential buildings the lower bound case is zero vertical load for shear wall tests.
- There is no significant difference in performance of OSB and plywood sheathed walls.

## Chapter 3

### Test Walls and Procedures

#### 3.1 General

Twelve straight<sup>1</sup> walls and four walls with corner framing were tested using a monotonic and a sequential phased displacement (SPD) pattern. Construction specifications matched those used by Johnson (1997) for the straight walls so that additional data could be used. The corner wall specimen configuration was provided by the National Association of Home Builders (NAHB). Straight wall specimens were 40 feet (12.2m) long and 8 feet (2.4m) high. Corner wall specimens measured 12 feet (3.7m) in length and were 8 feet (2.4m) tall. The size of the wing walls was either 2 feet by 8 feet (0.6m x 2.4m) or 4 feet by 8 feet (1.2m x 2.4m). Together with the results obtained by Johnson (1997), a total of five different wall configurations, three anchorage, and two loading conditions were included in this study (Table 3.1). The hatched areas in Table 3.1 represent the sheathing panels (OSB on one and gypsum sheathing on the other side). All walls were constructed with the sheathing panels oriented vertically (i.e. the long dimension of the panel ran parallel to the studs).

Each wall was composed of the same type of framing and sheathing nails. The nailing pattern was the same for every wall. Walls investigated by Johnson (1997) were sheathed with plywood but were constructed equivalently. All other walls had OSB sheathing. It is important to point out that all walls were tested without gravity load (in the form of dead or live load) applied. The intention was to test the most conservative condition such as possible uplift during high wind events that could exceed gravity loads or the contingency that the wall is a non-load bearing, partition wall in a building.

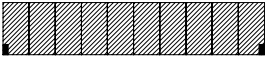
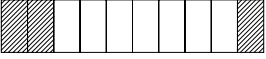
Because of the size of the specimens all walls were assembled and tested outside. During the assembly the walls were covered with a watertight plastic foil to protect them

---

<sup>1</sup> The term “straight” indicates that the walls did not contain corner framing

from rain. However, there was no control over ambient humidity and temperature. The measured moisture content of the lumber ranged between 8 and 12 percent at the time of testing. Moisture content was measured with an electric resistance meter.

Table 3.1: Specimen configurations

Wall Configurations - Straight Walls			Wall Type <sup>(2)</sup>	Testing Procedure
No Tie-down Anchors	Anchors at End of Wall Only <sup>(1)</sup>	Maximum Amount of Tie-down Anchors		
			A <sup>(3)</sup>	Monotonic and SPD
			D	Monotonic and SPD
			E	Monotonic and SPD
Wall Configurations - Walls with Corner Framing				
2 feet Corner Segments	4 feet Corner Segments			
No Tie-down Anchors	No Tie-down Anchors			
				SPD (one replication)

<sup>(1)</sup>These specimens were tested by Johnson (1997) and had plywood sheathing

<sup>(2)</sup>Wall types B and C were only tested by Johnson (1997) and are not included here

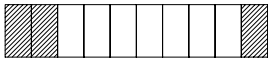
<sup>(3)</sup>Wall A had only two anchorage conditions due to it being fully sheathed

## 3.2 Description of Test Walls

### 3.2.1 Design and Construction of Straight Test Walls

Straight wall specimens included three different configurations. Table 3.2 lists the opening dimensions and pertinent sheathing area ratios determined using Equation 4.1 (Chapter 4). Wall A was fully sheathed. Wall D contained a garage door, a pedestrian door, and a window opening. Wall E had structural and gypsum sheathing at the ends only. Wall E was meant to represent conventionally constructed walls where a minimum of area was covered with structural sheathing. The middle area of this wall type is commonly sheathed with non-structural sheathing such as insulation board. The only deviation from conventional construction as defined in the 1994 or 1997 NEHRP Provisions was that the distance between structural sheathing panels was three feet (0.91m) greater than the 25 feet (7.62m) required.

Table 3.2: Opening sizes for wall configurations

Wall Configuration	Sheathing Area Ratio (r)	Wall Type	Opening Size	
			Door	Window <sup>(1)</sup>
	1.0	A	-	-
	0.48	D	6'-8" x 4'-0" 6'-8" x 12'-0"	4'-0" x 7'-10 <sup>1</sup> / <sub>2</sub> "
	0.30	E	(Sheathed at ends) <sup>2</sup> 8'-0" x 28'-0"	-

<sup>(1)</sup>The top of the window is located 16 inches from the top of the wall.

<sup>(2)</sup>Wall E has studs 16 in. o.c. for the full length of wall but is sheathed only at the ends of the wall.

The general wall assembly and the four different types of nails and different nail schedules used in constructing the wall specimens is shown in Figure 3.1. This system is recognized by the American model building codes. All framing connections used 16d

(3.8mm diameter and 82.6mm length) brite common nails. Brite common 8d (3.3mm diameter and 63.5mm length) nails attached OSB sheathing to the framing. Gypsum-to-framing connections used 13 gage x 1-1/2 inch ( $\text{Ø}2.4\text{mm}$  x 38.1mm) drywall nails. A nail spacing of 6 inches (152mm) around the perimeter and 12 inches (305mm) for intermediate framing was used for OSB sheathing and 7 inches (178mm) perimeter and 10 inches (254mm) field to fasten the gypsum wallboard to the framing (Figure 3.1). OSB sheathing fastened to the double end studs received double rows of nails, spaced 6 inches (152.4mm) on center. All nails were hand driven.

The bottom plate was bolted to a fixed steel structural tube 24 inches (610mm) on center, beginning one foot from the end of the wall with bolts 5/8 inch ( $\text{Ø}15.9\text{mm}$ ) diameter National Coarse thread. Steel plate washers, 3 inches x 3 inches square, 1/4 inch thick (76.2mm x 76.2mm x 6.4mm) distributed the load from the bolt head and prevented cross-grain bending in the wood. With the exception of the tie-down anchor bolts, all bolts were located a minimum of one foot from the edges of each sheathing panel and from the studs adjacent to openings. The steel load distribution beam and double top plate were connected in the same manner as the bottom plate with the rigid foundation (Figure 3.2).

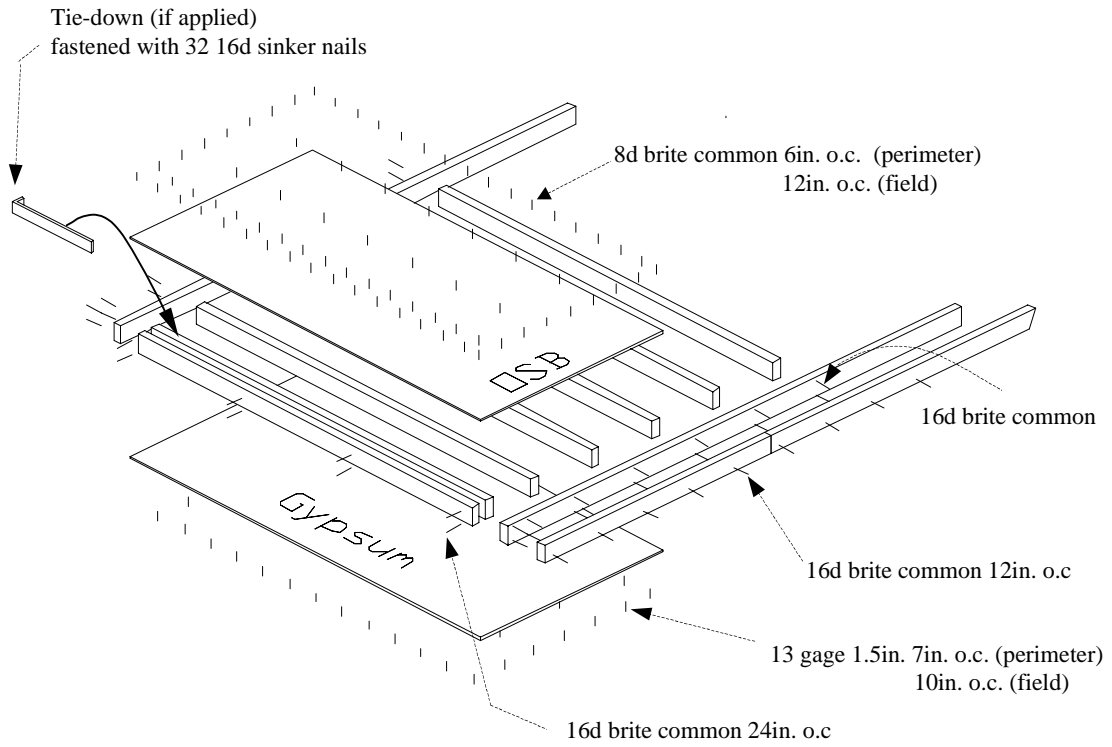


Figure 3.1: Wall assembly

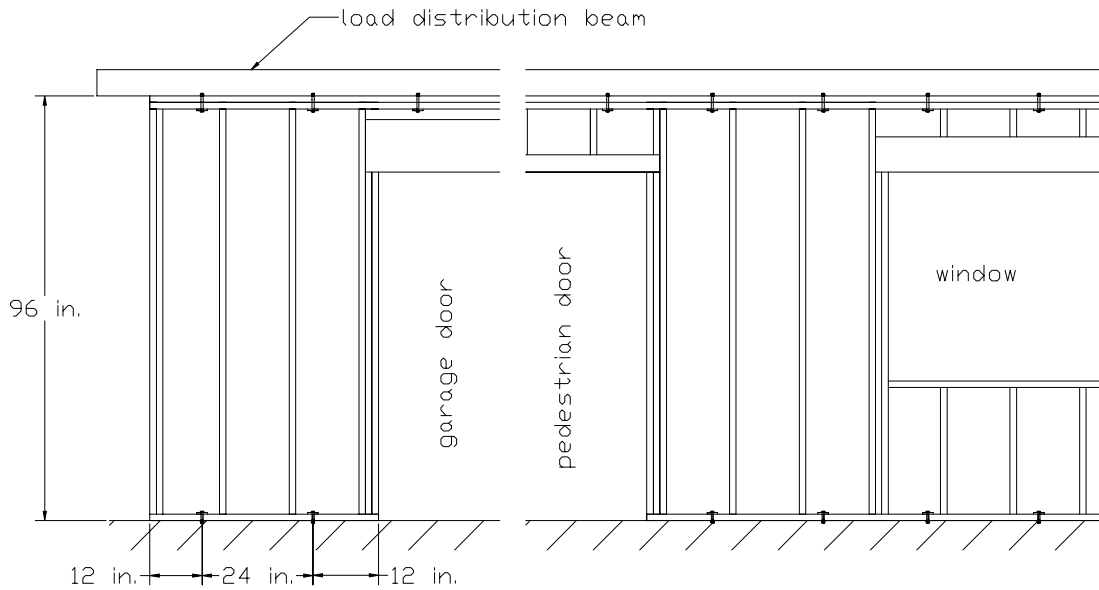


Figure 3.2: Wall construction

Studs, spaced 16 inches (406mm) on center, double top plates, single bottom plates, double end studs, and double or triple studs around doors and windows were the main components of the wall framing (Figure 3.2). A local lumberyard supplied the lumber for framing. All framing lumber was spruce-pine-fir and was graded “Stud or better”. Members were arbitrarily chosen when placed in the wall specimens. All lumber was stored at least two weeks prior to assembly in a covered laboratory.

The size of all full height sheathing panels was four feet by eight feet (1.2m x 2.4m). Exterior sheathing was 7/16 inch (11mm) OSB rated sheathing and interior sheathing consisted of 1/2 inch (13mm) gypsum wallboard. For the walls containing openings, the OSB and gypsum were cut to fit above and below the doors and windows without overlapping the header to jack stud connection. To be compatible with common construction practices, a gap of 1/8 inch (3mm) between OSB sheets was maintained to account for potential swelling of the sheets. All drywall joints were taped and covered with drywall compound. Compound drying times complied with manufacturer’s recommendation and were adjusted to ambient temperature and humidity. The steel test fixture was narrower than the top and bottom plates to allow free rotation of exterior and interior sheathing past the test fixture at the top and bottom. Materials and construction details for the wall specimens are summarized in Table 3. Included are the sizes of headers and jack studs used around openings.

Six specimens were tested monotonically and reversed cyclically without overturning restraint. Simpson Tie-down HTT22 with 5/8 inch ( $\varnothing$ 15.9mm) diameter anchor bolts were used on an additional six walls with one tie-down at the end of **each** fully sheathed segment (Table 3.3). Tie-down anchors were attached to the bottom of the end studs of the respective segment by thirty-two (32) 16d ( $\varnothing$ 3.8mm and 82.6mm length) sinker nails.

Table 3.3: Wall materials and construction data

Component	Fabrication and Materials
Framing Members	Stud, Spruce-Pine-Fir, 2 x 4 in. (nom.) (51 x 102mm) @ 16 in. (406mm) o.c.
Sheathing:	
Exterior	Structural oriented strandboard (OSB) <sup>(1)</sup> , 7/16 in., 4 ft. x 8 ft. (11mm x 1.2 x 2.4m) sheets installed vertically.
Interior	Gypsum wallboard, 1/2 in. (13mm), installed vertically, joints taped
Headers:	
4'-0" opening	(2) 2 x 4 in. (nom.) (51 x 102mm) with intermediate layer of 7/16 in. (11mm) structural OSB. One jack stud at each end.
7'-10 1/2" opening	(2) 2 x 8 in. (nom.) (51 x 203mm) with intermediate layer of 7/16 in. (11mm) structural OSB. Two jack studs at each end.
12' opening	(2) 2 x 12 in. (nom.) (51 x 305mm) with intermediate layer of 7/16 in. (11mm) structural OSB. Two jack studs at each end.
Tie-down	Simpson HTT 22, nailed to end studs with 16d (Ø3.8 x 82.6mm) sinker nails. 5/8 in. diameter (Ø 15.9mm) A307 bolt to connect to foundation.
Anchor Bolts	5/8 in. diameter (Ø 15.9mm) A307 bolt with 3 in. square x 1/4 in. (76 x 76x 6.35mm) steel plate washers.

<sup>(1)</sup>Exterior sheathing was plywood, 15/32 in. (12mm) in Johnson's (1997) specimens

### 3.2.2 Attachment to Test Frame and Instrumentation of Straight Walls

Walls were tested in horizontal position as depicted in Figure 3.3. To ease the installation of the measuring equipment and load cell, the walls were raised approximately 16 inches (406mm) above the ground. A hydraulic actuator, with a range of  $\pm 6$  inches (152mm) and capacity of 55,000 lbs. (245 kN), displaced the top right corner of each shear wall as shown in Figure 3.3. A 5 inch by 3 inch (127mm x 76mm)

steel tube distributed the loading to the wall's double top plate. Eight casters ensured horizontal motion of the wall top with minimum frictional loss. The casters were fixed to the load distribution beam parallel to loading (Figure 3.3). Johnson (1997) conducted a test to determine the amount of friction created by the wheels. He found that the magnitude of the friction was negligible (275lbs. or 1.2 kN) when compared to the capacity of the walls. Nevertheless, the friction was deducted from the absolute value of the recorded load resisted by each wall in both Johnson's and this study.

Figure 3.3 depicts the location of three linear variable differential transducers (LVDT) that were attached to the foundation to measure wall displacements. LVDT #0 was built into the hydraulic actuator, measuring the relative displacement of the actuator. The actuator also contained a sensor that recorded the load resisted by the wall. LVDT #1 and LVDT #2 recorded the compression and uplift displacement of the end studs relative to the foundation depending on which corner of the wall was in compression or tension, respectively. For walls with tie-down anchors, the data recorded were corrected to compensate for amplifications caused by the lever arm of the LVDT fixtures. This ensured that actual compression and uplift displacements of the end studs were measured. Anchored studs were assumed to rotate about the bolt attaching the anchor to the foundation (Figure 3.4). However, this assumption could not be made for the walls without overturning restraint because the end stud did not have a defined point of rotation. In this case the data recorded by LVDT #1 and #2 were not corrected.

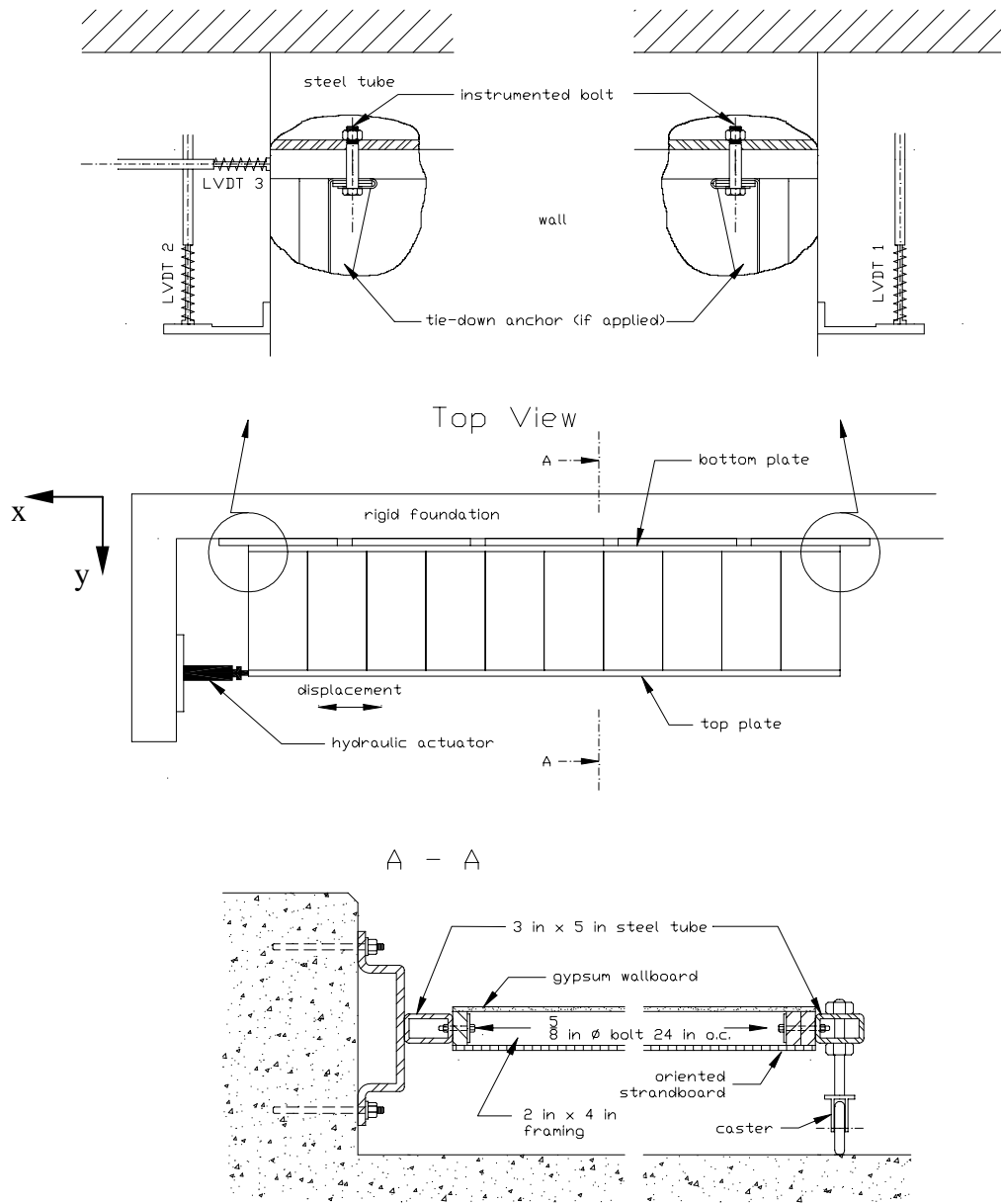


Figure 3.3: Straight wall orientation and test set-up

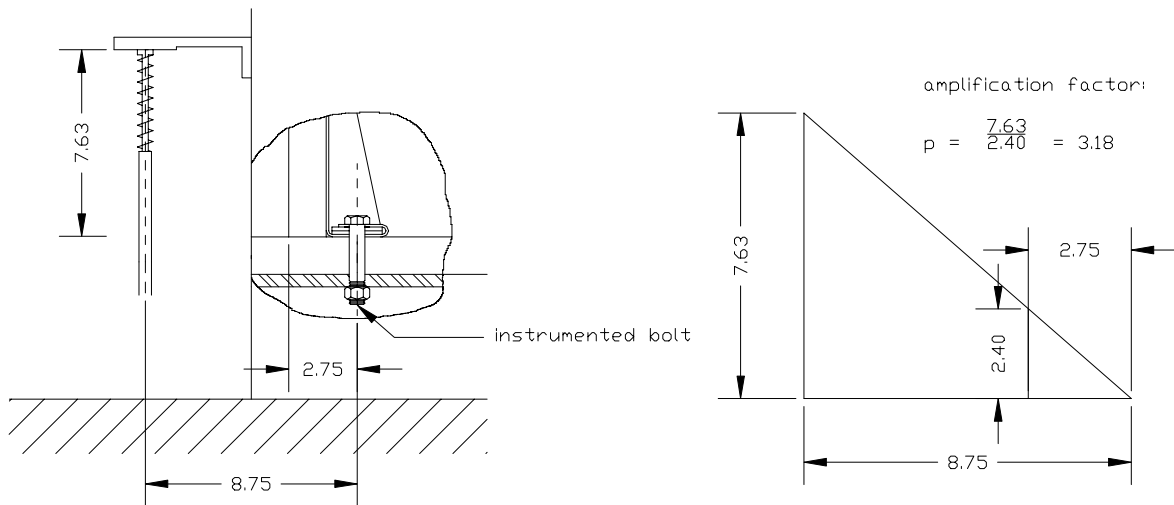


Figure 3.4: Geometry of LVDT fixture to measure stud uplift

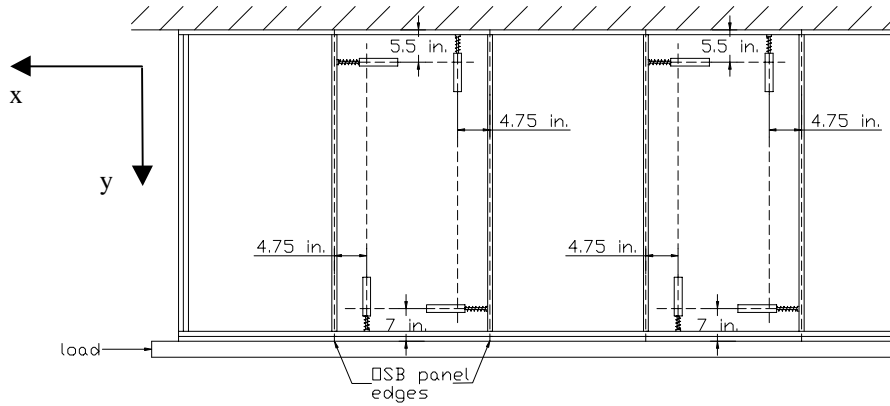
LVDT #3 measured the horizontal displacement of the bottom plate relative to the foundation. Through this measurement, rigid body translation of the wall could be subtracted from the global displacement to obtain interstory drift. Interstory drift is defined as the drift between top plate and bottom plate of the wall. Therefore, interstory drift was the reading of LVDT #0 less the reading of LVDT #3. Note that the interstory drift as measured here includes the shear wall deflection arising from rigid body rotation of the wall when tie-down anchors were omitted. By reason of the length of each specimen it was not possible to measure the change in diagonals to separate interstory drift arising from uplift.

To exclude slip between the load distribution beam and the top plate a fourth LVDT was originally included that measured the displacement of the top plate with respect to the foundation, rather than measuring the displacement of the load distribution beam (or hydraulic actuator). However, the data suggested that slip was negligible. Furthermore, at wall displacements greater than 3 inches (127mm), gaps formed between top plate and end stud, which often caught the core of the LVDT and the measurement

became unreliable. For these reasons, the displacement data recorded by the hydraulic actuator (LVDT#0) was used for all calculations.

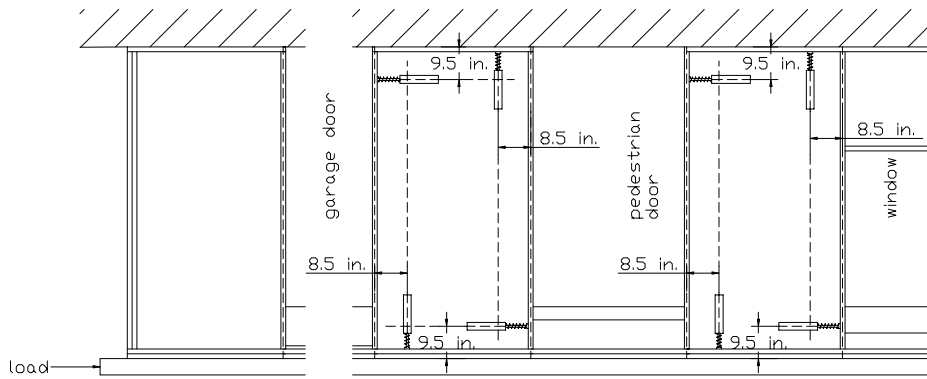
An instrumented tension bolt, replacing a normal bolt that attached the bottom plate to the foundation, was inserted close to the end stud. When tie-down anchors were applied, the tension bolt replaced the bolt that fastened the anchor and bottom plate to the foundation (Figure 3.3). Instrumented tension bolts were incorporated to measure uplift and compression forces in the stud and plate during testing. Since the tension bolts connected the tie-down anchors to the rigid foundation the measured force was equal to the tension force resisted by the anchors at the ends of the walls. In case of no overturning restraint, the recorded load was assumed to equal the uplift load resisted by the sheathing nails in the bottom plate close to the wall end. Compression forces could be measured by pretensioning each load bolt. Consequently, the compression force equals the tension load before the test less the recorded load during the test.

The interior of the five walls listed in Figure 3.5 was equipped with eight LVDTs each to measure the panel movement in respect to the framing. The LVDTs were fastened to the OSB sheathing. The dimensions given in Figure 3.5 are measured from the OSB edges. For better clarity, the intermediate studs are omitted in the drawing. The point of fixity of each LVDT is represented by the intersection of two dashed lines shown in Figure 3.5.



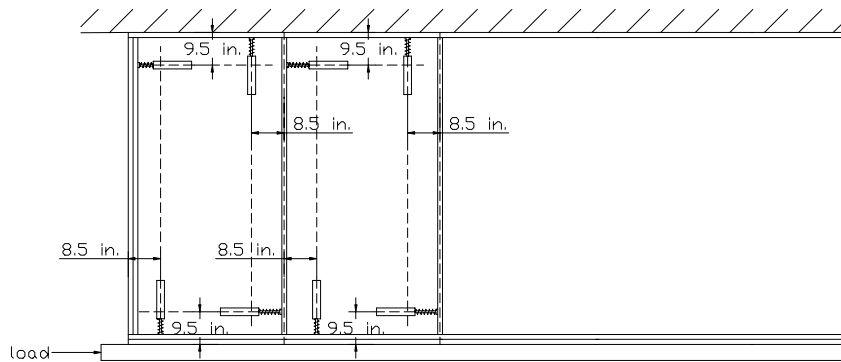
Wall A no anchors (SPD test)

Wall A anchors (SPD test)



Wall D max. amount of anchors (SPD test)

Wall D max. amount of anchors (monotonic test)



Wall E max. amount of anchors (SPD test)

Figure 3.5: Interior instrumentation of straight wall specimens

### 3.2.3 Design and Construction of Corner Walls

Walls with corner framing were essentially constructed in the same manner as the straight walls. Fastener types and schedules were identical. Figure 3.6 reveals the construction detail of the corner. Construction of the corner connection complied with the specifications provided by NAHB. The design is typical for American light-frame construction. At the end of each corner segment, double studs were incorporated to simulate the start of an opening. The corner walls were not restrained against uplift. In other words, no tie-down anchors were used.

As with the straight walls, all joints between the gypsum sheathing were taped and covered with drywall compound. For the 2 foot corners, the OSB and gypsum wallboard panels were cut in half lengthwise.

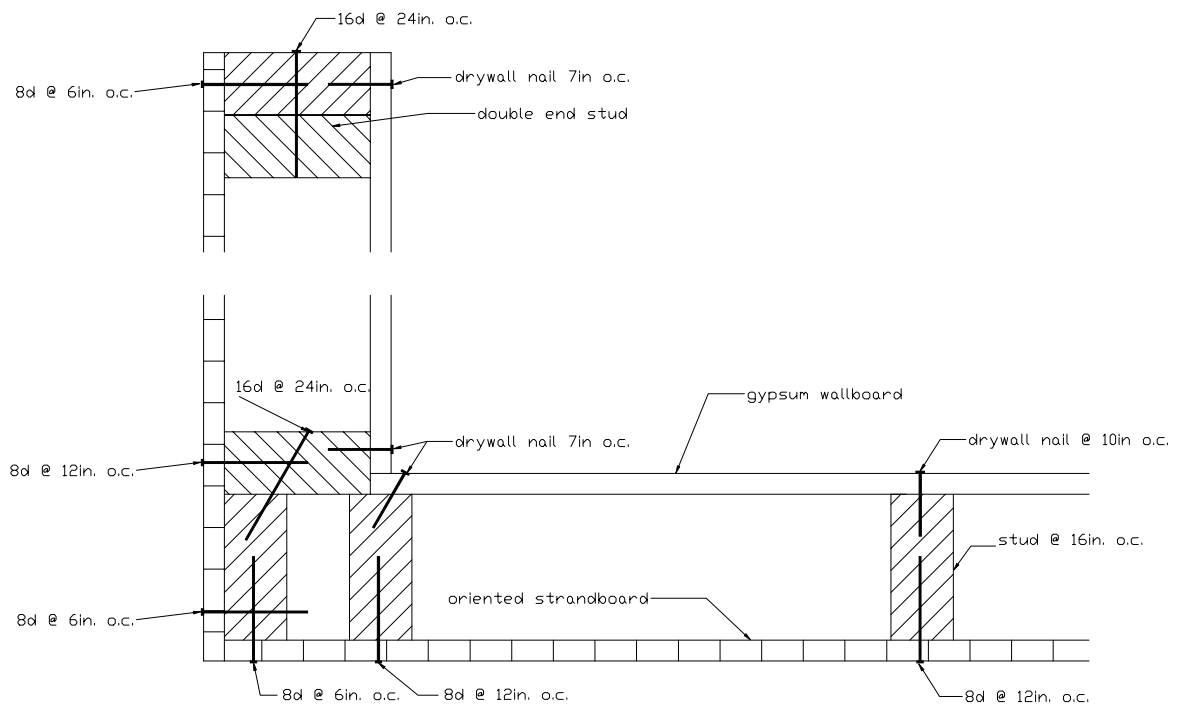


Figure 3.6: Construction detail corner

### 3.2.4 Attachment to the Test Frame and Instrumentation of Corner Walls

The test setup that was used for the straight wall specimens was not substantially changed when the corner wall specimens were tested. As with the straight walls, the corner walls were raised 16 inches off the ground. The same load distribution beam and rigid foundation were employed. Since the corner walls were 12 feet long, only four casters supported the load distribution beam. The amount of friction subtracted from the load data was divided in half, when compared to the straight wall specimens. A welded steel frame consisting of 3 inch by 5 inch (76mm x 127mm) steel tubes served as the rigid foundation for the wing walls (Figure 3.7). The steel frame was bolted to the concrete foundation with large steel braces that ensured sufficient sturdiness. At the top plate of each wall two 7/16 inch (11mm) thick OSB sheets were fastened to the end and main wall using 8d brite common nails ( $\varnothing 3.3\text{mm}$ , 63.5mm length), 6 inches (152mm) on center in order to simulate the assumed “lower bound” stiffening effect of a floor or ceiling diaphragm (Figure 3.7).

The exterior instrumentation of the walls is depicted in Figure 3.8. Four LVDTs were attached to the foundation and load distribution beam of each wall to record wall displacements. Due to the short length of the corner wall, large slip displacements were observed during preliminary tests. Therefore, LVDT# 0 was fixed to the load distribution tube and measured the slip between the tube and the wall. Again, two transducers, LVDT# 1 and # 2, were incorporated to measure the compression and uplift displacements of the end studs of the middle wall relative to the foundation. For uplift calculations, the corner wall sheathing was assumed to rotate about the outer bottom edge of either corner wall. Data from LVDT# 1 and # 2 were corrected to compensate for amplification effects caused by the geometry of the LVDT fixtures (Figure 3.9). LVDT #3 measured the horizontal displacement of the bottom plate relative to the foundation to subtract rigid body motion from the total wall displacement measured at the top plate. Total wall displacements were again recorded using the LVDT that was built in the hydraulic actuator; this time labeled as LVDT# 4. Interstory drift was calculated as readings of LVDT# 4 - (LVDT# 0 + LVDT# 3). Uplift and compression forces that were

exerted on connections between the bottom plate and the sheathing, as a result of the applied load, were measured by a tension bolt located close to the end stud of the middle wall (Figure 3.8).

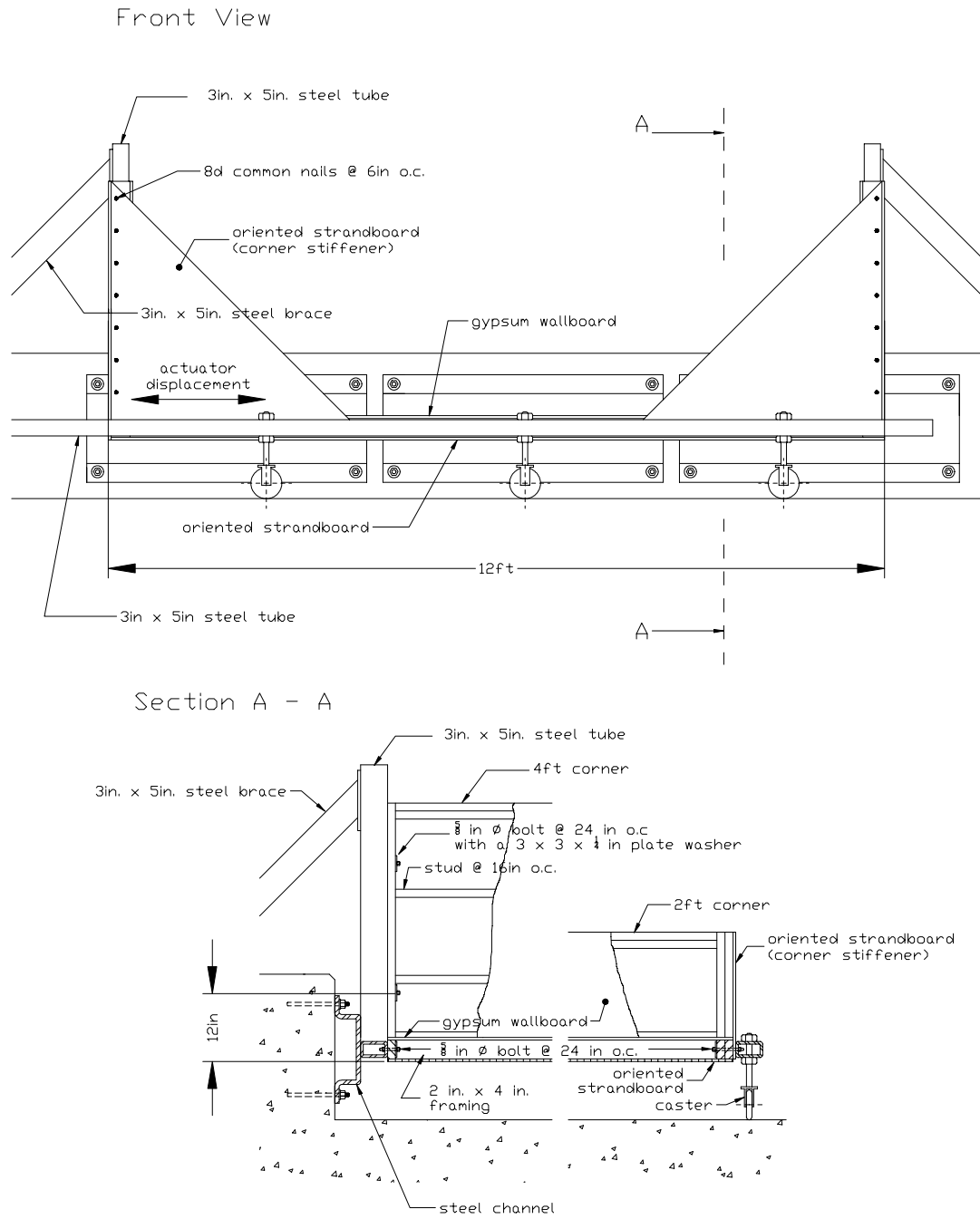


Figure 3.7: Test set up for corner walls

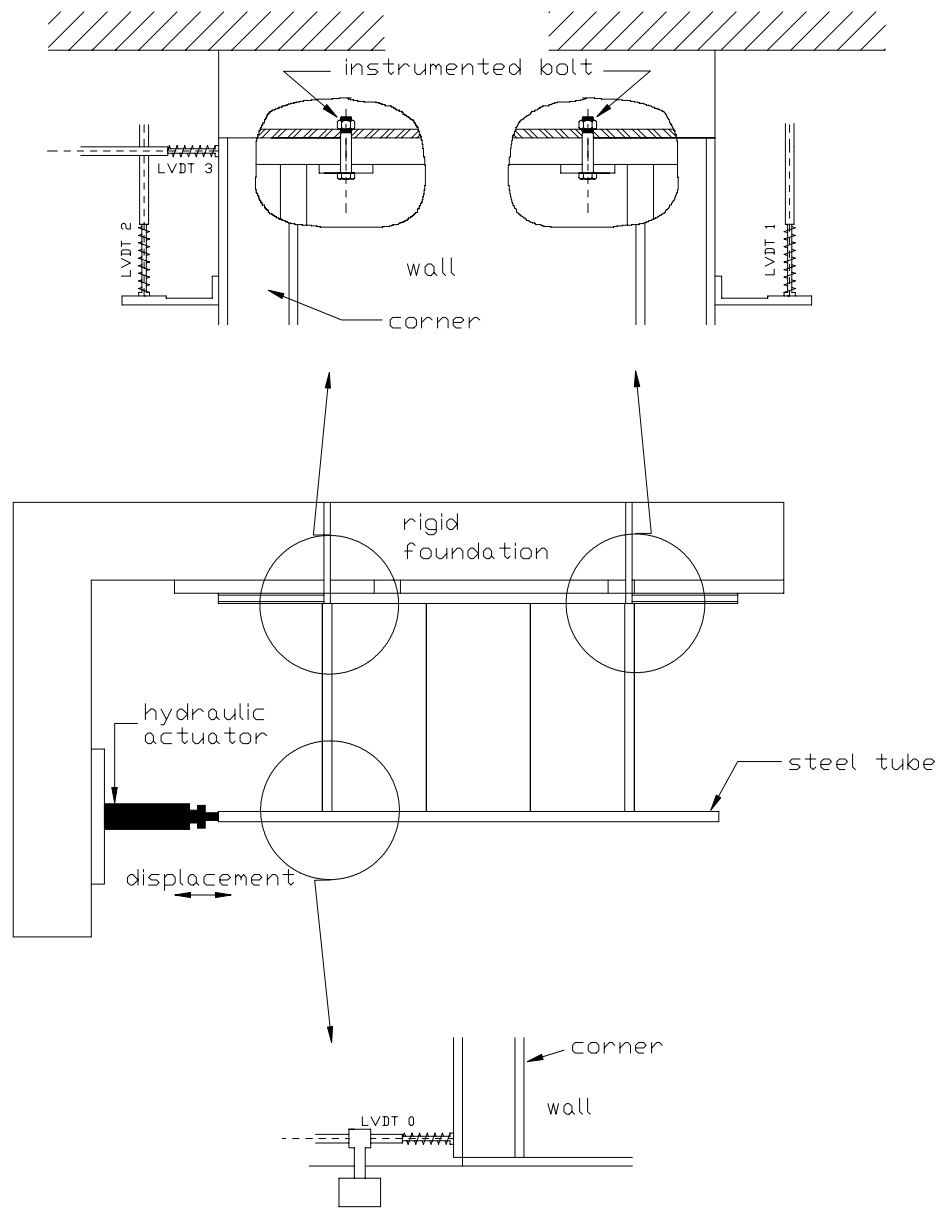


Figure 3.8: Corner wall instrumentation

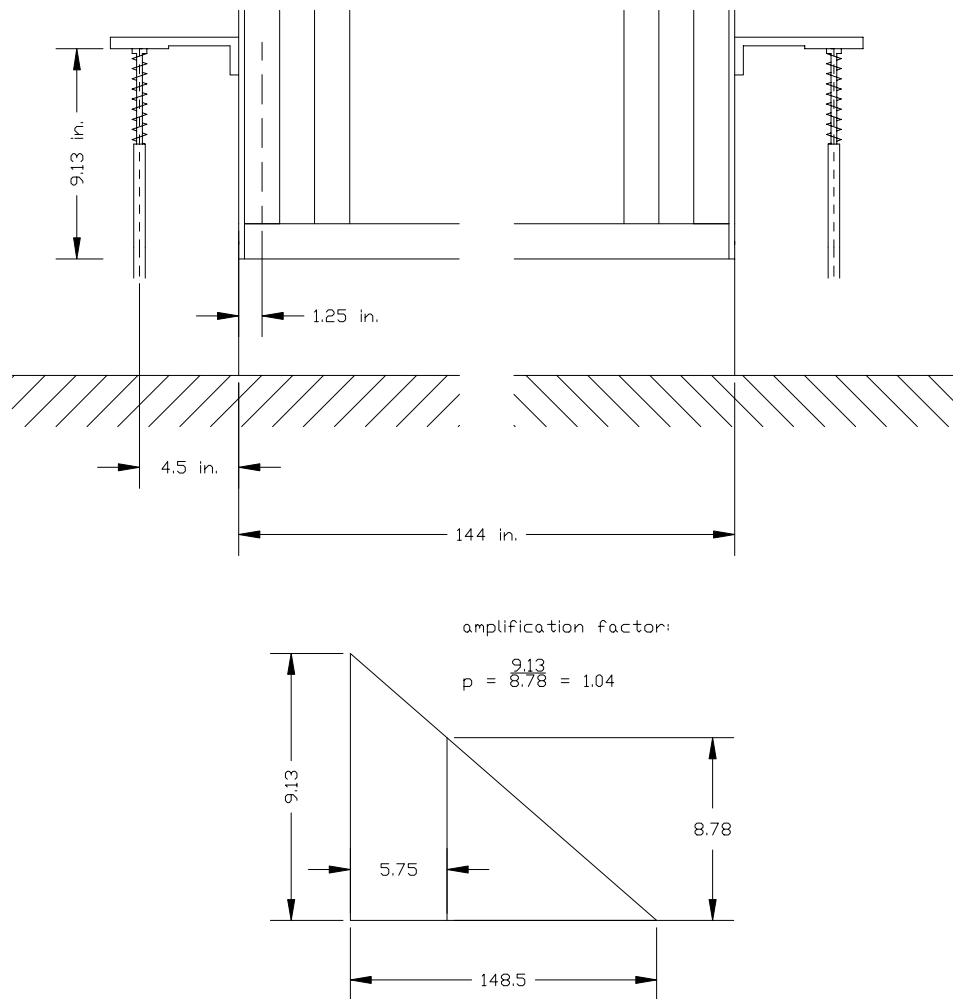


Figure 3.9: Measurement amplification of the LVDT fixture

Each specimen with corner framing was equipped with four interior LVDTs to record the displacement of the middle OSB panel in respect to the framing. The transducers were attached to the OSB panel at the same location in each wall (indicated by the intersection of the dashed lines in Figure 3.10).

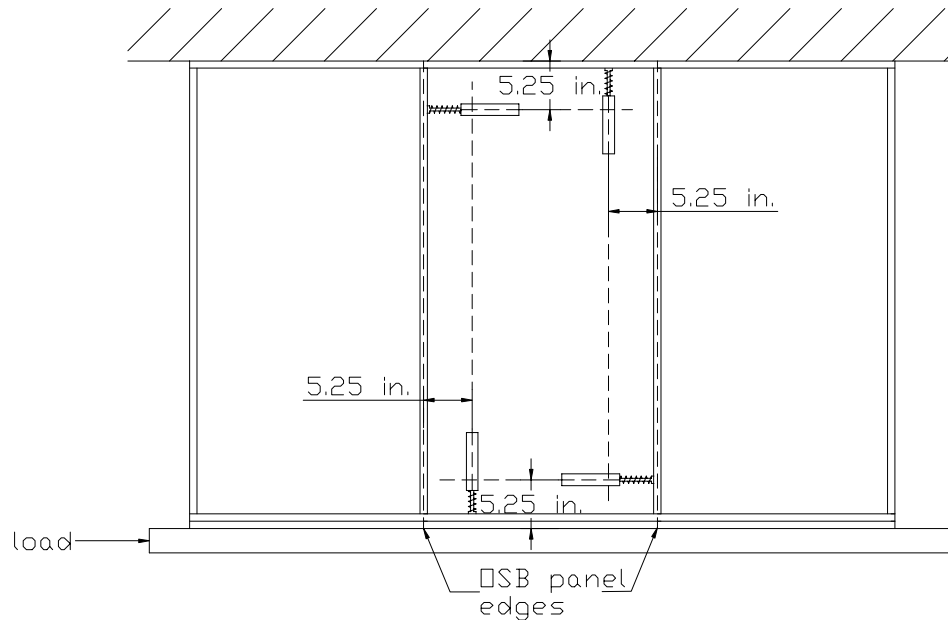


Figure 3.10: Interior instrumentation of corner walls

### 3.2.5 Precision of Instruments

The resolution of the LVDT built into the hydraulic actuator was 0.0024 inch using a 16 bit analog/digital converter card. All other LVDTs had a higher resolution. The resolution of the load cell using the same recording equipment was 50 lbs. The resolution of the tension bolts was  $\pm 12$  lbs. The reader should be aware that the results given are to be considered with the resolution of the respective instrument used to obtain them.

## 3.3 Testing Procedures

Monotonic and Sequential Phased Displacement (SPD) loading were applied to the straight walls. The corner walls were tested using SPD loading only.

### 3.3.1 Monotonic Loading

Monotonic (one-directional) loading displaced the walls at a constant rate of 0.6 inch per minute. This rate was approximately the same rate that the initial peaks

increased in magnitude during SPD loading procedure (Figure 3.11). The actual displacement rates used in the SPD protocol are significantly higher than the displacement rate used for the monotonic tests. The monotonic test specimens were not subjected to load increments as specified in the ASTM E72 procedure. Rather, the monotonic test was a continuous increase in displacement until failure occurred. As opposed to ASTM E 72, the walls were tested without a “stop” at the end of the wall. A LVDT monitored the potential slippage between wall and test frame during these tests. The stop in the ASTM procedure is applied to prevent slippage of the wall on the test frame. During monotonic tests, the data acquisition system recorded the data 10 times per second.

### **3.3.2 Sequential Phased Displacement Loading**

Cyclic loading protocol used in this study was a modification of the “Sequential Phased Displacement Procedure” developed by the Technical Coordinating Committee on Masonry Research (TCCMAR), a joint earthquake research project between USA and Japan. The procedure was first described by Porter (1987) and later revised by Dolan (1993), Dolan and Johnson (1996b), and the Structural Engineers Association of Southern California (SEAOSC) in 1996.

In general, the SPD protocol is displacement controlled and involves triangular reversed cyclic loading at incrementally increasing displacement levels. The incremental increase is controlled by the experimentally determined displacement at the first major event (FME) of the structure. The FME is defined as the displacement at which the structure starts to deform inelastically (anticipated yield displacement). For the walls tested in this study an FME of 0.1 inch (2.54mm) was determined. The cyclic frequency was held constant at 0.5 Hz. Note that with a fixed frequency and changing displacement amplitudes the displacement rate is not constant. Figure 3.11 depicts the displacement pattern of SPD loading employed along with the monotonic time-deflection plot for comparison.

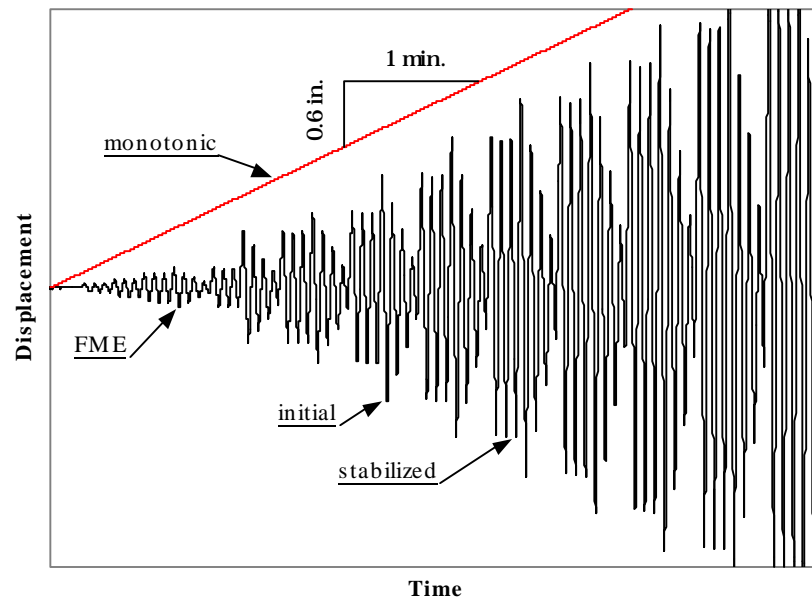


Figure 3.11: Displacement pattern of monotonic and SPD loading

In order to monitor the elastic performance of the structure, the SPD procedure embodies three phases, consisting of ordinary reversed cyclic displacement cycles at displacement levels smaller than FME displacement (Table 3.4). An initial displacement level of 25 percent of FME displacement, followed by 50 percent and 75 percent of FME for phase two and three, respectively, was used as described by Porter (1987). The displacement level of the fourth phase is increased to 100 percent of FME for the initial cycle which is followed by three degradation and three stabilization cycles. The degradation cycles are used to determine if there is a lower bound on displacement necessary for energy dissipation. The amplitude of each consecutive decay cycle decreases by a quarter of the initial displacement (Table 3.4). The displacement then increases to the initial displacement level and is kept constant over sufficient cycles to obtain the stabilized response of the system. Stabilized response is defined as a decrease in load between two successive cycles of not more than 5 percent. The stabilized

response is an important characteristic to assess structural performance after high wind events and during repetitive cyclic earthquake loading. Furthermore, the utilization of three cycles at the same displacement level allows the researcher to monitor the stiffness degradation of the system. For nailed wood joints and nailed shear walls, it has been determined that three stabilization cycles are sufficient to obtain a stabilized response. All following phases consist of initial, decay, and stabilization cycles. In this investigation the displacement amplitude increase between each successive phase was twice the FME displacement (i.e. 0.2 inch in this study). Porter (1987) proposed this rate for ductile or flexible systems. However, Table 3.4 reveals that between Phase 5 and 6 the displacement differs only by the amount of a FME displacement. Unfortunately this error was discovered after testing several walls and in order to be consistent with preceding tests the protocol was not altered. The displacement of each phase was increased until failure or a total of 6 inches displacement was obtained. The data was recorded between 15 and 35 times per second.

Table 3.4: SPD protocol of the first eight phases

Time (sec.)	Cycle No.	Displ. (in)	Phase No.
2	1	0.025	1
4	2	0.025	
6	3	0.025	
8	4	0.05	2
10	5	0.05	
12	6	0.05	
14	7	0.075	3
16	8	0.075	
18	9	0.075	4
20	10	<b>0.1 (FME)</b>	
22	11	0.075	
24	12	0.05	
26	13	0.025	
28	14	0.1	
30	15	0.1	
32	16	0.1	5
34	17	0.3	
36	18	0.225	
38	19	0.15	
40	20	0.075	
42	21	0.3	
44	22	0.3	
46	23	0.3	
48	24	0.4	6
50	25	0.3	
52	26	0.2	
54	27	0.1	
56	28	0.4	
58	29	0.4	
60	30	0.4	7
62	31	0.6	
64	32	0.45	
66	33	0.3	
68	34	0.15	
70	35	0.6	
72	36	0.6	
74	37	0.6	8
76	38	0.8	
78	39	0.6	
80	40	0.4	
82	41	0.2	
84	42	0.8	
86	43	0.8	
88	44	0.8	

### 3.4 Summary

Displacement controlled monotonic and SPD testing procedures were employed to assess the structural behavior of walls with maximum overturning restraint and without restraint. The testing scheme embodied two distinct corner wall structures and three different straight wall configurations. All sixteen walls were constructed inline with specifications used by Johnson (1997) and provided by NAHB in order to draw comparisons between the results of this testing and the results obtained by Johnson (1997). For safety reasons, each configuration was tested horizontally supported by casters to minimize friction. Various exterior and interior instrumentation of the specimens allowed close monitoring of the individual wall component and overall wall

response. The next three chapters introduce and discuss the results obtained from the experimental study that has been described herein.

## Chapter 4

### Property Definitions

#### 4.1 General

Key properties that describe the performance of a light-frame system acting as a shear wall are strength, stiffness, deformation characteristics and energy dissipation (i.e. damping) of the system. Numerous definitions of properties such as ductility, yield point and damping have been introduced in the past. In light of the fact that the obtained property indicators alter significantly with the chosen definition, a standardized test and evaluation procedure for timber structures has yet to be agreed upon. This chapter defines and elaborates on the methods that were used in this study to obtain key properties that are used to interpret the collected data and rate the performance of each wall.

#### 4.2 Perforated Shear Wall Method

Although the perforated shear wall method was derived for walls with one overturning restraint at each end, the empirically derived adjustment factors are applied to all wall configurations in this study. The perforated shear wall method relates the strength of shear walls with openings to fully sheathed shear walls by expressing the shear load ratio as a function of the sheathing area ratio. The method is based on empirical equations derived by Sugiyama and Matsumoto (1994). It was adopted by the *Standard Building Code* (SBC) in 1994 and provides an alternative to the traditional engineered method for designing shear walls with openings.

##### 4.2.1 Sheathing Area Ratio

Sheathing area ratio classifies walls based on the area of openings and total length of structural full-height sheathing panels present. Sheathing area ratio parameters are portrayed in Figure 4.1, and the ratio can be calculated by the following expressions:

$$r = \frac{1}{\left(1 + \frac{\alpha}{\beta}\right)} = \frac{1}{\left(1 + \frac{\sum A_i}{H \sum L_i}\right)} \quad (4.1)$$

$$\alpha = \frac{\sum A_i}{H \cdot L} \quad (4.2)$$

$$\beta = \frac{\sum L_i}{L} \quad (4.3)$$

where:

- $r$  = sheathing area ratio,
- $\alpha$  = opening area ratio,
- $\beta$  = wall length ratio,
- $\Sigma A_i$  = area of all openings,
- $\Sigma L_i$  = sum of the length of full-height sheathing,
- $L$  = shear wall length, and
- $H$  = wall height.

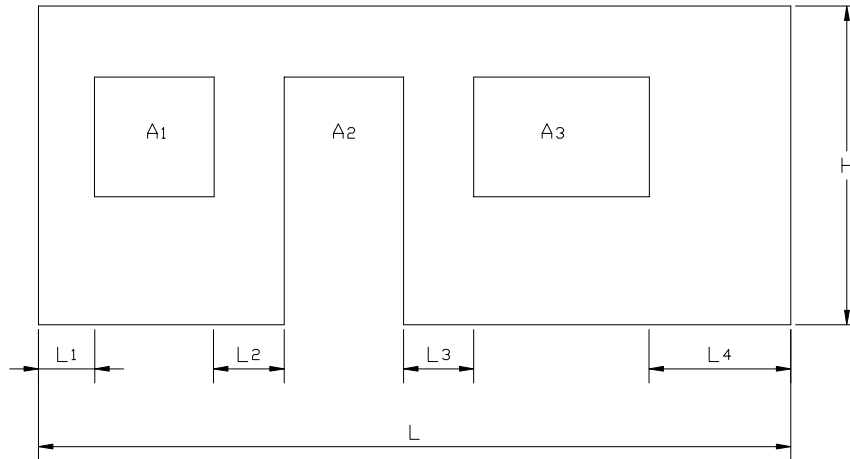


Figure 4.1: Sheathing area ratio variables

According to Equation (4.1) the sheathing area ratio of a fully-sheathed wall equals unity. Equation (4.1) approaches zero as the total area of openings increases.

#### 4.2.2 Shear Load Ratio

The shear load ratio is an empirically derived equation that incorporates sheathing area ratio to account for the fact that shear capacity for a wall with a given length decreases as the size of openings increases. The shear load ratio is determined as:

$$F = \frac{r}{3 - 2r} \quad (4.4)$$

where  $F$  stands for the shear load ratio and  $r$  is the sheathing area ratio. It is important to point out that the shear load ratio does not account for the location of openings.

#### 4.3 Sugiyama's Empirical Equations

Sugiyama and Matsumoto (1994) originally introduced Equation (4.4) to predict the shear load ratio for walls deflected at a shear deformation angle of 1/100 radian. For an 8 feet tall wall this corresponds to a 0.96 inch (24mm) interstory drift. Equation (4.4) has also been proposed to determine the shear load ratio at capacity and was therefore incorporated in the Perforated Shear Wall Method. Additionally, the two researchers derived an equation to determine the shear load ratio at a shear deformation angle of 1/300 radian (0.32 inch (8mm) interstory drift for 8 foot tall wall):

$$F = \frac{3r}{8 - 5r} \quad (4.5)$$

and for a shear deformation angle of 1/60 radian (1.6 inch (40mm) interstory drift for 8 foot tall wall):

$$F = \frac{r}{2 - r} \quad (4.6)$$

The above equations were developed based on test data of 1/3-scale walls with openings.

## 4.4 Capacity and Failure

All of the key properties can be determined from the load-interstory drift curves. For walls tested cyclically, the load-interstory drift plot is a series of hysteresis loops. In order to compare walls tested monotonically and reversed cyclically, the load envelope or backbone curve was introduced. A load envelope curve is the locus of extremities of the hysteresis loops and resembles the shape of a load-interstory drift curve obtained from static monotonic tests. Due to the loading pattern applied, two types of load envelope curves were obtained in this study (Figure 4.2). The initial envelope curve contains the peak load from the first cycle of each phase of SPD loading whereas the stabilized envelope curve represents the peak loads from the last cycle of each phase of SPD loading (refer to Chapter 3).

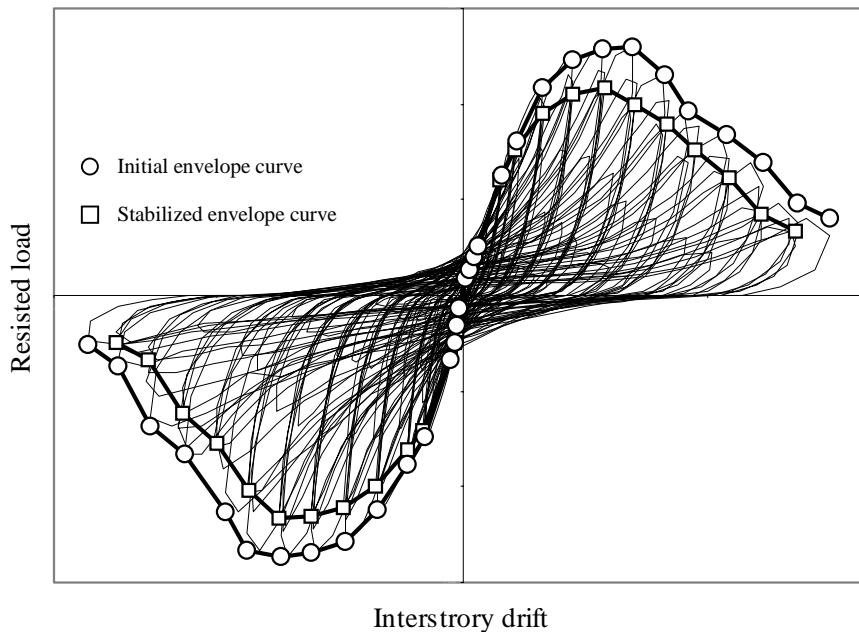


Figure 4.2: Typical hysteresis loops of a shear wall under SPD loading

### 4.4.1 Wall Capacity

Ultimate or initial capacity,  $F_{\text{peak,initial}}$ , is the highest average of the absolute positive and negative peak load occurring in the first cycles of each phase of SPD

loading. Likewise, the average value of the corresponding interstory drifts determined the displacement at initial capacity, denoted as  $\Delta_{\text{peak,initial}}$ . Stabilized capacity,  $F_{\text{peak,stabilized}}$ , is the highest average load resistance occurring in the last cycles of each phase of SPD loading, and  $\Delta_{\text{peak,stabilized}}$  stands for the corresponding average interstory drift at this capacity. Monotonic capacity is simply the highest load,  $F_{\text{peak}}$ , resisted by the wall, with the corresponding interstory drift  $\Delta_{\text{peak}}$ .

#### 4.4.2 Failure

Walls are considered to have failed after a significant drop in resistance or when the resistance reaches  $0.8 F_{\text{peak}}$  (or  $0.8 F_{\text{peak,initial}}$  depending on the test procedure), whichever first occurs. Often restrained shear walls do not exhibit a catastrophic failure. Instead, the resisted load declines in form of a parabola. If no sudden decrease in resistance is present, this definition sets a standard of what is to be considered as failure and limits variation between studies.

#### 4.5 Equivalent Energy Elastic-Plastic Parameters

As opposed to the idealized steel material response that undergoes an almost perfectly elastic-plastic behavior when loaded, light-frame systems do not exhibit typical yield behavior, and the proportional limit can not definitely be set. Various definitions of the yield point have been proposed in the past (Foliente 1996). In this study the yield point is obtained through the use of an equivalent energy elastic-plastic (EEEP) system as described by Porter (1987). The essence is to determine a perfectly elastic-plastic curve circumscribing an area equal to the area enclosed by the obtained load-interstory or load envelope curve between zero drift, failure, and the drift axis (Figure 4.3). This area is a measure of toughness of the system. Toughness is the energy required to fail a system. However, in case of cyclic loading the energy obtained from the area under the load envelope curve is less than the total dissipated energy by the structure until failure since the hysteresis loops in Figure 4.2 overlap. Nevertheless, the same definitions apply to the cyclic properties in order to obtain parameters for making comparisons.

Note that all parameters were computed from positive and negative performance indicators (at positive and negative drifts) and the absolute numbers of the results were averaged. One obtains slightly different values if the response is averaged first and then the parameters are calculated.

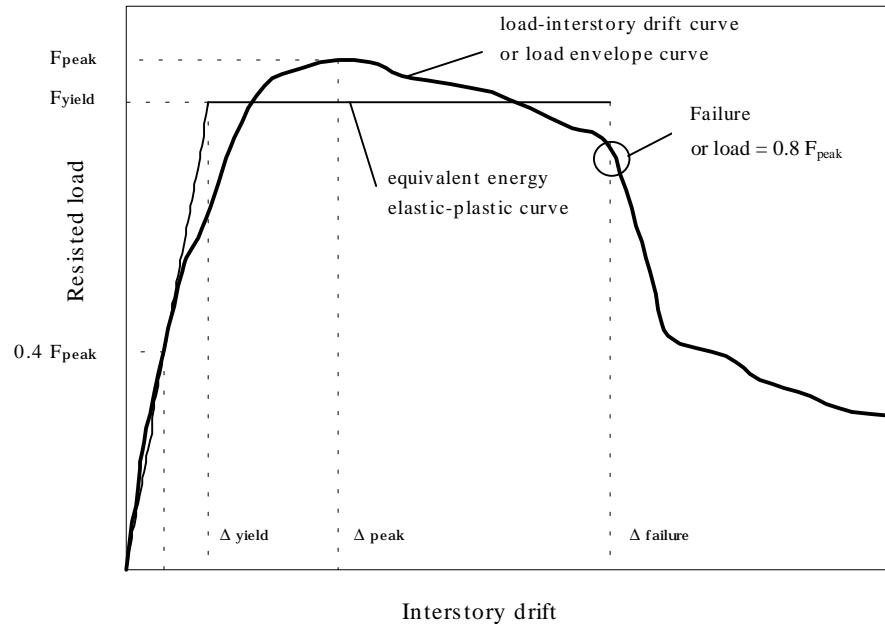


Figure 4.3: Equivalent elastic plastic curve and load-interstory drift (envelope) curve

#### 4.5.1 Elastic Stiffness

Elastic stiffness,  $k_e$ , is approximated by the slope of the secant passing through the origin and a point on the load envelope (or load-interstory drift curve) where the load equals 40 percent of  $F_{peak}$ . This definition has been used in European standards and is employed by the proposed ASTM E 06.11 connection test. For SPD loading, this point is in close vicinity to the load resisted at the first major event (FME). For both loading types  $0.4 F_{peak}$  is within the elastic range. Since two envelope curves describe the reversed cyclic behavior, the average initial and stabilized elastic stiffness from the positive and negative envelope curves were determined for each wall.

### 4.5.2 Yield Strength and Yield Displacement

The elastic portion of the EEEP curve contains the origin and has a slope equal to the elastic stiffness,  $k_e$ . The plastic portion is a horizontal line equal to  $F_{yield}$  (Figure 4.3). Porter (1987) suggested to obtain  $F_{yield}$  by moving the horizontal line until the areas circumscribed by the EEEP curve and the load-interstory drift (or load envelope curve) with the EEEP curve being the lower margin are equal to the areas with the EEEP line being the upper margin. However, with the definitions elaborated above,  $F_{yield}$  can clearly be determined by equation:

$$F_{yield} = \frac{-\Delta_{failure} \pm \sqrt{\Delta_{failure}^2 - \frac{2A}{k_e}}}{-\frac{1}{k_e}} \quad (4.7)$$

where,  $A$  is the area under the respective true load-interstory drift or load envelope curve. In case of a load envelope curve,  $F_{yield}$  represents the average value of  $F_{yield, positive}$  and absolute  $F_{yield, negative}$ . Per definition,  $F_{yield}$  must be greater or equal to  $0.8 F_{peak}$ . Displacement at yield,  $\Delta_{yield}$ , was defined as the displacement at the intersection of the elastic and plastic lines of the EEEP curve.

### 4.5.3 Ductility

A standard measure of a material's ductility is the specimen's elongation or reduction of area in a tension test. This deformation is related to the initial length or initial cross-sectional area and is expressed in percent. In case of shear walls, ductility is defined somewhat different since it is not an elongation or a reduction of area that is of interest but a distortion. For light-frame shear walls, ductility has been defined by relating the deformation at failure to the deformation at yield. As wood systems do not exhibit perfectly elastic-plastic behavior, deformations to determine ductility are obtained from the EEEP curve. The ratio of  $\Delta_{failure}$  and  $\Delta_{yield}$  defines the ductility  $D$ :

$$D = \frac{\Delta_{failure}}{\Delta_{yield}} \quad (4.8)$$

Note the ductility ratio as defined here does not necessarily quantify the ability of a structure to undergo large distortions without failure. The reason for that is that it weighs two variable deflections against each other. Deformation at yield primarily depends on elastic stiffness and capacity. Deformation at failure actually directly shows the ability of the system to deform and resist load. However, deformation at failure depends on the individual specimen and is therefore not a material property. Considering a structure with relatively low elastic stiffness, high capacity and large deflection at failure, the ductility value will remain low since  $\Delta_{\text{yield}}$  will be relatively large. Therefore, ductility should always be considered together with other performance indicators.

## 4.6 Earthquake Performance Indicators

### 4.6.1 Damping

When energy is removed from a vibrating system and transferred into heat or radiated away, it is called damping. For linearly or viscously damped elastic systems, that can be modeled as a dashpot in parallel with a spring, damping is quantified through the damping loss coefficient that compares the amount of damping energy per radian  $W_d/2\pi$  with the linear peak potential energy  $U_l$ :

$$\eta = \frac{W_d}{2\pi U_l} \quad (4.9)$$

Damping energy dissipated per cycle, also referred to as the hysteretic energy, is simply the area enclosed by a hysteresis loop. Linear peak potential energy is derived from viscously damped systems (dashed hysteresis loop in Figure 4.4) and is represented by the area of the triangle ABC and ADE for negative and positive displacements, respectively. In other words, the damping loss coefficient compares the energy dissipated with the total energy that can be released by the system in any form. In order to obtain the average damping loss coefficient per cycle, the dissipated damping energy is divided by the sum of the two potential energies, or the absolute areas enclosed by triangles ABC and ADE, respectively. The damping loss coefficient has frequently been used to

quantify damping of reversed cyclically loaded wood systems, and is referred to as *equivalent viscous damping ratio* (EVDR) in the literature. Considering wood structures, it is important to point out that the concept of EVDR is a good approach to approximate real damping values within the elastic range only (Chopra 1995). However, for the purpose of comparison between other tests, this study quantifies EVDR values obtained from data where the specimens were loaded beyond the elastic limit. EVDR values from this data are not adequate in evaluating the system response for inelastic dynamic analysis (Foliente 1997). Furthermore, the linear peak potential energy used to compute the EVDR is not the true potential energy since timber structures do not exhibit entirely viscous behavior but a rather complex mix of elastic-plastic and viscous-elastic performance. The true peak potential energy could better be approximated by the area enclosed by the centerline of the hysteresis loop (dashed line passing through CAE in Figure 4.4), the drift axis, and the lines BC and DE. However, the centerline is difficult to accurately compute from test data. For simplicity, the easier to determine linear peak potential energy has been used in the past to determine the (more conservative) damping ratio.

The amount of energy dissipated will change with changing excitation amplitude. Therefore an EVDR was determined for each phase. Since the EVDR is determined by a complete cycle, the corresponding interstory drift was specified to be the maximum positive interstory drift of the respective cycle (Point C).

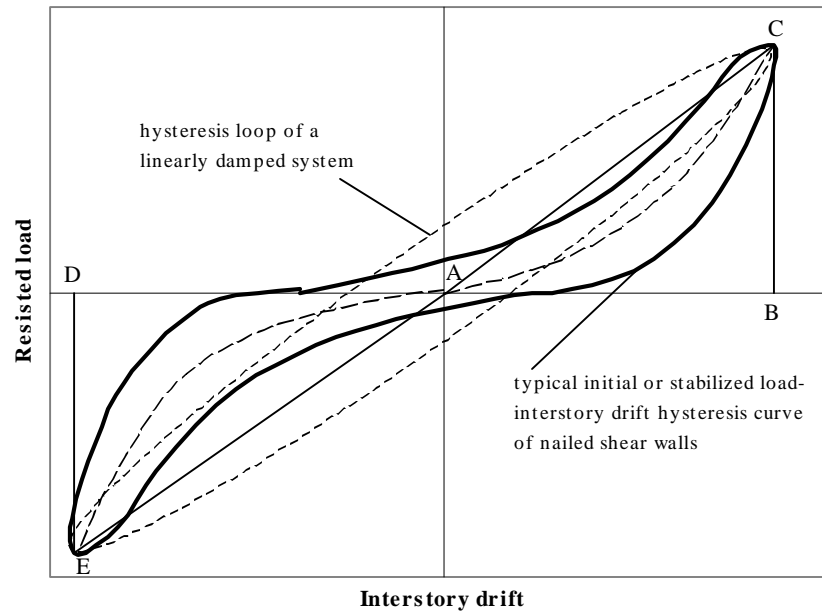


Figure 4.4: Typical initial or stabilized hysteresis loop plotted to determine cyclic stiffness and potential energy

#### 4.6.2 Cyclic Stiffness

Cyclic stiffness,  $k_c$ , is used to monitor the stiffness degradation of the structure during cyclic testing. Wood structures, when tested cyclically, typically exhibit pinched hysteresis loops with continuously changing stiffness as shown in Figure 4.4. Cyclic stiffness is defined as the average slope of the hypotenuse of the two triangles ABC and ADE in Figure 4.4. This is a computed value, and when considering that the slope is influenced by the length of the pinched part of the hysteresis loop, it can be taken as a measure to make inferences about stiffness degradation in wood structures.

#### 4.7 Concluding Remarks

The presented methods to obtain performance indicators were chosen to allow comparisons between the results obtained in this study and the study conducted by Johnson (1997). Outcomes of previous tests that used other methods should be re-analyzed when compared with results from this investigation. It is important that a

uniform format of property definitions and a constant notation and nomenclature be established in the near future to facilitate comparisons between test results.

## Chapter 5

### Monotonic Test Results of Straight Walls and Discussion

#### 5.1 General

The monotonic test program was comprised of six straight walls, 40 feet (12m) in length and 8 feet (2.4m) in height. Results obtained by Johnson (1997) were incorporated, and the effects of three anchorage conditions on a total of three different wall configurations were analyzed. Due to expense, each configuration was tested only once. The present chapter provides the results of the monotonic tests in the form of load-displacement curves, and lists performance indicators such as capacity, yield strength, elastic stiffness, and ductility. Furthermore, uplift forces and stud and sheathing displacements are included and discussed.

#### 5.2 Load-Drift Relationship

Load-deflection curves for a total of nine walls are depicted in Figures 5.1, 5.2, and 5.3. For the purpose of comparison, each graph is plotted using the same scale. Table 5.1 contains load resistance at capacity and elastic-plastic curve parameters. Wall A was tested with only two anchorage configurations, due to it being fully sheathed. In other words, Wall A was tested twice with tie-down anchors at the ends. Therefore, differences in capacities between the two tests cannot be explained by differences in the amount of tie-down anchors. Recall that Johnson (1997) tested plywood sheathed walls. Although OSB equivalency to plywood sheathed walls is given in all three building codes and has been shown by Foschi (1980) and Dolan (1987), differences could be a result of the two different sheathing materials and/or statistical variation between the two specimens.

The curves reveal that the amount of tie-down anchors influences the load-drift characteristic, dissipated energy, ultimate capacity, and failure mode. The magnitude of influence depends on the amount of openings in the wall. The fully sheathed Wall A

without overturning restraint reached 73 percent of the ultimate monotonic capacity of the OSB sheathed wall with maximum amount of overturning restraints (Table 5.2). In addition, the area under the load versus drift curve for Wall A without restraint is rather narrow compared to the curves shown for walls with restraint. Consequently, in case of Wall A without tie-down anchors, a substantial amount of induced energy was transformed into rigid body rotation, rather than racking resulting in lower ductility. The same trend, however, was not apparent for Walls D and E. For these configurations the elastic stiffness was significantly lower and therefore racking was the primary resistance component (Table 5.1). However, ultimate capacity decreased up to 59 percent (Wall E) if tie-down devices were omitted when compared to walls with maximum overturning restraint (Table 5.2).

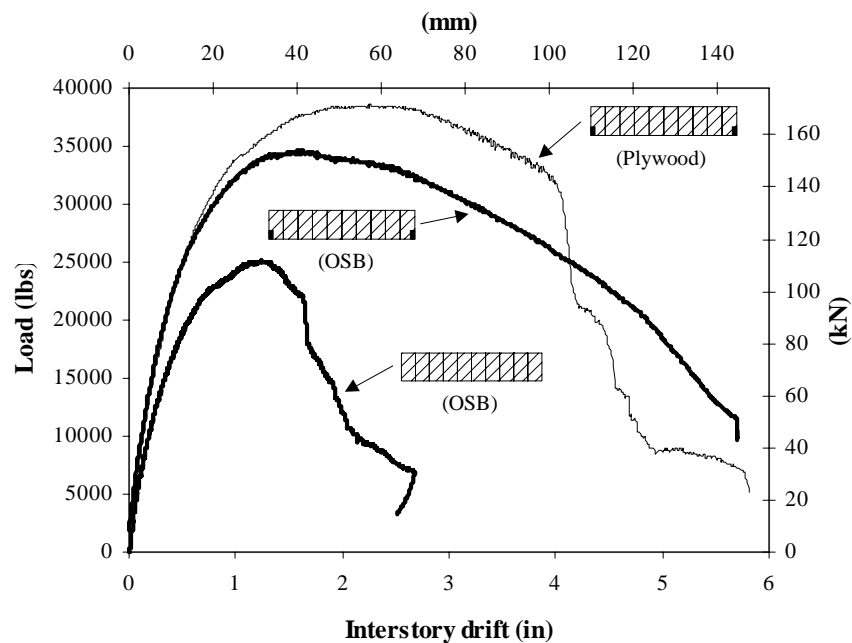


Figure 5.1: Load vs. interstory drift curves of wall configuration A

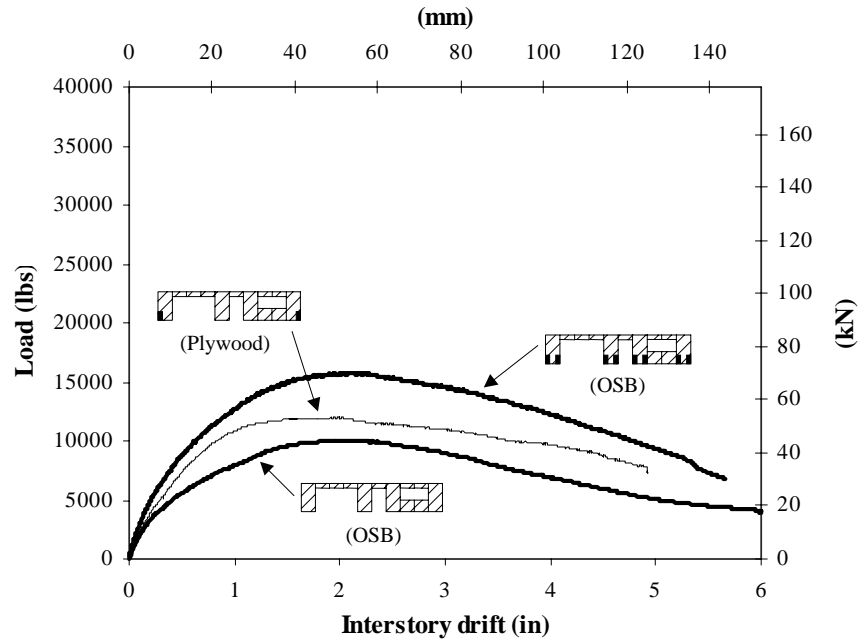


Figure 5.2: Load vs. interstory drift curves of wall configuration D

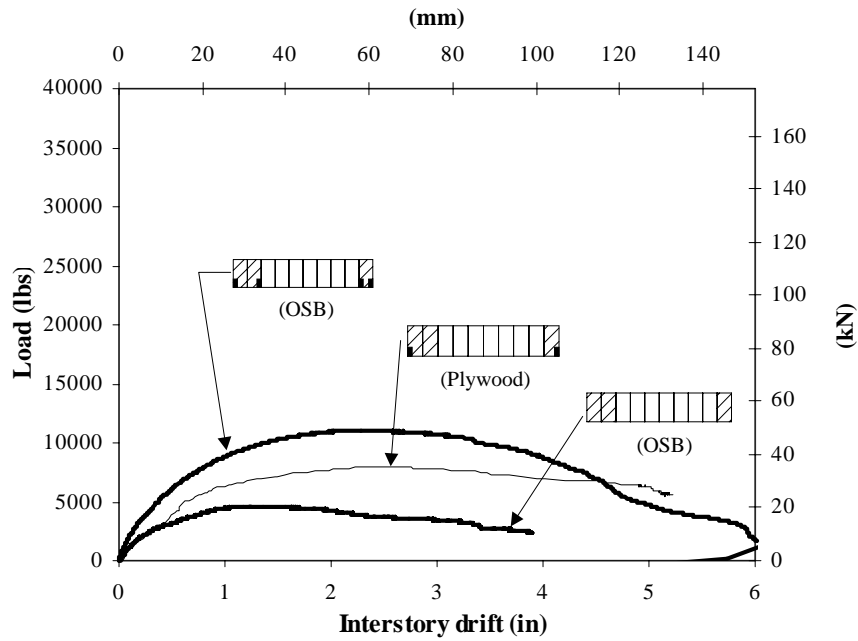


Figure 5.3: Load vs. interstory drift curves of wall configuration E

Table 5.1: Load-displacement data

	Wall Specimens								
	no tie-down anchors (OSB)			anchors at end of wall only <sup>(1)</sup> (Plywood)			maximum amount of tie-down anchors (OSB)		
	A	D	E	A <sup>(2)</sup>	D	E	A <sup>(2)</sup>	D	E
Peak Load (kips)	25.1	9.8	4.4	38.6	12.0	8.0	34.6	15.5	10.8
F <sub>yield</sub> (kips)	22.5	8.7	4.0	35.4	10.9	7.3	31.5	14.7	9.9
Elastic Stiffness (kips/in)	54.0	13.5	8.7	64.3	17.7	7.8	73.3	20.6	13.7
Δ <sub>yield</sub> (in)	0.4	0.6	0.5	0.6	0.6	0.9	0.4	0.7	0.7
Δ <sub>failure</sub> (in)	1.6	3.3	2.3	4.0	4.0	4.9	3.7	3.8	3.2
Ductility	3.9	5.1	5.0	7.3	6.6	5.3	8.6	5.3	4.5
Drift @ 0.8 F <sub>peak</sub>	1.7	3.3	2.3	4.0	4.0	4.9	3.7	3.8	3.8

<sup>(1)</sup> From Johnson (1997)

<sup>(2)</sup> Wall A has the same anchorage requirements for the anchors at the end of wall only and maximum amount of tie-down anchors due to being fully sheathed

Note: The numbers presented are rounded. All calculations were done using original values.

Table 5.2: Relative capacities based on engineered construction.

	Wall Specimens								
	no tie-down anchors <sup>(1)</sup>			anchors at end of wall only <sup>(2)</sup>			maximum amount of tie-down anchors <sup>(1)</sup>		
	A	D	E	A <sup>(3)</sup>	D	E	A <sup>(3)</sup>	D	E
Relative Capacity (%)	73	63	41	112	77	74	100	100	100

<sup>(1)</sup> These specimens had OSB sheathing

<sup>(2)</sup> These specimens had plywood sheathing (Dolan and Johnson 1996 a and b)

<sup>(3)</sup> Wall A has the same anchorage requirements for the anchors at the end of wall only and maximum amount of tie-down anchors due to being fully sheathed.

Ultimate capacity of Wall D and E with tie-downs at the ends only was 23 percent and 26 percent, respectively, lower than the capacity of the same walls with maximum amount of tie-down anchors (Table 5.2). The elastic stiffness of Wall E was almost doubled by increasing the amount of tie-down anchors from two to four. Wall D showed

a 16 percent increase in elastic stiffness as tie-down anchors were increased from two to eight. Thus, the perforated shear wall method, compared to traditional engineered design, decreases ultimate capacity and stiffness of the walls. This is due to the intermediate, fully-sheathed segments behaving more independently as the opening size increases resulting in end stud lifting from the bottom plate of each segment. Subsequently, when tie-down restraint is omitted, the sheathing nails have to transfer the entire uplift to the bottom plate resulting in higher nail slip and therefore higher wall displacement.

As expected, compared to unrestrained walls, the ultimate capacity and stiffness increased with increasing overturning restraint. It should be noted that these results are representative of conditions where no gravity load from dead and live loads are present. The ultimate capacity and stiffness may increase with an increase in gravity loads due to the probable reduction in uplift of the end stud. This probable increase would be largest for walls without overturning restraint.

### **5.3 Ductility**

Ductility values alone are not very informative regarding wall performance (Table 5.1). As previously mentioned, ductility is defined by dividing the interstory drift at failure by the interstory drift at the determined yield load. However, drift at yield load is decisively dependent upon stiffness. Ductility values ranged from 3.9 (Wall A, no anchors) to 8.6 (Wall A, anchors, OSB sheathing). The values obtained show no apparent trend.

Considering the load-deflection curves of all walls, the perforated shear Walls E and D appear to carry the highest proportion of maximum capacity over the greatest displacement, whereas Wall A without tie-down devices shows the most brittle behavior. Nevertheless, the values in Table 5.1 do not reflect that trend. Note that for all anchorage conditions the elastic stiffness of Walls D and E is significantly lower than that of the fully-sheathed configuration, Wall A. Although the ultimate capacity decreased with increasing opening size, the substantially lower stiffness led to relatively high yield displacements which in turn reduced the ductility ratio. Furthermore, there is some

variation in defining the point of failure. If no sudden load drop occurs, the load at failure and the corresponding displacement is taken at  $0.8 F_{\text{peak}}$ . However, a sudden load drop is not necessarily clearly identified since the shape of a load-displacement curve can be altered significantly when plotted on different scales. For that reason, the drift at  $0.8 F_{\text{peak}}$  was included in Table 5.1. Considering those drifts for all walls, anchors at the ends of the wall increased the deformation at failure (if consistently taken as  $0.8 F_{\text{peak}}$ ). Yet, this deformation did not increase when the number of tie-downs was increased from two to maximum.

#### **5.4 Perforated Shear Wall Method**

Table 5.3 contains actual and predicted shear strength ratios determined using Equation 4.4 (Chapter 4). Actual shear strength ratios are higher than the predicted ratios in all cases. Table 5.3 illustrates that the amount of conservatism increases as the amount of opening in the wall increases. The same behavior was found by Johnson (1997). Actual shear strength ratios range in conservatism from zero percent for a fully-sheathed wall to 240 percent for Wall E with maximum number of tie-down anchors. Wall A has an actual shear strength ratio of 1.0 because the predicted ratio given by Equation 4.4 is based on the fully-sheathed configuration.

Table 5.3: Capacities and actual and predicted shear strength ratios

	Wall Specimens								
	no tie-down anchors (OSB)			anchors at end of wall only <sup>(1)</sup> (Plywood)			maximum amount of tie-down anchors (OSB)		
	A	D	E	A <sup>(2)</sup>	D	E	A <sup>(2)</sup>	D	E
r=1.00	r=0.48	r=0.30	r=1.00	r=0.48	r=0.30	r=1.00	r=0.48	r=0.30	
Displacement (in) @ Peak Load	1.2	2.0	1.2	2.3	1.9	2.6	1.6	2.0	2.2
Peak Load (kips)	25.1	9.8	4.4	38.6	12.0	8.0	34.6	15.5	10.8
Predicted shear strength ratio, (F)	1.00	0.24	0.13	1.00	0.24	0.13	1.00	0.24	0.13
Actual shear strength ratio, (f)	1.00	0.39	0.17	1.00	0.31	0.21	1.00	0.45	0.31
Actual / Predicted	1.00	1.62	1.34	1.00	1.29	1.60	1.00	1.86	2.40

<sup>(1)</sup> From Johnson (1997)

<sup>(2)</sup> Wall A has the same anchorage requirements for the anchors at the end of wall only and maximum amount of tie-down anchors due to being fully sheathed

Note: The numbers presented are rounded. All calculations were done using original values.

Figure 5.4 shows the actual shear strength ratios from the load-interstory drift curves for the monotonic tests, along with the curve for predicted shear strength ratio given by Equation 4.4. Values from the walls with the maximum amount and without overturning restraint suggest rather linear relationships and indicate that the perforated shear wall method does predict conservative capacities for those walls but seems to be inaccurate. Yet, more tests are needed to confirm this observation. As expected, the amount of conservatism increases as the number of tie-downs is increased from two to maximum.

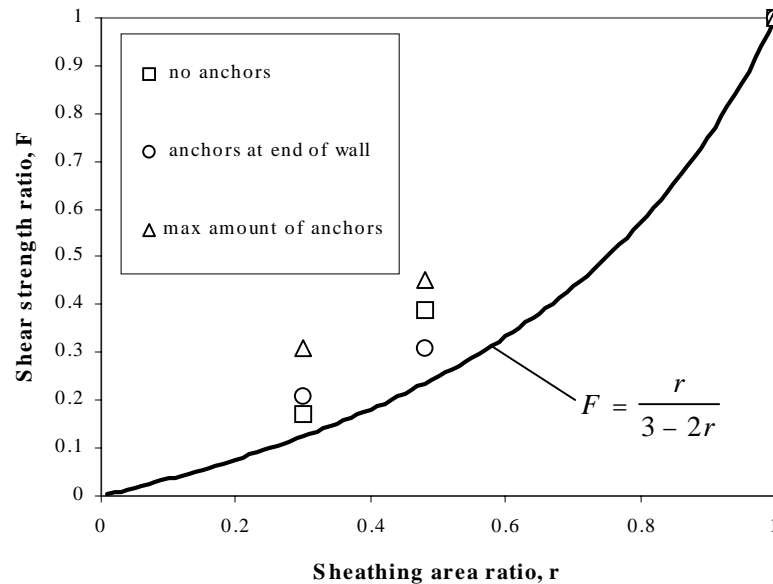


Figure 5.4: Shear strength ratios at capacity (Eq. 4.4)

## 5.5 Sugiyama's Equations

Sugiyama and Matsumoto (1994) derived Equations 4.4, 4.5, and 4.6 to predict the resistance reduction of a wall with openings compared to a fully-sheathed wall at shear deformation angles of 1/300, 1/100 and 1/60 radian. For an 8 feet tall wall this corresponds to the interstory drifts listed in Table 5.4. Johnson (1997) concluded that for walls with overturning restraints at the ends only, Sugiyama's equations predict conservative ratios. For comparison, Johnson's data is listed in Table 5.4 along with the actual and predicted shear strength ratios of the walls tested in this study.

The amount of conservatism of the predicted ratios at these displacements increases when applied to walls with maximum overturning restraint. However, the predictions using Equations 4.4, 4.5, and 4.6 for walls without overturning restraint, are between 8 and 41 percent higher than the actual values and still fairly conservative.

Table 5.4: Actual and predicted shear strength ratios at various interstory drifts

	Wall Specimens								
	no tie-down anchors (OSB)			anchors at end of wall only <sup>(1)</sup> (Plywood)			maximum amount of tie-down anchors (OSB)		
	A r=1.00	D r=0.48	E r=0.30	A <sup>(2)</sup> r=1.00	D r=0.48	E r=0.30	A <sup>(2)</sup> r=1.00	D r=0.48	E r=0.30
Load (kips) @ 0.32 in. int. drift	14.5	4.1	2.4	19.0	5.1	2.5	19.6	6.5	4.4
Actual shear strength ratio, (F)	1.00	0.28	0.17	1.00	0.27	0.13	1.00	0.33	0.22
Predicted shear strength ratio	1.00	0.26	0.14	1.00	0.26	0.14	0.14	0.26	0.14
Actual / Predicted	1.00	1.10	1.20	1.00	1.04	0.95	1.00	1.29	1.62
Load (kips) @ 0.96 in. int. drift	23.9	7.6	4.2	33.4	10.7	6.2	31.9	12.3	8.5
Actual shear strength ratio, (F)	1.00	0.32	0.18	1.00	0.32	0.19	1.00	0.39	0.27
Predicted shear strength ratio	1.00	0.24	0.13	1.00	0.24	0.13	1.00	0.24	0.13
Actual / Predicted	1.00	1.35	1.41	1.00	1.36	1.49	1.00	1.64	2.13
Load (kips) @ 1.6 in. int. drift	22.1	9.5	4.2	37.7	11.9	7.4	34.3	15.0	10.3
Actual shear strength ratio, (F)	1.00	0.43	0.19	1.00	0.32	0.20	1.00	0.44	0.30
Predicted shear strength ratio	1.00	0.32	0.18	1.00	0.32	0.18	1.00	0.32	0.18
Actual / Predicted	1.00	1.36	1.08	1.00	1.00	1.11	1.00	1.38	1.70

<sup>(1)</sup> From Johnson (1997)

<sup>(2)</sup> Wall A has the same anchorage requirements for the anchors at the end of wall only and maximum amount of tie-down anchors due to being fully sheathed

Note: The numbers presented are rounded. All calculations were done with original values.

As mentioned above, Equation 4.4 has been proposed to predict the shear strength ratio at capacity. Though this equation was derived from data obtained at a shear deformation angle of 1/100 radian or 0.96 inch interstory drift, the displacements at capacity listed in Table 5.3 are significantly higher than 0.96 inch. Consequently, Equation 4.6, which predicts the shear strength ratio at 1.6 inches of interstory drift, appears to be more appropriate to predict the shear strength ratio at capacity, which can be seen by comparing Figure 5.5 and Figure 5.4. Figure 5.5 depicts the actual shear strength ratios at capacity and the predicted ratio, which is plotted as a continuous line using Equation 4.6. Notice that the actual shear strength ratios are much closer than the predictions made with Equation 4.4.

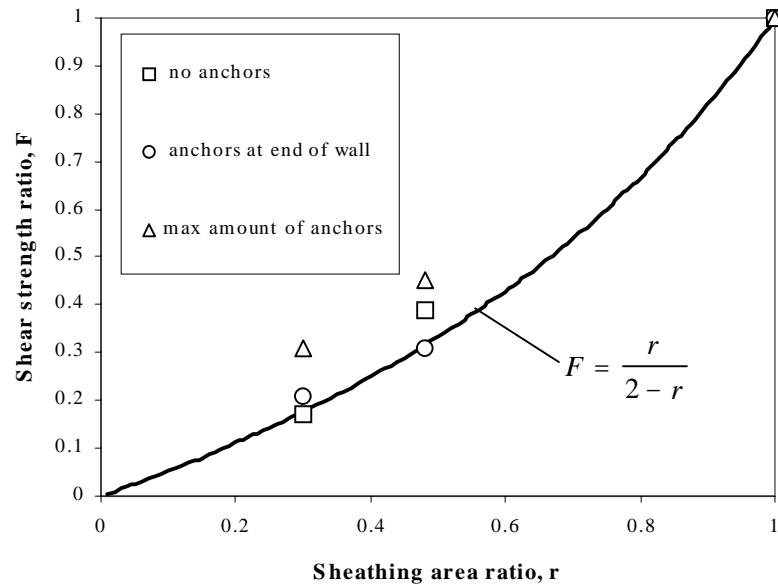


Figure 5.5: Predicted Shear strength ratio at capacity using Equation 4.6

## 5.6 Overall Wall Response

### 5.6.1 Tie-down Tension Bolts

Tension load bolts measured the uplift forces resisted by the tie-down anchors during monotonic loading. Correlation of racking load resisted by the shear wall to load resisted by the bolt was determined and the results are shown in Table 5.5. Unit shear was determined using the equation:

$$v = \frac{F_{peak}}{L} \quad (5.1)$$

where  $v$  is the unit shear,  $F_{peak}$  stands for wall capacity, and  $L$  is the sum of the widths of full-height sheathing panels. Consequently, the theoretical uplift was obtained by multiplying the unit shear  $v$  by the normal distance between applied load and foundation, which equals the wall height in this investigation.

The ratio of actual to theoretical uplift exceeds unity for Wall D with tie-down anchors. The significantly smaller peak loads recorded by the bolts in walls without

overturning restraint elucidate how little uplift force is transferred to the foundation in a concentrated manner if tie-down anchors are omitted. The lower forces experienced by the instrumented bolts were due to the inability of the sheathing nails to transfer the overturning loads. The associated damage to the sheathing nails resulted in significantly reduced capacities. This indicates a possible advantage for using “lighter” but more disperse tie-down devices if lower ultimate capacities are adequate. Tension bolts experienced their maximum load at wall displacements lower than where ultimate capacity was reached in walls with no overturning restraint (Figure 5.6). This is attributed to the fact that the sheathing started to separate from the bottom plate at the end stud and progressed towards the middle of the wall at loads below capacity. Subsequently, less uplift forces could be transferred to the bottom plate in close vicinity of the end stud where the tension bolt was located. The bolt load values in Table 5.5 for walls without overturning restraint are the maximum loads recorded by the tension bolts. With tie-down anchors applied, maximum load in the tension bolts was reached at displacements higher than where wall capacity was reached (Figure 5.7). Again, this was a result of the nailed sheathing-to-frame connection starting to fail in the corners where the fasteners were most heavily loaded. The sheathing transferred less uplift forces to the foundation. Consequently the tie-down devices resisted higher loads as displacements increased past capacity. Tension bolt loads in Table 5.5 for walls with overturning restraint are the loads recorded at wall capacity, not the maximum loads experienced by the bolts.

Table 5.5: Force resisted by tension bolt at or near wall capacity

	Wall Configuration								
	no tie-down anchors <sup>(1)</sup>			anchors at end of wall only <sup>(2)</sup>			maximum amount of tie-down anchors <sup>(1)</sup>		
	A	D	E <sup>(4)</sup>	A <sup>(3)</sup>	D	E	A <sup>(3)</sup>	D	E
F <sub>tension bolt</sub> (lbs.)	755	697	N/A				3865	8014	6592
Wall capacity (kips)	25.1	9.8	4.4				34.6	15.5	10.8
Unit shear (lbs./ft) @ F <sub>peak, wall</sub>	628	613	367				865	969	900
Theoretical uplift (lbs.)	5020	4900	2933				6920	7750	7200
actual / theoretical	0.15	0.14	-				0.56	1.03	0.92

<sup>(1)</sup> These specimens had OSB sheathing.

<sup>(2)</sup> Johnson (1997) did not measure uplift forces for these configurations.

<sup>(3)</sup> Wall A has the same anchorage requirements for the anchors at the end of wall only and maximum amount of tie-down anchors due to being fully sheathed.

<sup>(4)</sup> Data not available due to damaged leads to tension bolt.

Note: The numbers presented are rounded. All calculations were done with original values.

All bolts were pretensioned prior to testing. The load histories in Figures 5.6 and 5.7 are offset from zero due to that pretensioning. The actual tension load is the total load recorded by the bolts less the respective pretension recorded at the beginning of each test. Figure 5.6 includes the recording of the pretensioned tension bolt on the compression ends of Walls A and E. For all other walls the measurement could not be obtained due to a malfunctioned bolt. The total magnitude of compression is simply the maximum load less the minimum load recorded by the bolt assuming that no relaxation of the wood fibers occurred during the test. The compressive force near the stud was 605 lbs in Wall A and 716 lbs in Wall E. The load histories of the two “compression” bolts show a minimum at a displacement lower than and close to the capacity displacement. The steady load increase at increasing drifts is associated with the accumulated damage experienced by the walls beyond capacity.

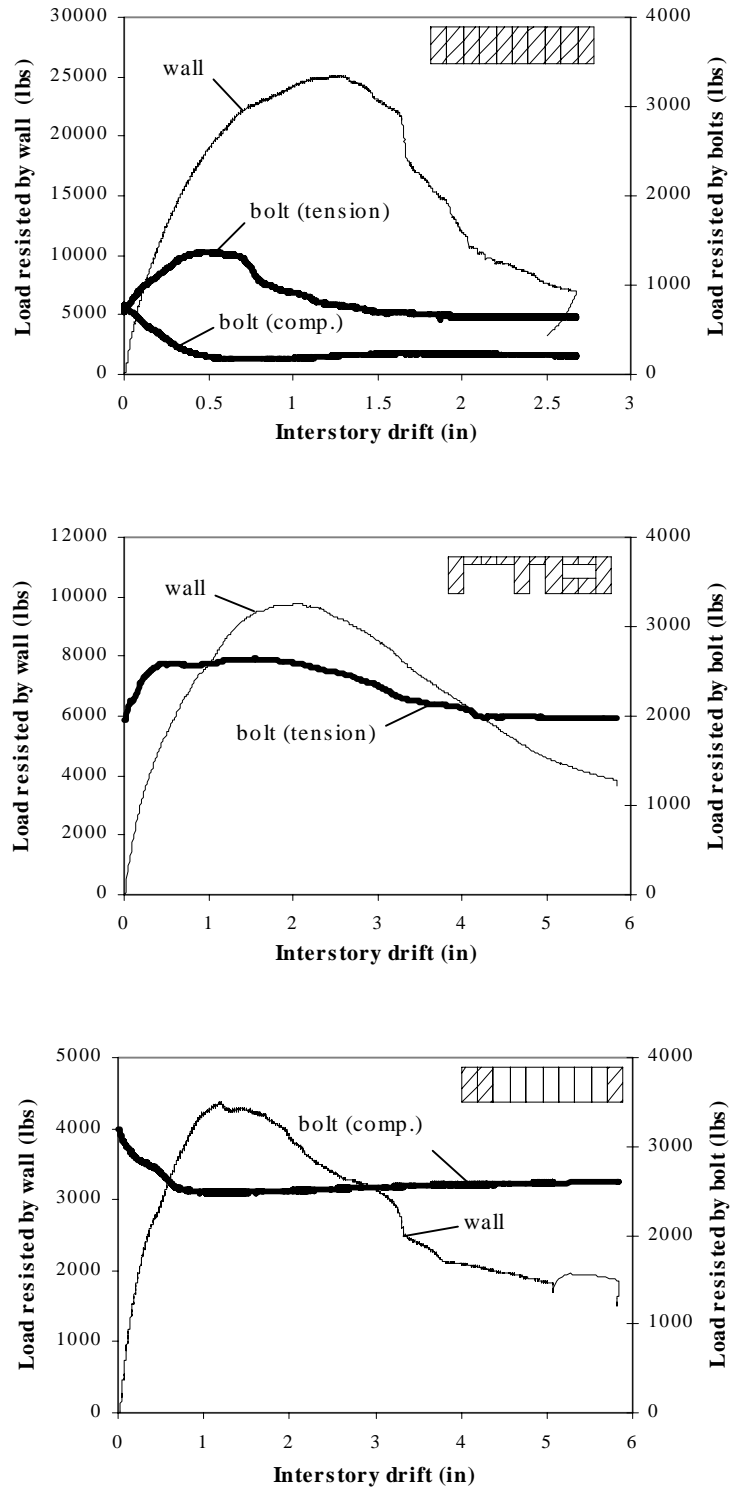


Figure 5.6: Resisted load by tension bolts of Walls A, D, E, respectively, not restrained against uplift, along with the corresponding load envelope curves

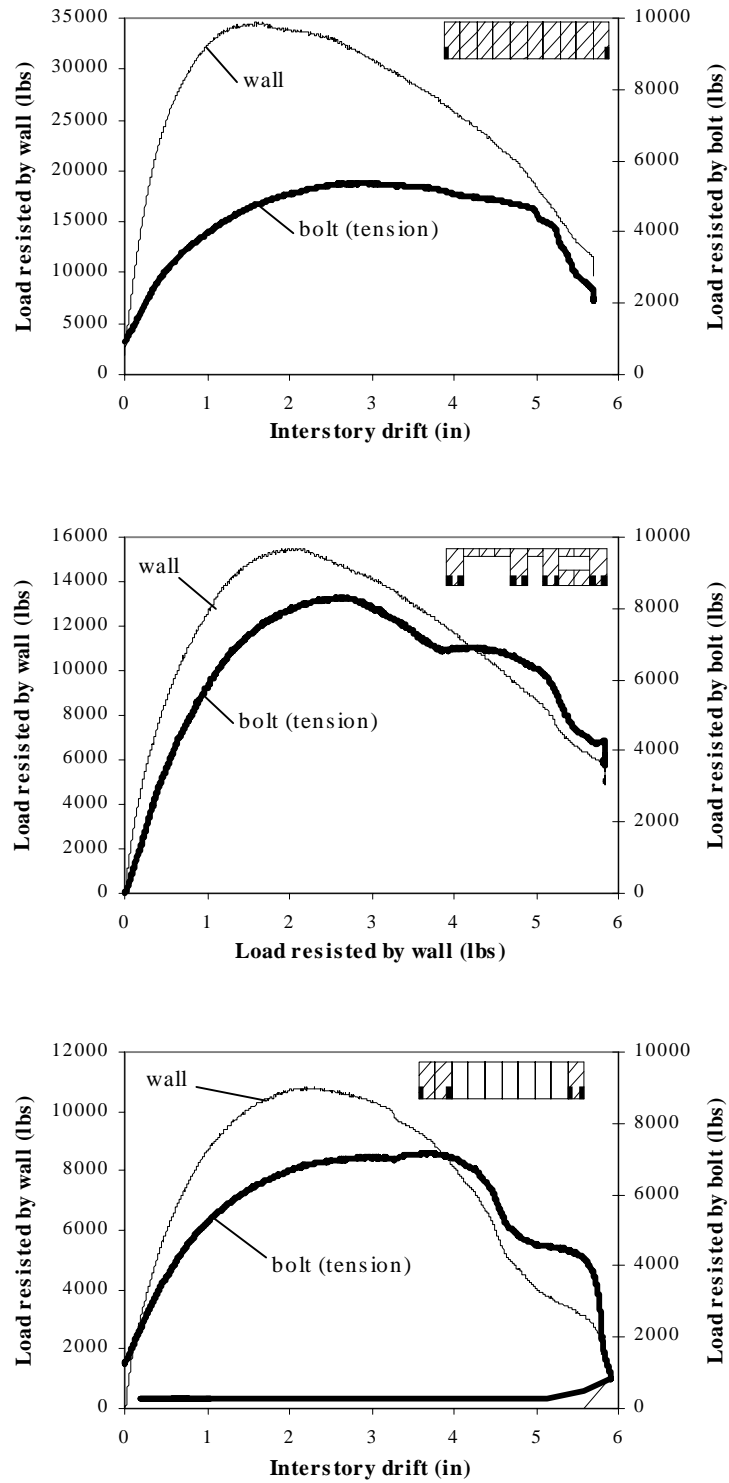


Figure 5.7: Resisted load by tension bolts of Walls A, D, E, respectively, with maximum uplift restraints, along with the corresponding load envelope curves

### 5.6.2 End Stud Uplift Displacement

Vertical displacements of the end studs for each wall configuration at ultimate capacity are listed in Table 5.6. Due to computer error, the data pertaining to the end stud behavior for Wall E (with tie-down at the ends of the wall only) was not recorded correctly and was not available. For all walls, the displacement given in Table 5.6 for the compression end stud was due to crushing of the sill plate and closing of sometimes small gaps between stud and sill plate.

With anchors attached, the end studs were presumed to rotate about the anchor bolt. Considering that the change of the wall diagonal was not measured, a significant part of the uplift measured is due to the shear distortion of the framing (refer to Chapter 3 for geometry of LVDT fixture). At 2 inches (51mm) interstory drift, where most walls tested monotonically reached capacity,  $dx$  as shown in Figure 5.8 is approximately 0.1 inch (2.5mm) depending on how much racking distortion of the framing actually occurred. Taking the amplification effect of the LVDT fixture into account (Figure 3.4), a  $dx$  of 0.1 inch corresponds to an erroneous uplift displacement of 0.03 inch. Therefore, the numbers displayed in Table 5.6, for walls containing anchors are approximate numbers only and the actual values are smaller. Differences of the stud displacements between walls with restraint at the ends of the wall and walls with maximum overturning restraint are not significant. Relatively small displacements of the compression end studs of wall configuration E compared to the configurations A and D indicate that the two fully sheathed segments at the ends of Wall E behave more or less independently. Compression end stud displacements did not differ significantly between anchorage conditions. Tension end stud displacements, however, are substantially higher for walls not restrained against uplift, as expected. Due to its higher stiffness, Wall A of this group showed the greatest separation (0.95in or 24mm) of the tension end stud from the sill plate. It should be noted that the unrestrained stud displacements were not corrected to compensate for amplifications caused by the lever arm of the LVDT fixtures since no movement pattern of the studs could be accurately assumed. Unfortunately, without correction there could be a significant amount of “uplift displacement” measured which

was in reality stud rotation (Figure 5.8). As upper bound for walls without tie-down anchors, an error of 0.1 inch ( $dx$  not corrected for amplification) can be assumed. Again, the numbers in Table 5.6 for walls without restraints, are to be considered as approximate values only.

Table 5.6: Vertical end stud displacement at wall capacity

LVDT Location	Wall Specimens								
	no tie-down anchors (OSB)			anchors at end of wall only <sup>(1)</sup> (Plywood)			maximum amount of tie-down anchors (OSB)		
	A	D	E	A <sup>(2)</sup>	D	E	A <sup>(2)</sup>	D	E
Compression End Stud (in)	0.14	0.14	0.07	0.11	0.15	N/A	0.11	0.15	0.08
Tension End Stud (in)	0.95	0.86	0.82	0.11	0.11	N/A	0.11	0.11	0.13

<sup>(1)</sup> From Johnson (1997)

<sup>(2)</sup> Wall A has the same anchorage requirements for the anchors at the end of wall only and maximum amount of tie-down anchors due to being fully sheathed

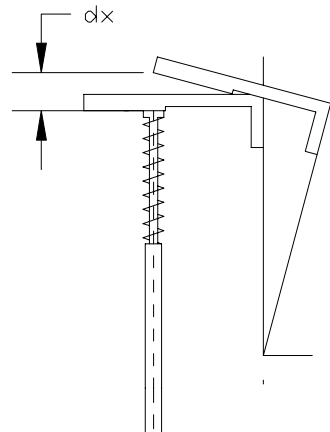


Figure 5.8: False uplift displacement measured if wall is only racking (no anchors)

### 5.6.3 Sheathing Displacement

During monotonic testing, displacements of OSB sheathing panels relative to the framing were only recorded from Wall D with maximum amount of anchors. The reason is that the scope of the study was augmented and these measurements were included after several specimens had already been tested. Johnson (1997) did not record sheathing displacements. Hence, comparisons between different wall configurations for walls loaded monotonically cannot be made. However, the recorded data from Wall D represent preliminary results and give general information about sheathing displacements relative to the framing. For the analysis, it was assumed that each OSB panel was perfectly rigid and did not distort during loading. In addition, the assumption was made that the top plate attached to the load distribution beam did not bend. Any two-dimensional displacement of a rigid panel can then be described by a  $x$ - and  $y$ -displacement of the panel midpoint and a rotation about the normal passing through the midpoint (Refer to Chapter 3, Section 3.2.2 for LVDT arrangements). Note that the two LVDTs recording the rotation of the sheathing against the bottom or top plates measured a higher rotation than actually experienced by the sheathing. As a shear wall is deflected the distance between top and bottom plate decreases. Associated with the position of the two LVDTs, that decrease will bias the measurements. Assuming that the loaded end stud and the top plate did not bend, at wall capacity the recorded angle of rotation relative to top and bottom plate is approximately 10 percent high. However, there was not sufficient information to correct the data accordingly, as the exact decrease of the distance between the two plates was not measured. At interstory drifts greater than 4 inches (102mm) the data becomes unreliable because sometimes the LVDT core was caught in the gap generated between sheathing and framing.

#### 5.6.3.1 Midpoint Movement

Figures 5.9 and 5.10 depict the midpoint movement of Panels 5 and 7, respectively, relative to the framing along with the corresponding interstory drift. Drift during contraction of the hydraulic actuator was specified as positive. However, the

interstory drift values shown in Figures 5.9 and 5.10 are absolute values. The reader is referred to Figure 5.11 that specifies x- and y- direction.

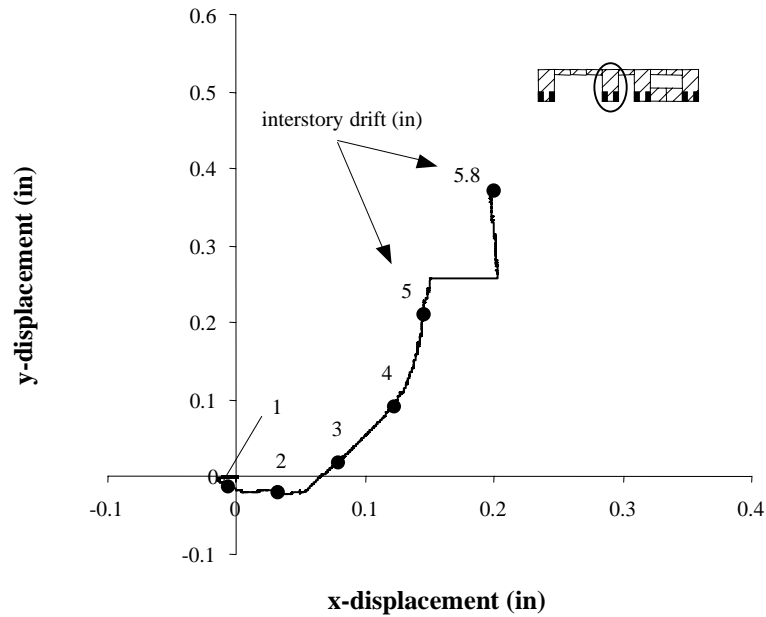


Figure 5.9: Midpoint movement OSB Panel 5, Wall D, maximum amount of anchors

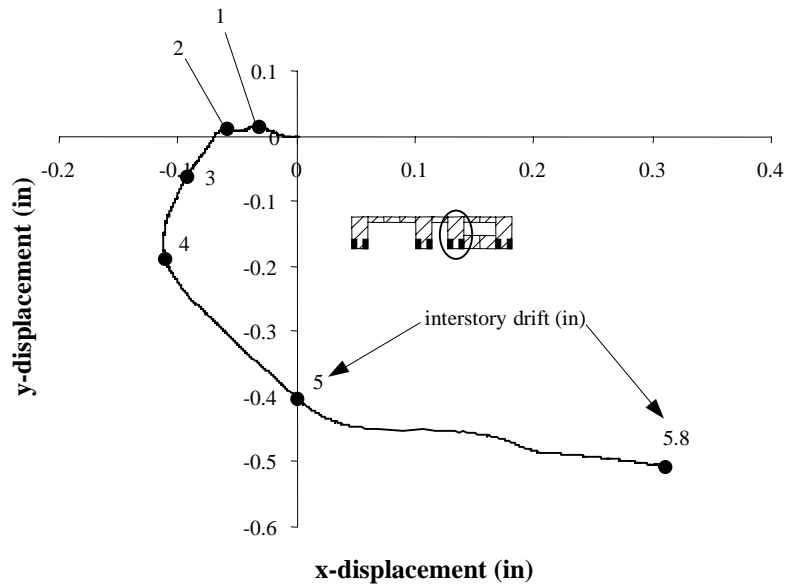


Figure 5.10: Midpoint movement OSB Panel 7, Wall D, maximum amount of anchors

Wall D reached capacity at 2 inches (51mm) interstory drift. It is apparent from Figures 5.9 and 5.10 that midpoint movements of both panels are insignificant at interstory drifts of less than 2 inches. Consequently, up to wall capacity it is safe to assume that the sheathing rotates about its centroid. At higher interstory drifts both panels “accelerate” and the midpoint drift with respect to the framing becomes more pronounced with the midpoint of Panel 5 moving towards the top plate and that of Panel 7 drifting towards the bottom plate. Since the midpoint movements are fairly small they could very well be arbitrary. The sample size of one does not allow further inferences to be made.

#### *5.6.3.2 Sheathing Rotation*

Because the framing distorts into a parallelogram during loading, the rotation relative to the studs and relative to top and bottom plate of panels 5 and 7 was determined. Figure 5.11 depicts how positive and negative rotation is specified. A negative angle in Figures 5.12 and 5.13 indicates a clockwise rotation of the sheathing with respect to the corresponding framing member (stud or plate) when viewed from the sheathing side of the wall. The line labeled lozenge rotation represents the rotation angle  $\gamma$  (Figure 5.11) of the end stud where the load was applied, assuming that the stud did not bend during loading.

Considering the two graphs, panels 5 and 7 rotated during the test as shown in Figure 5.11. The panel rotation relative to the studs was significantly less than the rotation with respect to top and bottom plate shown in Figures 5.12 and 5.13. This demonstrates that the fasteners located in the corner attaching sheathing and plates are most heavily loaded and will fail first. The rotation of Panel 7 relative to the studs is essentially zero. The adjacent panels may have caused Panel 7 to bend and restrained it from rotating past the studs.

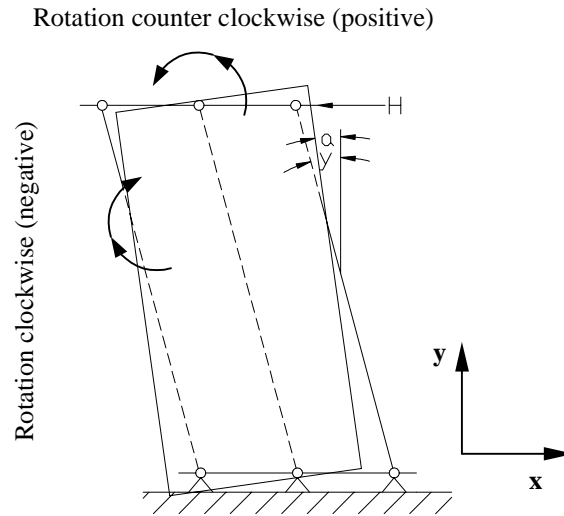


Figure 5.11: General sheathing rotation relative to the framing

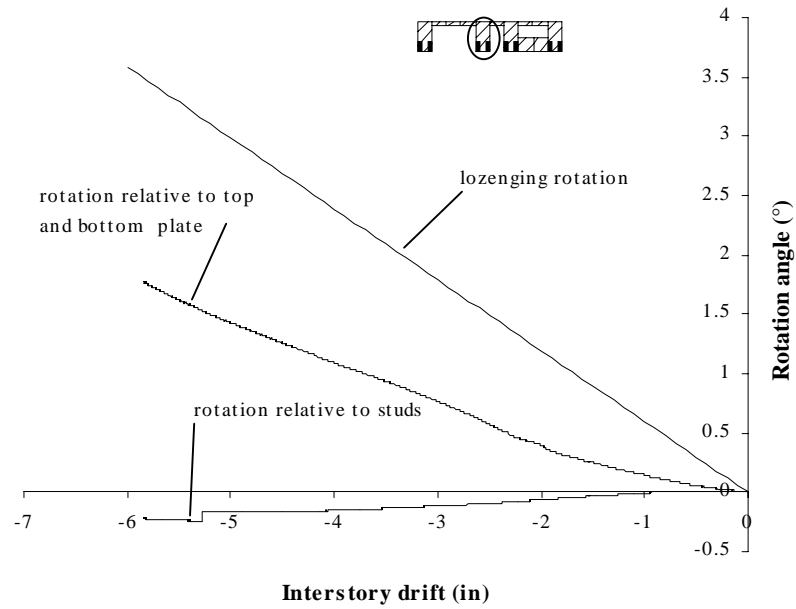


Figure 5.12: Rotation of OSB Panel 5, Wall D, maximum amount of anchors

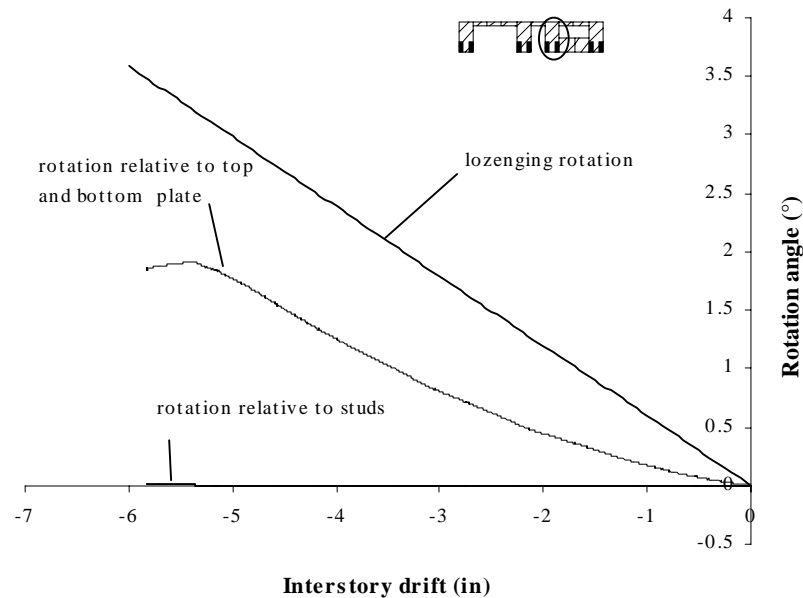


Figure 5.13: Rotation of OSB Panel 7, Wall D, maximum amount of anchors

According to simple diaphragm theory and considering the sign specification mentioned above, the angle of rotation of the end stud (lozenging rotation) can be expressed as:

$$\gamma = \alpha - \beta \quad (6.1)$$

where  $\alpha$  is the rotation relative to the top and bottom plate and  $\beta$  stands for the rotation relative to the studs. If  $\alpha$  is specified as positive,  $\beta$  has to be negative if the wall behaves as indicated in Figure 5.11. However, when superpositioning the two curves in Figures 5.12 and 5.13 the rotation angle remains well below the lozenging rotation. The difference increases with increasing interstory drift. The neglected shear deformation of the panels may explain a small amount of the difference since a part of the interstory drift is due to shear deformation of the sheathing only. Assuming a shear modulus through the thickness of 168,640 psi for one OSB panel (APA 1997) the maximum possible shear distortion of an OSB panel in Wall D is about 0.06 degrees presuming there is no nail slip. Another reason for the difference is that bending of the framing elements elucidates some of the recorded interstory drift rather than just segment rotation. This is especially

pronounced in the case of Wall D with only four fully sheathed panels. Furthermore, as previously mentioned in Chapter 3, the recorded interstory drift contains the shear wall deflection arising from rigid body rotation. As Table 5.6 displays, the uplift at capacity of Wall D fully restrained was approximately 0.11 inch (2.8mm). That corresponds to a maximum possible rotation angle of 1.6 degrees if it is assumed that the stud rotates about the anchor. Put together, these two additional components compensate for the full difference between the combined measurements and the lozenging measurement.

## **5.7 General Observations**

These tests were performed without an applied gravity (dead and live) load in order to test the most conservative condition. If gravity load had been present, the studs next to openings that had no overturning restraint (i.e., no tie-down connectors) would not have lifted from the test frame as much. This would have reduced damage to the nails attaching the sheathing to the bottom plate in these regions. The result may have been an improved overall performance. This is especially clear when one considers that studs next to openings have the highest compressive load due to applied dead load.

With the exception of Wall A without overturning restraint, all walls showed the ability to support loads close to capacity at displacements well beyond peak capacity.

Failure modes for walls with maximum overturning restraint were similar to the observed modes by Johnson (1997). Typical failures for these wall types often included buckling of the OSB panel adjacent to the load cell after maximum load was achieved, and at larger displacements, nail tear through at the bottom edge of the OSB panels, and nail tear through or head pull through of the gypsum wallboard panel edges. OSB edges between two panels failed in bearing and were crushed due to racking forces. Some OSB and gypsum panels started overlapping at displacements well beyond failure. In addition, end stud bending in the wall plane was apparent. At displacements beyond failure, the top plate started to separate from the compression end stud. Panels above and below openings acted more or less as rigid bodies.

Failure modes for walls with no overturning restraint were conspicuously different. For all three walls, the typical failure mode was the tension end stud separating

from the bottom plate and the sheathing unzipping from the bottom plate. As the tension stud started to separate from the bottom plate the few nails at the bottom of the sheathing resisted the entire overturning force. Consequently nails at this location started to tear through the OSB and gypsum panel edges. The result was a progressive failure of the nails at the bottom of the wall. At larger displacements, (much larger than displacements near capacity) studs and sheathing totally separated from the bottom plate. Crushing of panel edges between sheathing panels, was observed occasionally. Damage of gypsum edges was less apparent for walls with no overturning restraint. In all walls, cracking and failure of taped joints between gypsum panels occurred at displacements of approximately 1 inch.

## **5.8 Summary**

In summary, the major effects of overturning restraint on full-size wood frame shear walls with and without openings, tested monotonically are:

- 1) In general, tie-down anchors enhance the overall performance of a shear wall. Without tie-down anchors applied the structure exhibits a pronounced rigid body rotation arising from uplift and separation along the bottom plate.
- 2) Shear walls constructed according to the perforated shear wall method, as opposed to traditional engineered design, are less stiff. Ultimate capacity was significantly lower. Stiffness and capacity were further reduced when tie-down anchors were omitted. The fully-sheathed wall with no overturning restraint showed the largest rigid body rotation and the least ability to dissipate energy. Thus, a shear wall containing the maximum amount of tie-down anchors utilizes overall material strength most efficiently, but the performance improvements may not be justified depending on construction costs and design criteria.
- 3) Walls with overturning restraint at the ends of the wall, and walls with maximum overturning restraint, showed similar failure modes. Ultimate capacity was reached when sheathing nails of both, OSB and gypsum wallboard started to tear through the panel, and when the panel edges started to fail in compression.

- 4) Walls with no overturning restraint, failed due to nail tear through and stud separation along the bottom plate. These walls had the lowest stiffness and capacity. However, the performance appears adequate for many design conditions where the expected lateral loads are low to moderate in magnitude. This is especially evident if smaller structures are considered along with the effects of gravity loads and corner framing.
- 5) The data suggest that the empirical perforated shear wall design approach gives conservative design values for all wall configurations tested in this study. The amount of conservatism increased with increasing opening size in the wall and increase in overturning restraint. Equation 4.6 appears to be a better approximation to predicting shear strength ratios at capacity than predictions made by Equation 4.4, which has been incorporated in the Perforated Shear Wall Method.

## Chapter 6

### SPD Test Results of Straight Walls and Discussion

#### 6.1 General

Results presented in this chapter were obtained from six straight walls, 40 feet (12m) in length and 8 feet (2.4m) in height. The walls were tested using a sequential phased displacement pattern (SPD) as described in Chapter 3. Due to expense, every configuration was tested only once. As with the monotonic tests, results of plywood sheathed and SPD tested walls of identical configuration obtained by Johnson (1997) are incorporated. Effects of three different anchorage conditions on three wall configurations are compared and discussed here. Data analysis includes the determination of performance indicators such as capacity, yield strength, elastic and cyclic stiffness, and ductility. In addition, for future reference equivalent viscous damping ratios are computed for each configuration. Uplift forces, and stud and sheathing displacement histories are also presented. The discussion closes with a general description of the overall behavior of the walls.

#### 6.2 Load-Drift Relationship

Please note that Wall A was tested cyclically with only two anchorage conditions due to it being fully sheathed. As with the monotonic results, differences in capacities or other performance indicators between the two specimens cannot be explained by the amount of tie-down anchors but may be a result of statistical variation or a slight difference between plywood and OSB nail bearing strength.

Initial load envelope curves of each wall configuration are depicted in Figures 6.1, 6.2, and 6.3. It has been proposed that data from the initial curve can be used to establish design values for shear walls subjected to a one time peak load such as wind loading. Data from the stabilized curve can be used to set conservative design values for shear walls subjected to repetitive cycling such as a seismic event. However, an adjustment in

the system response factor,  $R$ , which is used in calculating base shear, may be needed to compensate or calibrate the design process to expected response. Load resistance at capacity was determined from the initial and stabilized load envelope curves and is presented in Table 6.1. All performance indicators listed in Table 6.1 represent average values from the respective positive and negative load envelope curves.

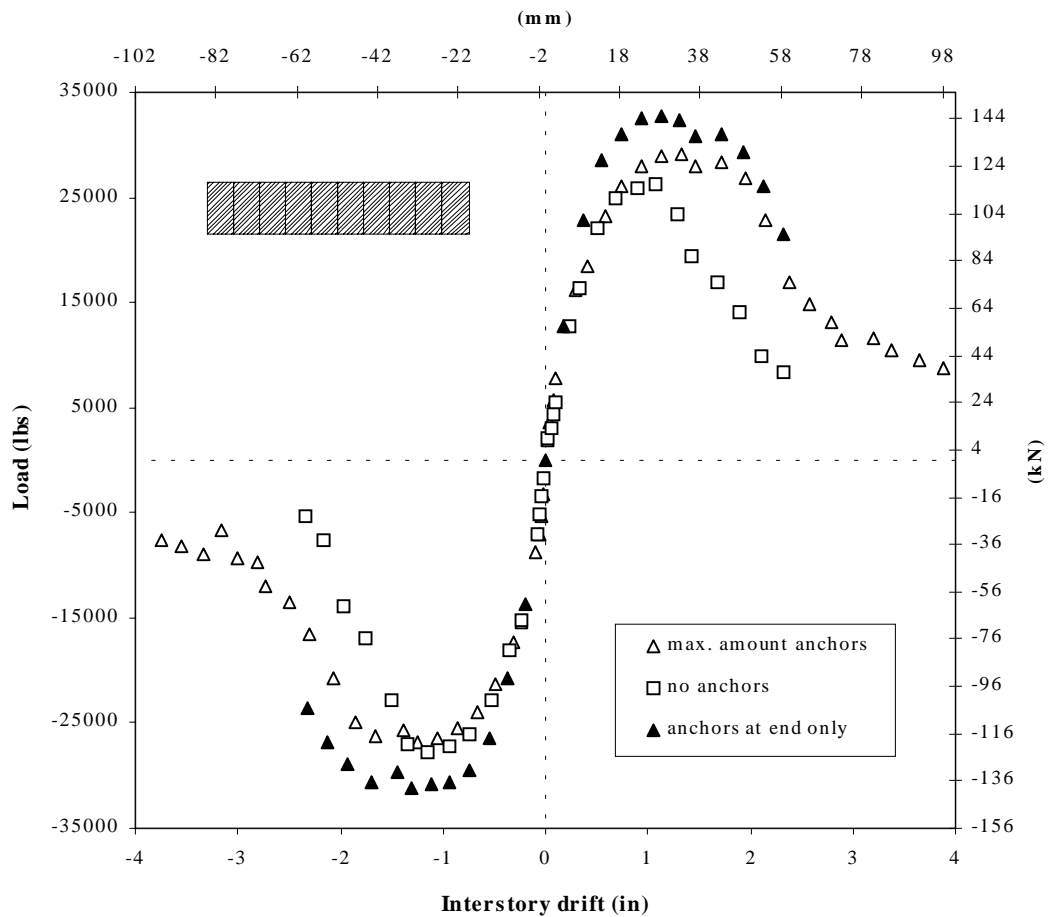


Figure 6.1: Load vs. Interstory drift envelope curves of wall configuration A

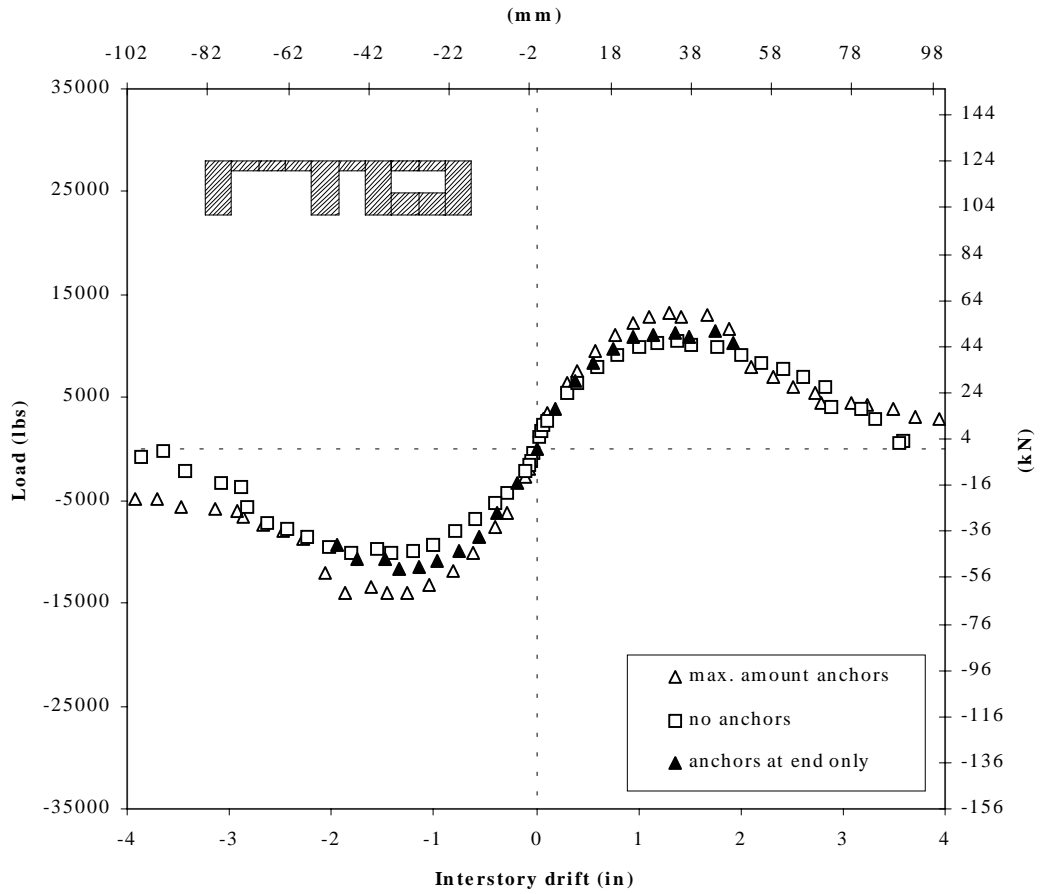


Figure 6.2: Load vs. Interstory drift envelope curves of wall configuration D

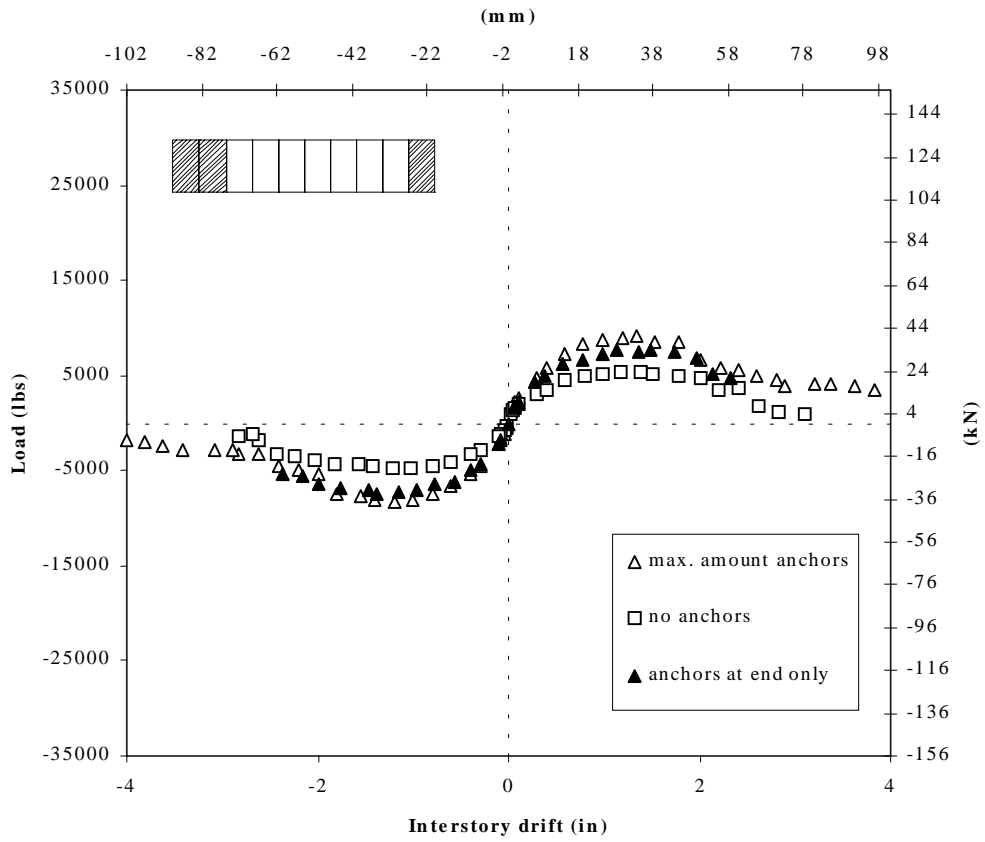


Figure 6.3: Load vs. Interstory drift envelope curves of wall configuration E

Table 6.1: Initial cyclic and stabilized cyclic load resistance data

	Wall Specimens								
	no tie-down anchors <sup>(1)</sup>			anchors at end of wall only <sup>(2)</sup>			maximum amount of tie-down anchors <sup>(1)</sup>		
	A	D	E	A <sup>(3)</sup>	D	E	A <sup>(3)</sup>	D	E
<b>Capacity</b>									
Initial SPD (kips)	26.7	10.1	4.8	32.0	11.2	7.3	27.7	13.4	8.4
Stabilized SPD (kips)	22.5	8.7	4.1	27.4	9.6	6.3	23.7	11.7	7.1
Stabilized/Initial	0.84	0.86	0.85	0.86	0.86	0.87	0.85	0.87	0.85
<b>F<sub>yield</sub></b>									
Initial SPD (kips/in)	24.3	9.0	4.3	29.9	10.3	6.3	25.3	12.2	7.6
Stabilized SPD (kips/in)	20.2	7.7	3.7	25.8	9.6	5.3	21.6	10.5	6.5
Stabilized/ Initial	0.83	0.86	0.86	0.86	0.94	0.84	0.85	0.86	0.85
<b>Elastic Stiffness</b>									
Initial SPD (kips/in)	61.6	16.5	11.0	70.4	17.6	16.7	69.0	21.9	16.8
Stabilized SPD (kips/in)	61.1	16.4	11.1	70.1	17.4	16.0	67.8	21.2	16.8
Stabilized/ Initial	0.99	0.99	1.01	1.00	0.99	0.96	0.98	0.97	1.00

<sup>(1)</sup> These specimens had OSB sheathing

<sup>(2)</sup> These specimens had plywood sheathing (Johnson1997)

<sup>(3)</sup> Wall A has the same anchorage requirements for the anchors at the end of wall only and maximum amount of tie-down anchors due to being fully sheathed.

Note: The numbers presented are rounded. All calculations were done with original values.

Peak load of the initial and stabilized cycles is correlated with the amount of tie-down anchors. For all wall configurations, capacity increased with increasing overturning restraint. The increase in capacities with the number of tie-down anchors was also affected by the size of openings. Wall E with the largest opening shows the greatest increase measured as proportion of capacity, while the capacity of Wall A experienced the least amount of relative increase. This trend is better described in Table 6.2. The relative capacities based on engineered construction with maximum amount of tie-down devices are shown for each wall configuration. Initial and stabilized peak loads of Wall A decreased by less than 5 percent when overturning restraints were omitted, whereas the capacities of Wall E with the largest opening and no tie-down devices decreased 43 percent compared to the same configuration with maximum restraint. It should be noted that these test observations are relative to the nature of the test method

and conditions. When corner framing is considered as discussed in Chapter 7, the strength and stiffness of conventionally-built (unrestrained) walls is enhanced. Consideration of gravity load effects may also provide expected improvements in tested or predicted performance.

Table 6.2: Relative capacities based on engineered construction.

	Wall Specimens								
	no tie-down anchors <sup>(1)</sup>			anchors at end of wall only <sup>(2)</sup>			maximum amount of tie-down anchors <sup>(1)</sup>		
	A	D	E	A <sup>(3)</sup>	D	E	A <sup>(3)</sup>	D	E
Relative capacity (%)									
Initial SPD (kips)	96	75	57	116	84	87	100	100	100
Stabilized SPD (kips)	95	74	58	116	82	89	100	100	100

<sup>(1)</sup> These specimens had OSB sheathing

<sup>(2)</sup> These specimens had plywood sheathing (Johnson 1997)

<sup>(3)</sup> Wall A has the same anchorage requirements for the anchors at the end of wall only and maximum amount of tie-down anchors due to being fully sheathed.

The ratio of stabilized to initial peak load is almost constant for all wall configurations. According to the ratio, the reduction of ultimate resistance between initial and stabilized SPD cycles is, on average, 14 percent (Std Dev = 1%). This demonstrates that strength degradation of shear walls is a result of crushing of the timber around the nail shanks, partial nail withdrawal, and is independent on size of openings and anchorage conditions. Table 6.1 includes the two parameters  $F_{yield}$  and elastic stiffness determined from the EEEP curve. The average reduction of  $F_{yield}$  between initial and stabilized cycles is 14 percent (Std Dev = 3.1%) for all wall configurations. Again, this confirms that the damage experienced by the walls was fairly uniform regardless of the amount of overturning anchorage present. As expected,  $F_{yield}$  increased as the number of overturning restraints increased from zero to maximum.

Stabilized and initial elastic stiffness values for a given configuration differ a maximum of 4 percent, which is not significant for most practical applications. Table 6.1 further shows that stiffness values also increase with an increasing amount of overturning

restraint for a given wall, but the increase is not as pronounced. This condition is unique to the small amplitude of displacements used in the elastic stiffness region, resulting in minor damage to the sheathing nails. In all three wall groups, the highest elastic stiffness values were determined for Wall A, fully-sheathed. As with load resistance and capacity, stiffness values increased in magnitude as area of openings decreased. Stiffness values for Wall E reached only an average of 20 percent (Std Dev = 4.3%) of the stiffness of Wall A, regardless of the number of tie-downs.

### 6.3 Ductility

Recall that ductility is obtained through division of the drift at failure by yield displacement. Ductility values reported in Table 6.3, as well as the ratio of stabilized to initial ductility, show no apparent trend. Initial ductility ranged from 2.7 to 5.2, while stabilized ductility ranged from 3.5 to 7.3. As already mentioned in the monotonic section, ductility values are dependent upon initial or stabilized stiffness that indirectly determines yield displacement. Furthermore, since the determination of a sudden load drop that identifies failure can be ambiguous, the associated drift at failure can be questionable as well. For that reason, the clearly defined drift at  $0.8 F_{\text{peak}}$  was included in Table 6.3. However, even when considering those values, there was no recognizable effect of tie-down anchors on ductility.

It is conspicuous that Wall D, not restrained against uplift, shows a fairly high failure displacement. It is also apparent that the drifts at  $0.8 F_{\text{peak}}$  are almost constant when overturning restraints are applied. The load is distributed more uniformly in walls containing tie-down anchors. The relatively constant drift is a result of nail fatigue occurring after a certain amount of cycles at large displacements. Wall A without tie-down anchors shows the lowest initial and stabilized ductilities. This indicates that this wall failed in a rather brittle manner when compared to the other configurations (Figure 6.1). The wall experienced little racking and the energy dissipation was lower, implying that overturning restraints help utilize material strengths more effectively.

Table 6.3: Initial cyclic and stabilized cyclic ductility

	Wall Specimens								
	no tie-down anchors <sup>(1)</sup>			anchors at end of wall only <sup>(2)</sup>			maximum amount of tie-down anchors <sup>(1)</sup>		
	A	D	E	A <sup>(3)</sup>	D	E	A <sup>(3)</sup>	D	E
$\Delta_{yield}$									
Initial SPD (in)	0.4	0.6	0.4	0.4	0.6	0.4	0.4	0.6	0.5
Stabilized SPD (in)	0.3	0.5	0.3	0.4	0.6	0.3	0.3	0.5	0.4
$\Delta_{failure}$									
Initial SPD (in)	1.3	2.2	2.0	1.9	1.9	2.0	1.9	1.7	1.8
Stabilized SPD (in)	1.3	2.1	1.9	1.9	2.0	2.0	1.9	1.9	1.7
Ductility:									
Initial SPD ductility	2.7	4.0	5.0	4.6	3.3	5.2	5.1	3.5	3.9
Stabilized SPD ductility	4.1	3.7	7.3	5.2	3.5	6.0	5.9	3.5	4.3
Stabilized/ Initial ductility	1.5	0.9	1.5	1.2	1.0	1.0	1.2	1.0	1.1
Drift @ 0.8 F <sub>peak</sub>									
Initial SPD (in)	1.4	2.2	2.0	1.9	1.9	2.0	2.0	2.0	1.9
Stabilized SPD (in)	1.3	2.1	1.9	1.9	2.0	2.0	1.9	1.8	1.8

<sup>(1)</sup> These specimens had OSB sheathing

<sup>(2)</sup> These specimens had plywood sheathing (Johnson 1997)

<sup>(3)</sup> Wall A has the same anchorage requirements for the anchors at the end of wall only and maximum amount of tie-down anchors due to being fully sheathed.

Note: The numbers presented are rounded. All calculations were done with original values.

## 6.4 Perforated Shear Wall Method

Table 6.4 shows actual shear capacity ratios from the initial curves along with the predicted shear strength ratio calculated using Equation 4.4. Actual shear strength ratios are higher than predicted ratios in all cases except for Wall A. Wall A has an actual shear capacity ratio of 1.0 because the predicted ratio given by Equation 4.4 is based on the fully-sheathed configuration. The actual shear strength ratios are based on the capacity of the fully-sheathed configuration with the same overturning restraint conditions. The amount of conservatism increases as the amount of openings in the wall increases. Johnson (1997) noted the same trend. The actual shear capacity ratio ranges in

conservatism from zero percent for a fully sheathed wall to 233 percent for Wall E with maximum number of tie-down anchors. Similar values were obtained from monotonic tests (Chapter 5) on the same wall configurations.

Table 6.4: Comparison of actual initial capacity with theoretical predicted capacity

	Wall Specimens								
	no tie-down anchors (OSB)			anchors at end of wall only <sup>(1)</sup> (Plywood)			maximum amount of tie-down anchors (OSB)		
	A	D	E	A <sup>(2)</sup>	D	E	A <sup>(2)</sup>	D	E
Displacement (in) @ peak load	1.06	1.34	1.15	1.20	1.51	1.23	1.23	1.33	1.23
Predicted shear load ratio, (F) (Eq. 1)	1.00	0.24	0.13	1.00	0.24	0.13	1.00	0.24	0.13
Peak load (kips)	26.7	10.1	4.8	32	11.2	7.3	27.7	13.4	8.4
Actual shear load ratio, (F)	1.00	0.38	0.18	1.00	0.35	0.23	1.00	0.48	0.30
Actual / predicted shear load ratio	1.00	1.58	1.38	1.00	1.46	1.75	1.00	2.02	2.33

<sup>(1)</sup> From Johnson (1997)

<sup>(2)</sup> Wall A has the same anchorage requirements for the anchors at the end of wall only and maximum amount of tie-down anchors due to being fully sheathed

Note: The numbers presented are rounded. All calculations were done using original values.

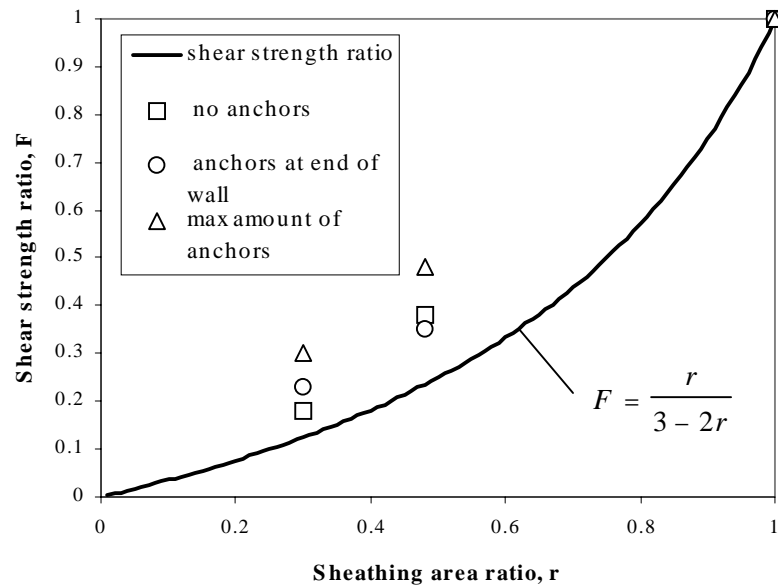


Figure 6.4: Shear strength ratios at capacity (Eq. 4.4) as a function of sheathing area ratio

Figure 6.4 illustrates the conservatism of the predicted shear strength ratio by plotting the actual shear strength ratios and the calculated shear strength ratio according to Equation 4.4 against the sheathing area ratio (Equation 4.1).

## 6.5 Sugiyama's Equations

Although the empirical Equations 4.4, 4.5, and 4.6, introduced by Sugiyama and Matsumoto in 1994, were derived from monotonic racking tests, their applicability to predicting cyclic shear strength ratios is presented below. As previously mentioned, Equation 4.4 may be used to predict the shear strength ratio of an 8 feet high wall at 0.96 inch (24mm) interstory drift, whereas Equations 4.5 and 4.6 were introduced to predict the shear strength ratio at 0.32 inch (8mm) and 1.6 inch (41mm) interstory drifts, respectively.

For wall configurations D and E, Sugiyama's equations predict conservative shear strength ratios (Table 6.5). Again, Wall A was fully sheathed, and therefore, the predicted and actual shear strength ratios are unity. The amount of conservatism ranges from 6 percent for Wall D with restraints at the ends only up to 241 percent for Wall E

restraint at maximum amount. As expected the three equations predict more conservative values for walls with maximum overturning restraint. But even for walls not restrained against uplift, the predictions are conservative. Indicated by the high variation among the predicted values in Table 6.5, Equations 4.4, 4.5, and 4.6 seem not to be accurate in predicting shear strength ratios at respective interstory drifts for cyclically tested walls even with tie-downs at the ends only.

Equation 4.4 has been proposed to predict the shear strength ratio at capacity, although this equation was derived from data obtained at a shear deformation angle of 1/100 radian or 0.96 inch interstory drift. However, most displacements at capacity listed in Table 6.4 are significantly higher than 0.96 inch. Given the fact that Equation 4.4 predicts fairly conservative values, Equation 4.6, which predicts the shear strength ratio at 1.6 inch interstory drift, may be more appropriate to predict the shear strength ratio at capacity. That can be seen by comparing Figures 6.4 and 6.5. Figure 6.5 depicts the actual and predicted shear strength ratios at capacity. The predicted ratio is plotted as a continuous line using Equation 4.6.

Table 6.5: Initial cyclic and stabilized cyclic load resistance data

	Wall Specimens								
	no tie-down anchors <sup>(1)</sup>			anchors at end of wall only <sup>(2)</sup>			maximum amount of tie-down anchors <sup>(1)</sup>		
	A	D	E	A <sup>(3)</sup>	D	E	A <sup>(3)</sup>	D	E
	r=1.00	r=0.48	r=0.30	r=1.00	r=0.48	r=0.30	r=1.00	r=0.48	r=0.30
Load (kips) @ 0.32 in. int. drift									
Initial SPD (kips)	16.5	4.9	2.8	19.8	5.4	4.4	16.9	6.5	4.7
Actual shear strength ratio, (F)	1.00	0.30	0.17	1.00	0.27	0.22	1.00	0.38	0.28
Predicted shear strength ratio	1.00	0.26	0.14	1.00	0.26	0.14	1.00	0.26	0.14
Actual / Predicted	1.00	1.15	1.23	1.00	1.06	1.60	1.00	1.50	2.01
Load (kips) @ 0.96 in. int. drift									
Initial SPD (kips)	26.4	9.2	4.7	31.7	10.7	7.0	26.9	12.4	8.1
Actual shear strength ratio, (F)	1.00	0.35	0.18	1.00	0.34	0.22	1.00	0.46	0.30
Predicted shear strength ratio	1.00	0.24	0.13	1.00	0.24	0.13	1.00	0.24	0.13
Actual / Predicted	1.00	1.48	1.42	1.00	1.43	1.77	1.00	1.96	2.41
Load (kips) @ 1.6 in. int. drift									
Initial SPD (kips)	18.1	9.6	4.4	30.6	10.7	7.0	27.0	13.0	7.8
Actual shear strength ratio, (F)	1.00	0.53	0.24	1.00	0.35	0.23	1.00	0.48	0.29
Predicted shear strength ratio	1.00	0.32	0.18	1.00	0.32	0.18	1.00	0.32	0.18
Actual / Predicted	1.00	1.68	1.38	1.00	1.11	1.30	1.00	1.52	1.64

<sup>(1)</sup> These specimens had OSB sheathing

<sup>(2)</sup> These specimens had plywood sheathing (Johnson 1997)

<sup>(3)</sup> Wall A has the same anchorage requirements for the anchors at the end of wall only and maximum amount of tie-down anchors due to being fully sheathed.

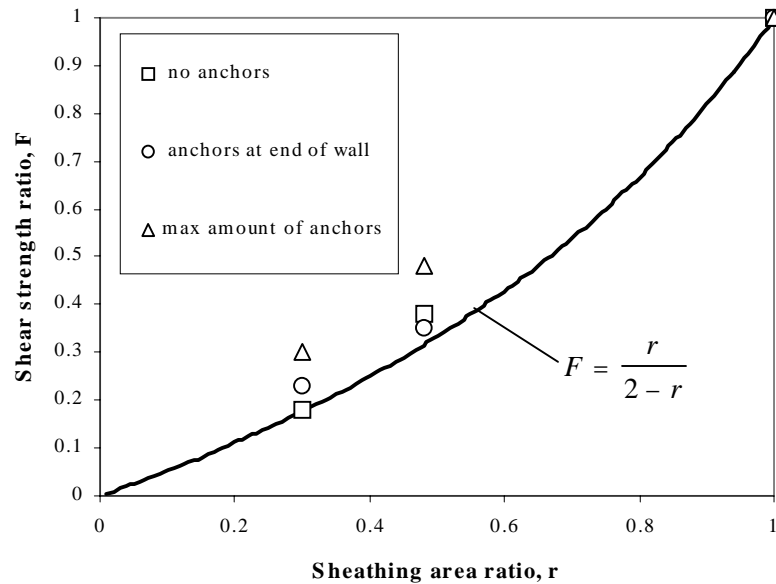


Figure 6.5: Shear strength ratio at capacity using Equation 4.6

## 6.6 Earthquake Performance

Along with strength and ductility, damping and stiffness degradation are the other two most important earthquake performance indicators. Response of an excited structure depends on the type of excitation and the amount of damping present.

### 6.6.1 Equivalent Viscous Damping

Initial and stabilized damping ratios for walls not restrained against uplift are consistently higher than the damping ratios for the other two anchorage conditions, especially at load levels at displacements beyond capacity (Figures 6.6 and 6.7). The reason for that is that the linear peak potential energy at a given interstory drift is lower for walls without tie-down devices (refer to Chapter 4). After the wall has started to separate across the bottom, interstory drift arising from that separation can be viewed similar to a plastic deformation which stores no potential energy. Anchors on the other hand, prevent the wall from separating from the bottom plate, and therefore, the structure behaves more elastically. However, as can be seen from the graphs in Figures 6.6 and

6.7, the difference in damping ratios is rather small and is evident mainly when the walls begin to separate from the bottom plate.

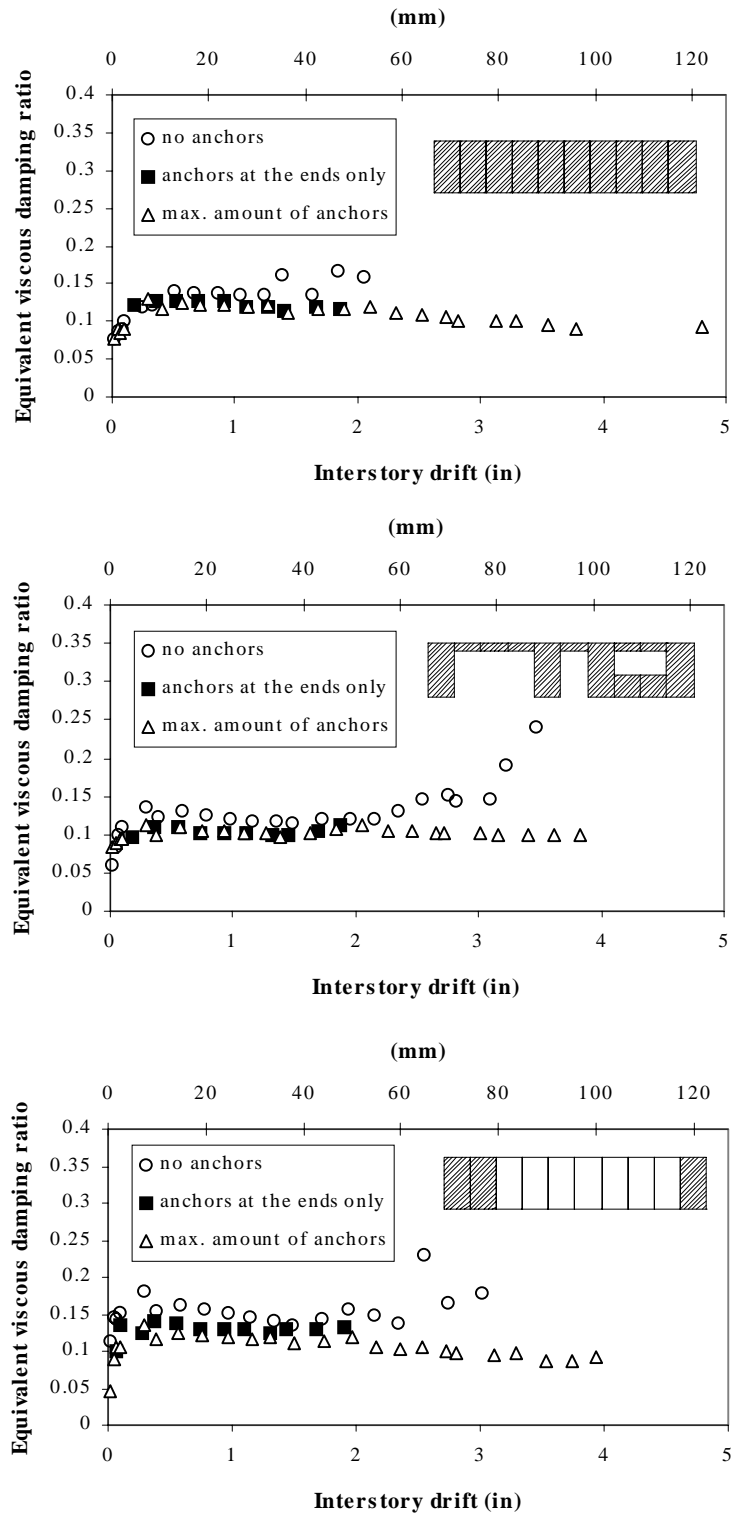


Figure 6.6: Initial EVDR vs. interstory drift of wall configurations A, D, and E

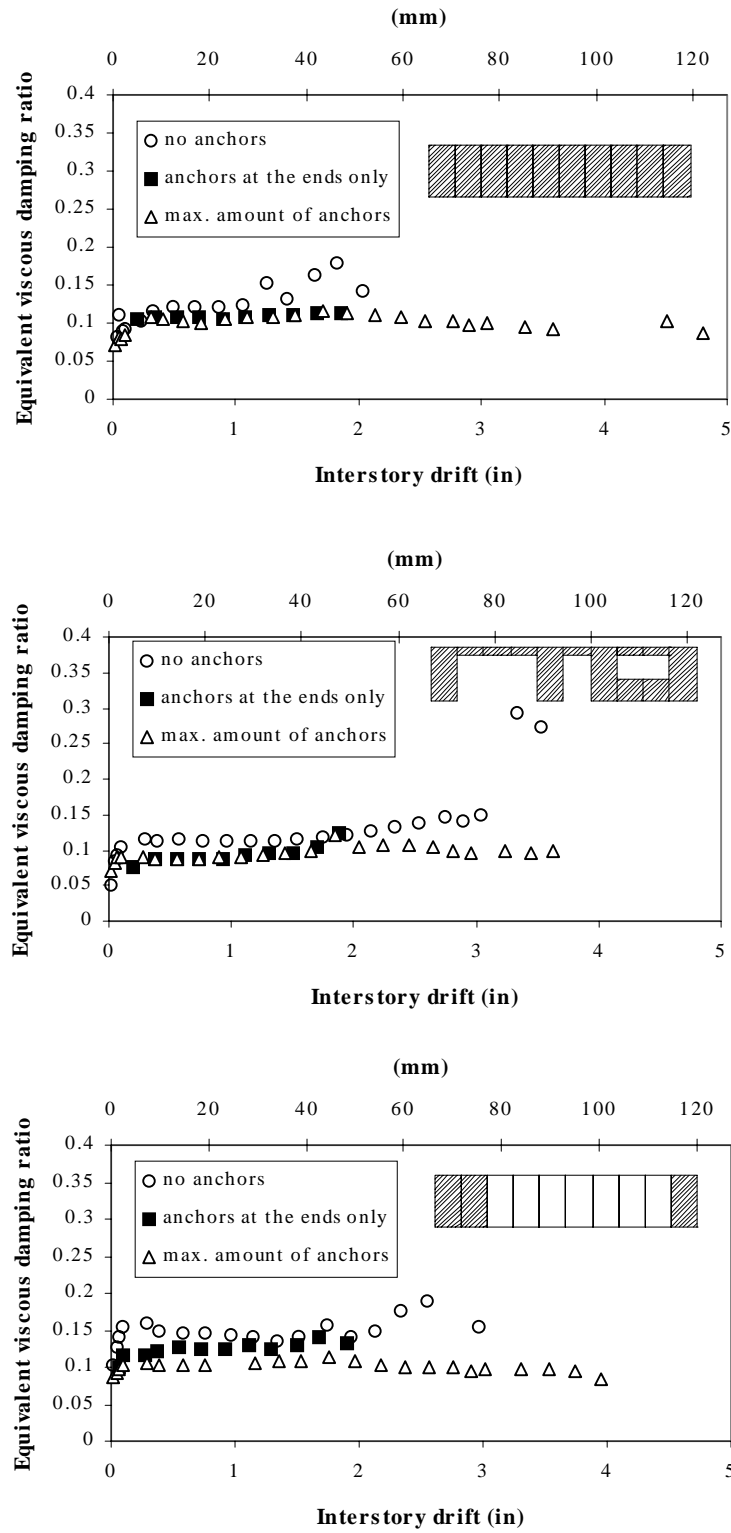


Figure 6.7: Stabilized EVDR vs. interstory drift of wall configurations A, D, and E

With the exception of Wall E, initial and stabilized EVDR for walls containing anchors at the ends and maximum amount of anchors almost coincide. This is also reflected in Table 6.6 where the mode of all EVDR obtained for each wall together with the pertaining relative frequency is listed. The mode is a statistical term and represents the value of a sample that occurs with the greatest frequency. Note that in order to obtain a mode the EVDR values were rounded. According to Table 6.6 the damping ratios are fairly constant and range between 0.09 and 0.15. Stabilized EVDRs tend to be slightly lower than initial EVDRs.

Note that EVDR is only an approximation since the walls were loaded quasi-statically beyond the elastic limit. At low loading rates, where no inertia forces are involved such as during quasi-static loading, the viscous damping is in principle zero. In addition, timber structures exhibit a highly non-linear behavior and a complex mix of Coulomb damping, internal friction and rupture of material when loaded beyond the elastic region. Beyond the elastic limit, the equivalent viscous damping approach is not appropriate to compare timber structures with structures of other materials (Lowe and Edwards 1984; Polensek 1988; Foliente 1994). For future reference the EVDR of the first three phases (at displacements below FME) are listed in Table 6.7. Values represent damping ratios within the elastic range, and can be used for dynamic analysis. Theoretically, hysteresis damping within the elastic range is zero. Nevertheless some energy is dissipated due to friction in nailed sheathing-to-framing connections and compression of the grain. In fact, Wall E without tie-down anchors exhibited an EVDR of more than 10 percent (Table 6.7). In the literature an EVDR of 5 percent for timber structures has been assumed within the elastic range (Ceccotti 1995).

Table 6.6: EVDR mode and its relative frequency

	Wall Specimens								
	no tie-down anchors <sup>(1)</sup>			anchors at end of wall only <sup>(2)</sup>			maximum amount of tie-down anchors <sup>(1)</sup>		
	A	D	E	A <sup>(3)</sup>	D	E	A <sup>(3)</sup>	D	E
Initial									
EVDR mode	0.14	0.12	0.15	0.12	0.10	0.13	0.12	0.10	0.12
Relative frequency	0.33	0.39	0.32	0.50	0.70	0.50	0.38	0.29	0.29
Stabilized									
EVDR mode	0.12	0.11	0.15	0.11	0.09	0.12	0.11	0.09	0.10
Relative frequency	0.33	0.36	0.28	0.90	0.50	0.42	0.29	0.43	0.25

<sup>(1)</sup> These specimens had OSB sheathing

<sup>(2)</sup> These specimens had plywood sheathing (Johnson 1997)

<sup>(3)</sup> Wall A has the same anchorage requirements for the anchors at the end of wall only and maximum amount of tie-down anchors due to being fully sheathed

Note: The mode was computed using rounded numbers.

Table 6.7: EVDR from the first three phases of SPD loading (elastic range)

	Interstory drift (in)	Wall Specimens								
		no tie-down anchors <sup>(1)</sup>			anchors at end of wall only <sup>(2)</sup>			maximum amount of tie-down anchors <sup>(1)</sup>		
		A	D	E	A <sup>(3)</sup>	D	E	A <sup>(3)</sup>	D	E
Initial										
	0.025	0.08	0.06	0.11				0.08	0.08	0.05
EVDR	0.050	0.09	0.08	0.15				0.09	0.09	0.09
	0.075	0.09	0.10	0.14				0.08	0.09	0.10
Stabilized										
	0.025	0.08	0.05	0.10				0.07	0.07	0.09
EVDR	0.050	0.11	0.09	0.13				0.08	0.08	0.09
	0.075	0.09	0.09	0.14				0.08	0.09	0.10

<sup>(1)</sup> These specimens had OSB sheathing

<sup>(2)</sup> Johnson (1997) did not list values

<sup>(3)</sup> Wall A has the same anchorage requirements for the anchors at the end of wall only and maximum amount of tie-down anchors due to being fully sheathed.

### 6.6.2 Cyclic Stiffness

Cyclic stiffness is a measure to monitor the approximate stiffness degradation of a timber structure subjected to cyclic loading (refer to Chapter 4). Inherent to the response history of timber structures, cyclic stiffness is correlated with elastic stiffness. As a result, wall configuration A starts off with the highest initial and stabilized cyclic stiffness (Figures 6.8 and 6.9). Furthermore the stiffness degradation is highest for this wall configuration. Cyclic stiffness degradation is a result of the sheathing nail shank crushing the wood fibers surrounding it at each progressive phase beyond the elastic limit. A cavity is formed around the nail shank, leaving the nail unsupported during successive cycles until the actuator displacement increases and the nail shank becomes supported by the previously crushed timber again. However, until the shank contacts the crushed timber, only bending resistance of the nail shank within the cavity and friction counteracts the external force. This is reflected in the pinched part of the hysteresis loops. As the wall displacement increases the fibers crush around more fasteners and the cavities enlarge. The part where the external force is resisted by nail bending only increases. Consequently the pinched sections of the hysteresis loops become longer, and since the resisted load increases at a lower rate, the cyclic stiffness degrades after the first phase. Wall configuration A exhibits the highest degradation of cyclic stiffness because it contains the most sheathing fasteners, due to being fully sheathed. For all walls, the stiffness degrades nonlinearly and approaches zero (Figures 6.8 and 6.9).

There is almost no difference between the course of the cyclic stiffness plots when compared for each anchorage condition. According to the graphs (Figures 6.8 and 6.9) the cyclic stiffness values of the walls without tie-down devices are typically slightly below the other values. The same trend was found for elastic stiffness in section 6.2. The separation of wall and bottom plate probably adds some plastic type displacement that reduces cyclic stiffness.

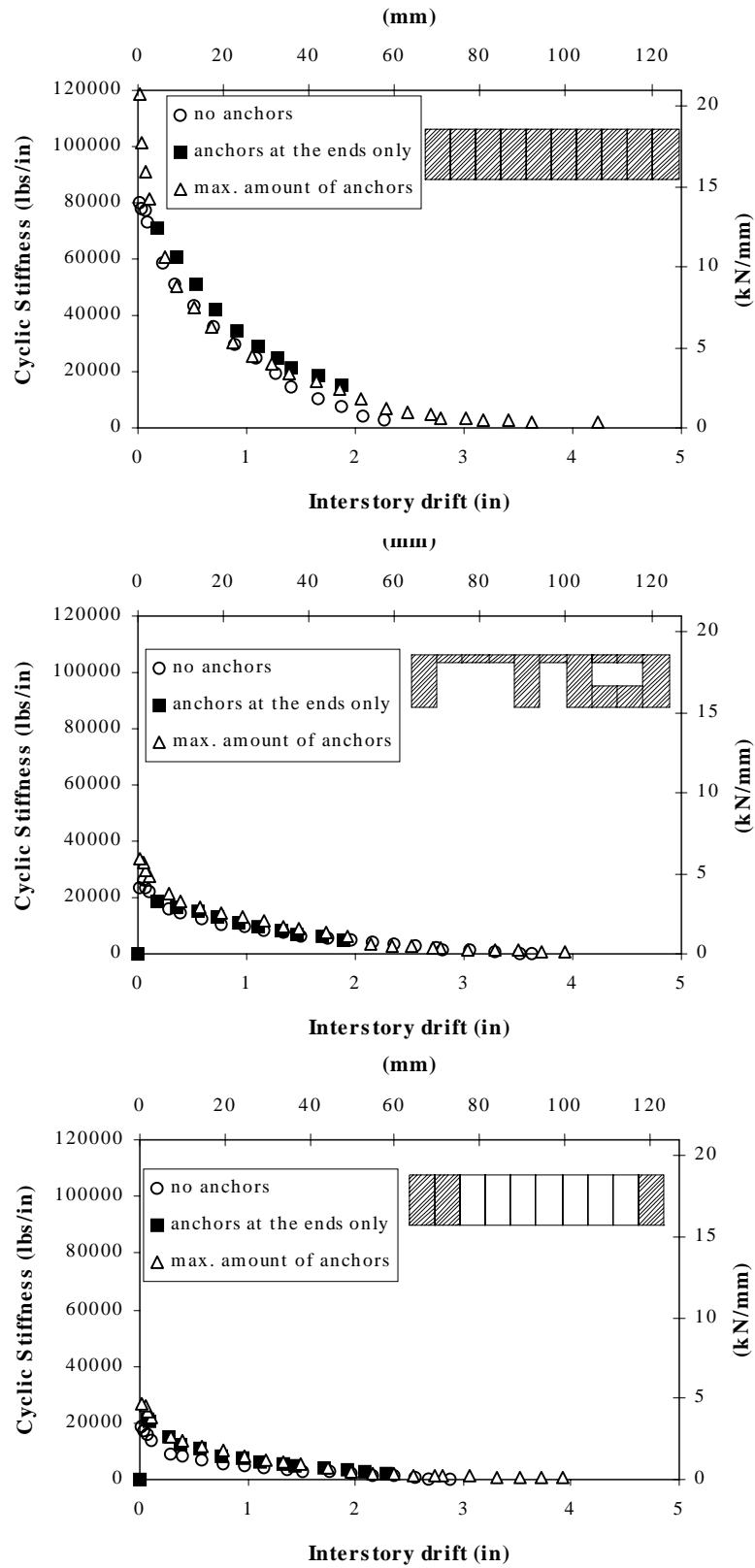


Figure 6.8: Initial cyclic stiffness vs. interstory drift of wall configurations A, D, and E

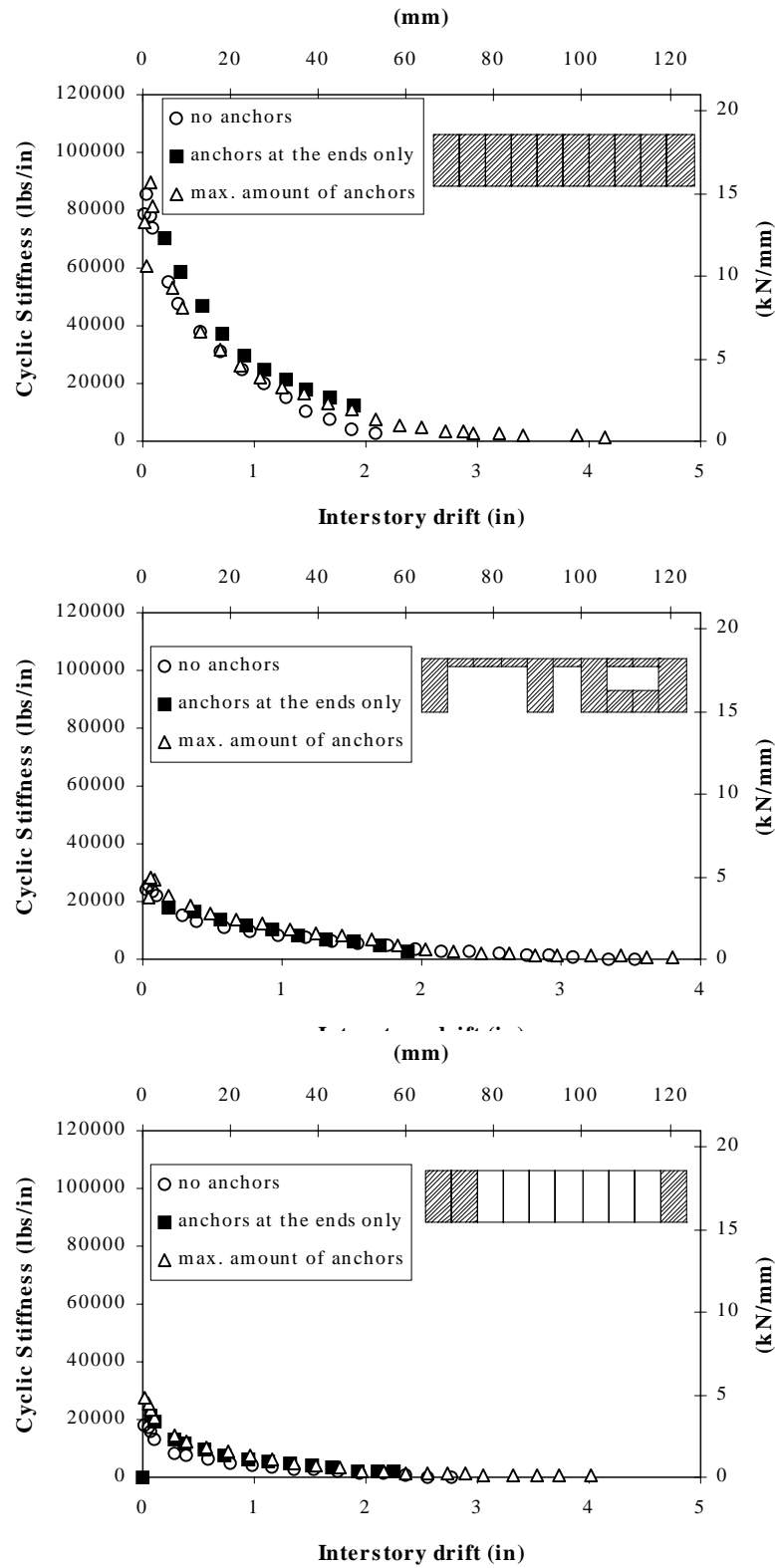


Figure 6.9: Stabilized cyclic stiffness vs. interstory drift of wall configurations A, D, E

## 6.7 Overall Wall Response

### 6.7.1 Tie-down Tension Bolts

Calibrated tension load-cell bolts measured the uplift resisted by the tie-down anchors during SPD loading. The graphs in Figures 6.10 and 6.11 show the tensile load distribution of the respective tension load bolt together with the load initial envelope curve of the corresponding specimen without tie-down anchors and with maximum amount of anchors installed, respectively. Johnson (1997) did not use load bolts in the wall configurations tested in his study and therefore, the anchorage condition for the perforated shear wall method cannot be included. The location of the bolt discussed here was adjacent to the end stud where the load was applied (circled corner). Data of the second load bolt (refer to Chapter 3) could only be obtained for Wall A (max. amount of anchors) due to instrumentation damage and is therefore not included here. The square shaped marks in the graphs represents that part of the initial load envelope curve where the bolt was in tension.

Considerable load loops at positive interstory drift in the graphs of Figure 6.11 are not real tension load values. At positive interstory drift the hydraulic actuator was contracting and the bottom plate underneath the load bolt was in compression. However, the bolts used could only record tension load. The reason for the erroneous load at positive drifts is that the bolt fastened both the tie-down anchor and bottom plate to the foundation. Arising from the stud rotation the bolt was also stressed in bending and tension especially at larger interstory drifts and recorded false data.

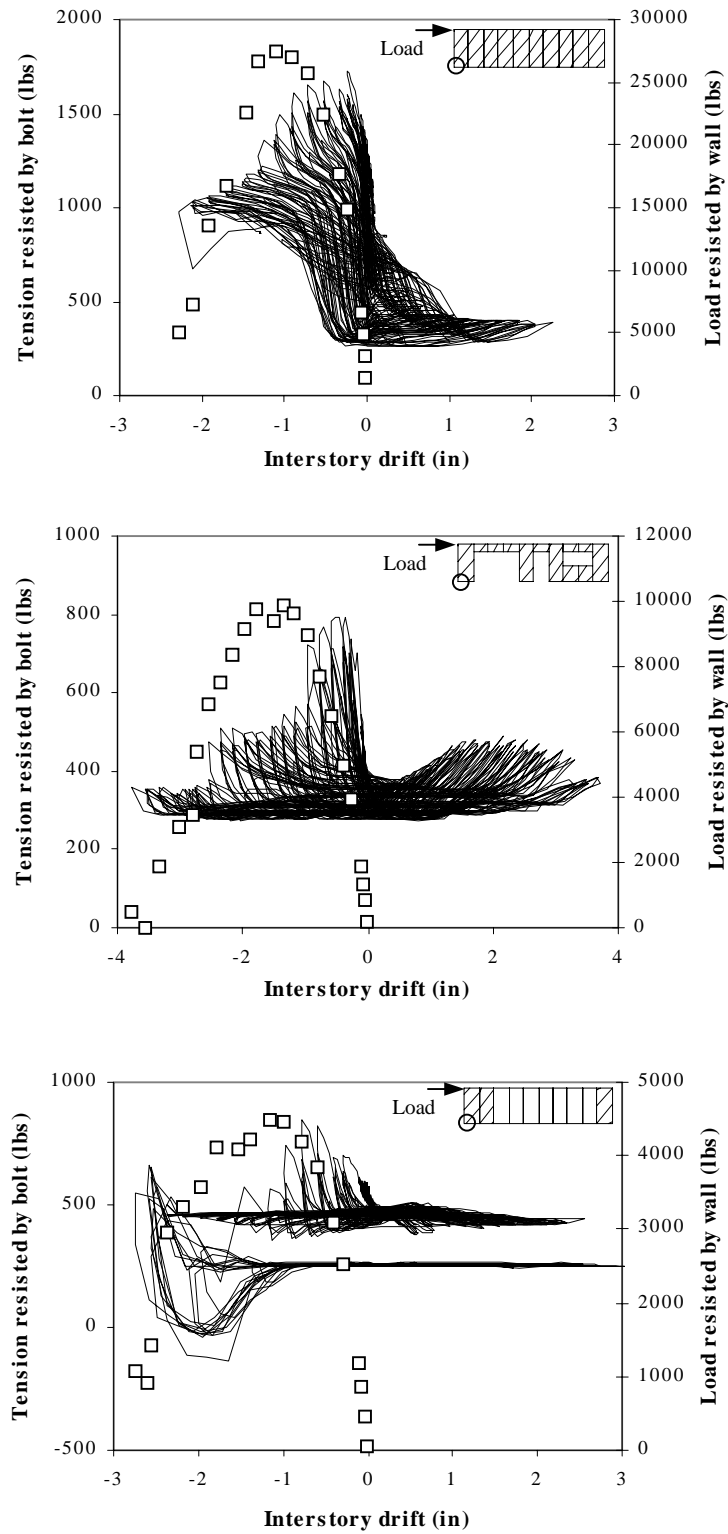


Figure 6.10: Resisted load by tension bolts of Walls A, D, and E, respectively, not restrained against uplift, along with the corresponding initial load envelope curves

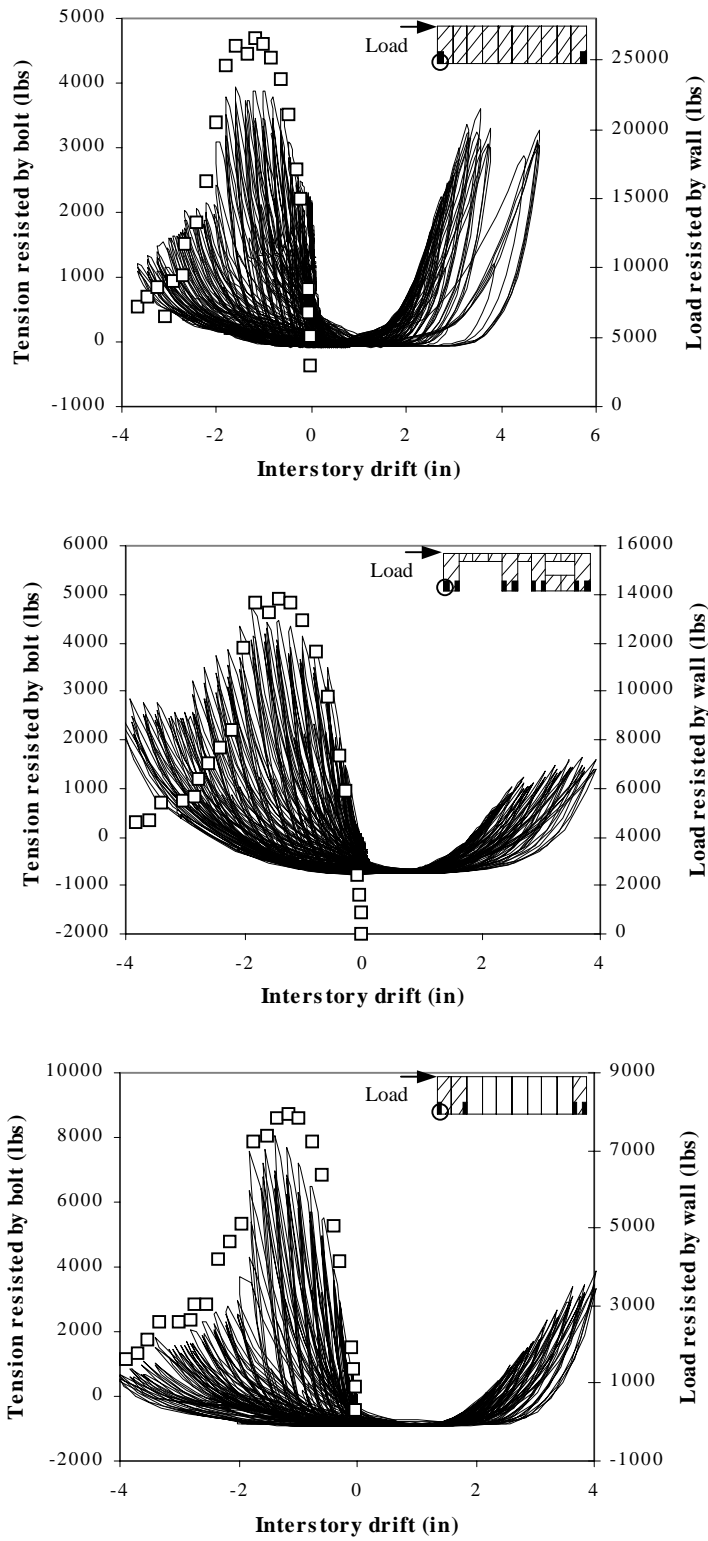


Figure 6.11: Resisted load by tension bolts of Walls A, D, and E, respectively, with maximum uplift restraints, along with the corresponding initial load envelope curves

Prior to testing, all bolts were pretensioned to indirectly measure compression loads. For that reason the bolt load histories shown in Figure 6.10 are notably offset from zero. However, the bolts had to be tightened before the last sheathing panel was applied, which was a considerable amount of time before testing. As a result some pretension was lost due to relaxation of the wood, and there was no control over the amount of pretension at the beginning of the test. During the test further relaxation and additional crushing of the wood fibers of the bottom plate underneath the bolt and around the bolt shank occurred resulting in a continuous decrease of pretension with each successive cycle. Compressive load onto the bottom plate is therefore difficult to assess. During the cycle where the tension bolts reached their maximum only the bottom plate in Wall A without tie-down anchors experienced a compressive load of 273 lbs underneath the end stud. This value was obtained by subtracting the minimum load recorded at wall capacity from the tension load recorded at zero interstory drift (i.e. between positive and negative  $\Delta_{\text{peak}}$ ). Note that in order to obtain the maximum tension load, the pretension has to be deducted from the acquired data.

The recorded load underwent a sign change for walls containing anchors. The data was offset by the bending stress induced to the bolt. The correct tension load in these cases is therefore the positive amplitude of the recorded load curve plus the minimum negative load recorded, rather than the load shown on the scale.

The peaks of the hysteresis loops acquired by the load bolts follow closely the load envelope curve as the maximum amount of anchors was applied (Figure 6.11). However, when anchors were omitted, the two curves are offset and the shapes do not resemble each other. The sudden tensile load drop, especially in the graphs for Walls D and E, elucidates the relatively abrupt separation of sheathing and end stud from the bottom plate. After separation, little uplift load could be transferred to bottom plate and foundation.

Correlation of racking load resisted by the shear wall to load resisted by the bolt for each cycle in the test was determined and the results are shown in Table 6.8. Unit shear was determined according to Equation 5.1. Tension bolts in walls without tie-down

devices applied experienced their maximum load at wall displacements lower than where ultimate wall capacity was reached. In contrast, for walls with tie-down anchors applied, maximum load in the tension bolts was reached at displacements slightly higher than where wall capacity was reached. The reasons for this are essentially the different failure modes and were previously elaborated in Section 5.4 (Monotonic loading). The load bolt values in Table 6.8 for walls not restrained against uplift are the maximum loads recorded by the tension bolts. The values for walls maximally restrained, however, represent the loads recorded at wall capacity, not the ultimate loads experienced by the bolts.

Table 6.8 lists a significantly higher tensile load for the bolt in Wall A (maximum amount of anchors) than the graph in Figure 6.11 actually shows. The value presented in Table 6.8 is the tensile load measured by the second load bolt (this is the only test where useful data was obtained for both load bolts). This bolt was located at the end stud away from the hydraulic actuator. To be conservative, the tensile load of the second bolt was incorporated into Table 6.8. For comparison the tensile load of the bolt close to the actuator at wall capacity was 3970 lbs.

The ratio of actual to theoretical uplift exceeds unity for Wall E with maximum amount of tie-downs. The significant smaller peak loads recorded by the bolts in walls without overturning restraint elucidate how little uplift force is transferred to the foundation in a concentrated manner if tie-down anchors are omitted. The lower force experienced by the instrumented bolts were due to the inability of the sheathing nails to transfer the overturning loads. The associated damage to the sheathing nails resulted in significantly reduced capacities of the walls.

Table 6.8: Force resisted by tension bolt at or near wall capacity

	Wall Configuration								
	no tie-down anchors <sup>(1)</sup>			anchors at end of wall only <sup>(2)</sup>			maximum amount of tie-down anchors <sup>(1)</sup>		
	A	D	E	A <sup>(3)</sup>	D	E	A <sup>(3)</sup>	D	E
F <sub>tensionbolt</sub> (lbs.)	716	475	475				5221	5228	8633
Initial wall capacity (kips)	26.7	10.1	4.8				27.7	13.4	8.4
Unit shear (lbs./ft) @ F <sub>peak, wall</sub>	668	631	400				693	838	700
Theoretical uplift (lbs.)	5340	5050	3200				5540	6700	5600
actual / theoretical	0.13	0.09	0.15				0.94	0.78	1.54

<sup>(1)</sup> These specimens had OSB sheathing

<sup>(2)</sup> Johnson (1997) did not measure uplift forces for these configurations

<sup>(3)</sup> Wall A has the same anchorage requirements for the anchors at the end of wall only and maximum amount of tie-down anchors due to being fully sheathed.

### 6.7.2 End Stud Uplift Displacement

Vertical movement (in y-direction, Figure 3.3) of the end studs relative to the bottom plate was measured. The distance traveled by the end studs between peak positive and negative interstory drifts, recorded during the initial cycle at  $\Delta_{\text{peak load}}$  and  $\Delta_{\text{failure}}$ , are given in Table 6.9. At this point, it should be mentioned that no pattern of movement for the end studs of walls without overturning restraint could reasonably be assumed. When comparing the displacements depicted in Table 6.9, recall that the values for walls without restraint were not corrected regarding geometric measurement amplification effects. Furthermore, the same error considerations apply as elaborated in Section 5.6.2 for monotonically tested walls. Thus, the figures in Table 6.9 are to be considered as approximate values only. The vertical stud movement for walls without tie-down anchors is an order of magnitude higher than for walls with anchors. This illustrates why walls tested without tie-down anchors tend to fail along the line of sheathing nails at the bottom of the wall in an unzipping manner, while walls with anchors show a distribution of load to all sheathing nails indicating a higher degree of

load sharing. However, if corner framing effects are considered, stud uplift is significantly reduced for walls without tie-down anchors (see Chapter 7)

Table 6.9: End stud displacement between positive and negative peak drifts during initial cycle of  $\Delta_{\text{peak load}}$

	Wall Configuration								
	no tie-down anchors <sup>(1)</sup>			anchors at end of wall only <sup>(2)</sup>			maximum amount of tie-down anchors <sup>(1)</sup>		
	A	D	E	A <sup>(3)</sup>	D	E	A <sup>(3)</sup>	D	E
End stud (at actuator) @ $\Delta_{\text{peak load}}$	0.90	0.77	1.06	0.14	0.10	0.10	0.16	0.15	0.18
End stud (away from actuator) @ $\Delta_{\text{peak load}}$	1.21	1.02	0.67	0.14	0.14	0.14	0.26	0.16	0.15

<sup>(1)</sup> These specimens had OSB sheathing

<sup>(2)</sup> These specimens had plywood sheathing (Dolan and Johnson 1996 a and b)

<sup>(3)</sup> Wall A has the same anchorage requirements for the anchors at the end of wall only and maximum amount of tie-down anchors due to being fully sheathed.

For all walls, vertical stud displacements increase at racking displacements beyond wall capacity. This is partly attributed to the fact that stud rotation about the anchor bolt increases with increasing drift of the wall. In case of no overturning restraints, the applied force causes the wall to separate along the bottom plate and stud uplift increases until catastrophic failure.

Since stud uplift of walls with tie-down anchors is relatively small, it is doubtful that axial loading (i.e. dead load) would increase shear load capacity for walls with maximum amount of tie-down anchors of the kind used in this investigation. Conversely, significant increases could be expected for the unrestrained walls.

### 6.7.3 Sheathing Displacement

LVDTs were incorporated in four walls tested cyclically to monitor the OSB sheathing rotation and translation relative to the framing members. These measurements should be considered as preliminary tests because the scope of this study was augmented and the measurements were included after several walls had already been tested. The

results give general information about the motion of particular sheathing panels during cyclic testing. Johnson (1997) did not record sheathing displacements. The same assumptions and limitations as discussed in Chapter 5, Section 5.6 apply here.

Figures 6.12 to 6.18 reveal the rotation and midpoint translation of the respective panels of Wall A without tie-down anchors, Wall A ultimately restrained against uplift and Walls D and E both fully restrained against uplift. Although Panel 2 in Wall E was also monitored for displacement and rotation, the data could not be analyzed because the leads to one LVDT were damaged. For clarity, only the envelope curves of the rotation angle are plotted against interstory drift. However, since there was no systematic movement of the panel midpoints, the graphs depict the consecutive displacement history. Included as white dots in the displacement graphs are positive interstory drift values that correlate the panel displacements with wall deflections. Unfortunately, due to the nature of the cyclic test, lines pertaining to larger displacements often cover the lines recorded at the beginning of the test. For that reason, a small graph showing the panel displacement up to 1 inch (25mm) interstory drift was added. The figures also contain measured panel rotation relative to the studs and relative to the top and bottom plate. Moreover, the graphs show the rotation of the end stud caused by the lozenge rotation of the framing. Drift during contraction of the hydraulic actuator was specified as positive. The reader is referred to Figure 6.19 that details the sign convention of panel rotation and specifies x- and y-directions.

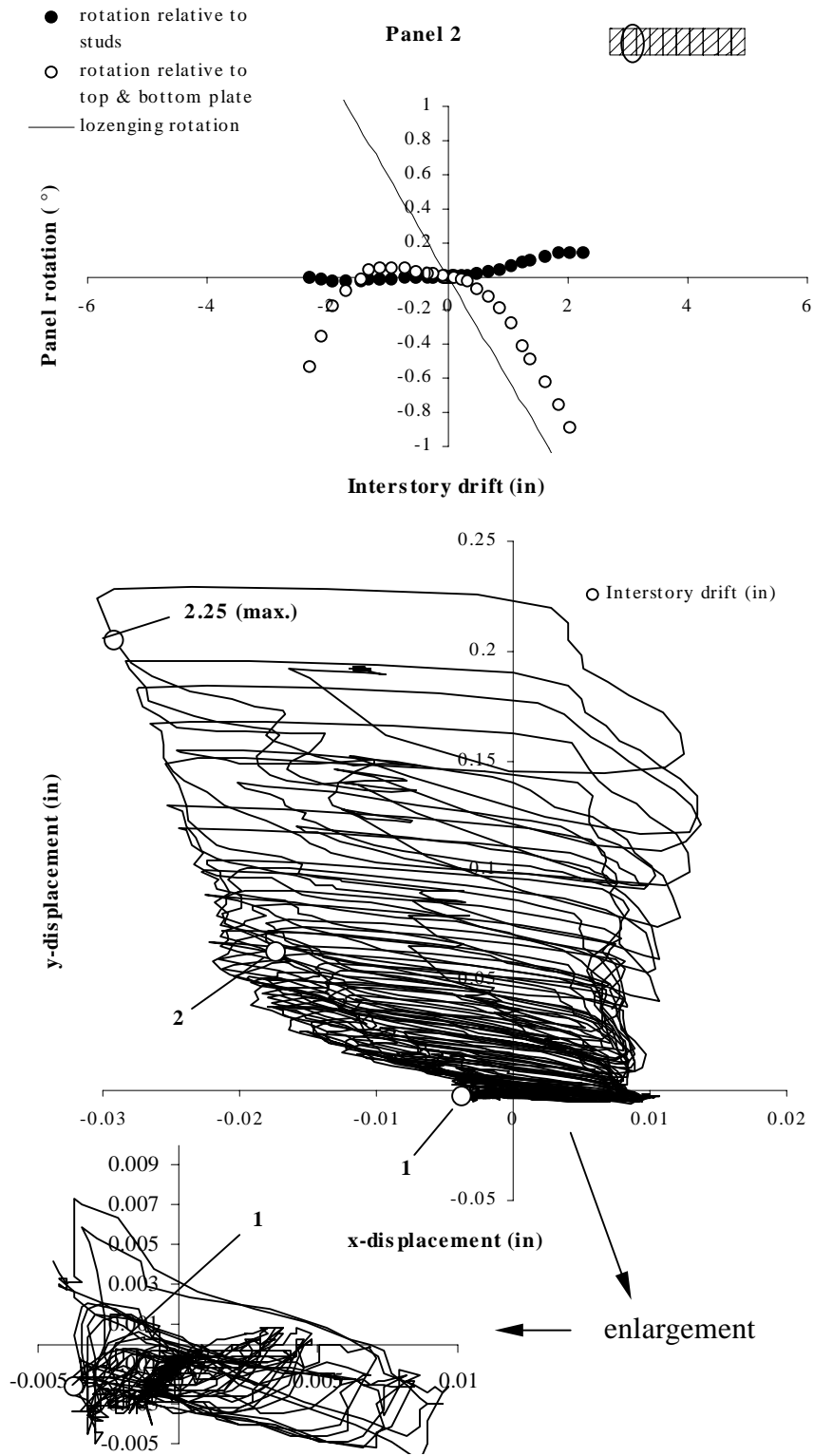


Figure 6.12: Rotation and midpoint movement of OSB Panel 2, Wall A, no anchors

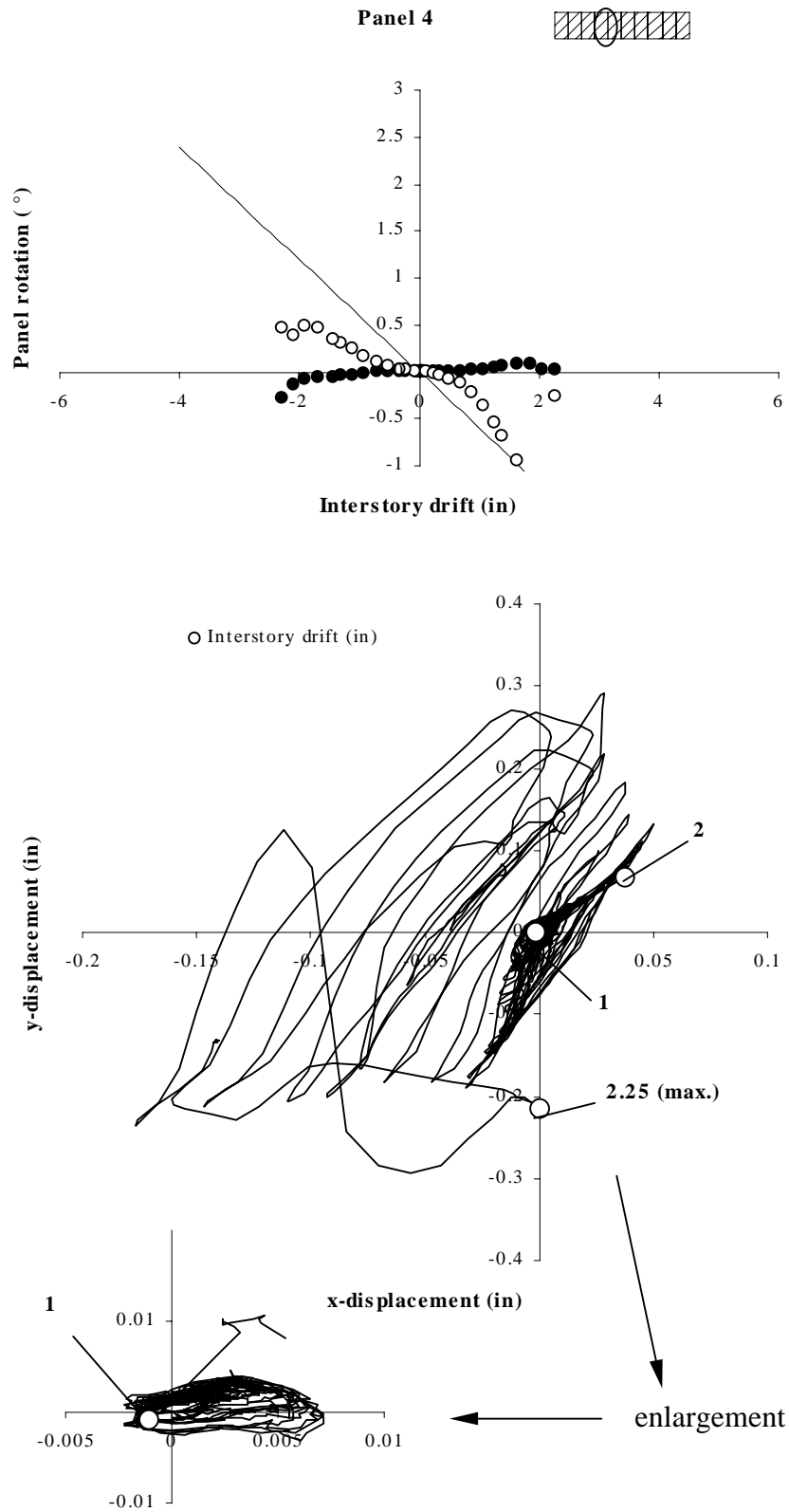


Figure 6.13: Rotation and midpoint movement of OSB Panel 4, Wall A, no anchors

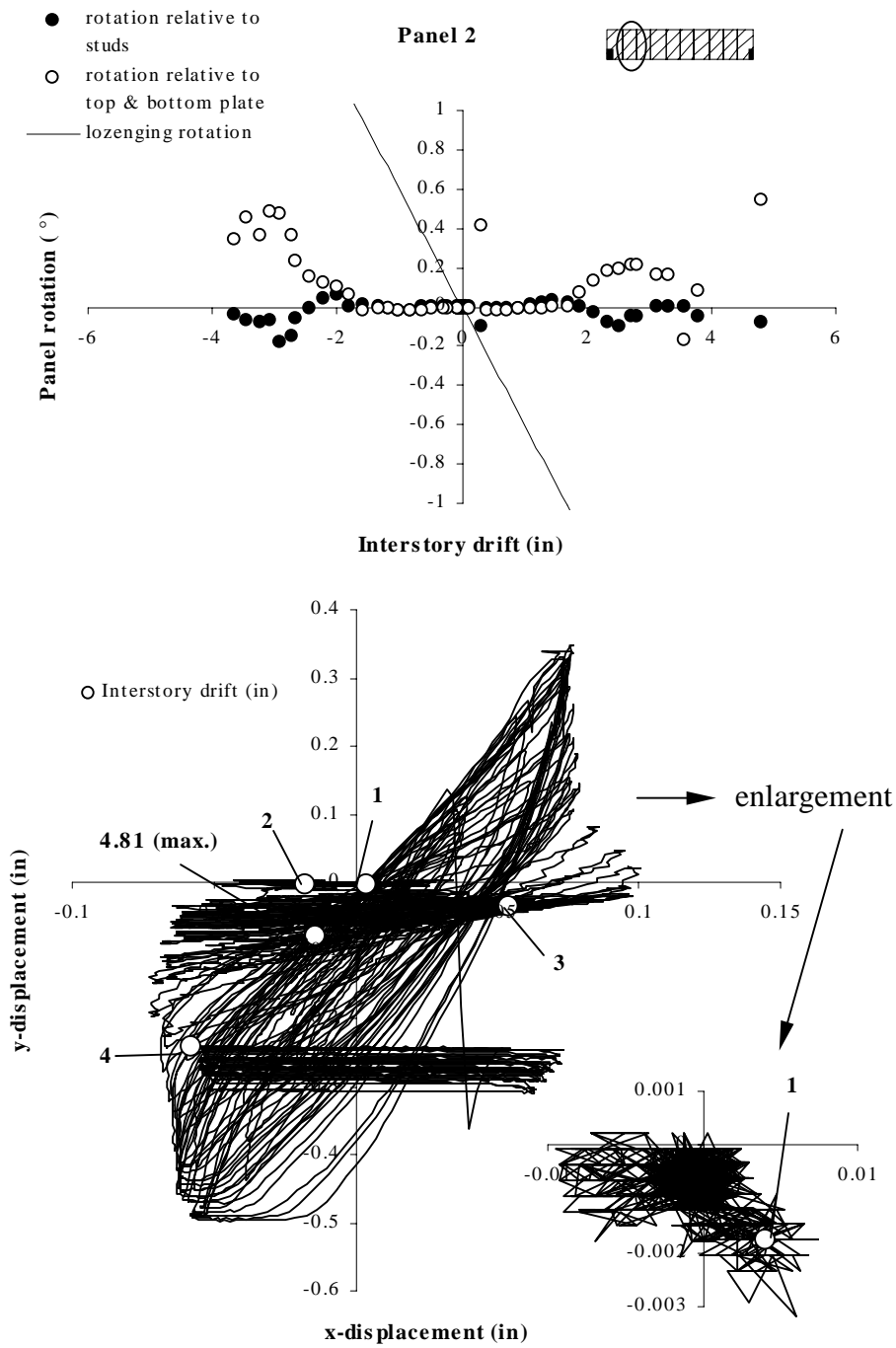


Figure 6.14: Rotation and midpoint movement of OSB Panel 2, Wall A, maximum amount of anchors

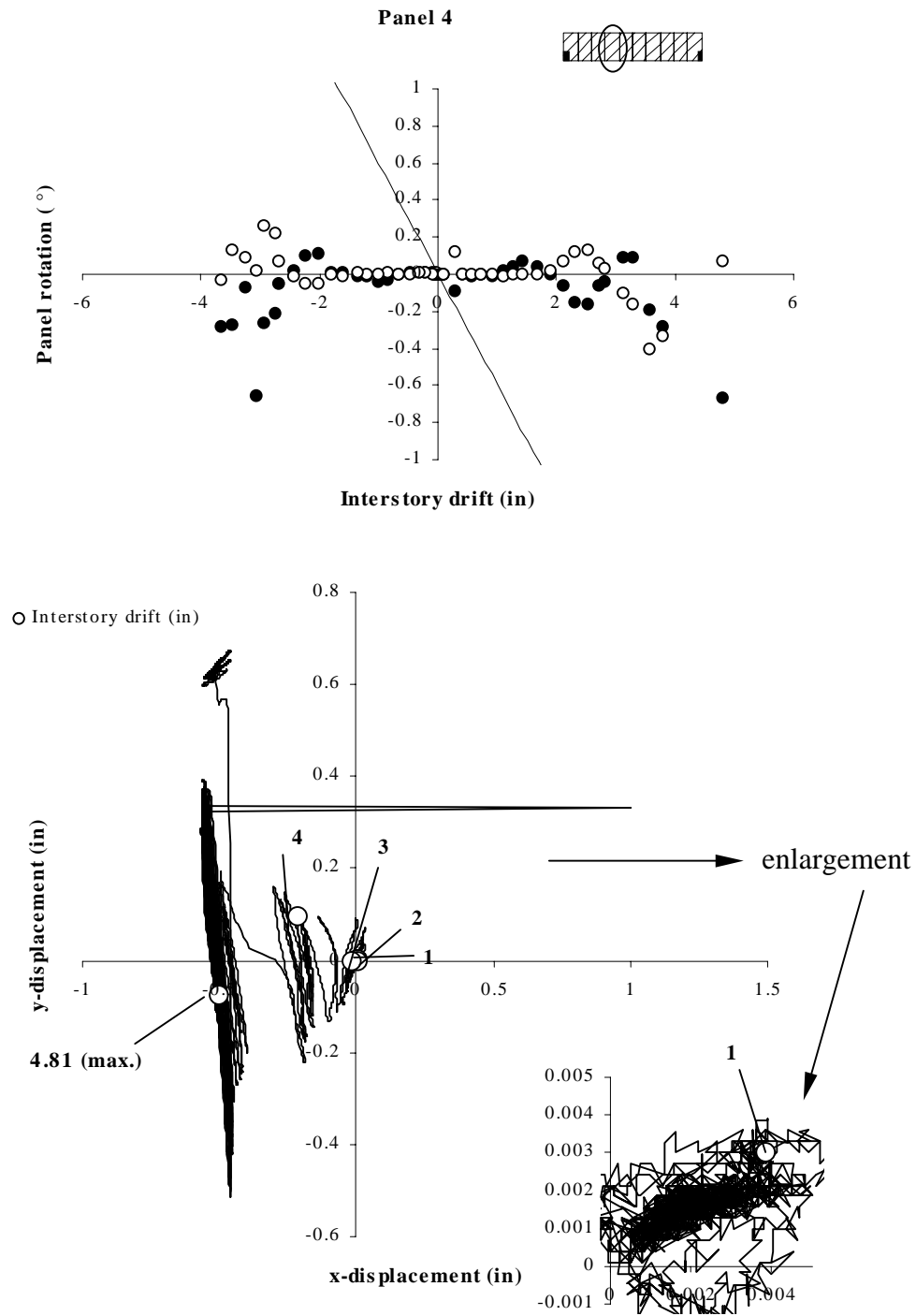


Figure 6.15 Rotation and midpoint movement of OSB Panel 4, Wall A, maximum amount of anchors

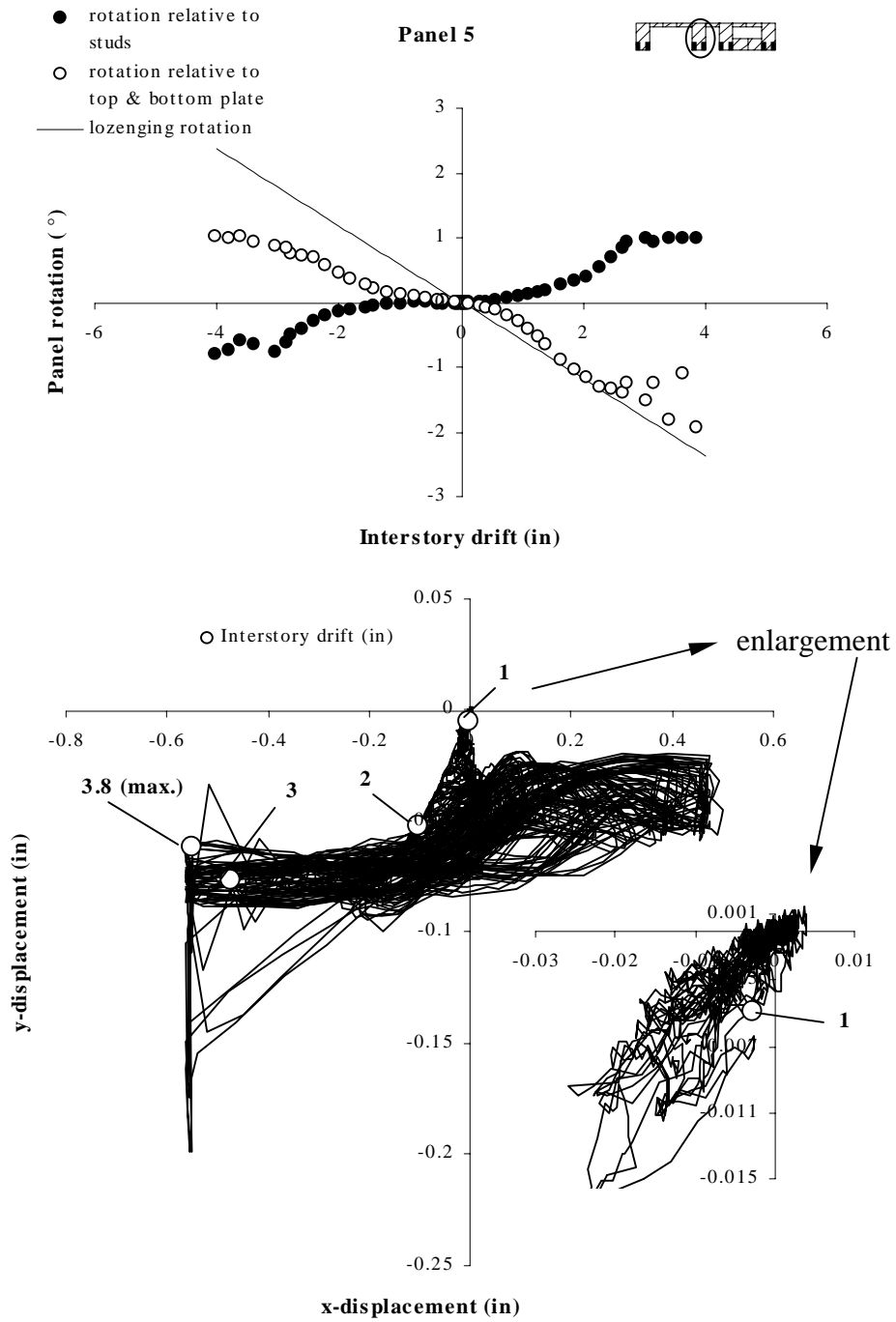


Figure 6.16: Rotation and midpoint movement of OSB Panel 5, Wall D, maximum amount of anchors

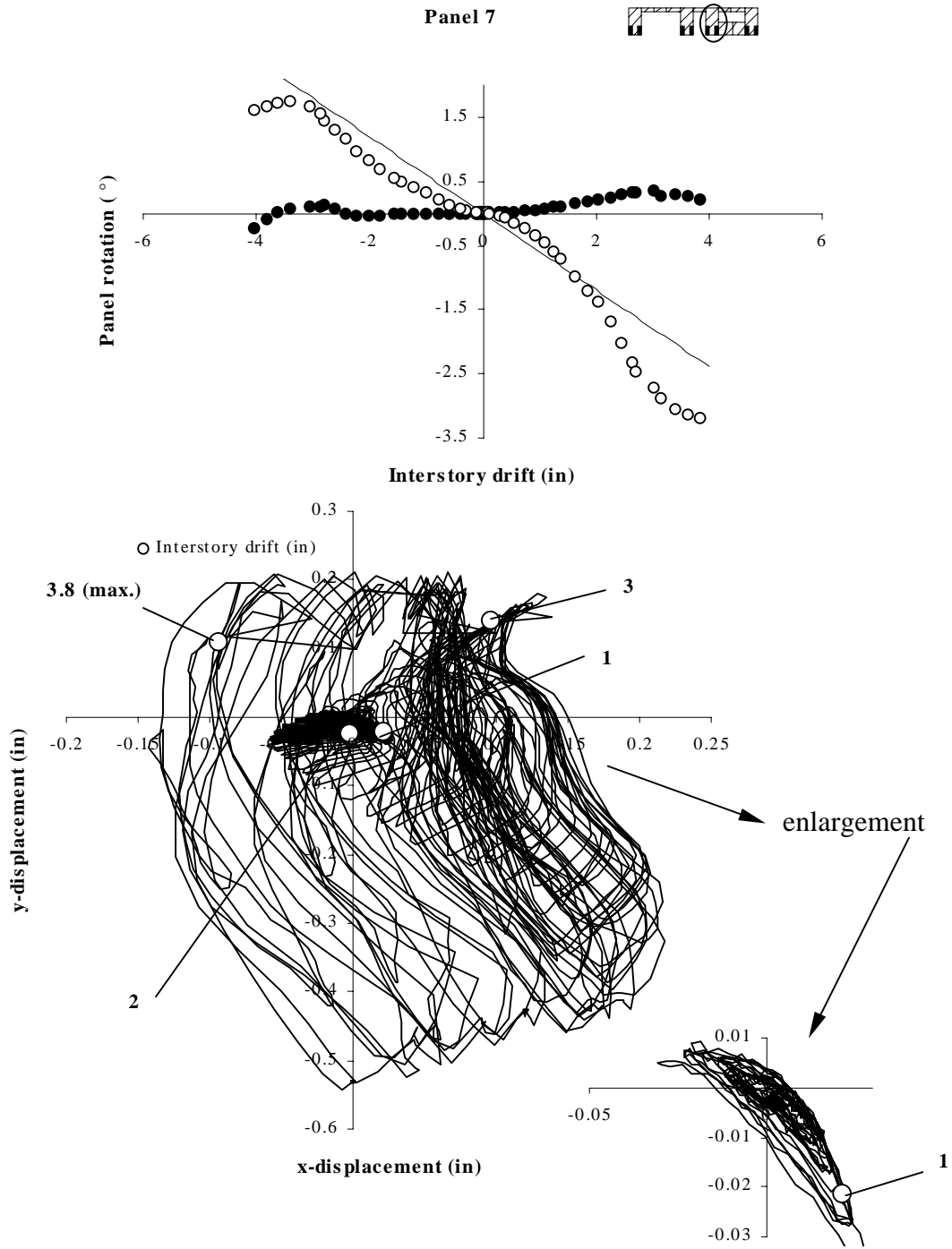


Figure 6.17: Rotation and midpoint movement of OSB Panel 7, Wall D, maximum amount of anchors

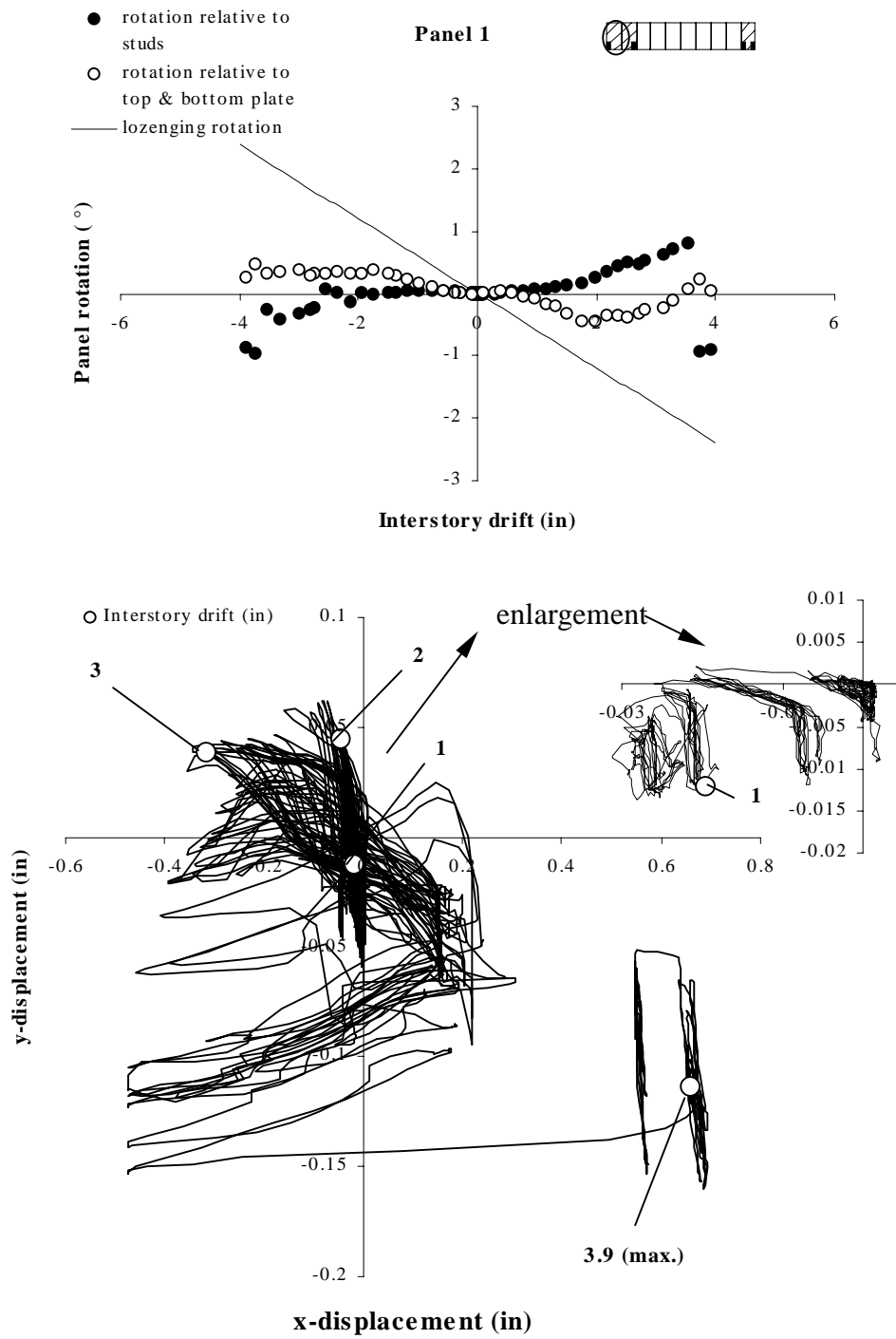


Figure 6.18: Rotation and midpoint movement of OSB Panel 1, Wall E, maximum amount of anchors

The displacement graphs in Figures 6.12 to 6.18 are not plotted in the same scale. For all walls depicted in Figures 6.12 to 6.18 the midpoint movement of the OSB sheathing is negligible up to an interstory drift of 1 inch (25mm). The displacement of the panel midpoint increases substantially after wall capacity, which is associated with nail fatigue, starting to occur. In general, the midpoint displacement relative to framing members appears to be completely random. Yet, this is not true for panel rotation. Considering the rotation graphs of Walls D and E in Figures 6.16 to 6.18, each panel rotates as expected and as displayed in Figure 6.19. It is apparent, however, that the rotation relative to the plates is higher at positive interstory drift. This trend becomes even more apparent if the measurement error of the panel rotation relative to top and bottom plate is taken into account. Due to the reduction of the normal distance between top and bottom plate when a wall is deflected in its plane, the LVDTs measured too high an angle relative to the plates at negative drifts and too low an angle at positive interstory drifts. The error greatly depends on the amount of panel rotation at the corresponding interstory drift, and becomes significant at displacements beyond capacity for all walls. The asymmetric rotation relative to the plates may be explained by the displacement history used to deflect the walls. Each progressive phase started with a positive displacement forcing the sheathing to rotate further than during previous cycles. Subsequently, sheathing panels may not have rotated back to the original position when cycled the opposite direction.

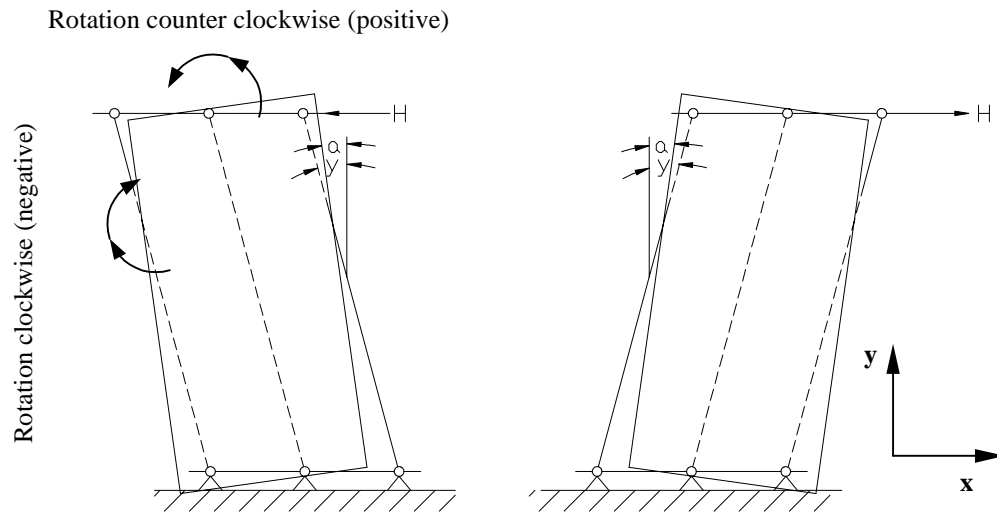


Figure 6.19: General sheathing rotation relative to the framing, cyclic loading

Included in all rotation graphs and displayed as a solid line is the lozenge rotation of the frame as a function of interstory drift. Assuming that no stud bending occurred, this value is the measured rotation angle of at least the end stud where the load was applied. As already elaborated in Chapter 5, superpositioning the two curves for panel rotation against the studs and the plates, respectively, should approximately match the lozenge rotation line. However, there are several reasons why the curves don't match exactly. First, stud bending was neglected and it is also true that the first stud does not necessarily rotate in the same manner as any other stud in the system. Furthermore, as elaborated in Chapter 5, the actual lozenge rotation was less due to uplift. Second, the reduction of the normal distance between top and bottom plate adds an error to the data. Third, beyond drift at failure, the data becomes unreliable because the cores of the LVDTs were sometimes caught between sheathing and framing. And last, the shear distortion of the sheathing was neglected and it was assumed that the sheathing does not bend and rotates as a rigid body. However, this assumption is reasonable since the distortion is insignificantly small compared to wall deflection (Chapter 5, Section 5.6).

There is no match with the frame lozenge rotation when superpositioning the two rotation curves for wall configuration A with maximum amount of anchors. Graphs of panel rotation for this wall (Figure 6.14 and Figure 6.15) are substantially different

than the graphs discussed above. Rotation angles relative to top and bottom plates are significantly smaller. Further, the directions of these rotations are not in accord with the simple diaphragm theory depicted in Figure 6.19. Another perceptible difference is that up to the displacement at capacity (Table 6.4) the rotation relative to the studs and the plate is almost zero. It is possible that the sheathing panels rotated less because the walls were fully sheathed. But it is fact that each wall was deflected the same amount. Therefore, despite the sheathing rotation being less, the studs still rotate relative to the sheathing. This rotation increases as the total sheathing rotation decreases. Yet, this is not reflected in the graphs of Figures 6.14 and 6.15. Considering the conspicuous resemblance of both rotation graphs of Panels 5 and 7 it is likely that the data acquisition system did not record the data correctly.

In case of Wall A without tie-down anchors, the wall unzipped across the bottom plate during the test (Figure 6.12). This resulted in a rigid body rotation of the wall as a whole and enhanced top plate bending, especially at negative drifts. At larger displacements, the wall unzipped along the bottom plate starting at the extreme ends. Since the LVDT in Panel 2 was located close to the end of the wall, the recorded data was altered by the separation of studs and bottom plate (refer to Figure 3.5 that specifies LVDT locations). This may explain why the rotation angle relative to the plates of Panel 2, that was closest to the applied load, is so much smaller and even changes direction at negative interstory drifts. Panel 4 rotated as expected (Figure 6.13).

#### **6.7.4 General Observations**

To be consistent with the monotonic tests, these tests were performed without an applied dead load in order to test the most conservative condition. As previously stated, dead load may have reduced the damage to the nails attaching the sheathing to the bottom plate in these regions, and the result may have been an improved overall performance.

The predominant mode of failure for walls with maximum overturning restraint was nail fatigue between framing and OSB sheathing at larger displacements (greater than that associated with wall capacity), and nail tear through at the top and bottom of sheathing panels after peak load was reached. Nail fatigue evolved because the clamping

force of the framing around the nail shank was so high that the nail only partially withdrew and developed two plastic hinges according to Mode IV (Chaper 2, Figure 2.1). During successive cycles, the nail reversibly bent about the same location and eventually failed.

Close to capacity, OSB panel edges between adjacent panels started to interfere and fail in bearing. At larger displacements, much greater than at capacity, studs and sheathing started to separate from the top plate, especially at the end of the wall away from the applied load. Nails attaching OSB sheathing to the framing partially withdrew on the perimeter of the panels near corners, but failed predominantly due to fatigue.

Walls with no overturning restraint separated almost completely from the bottom plate at large displacements, which was the typical failure mode. Panels above and below openings, more or less, rotated as rigid bodies. Nail fatigue occurred less in walls with no tie-down anchors than in walls with maximum amount of tie-down anchors because the racking of the sheathing relative to the framing was less distinct.

Bolts attaching the bottom plate were located a minimum of 12 inches away from the studs adjacent to openings. This resulted in the bottom plate lifting when the stud next to an opening was in tension and did not have a tie-down anchor to resist the force. In turn, the nails attaching the sheathing to the bottom plate had to transfer this tension and were damaged significantly more than nails near tie-down anchors.

Gypsum panels were observed to be damaged quickly during the cyclic tests. Even at low displacement magnitudes, drywall nails tore a path in the gypsum panels. Taped joints failed at lower interstory drifts than during monotonic tests. This matches experience in large magnitude seismic events (APA 1994).

## **6.8 Summary**

Six long fully-sheathed and perforated walls were tested under SPD loading providing quantitative information about earthquake performance and the effect of overturning restraint. Based on the results that have been presented, the following conclusions can be drawn:

- 1) Ultimate capacity of walls subjected to SPD loading increased with increasing overturning restraint. The increase was greatest for walls containing the largest openings.
- 2) The strength reduction from initial to stabilized response was 14 percent and practically constant.
- 3) Elastic stiffness was positively correlated with the amount of tie-down anchors, whereas, cyclic stiffness was not significantly influenced by the different anchorage conditions. For all six walls, cyclic stiffness degraded and approached zero.
- 4) EVDR's within the elastic range were between 8 and 14 percent. Damping ratios were fairly constant beyond the elastic range with values for unrestrained walls being slightly higher than for walls containing anchors.
- 5) Gypsum panel sheathing was observed to perform poorly during the reversed cyclic tests. Extensive damage to gypsum sheathing around nails and taped joints occurred.
- 6) Typical failure mode for walls with no tie-down anchors was the almost complete separation of studs and sheathing from the bottom plate. The predominant mode of failure for walls with maximum overturning restraint was nail fatigue and nail tear through on the perimeter of the OSB panels.
- 7) The perforated shear wall design approach gives highly conservative values when predicting shear strength ratios for cyclically tested walls. It was found that Equation 4.6 developed by Sugiyama (1994) more accurately predicts shear strength ratios at ultimate capacity than does Equation 4.4.

## Chapter 7

### SPD Test Results of Walls with Corners and Discussion

#### 7.1 General

Two mutually perpendicular walls provide some uplift restraint when intersecting in the corner of a building. In order to quantify the uplift restraint of corners, four walls, 12 foot (3.7m) in length and 8 foot (2.4m) in height with 4 foot (1.2m) by 8 foot (2.4m) and 2 foot (0.6m) by 8 foot (2.4m) corner segments attached were included in this study. Each configuration was tested twice using the sequential phased displacement (SPD) pattern as described in Chapter 3. As with the SPD tested straight walls, the data analysis includes the determination of performance indicators such as capacity, yield strength, elastic and cyclic stiffness, and ductility. In addition, for future reference, equivalent viscous damping ratios are computed for each configuration. Uplift forces and stud and sheathing displacements are also presented.

The investigation conducted here covers only a small portion of what is necessary to fully understand the interaction of two mutually perpendicular walls. Due to the small number of specimens and configurations tested, the results are to be viewed as preliminary.

#### 7.2 Load-Drift Relationship

The SPD test protocol could not be performed completely because every corner wall specimen tested had entirely separated from the bottom plate at around 2 inch (51mm) interstory drift. The obtained initial load versus interstory drift envelope curves are depicted in Figure 7.1. Table 7.1 includes information about initial and stabilized peak loads and equivalent elastic plastic parameters.

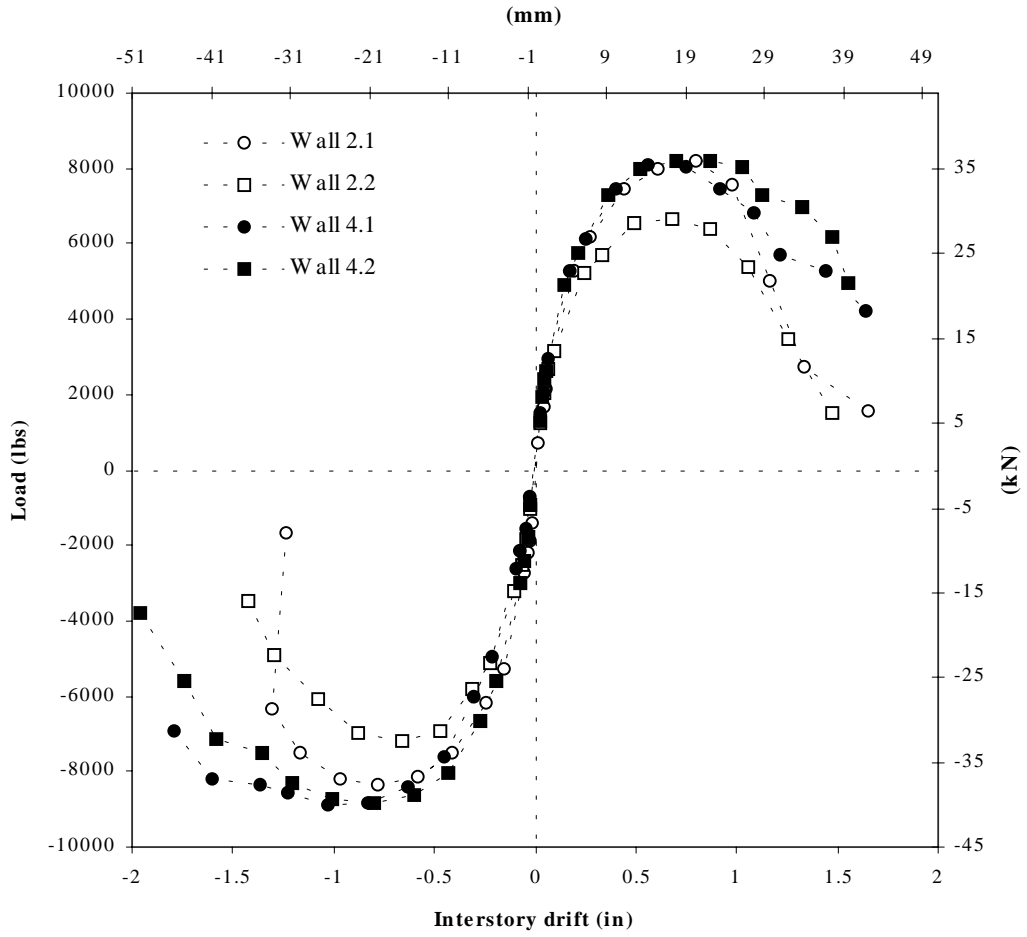


Figure 7.1: Initial load vs. interstory drift envelope curves of all corner walls

Table 7.1: Initial cyclic and stabilized cyclic load resistance data

	Wall Specimen					
	2ft corners			4ft corners		
	Wall 2.1	Wall 2.2	average	Wall 4.1	Wall 4.2	average
<b>Capacity</b>						
Initial SPD (kips)	8.3	6.9	7.6	8.5	8.5	8.5
Stabilized SPD (kips)	6.8	5.6	6.2	7.2	7.1	7.2
Stabilized/Initial	0.82	0.82	0.82	0.84	0.84	0.84
<b>F<sub>yield</sub></b>						
Initial SPD (kips)	7.5	6.2	6.8	7.7	7.8	7.8
Stabilized SPD (kips)	6.1	5.1	5.6	6.5	6.5	6.5
Stabilized/Initial	0.82	0.82	0.82	0.84	0.84	0.84
<b>Elastic Stiffness</b>						
Initial SPD (kips/in)	38.7	36.8	37.7	32.3	39.9	36.1
Stabilized SPD (kips/in)	44.7	39.7	42.2	35.9	44.2	40.1
Stabilized/Initial	1.15	1.08	1.12	1.11	1.11	1.11

Note: The numbers presented are rounded. All calculations were done with original values.

The walls with 2 foot wide corners attached show a fairly high variation in capacity. The sample size of two walls is not sufficient to make inferences whether the variation is due to statistical error. Additional tests are needed to obtain more reliable results. However, the values obtained from walls with 4 foot corners are almost equivalent. On average, walls with 4 foot long wing walls reached higher ultimate capacities than walls with shorter, 2 foot long, perpendicular segments. The average reduction between initial and stabilized capacity was 17 percent (Std. Dev. =1.1%) and practically constant. This indicates that the damage experienced by the walls is fairly uniform regardless of the length of perpendicular wall segments attached, implying that the performance of timber framed shear walls is primarily governed by the sheathing nails.

Elastic stiffness, was not significantly influenced by the length of the corner segments. Figure 7.1 clearly shows that within the elastic range, the four initial envelope curves almost coincide. Stabilized stiffness was consistently higher than initial stiffness

(Table 7.1). The reason is found in the definition of elastic stiffness (refer to Chapter 4). In the elastic range, stabilized and initial envelope curves coincide. Since stabilized capacity will always be lower than initial capacity the secant of stabilized elastic stiffness will pass through a point on the envelope curve closer to origin where the curve has a steeper slope. Consequently, the slope of the secant is also steeper and the stiffness is higher. The ratio of stabilized to initial elastic stiffness is therefore similarly constant as the ratio of stabilized to initial capacity. However, cyclically tested straight walls did not show this trend. The interstory drift at 40 percent  $F_{\text{peak}}$  was found by interpolation between two adjacent data points. Since the capacity of the shorter corner walls is obviously less than the capacity of straight 40 feet long walls, the data points on the load envelope curve are closer together, especially within the elastic region. Hence, an interpolation is more accurate. This explains why the stabilized elastic stiffness for straight walls was not consistently higher than the initial stiffness.

The same variation that occurred between ultimate capacity values of the two walls with 2 foot long perpendicular segments is reflected in the  $F_{\text{yield}}$  values. As with the recorded ultimate capacities,  $F_{\text{yield}}$  increased with increasing corner length.

### 7.3 Ductility

Ductility as presented in Table 7.1 was determined by dividing the positive and negative interstory drift at failure by the respective positive and negative interstory drift at yield load and by taking the average of the absolute results (Chapter 4). Note that both  $\Delta_{\text{yield}}$  and  $\Delta_{\text{failure}}$  values listed in Table 7.1 are average values and may yield a slightly different ductility. Since drift at yield load is decisively dependent upon initial stiffness, stabilized ductility values in Table 7.2 are consistently higher than pertinent initial values, as expected. Average initial ductility values for both wall configurations are equivalent. However, considering Figure 7.1, the walls with 4 foot corner framing sustained higher loads beyond failure than the walls with the shorter corner segments, indicating a tougher (or more robust) structural response. This is reflected in the higher drifts at failure of

Walls 4.1 and 4.2, suggesting that interstory drift at failure may be a better measure to compare ductile behavior among walls with the same height.

Table 7.2: Corner wall ductility

	Wall Specimen					
	2ft corners			4ft corners		
	Wall 2.1	Wall 2.2	average	Wall 4.1	Wall 4.2	average
$\Delta_{\text{yield}}$						
Initial SPD (in)	0.2	0.2	0.2	0.3	0.2	0.2
Stabilized SPD (in)	0.1	0.1	0.1	0.2	0.1	0.2
$\Delta_{\text{failure}}$						
Initial SPD (in)	1.1	1.1	1.1	1.4	1.3	1.4
Stabilized SPD (in)	1.0	1.0	1.0	1.3	1.4	1.4
Ductility						
Initial SPD ductility	5.9	6.5	6.2	5.8	6.6	6.2
Stabilized SPD ductility)	7.6	7.4	7.5	6.9	9.5	8.2
Stabilized/Initial	1.29	1.14	1.21	1.19	1.44	1.32

Note: The numbers presented are rounded. All calculations were done with original values.

## 7.4 Earthquake Performance

In general, it is desired that a structure shows the ability to dissipate large portions of the excitation energy to limit internal stresses. The energy dissipation characteristic is reflected by the equivalent viscous damping ratio. In addition to energy dissipation, the response of an earthquake excited structure is determined by its stiffness. The higher the stiffness the higher will be inherent inertia forces the structure has to withstand. On the other hand, if the structure is not stiff enough, damage arising from large deformations will occur.

### 7.4.1 Equivalent Viscous Damping

One can note the effect of corner length on equivalent viscous damping ratios (EVDR) when considering the graphs in Figure 7.2. The two walls with the shorter

corners attached show slightly higher EVDRs at drifts beyond the elastic limit. The reduced hold-down effect of the narrower corner framing led to more pronounced rigid body rotation of the structure and increased separation along the bottom plate. Rigid body rotation due to uplift and progressive separation along the bottom plate was an indifferent movement that did not add potential energy to the system. At a given interstory drift, the linear peak potential energy was lower for walls with 2 foot transverse segments, accordingly. The same effect explains the slight upward trend of all EVDRs with increasing wall displacements since the separation along the bottom plate increased with increasing drifts.

It is noteworthy that as wall displacements increase, between elastic range and failure, the EVDRs approach the value 0.16 which is  $1/(2\pi)$ . This indicates that beyond the elastic limit, linear peak potential energy and hysteretic energy approach the same value.

As already elaborated in Chapter 6, inherent to its definition, EVDR can only be an approximation for timber structures as such structures exhibit no purely viscous behavior. This is especially true when the structure is loaded beyond the elastic limit. For future reference, EVDRs in the elastic range are listed in Table 7.3.

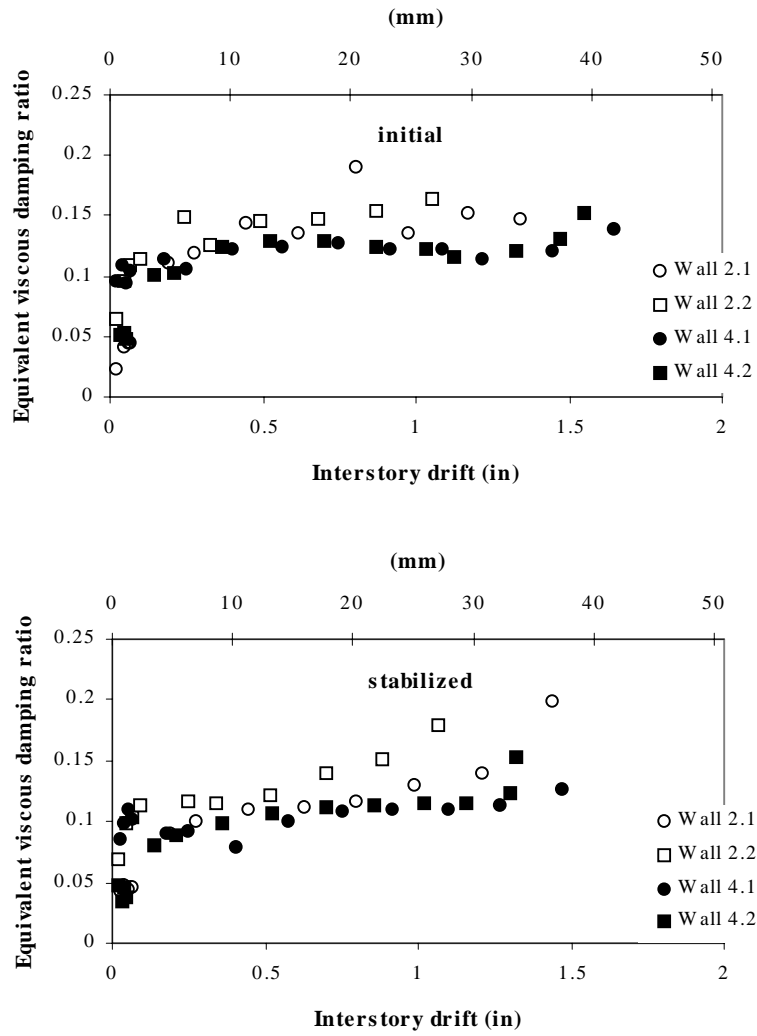


Figure 7.2: Initial and stabilized EVDR vs. interstory drift of all corner walls

Table 7.3: EVDR from the first three phases of SPD loading (elastic range)

	Interstory drift (in)	Wall Specimen			
		2ft corners		4ft corners	
		Wall 2.1	Wall 2.2	Wall 4.1	Wall 4.2
Initial					
	0.03	0.02	0.07	0.10	0.05
EVDR	0.05	0.04	0.10	0.11	0.05
	0.08	0.04	0.11	0.10	0.05
Stabilized					
	0.03	0.04	0.07	0.09	0.05
EVDR	0.05	0.05	0.10	0.10	0.03
	0.08	0.04	0.10	0.11	0.05

#### 7.4.2 Cyclic Stiffness

Light-frame structures have performed well during earthquakes because of stiffness degradation. Decline in stiffness of light-frame shear walls causes the natural frequency to differ from the excitation frequency, and a condition of sustained resonance is never encountered. The cause of stiffness degradation in reversed cyclically loaded timber structures is discussed in Chapter 6 and is also applicable to walls containing corner framing. Cyclic stiffness degrades exponentially and approaches zero as wall displacement increases (Figure 7.3). More nails being inelastically loaded at higher interstory drifts explain the exponential decrease. Zero stiffness is a result of entire detachment between bottom plate and wall sheathing and stud. Among the four walls, there is almost no difference in cyclic stiffness at a given interstory drift suggesting that stiffness degradation is governed by the amount of fasteners in the wall system rather than the length of corner framing.

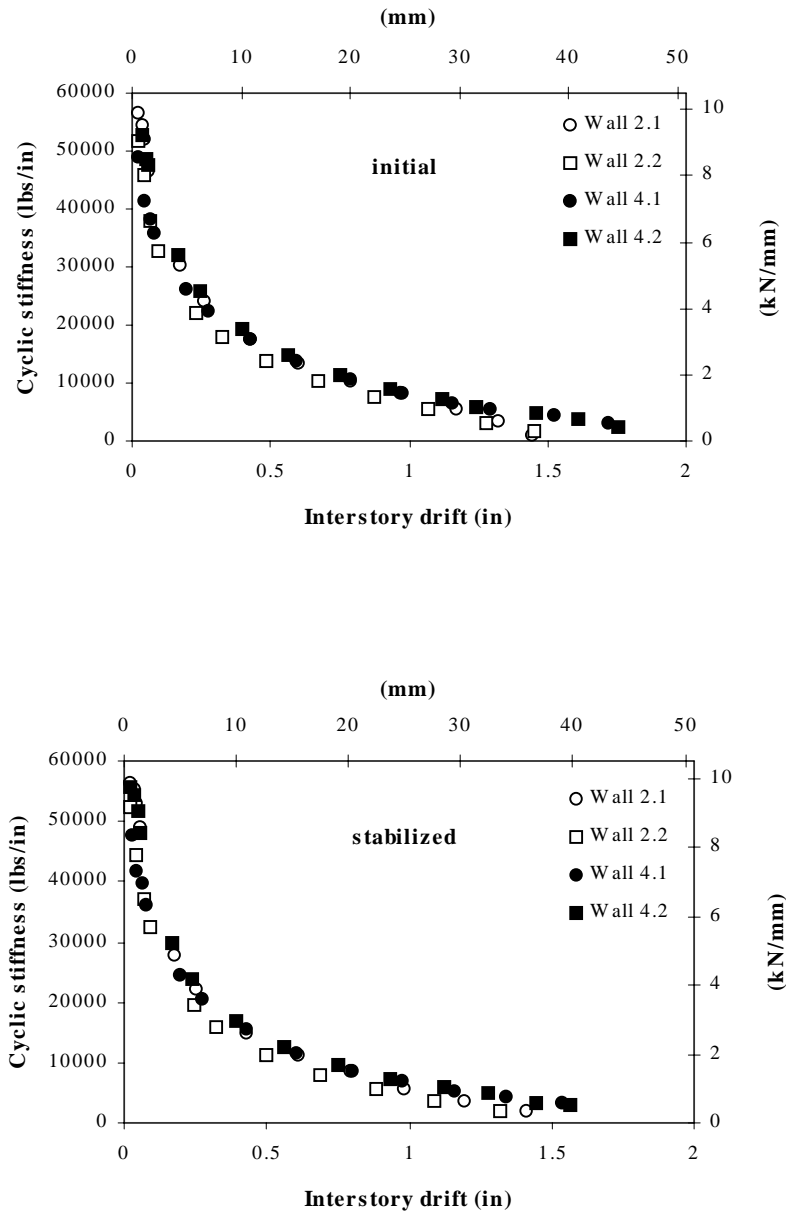


Figure 7.3: Initial and stabilized cyclic stiffness of all corner walls

## 7.4 Overall Wall Response

### 7.4.1 Tension bolts

Recorded tension loads measured by the instrumented bolts located adjacent to each end stud (circled area) are shown in Figures 7.4 through 7.7. Each graph also contains the respective load envelope curve pertaining to positive or negative interstory drifts. The tension load bolt of Wall 4.1 located away from the actuator did not record data due to damaged wires. Considering the graphs, it becomes apparent that the data acquisition system did not function properly. All curves are offset with extremely varying amplitudes among wall configurations. Possibly the amplifier setting was erroneous. The data is highly unreliable, which should be considered when making judgments about wall performance. However, the trends in tension load versus interstory drift are similar to those seen for straight wall segments indicating a similar hold-down response. The load amplitudes recorded are lower for walls with 4 foot corner segments than for walls with shorter, 2 foot segments suggesting an increased hold-down effect of the longer transverse walls.

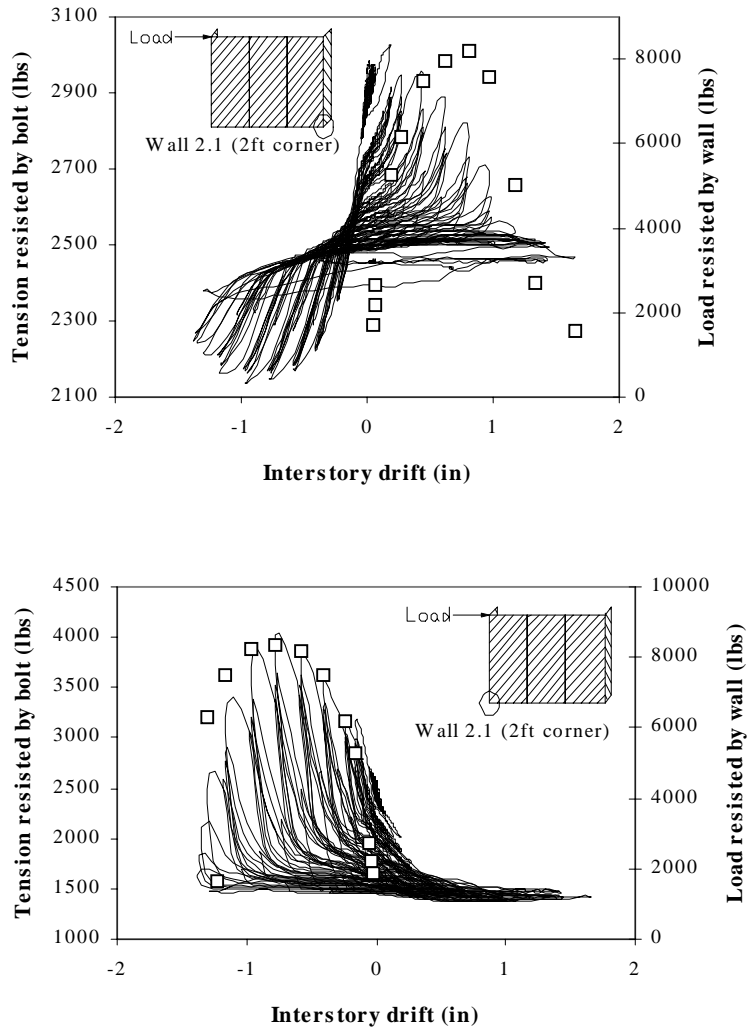


Figure 7.4: Resisted load by tension bolts of Wall 2.1 with 2 foot corner framing along with the corresponding initial load envelope curve

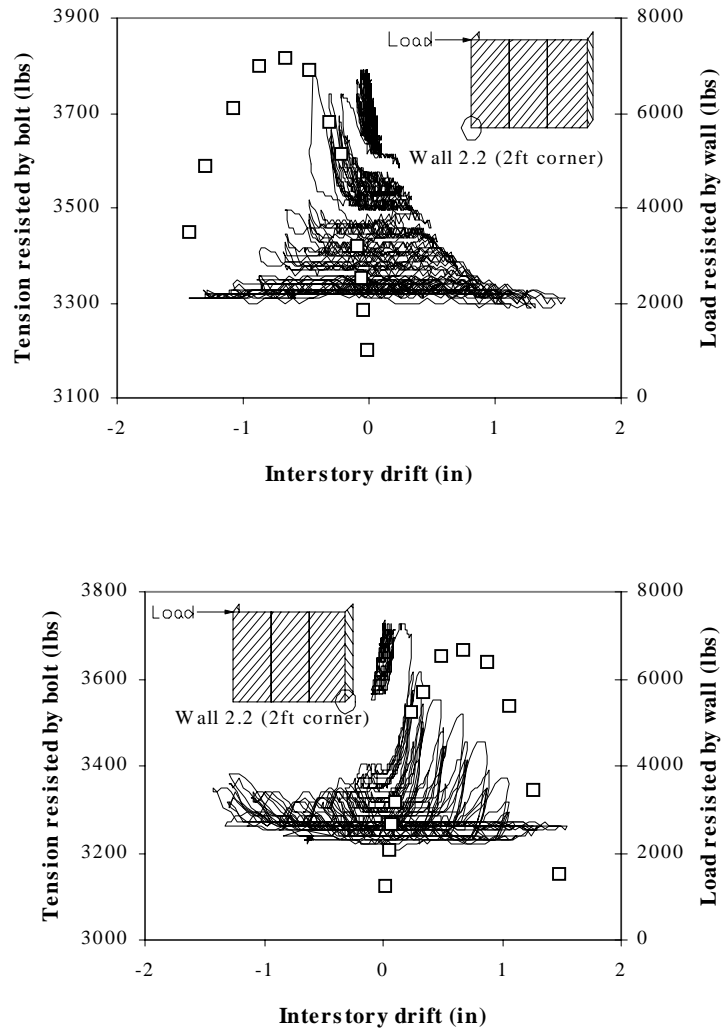


Figure 7.5: Resisted load by tension bolts of Wall 2.2 with 2 foot corner framing along with the corresponding initial load envelope curve

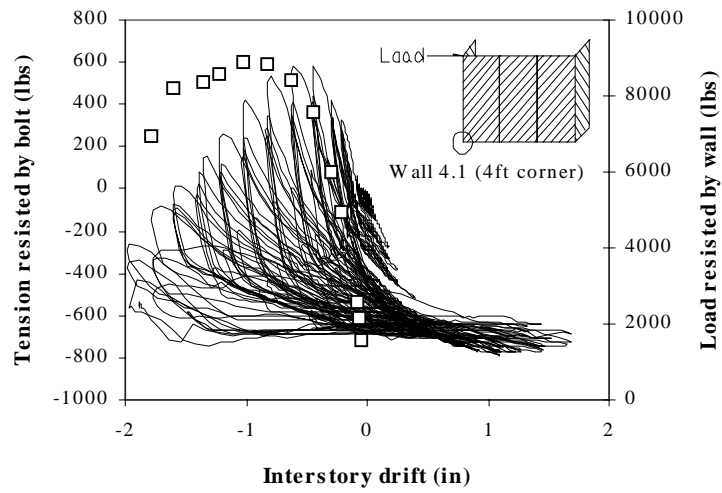


Figure 7.6: Resisted load by tension bolts of Wall 4.1 with 4 foot corner framing along with the corresponding initial load envelope curve. Leads to one bolt were defective.

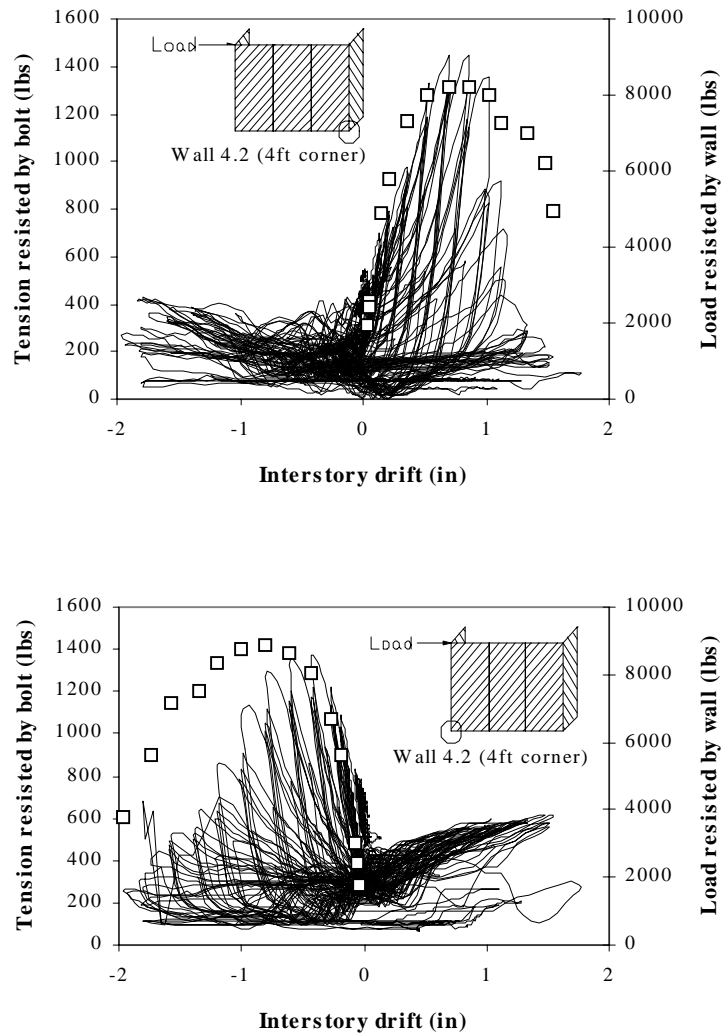


Figure 7.7: Resisted load by tension bolts of Wall 4.2 with 4 foot corner framing along with the corresponding initial load envelope curve

### 7.4.2 End Stud Displacement

The recorded compression and uplift displacement of the stud in each corner was corrected to compensate amplifications caused by the geometry of the LVDT fixture (Section 3.2.4). The walls were assumed to rotate about the outer bottom edge of either wing wall depending on the direction of the load exerted on the wall. Table 7.4 lists the total displacements of both corner studs at ultimate capacity and at failure of the walls with 2 foot and 4 foot wide corner framing and of the 40 feet long straight walls tested and described in Chapter 6.

Table 7.4: End stud displacement between positive and negative peak drifts during initial cycle of  $\Delta_{\text{peak load}}$  and  $\Delta_{\text{failure}}$

	Wall Specimen			
	12 ft Walls with corner framing		40 ft walls no corner framing	
	2 ft corner <sup>(1)</sup>	4 ft corner <sup>(1)</sup>	no overturning restraint <sup>(2)</sup>	overturning restraint <sup>(1)</sup>
End stud (at actuator) @ $\Delta_{\text{peak load}}$	0.64	0.64	0.90	0.15
End stud (away from actuator) @ $\Delta_{\text{peak load}}$	0.70	0.57	1.21	0.20
Theoretical uplift @ capacity (lbs.)	5056	5664	5340	5968

<sup>(1)</sup> Average values out of two specimens

<sup>(2)</sup> Values obtained from one specimen only

<sup>(3)</sup> Data not available due to failure mode

The values suggest that perpendicular wall segments reduce the uplift by providing some hold-down effect. On average, total stud movement at capacity was reduced by 36 percent and 41 percent for walls with 2 foot and 4 foot wide corner framing, respectively, compared to a straight wall with no overturning restraint.

### 7.4.3 Sheathing Displacement

Each corner wall contained four internal LVDTs that monitored the drift and rotation of the middle OSB sheathing panel relative to top plate, bottom plate and studs. As previously mentioned, shear distortion of the sheathing panel was assumed to be zero, as was stud bending and the reduction of the normal distance between top and bottom plate (refer to section 5.6.3).

Uplift displacement and detachment of bottom plate from the wall influenced the recording of the panel rotation and midpoint translation (Figures 7.8 through 7.11). The midpoint of each panel conspicuously moved in positive y-direction (Figure 7.12). The magnitude of that translation was more than 0.1 inch (2.5mm) at 1 inch (25mm) interstory drift in three specimens (small graphs in Figures 7.8 through 7.11). However, this translation is more or less the recorded movement relative to the bottom plate only. Considering the circled LVDT in Figure 7.12, it becomes clear that during separation of wall and bottom plate, this device extended and recorded a panel movement. Since the walls were relatively short, separation started at each end, and according to the drift history of the panel midpoint, the walls literally “withdrew” from the bottom plate by rotating about the outer edge of each end stud. At 1 inch (25mm) interstory drift, the magnitude of withdrawal did not significantly differ among the two wall configurations. Whether the midpoint translation was in the positive or negative x-direction in relation to the studs seems to be arbitrarily.

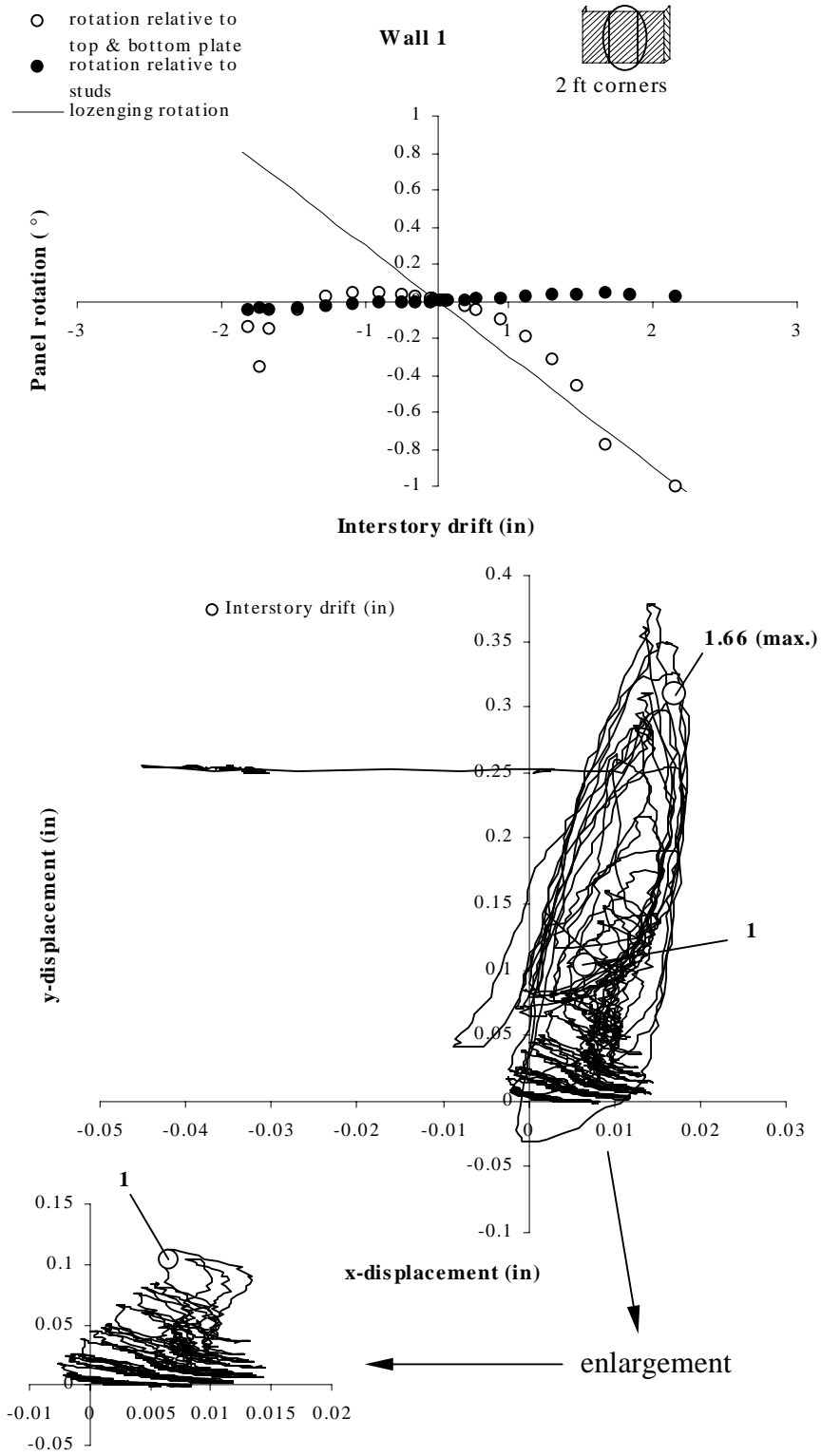


Figure 7.8: Rotation and midpoint translation of the mid OSB panel, Wall 2.1

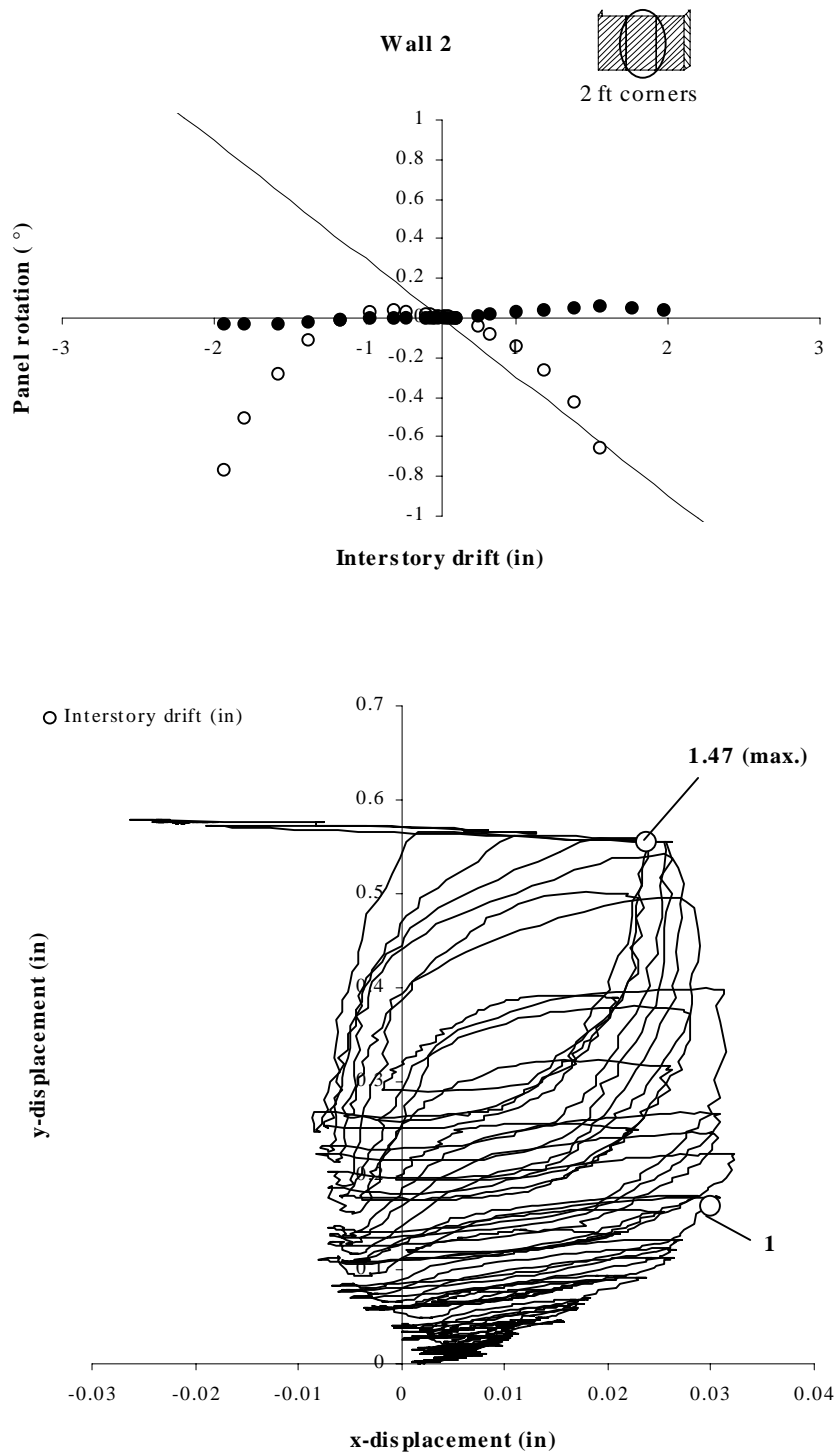


Figure 7.9: Rotation and midpoint translation of the mid OSB panel, Wall 2.2

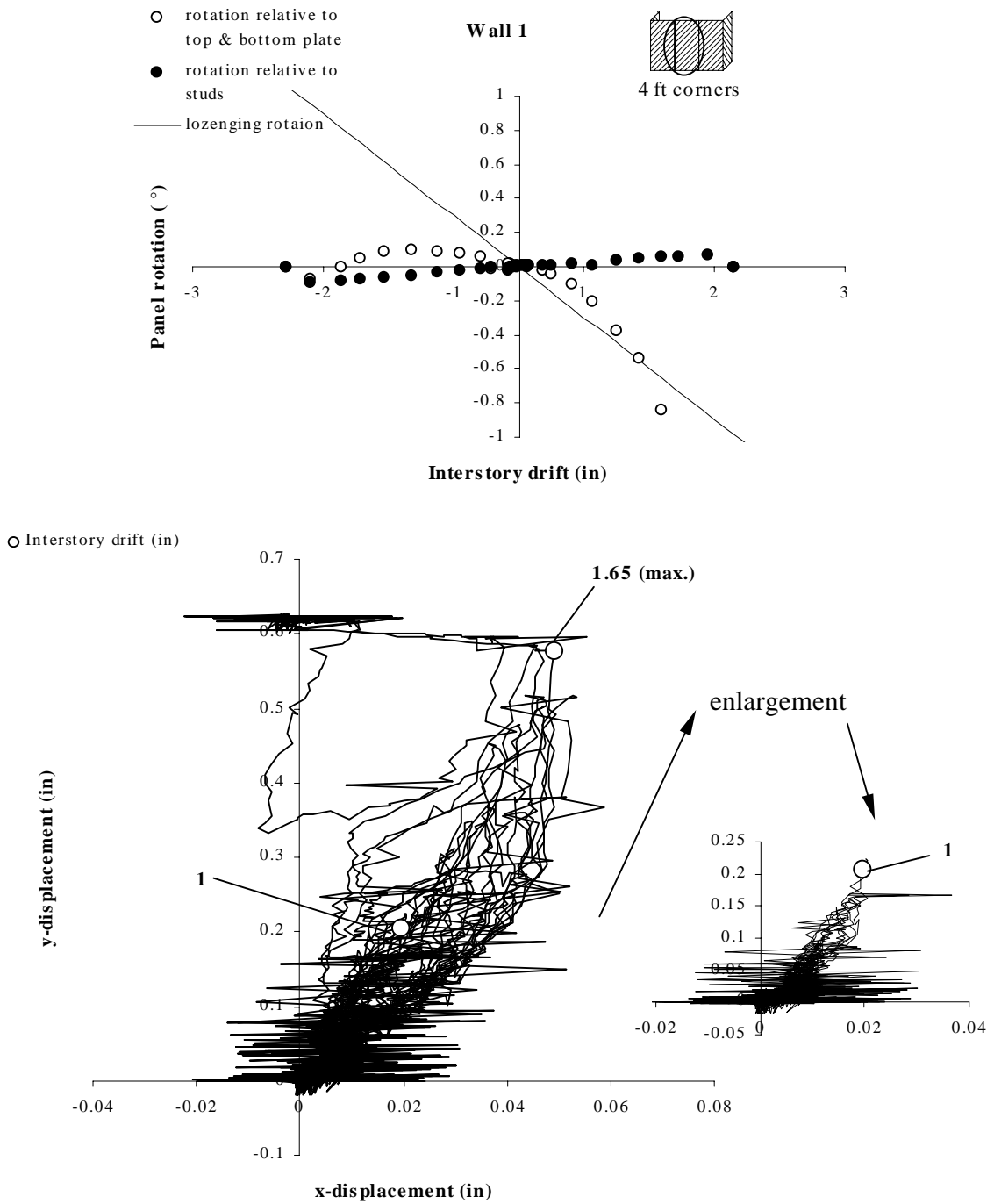


Figure 7.10: Rotation and midpoint translation of the mid OSB panel, Wall 4.1

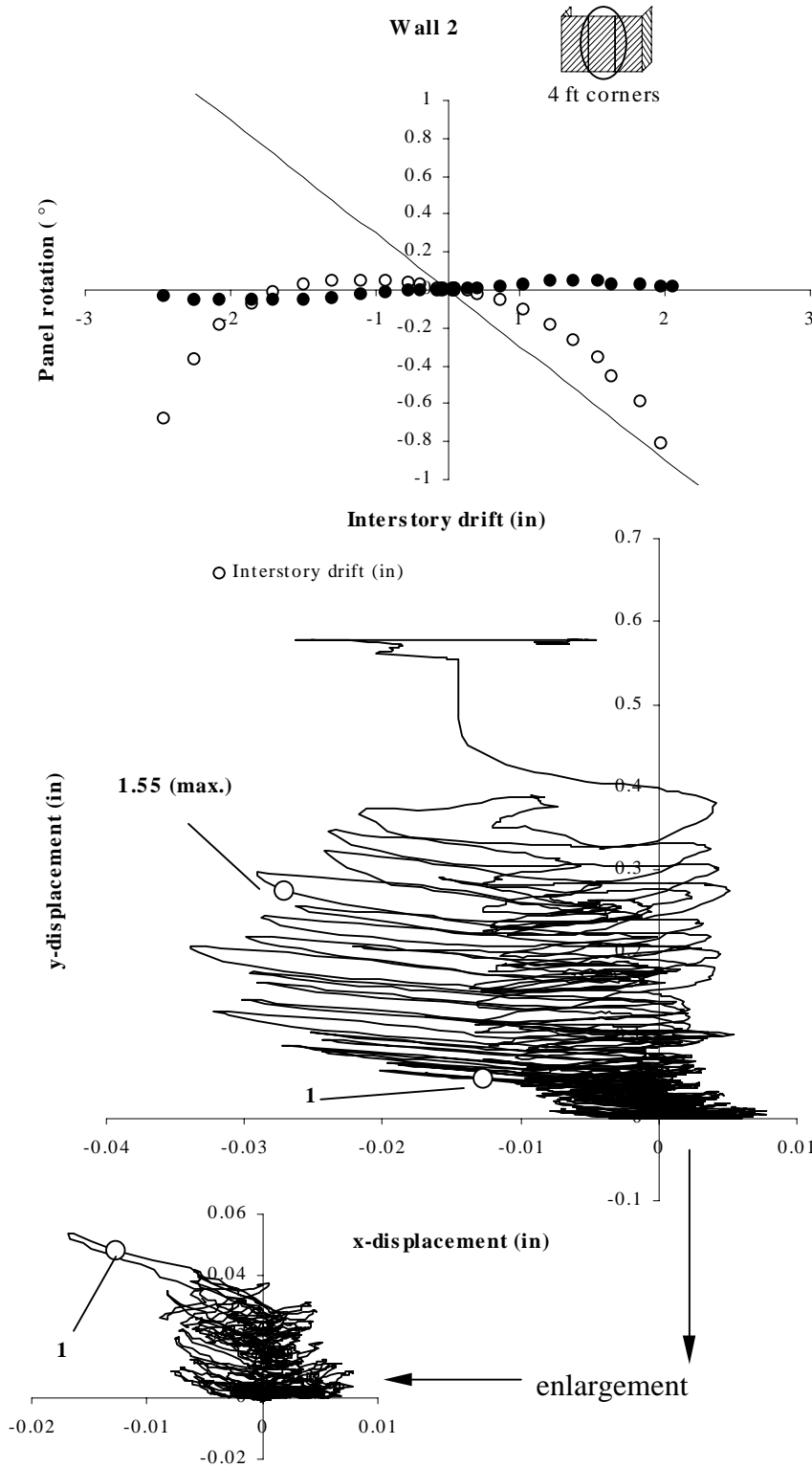


Figure 7.11: Rotation and midpoint translation of the mid OSB panel, Wall 4.2

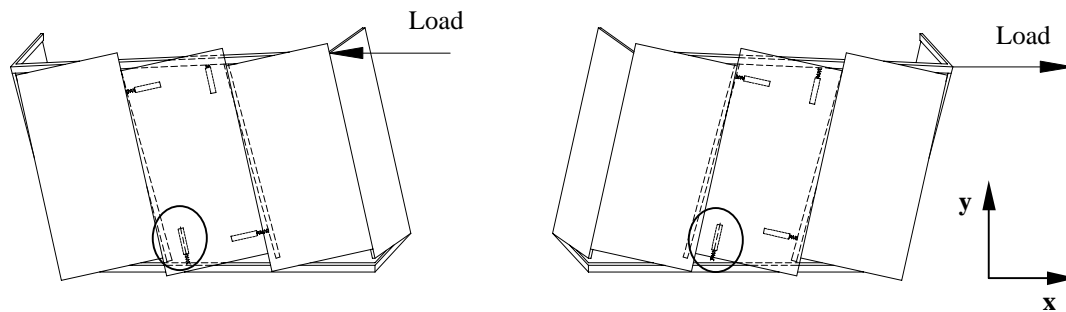


Figure 7.12: Sheathing rotation relative to the framing when uplift is considered

In light of the significant movement of the sheathing panel below 1 inch (25mm) interstory drift, it can not be assumed that the panel rotates about the normal passing through its centroid. Note that the rotational behavior of each panel in Figures 7.8 through 7.11 is similar to that of Panel 2 in Wall A with no anchors (described in Chapter 6). Envelope curves of the rotation relative to the studs are presented by black dots, whereas white dots represent the envelope curves of the rotation relative to top and bottom plate. The solid line indicates the rotation of the end stud where the load was applied. Presuming that every stud rotates equally in the system and neglecting stud bending, this line represents the lozenge deflection of the framing. Inasmuch as the studs rotate, the rotation of the sheathing relative to the studs was comparatively small. In all graphs, the measured extremities of the rotation history in relation to stud rotation are in line with the sign convention shown in Figure 6.19 (Chapter 6). However, this is not true for the U-shaped envelope curves showing the rotation against top and bottom plate. Due to the separation of the wall across the bottom plate, the measurement of the rotation relative to the plates was altered by this uplift motion. Being located close to the middle of the wall, the LVDT extended when the wall was deflected in both positive and negative x-directions. As previously mentioned, at increasing interstory drifts the walls withdrew from the bottom plate increasing the normal distance between top and bottom plate. This led to an amplified recording of the rotation angle at positive drifts and to a decreased recording at negative interstory drifts. Since the displacements measured by the LVDTs were small, an uplift movement of 0.1 inch (2.5mm) was sufficient to have

the effect of a sign change on the rotation angle at negative interstory drifts. As a result of the increased hold-down effect when 4 foot corner framing was applied, the rotation against the plates at negative drifts is not depressed as much as for walls with 2 foot wide corners attached. Taking into account the considerable rigid body rotation and inherent separation of the corner walls from the bottom plate, the sheathing rotated as revealed in Figure 7.12.

#### **7.4.4 General Observations**

It is remarkable that there were no typical damage signs of racking of the sheathing panels with corner framing. The taped joints between the drywall panels experienced no damage. The corner segments hindered the free rotation of the drywall sheathing with respect to the framing. The walls more or less rotated as rigid bodies and eventually separated from the bottom plate. This behavior may be a result of the relatively short wall length of 12 foot. The rigid body rotation was more pronounced when the 2 foot corner wing walls were attached arising from the lower hold-down effect. Due to the hold-down effect provided by the corner framing, the separation of the wall from the bottom plate started to occur at relatively high loads.

At the bottom plate, nails tore and pulled through the sheathing. Nails simply withdrew along the bottom of the wing walls. There was no nail fatigue observed in the corner specimens, which is a significant change from the behavior observed during SPD tests of the long and straight walls. This is attributed to the fact that almost no racking of the sheathing panels occurred. The wing walls rotated about the nail furthest away from the corner of the specimens (Figure 7.12).

Walls with 4 foot corner framing exhibited out-of-plane distortion during loading. This behavior arose from the corner segments that shifted the wall rotation point out of the wall plane.

### **7.5 Summary**

Four walls with two different corner framings were tested under reversed cyclic loading. Based on the results, the following conclusions can be drawn:

- 1) On average, walls with 4 foot corners reached higher ultimate capacities than walls with 2 foot long perpendicular segments.
- 2) Average strength reduction between initial and stabilized capacity was consistently 17 percent.
- 3) Elastic and cyclic stiffness were not significantly influenced by the length of the corner segments.
- 4) Damping ratios were slightly higher for walls with shorter corner segments attached. At displacements between elastic limit and failure, linear peak potential energy and hysteretic energy tended to the same value for all specimens, and the EVDR approached 16%.
- 5) Walls with corner framing showed no apparent racking of the sheathing. The walls responded mainly through rigid body rotation until complete separation from the bottom plate occurred. No nail fatigue was observed and there were no signs of damage at joints between drywall panels.

## Chapter 8

### Comparisons Between Tests

#### 8.1 General

This chapter draws comparisons between the three test schemes presented in earlier chapters. Performance indicators of monotonic and sequential phased displacement tests are compared and differences are elaborated. The remainder of the chapter describes the effect of corner framing, and results of the corner wall investigation are compared to results of the SPD test of wall configuration A (fully-sheathed) on a unit-length basis. At this point the reader is reminded of some limitations that apply:

Performance of cyclically tested walls, employing the SPD procedure, were considerably influenced by nail fatigue. During earthquake events, however, nail fatigue in timber structures has rarely, if ever, been observed, because an earthquake is shorter in duration and the number of cycles a structure actually experiences during an earthquake is less than those tested in this study. Future tests of nailed shear walls using SPD procedure should be altered to eliminate the “decay cycles”. This will reduce the number of cycles, and will therefore reduce nail fatigue. Nail fatigue also diminishes if the clamping force of the framing members around the nail shank is less than the clamping force of the sheathing. During reversed cyclic loading, the nail then continuously withdraws from the framing. A single plastic hinge is less likely to develop since the nail is not repeatedly bent at the same location. For instance, to reduce the clamping force of the framing, the building code in New Zealand requires a maximum penetration depth of the nails into the framing. Consequently the nails are shorter than in American light-frame construction.

For 40 foot long walls, only one specimen per configuration was tested due to the high cost and effort associated with full-scale testing. As a result, no statistical information can be revealed. However, it is well established, and the results of this study show that the response of a light-frame shear wall is primarily influenced by the

sheathing-to-framing nail load slip characteristics (Dowrick 1986; Stewart 1987; Dolan 1989; Dolan and Madsen 1992a). In light of the fact that a full scale specimen as tested in this investigation contains a high number of nails, the average response of the nails and therefore the wall, can be expected and comparisons can be made.

Comparisons between corner and straight walls were made on unit shear basis. However, there was a significant difference in length between the specimens. The substantially shorter corner walls exhibited out-of-plane distortions and different racking characteristics. Future tests should confirm whether the influence of corners decreases with increasing wall length.

## **8.2 Monotonic vs. SPD Performance of Straight Walls**

### **8.2.1 Strength**

Monotonic load versus drift curves, along with initial and stabilized envelope curves, are depicted in Figures 8.1 through 8.3. Values for stabilized and initial response in all graphs are average values of the positive and negative curves for each wall. It is apparent from the graphs that the monotonic testing procedure yields capacities in between the stabilized and initial response from the SPD test method for Walls A, D, and E without tie-down anchors. Initial capacities were between 3 and 8 percent higher than monotonic capacities (Table 8.1). All other wall configurations reached higher peak loads during monotonic tests than during the SPD procedure. According to Table 8.1, the ratio of reduction between monotonic and initial SPD cycles for walls with overturning restraints ranged between 23 percent (Wall E, maximum amount of anchors) to 6 percent (Wall D, anchors at the ends only). Stabilized peak loads for all specimen configurations were consistently below monotonic capacities (Table 8.1).

One reason why monotonic capacities were lower than cyclic, when tie-down anchors were omitted is that wall specimens separated from the bottom plate at both ends during the SPD procedure. The wall crushed the bottom plate at one end and unzipped at the other end, and vice versa. Until nails were completely withdrawn from the studs and

the wall was separated from the bottom plate there was more friction involved than during monotonic testing. Consequently more energy was dissipated.

For all wall configurations, the difference between monotonic and SPD capacity (initial and stabilized) increased with increasing overturning restraint. The highest disparity is experienced by Wall E with maximum restraint for both ratios, initial over monotonic and stabilized over monotonic (Table 8.1). This is due to increased restraint producing a more uniform distribution of the load to the sheathing nails, which increased the overall damage to the sheathing connections prior to reaching peak load during the SPD tests. Because the initial and stabilized curves really represent envelopes of hysteretic loops, the walls have actually dissipated more energy at a given displacement relative to the monotonic tests.

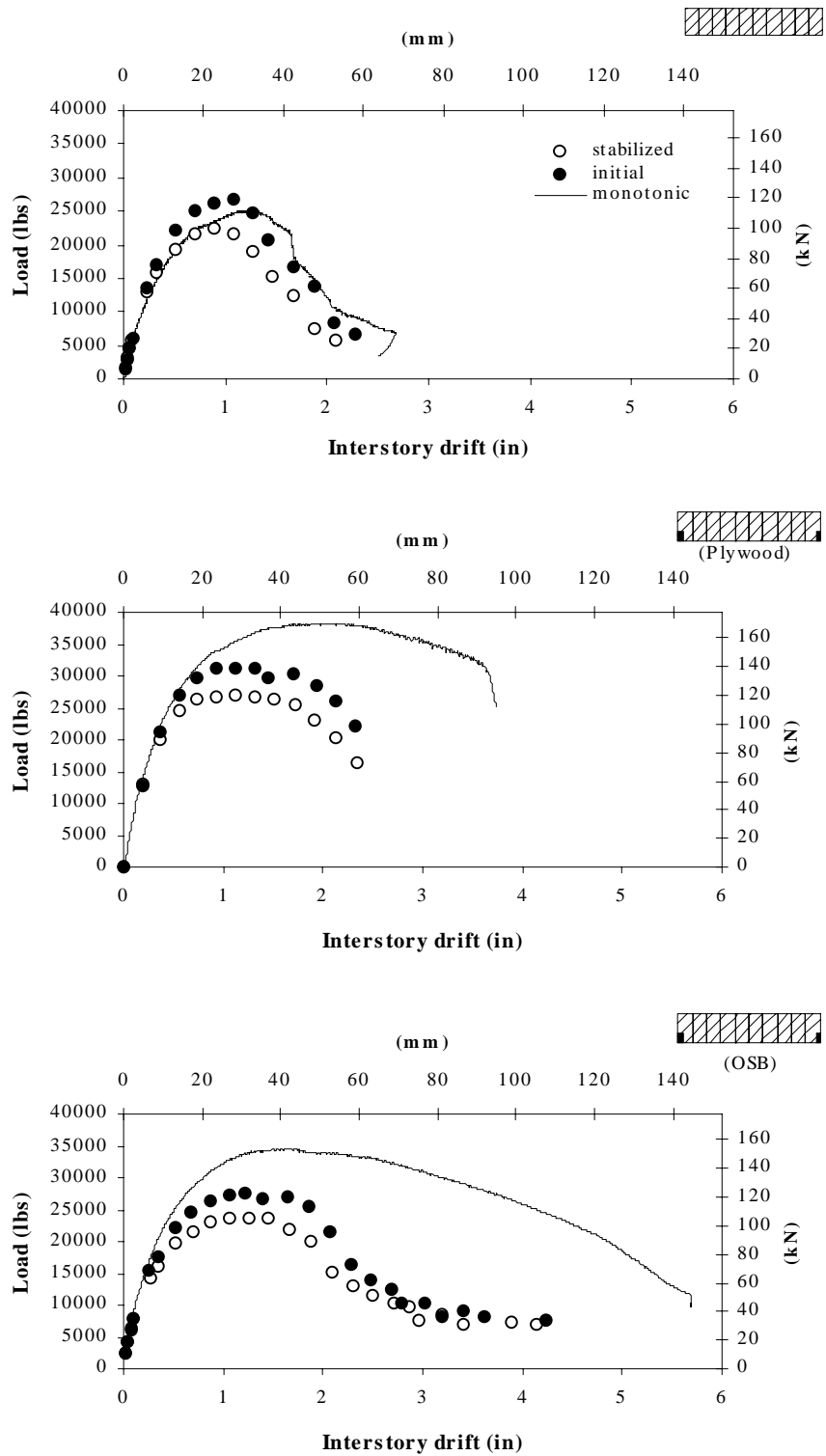


Figure 8.1: Monotonic load vs. drift curves, initial envelope, and stabilized envelope curves for wall configuration A

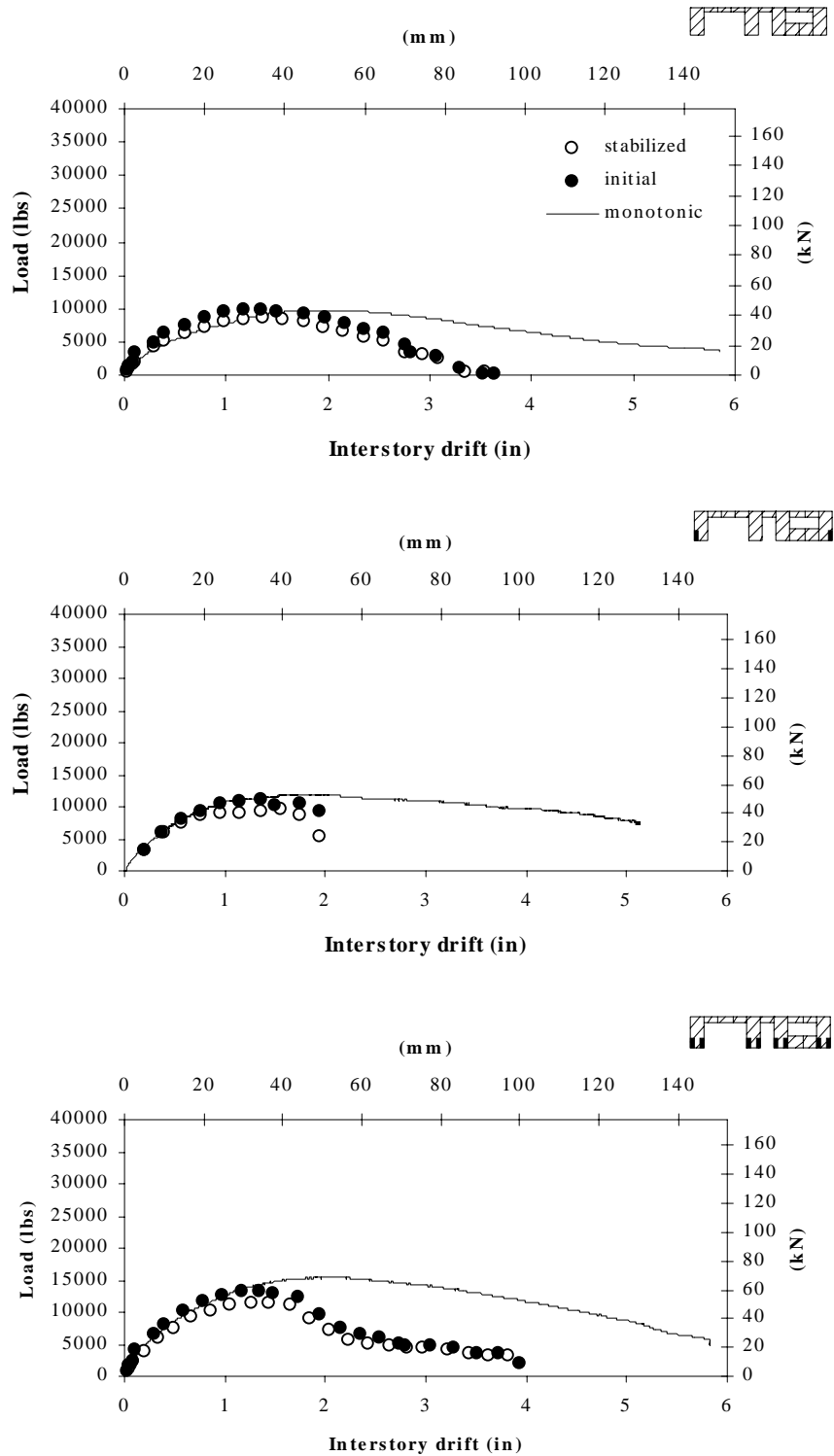


Figure 8.2: Monotonic load vs. drift curves, initial envelope, and stabilized envelope curves for wall configuration D

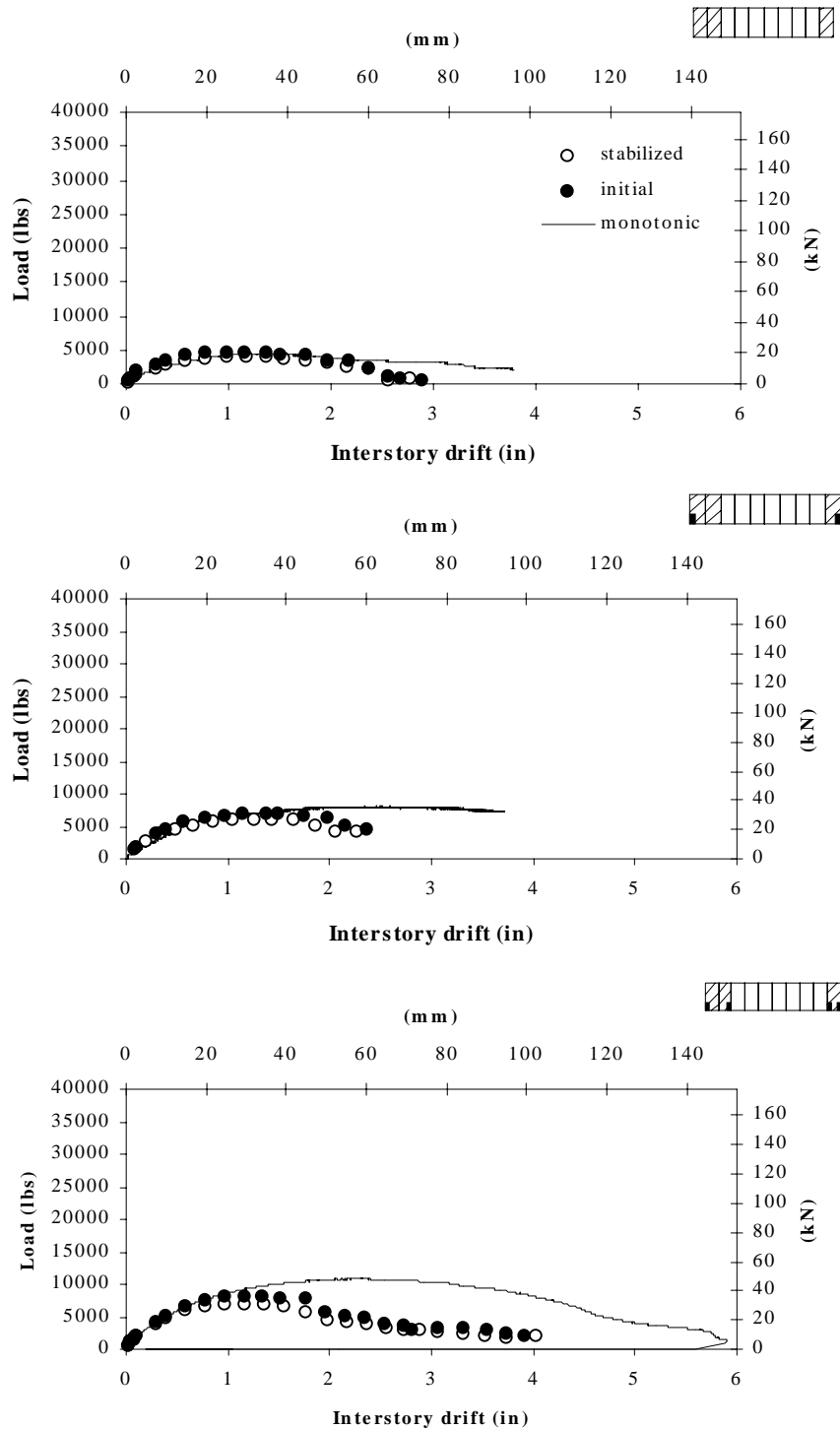


Figure 8.3: Monotonic load vs. drift curves, initial envelope, and stabilized envelope curves for wall configuration E

Table 8.1: Capacities of monotonic and SPD tested straight walls

	Wall Specimens								
	no tie-down anchors <sup>(1)</sup>			anchors at end of wall only <sup>(2)</sup>			maximum amount of tie-down anchors <sup>(1)</sup>		
	A	D	E	A <sup>(3)</sup>	D	E	A <sup>(3)</sup>	D	E
$F_{peak}$									
Monotonic	25.1	9.8	4.4	38.6	12.0	8.0	34.6	15.5	10.8
Initial SPD (kips)	26.7	10.1	4.8	32.0	11.2	7.3	27.7	13.4	8.4
Stabilized SPD (kips)	22.5	8.7	4.1	27.4	9.6	6.3	23.7	11.7	7.1
Initial/Monotonic	1.06	1.03	1.08	0.83	0.94	0.91	0.80	0.86	0.77
Stabilized/Monotonic	0.90	0.89	0.93	0.71	0.81	0.79	0.68	0.75	0.66

<sup>(1)</sup> These specimens had OSB sheathing

<sup>(2)</sup> These specimens had plywood sheathing (Johnson 1997)

<sup>(3)</sup> Wall A has the same anchorage requirements for the anchors at the end of wall only and maximum amount of tie-down anchors due to being fully sheathed.

## 8.2.2 Equivalent Energy Elastic-Plastic Parameters

The equivalent energy elastic-plastic parameters are listed in Table 8.2 Recall that the equivalent energy elastic-plastic parameters were obtained from the equivalent energy elastic-plastic system (EEEP) as described by Porter (1987) and elaborated on in Chapter 4. Each parameter represents the average of two values of the EEEP, at positive and negative interstory drifts.

### 8.2.2.1 Yield Load

$F_{yield}$  is correlated to  $F_{peak}$  and therefore shows similar trends. The ratio between initial cyclic and monotonic yield load exceeds unity for walls that were not restrained against uplift. For all other walls initial  $F_{yield}$  was smaller than monotonic yield load with Wall E (ultimately restrained) exhibiting the highest difference (Table 8.2). Stabilized yield loads were consistently below monotonic yield loads for all wall configurations.

### 8.2.2.2 Elastic Stiffness

Monotonic and initial load versus interstory drift curves almost coincide in the elastic range when walls were ultimately restrained against uplift. On the other hand, walls without restraint typically showed lower elastic stiffness during monotonic tests than during SPD testing. The elastic stiffness was on average 17 percent (Std Dev = 4.6%) lower for walls tested monotonically than for walls tested using the SPD method (Table 8.2). This change in performance is in part attributed to the fact that energy was dissipated through increasing racking and cold-working of the sheathing nails during the cyclic test when anchors were applied, whereas all the energy was absorbed through racking of the sheathing nails for all monotonic tests. When anchors were omitted, however, the internal damage experienced by the wall was mainly withdrawal from the bottom plate.

### 8.2.2.3 Drifts and Ductility

Walls containing tie-down anchors showed 111 percent (Std Dev = 23%) higher interstory drifts at failure when tested monotonically than when tested using SPD protocol (Table 8.4). Again, this difference in performance was caused by nail fatigue that occurred in walls exposed to the SPD procedure. Failure at smaller drifts is also an indication of higher energy dissipation of cyclically tested walls due to the SPD loading history. However, when anchors were omitted, monotonic drifts were only 29 percent (Std Dev = 18%) above initial SPD values. This elucidates that more rigid body rotation was involved, since the walls were not restrained against uplift. In turn, the walls exhibited less racking and less nail fatigue during SPD tests. In other words, without tie-down anchors, the damage performance was more alike during the two different testing procedures. Ductility values listed in Table 8.2 only partially reflect this trend since ductility compares drift at failure to drift at yield. Ductility ranges from 2.7 (Wall A no anchors, SPD initial) to 8.6 (Wall A max. anchors, monotonic). Most of the time monotonic ductility was higher than initial and stabilized SPD ductility.

Interstory drifts at peak loads followed the same trend as the drifts at failure (Table 8.4). Note that the drift at capacity for SPD loaded and maximum restrained walls

was fairly constant arising from a more uniform load distribution throughout the wall when maximum amount of tie-downs was applied. The more restraints applied, the more the wall was forced to deflect through racking rather than rigid body rotation and capacity was increasingly influenced by nail fatigue.

Table 8.2: Equivalent energy elastic-plastic parameters

	Wall Specimens								
	no tie-down anchors <sup>(1)</sup>			anchors at end of wall only <sup>(2)</sup>			maximum amount of tie-down anchors <sup>(1)</sup>		
	A	D	E	A <sup>(3)</sup>	D	E	A <sup>(3)</sup>	D	E
<b>F<sub>yield</sub></b>									
Monotonic	22.5	8.7	4.0	35.4	10.9	7.3	31.5	14.7	9.9
Initial SPD (kips/in)	24.3	9.0	4.3	29.9	10.3	6.3	25.3	12.2	7.6
Stabilized SPD (kips/in)	20.2	7.7	3.7	25.8	9.6	5.3	21.6	10.5	6.5
Initial/Monotonic	1.08	1.03	1.08	0.84	0.94	0.86	0.80	0.83	0.77
Stabilized/Monotonic	0.90	0.89	0.93	0.73	0.88	0.73	0.69	0.71	0.66
<b>Elastic Stiffness</b>									
Monotonic	54.0	13.5	8.7	64.3	17.7	7.8	73.3	20.6	13.7
Initial SPD (kips/in)	61.6	16.5	11.0	70.4	17.6	16.7	69.0	21.9	16.8
Stabilized SPD (kips/in)	61.1	16.4	11.1	70.1	17.4	16	67.8	21.2	16.8
Initial/Monotonic	1.14	1.22	1.26	1.09	0.99	2.14	0.94	1.06	1.23
Stabilized/Monotonic	1.13	1.21	1.28	1.09	0.98	2.05	0.92	1.03	1.23
<b>Ductility:</b>									
Monotonic	3.9	5.1	5.0	7.3	6.6	5.3	8.6	5.3	4.5
Initial SPD ductility	2.7	4.0	5.0	4.4	3.2	5.6	5.1	3.5	3.9
Stabilized SPD ductility	4.1	3.7	7.3	5.1	3.2	5.5	5.9	3.5	4.3
Initial/Monotonic	0.69	0.78	1.00	0.60	0.48	1.06	0.59	0.66	0.87
Stabilized/Monotonic	1.05	0.73	1.46	0.70	0.48	1.04	0.69	0.66	0.96

<sup>(1)</sup> These specimens had OSB sheathing

<sup>(2)</sup> These specimens had plywood sheathing (Johnson 1997)

<sup>(3)</sup> Wall A has the same anchorage requirements for the anchors at the end of wall only and maximum amount of tie-down anchors due to being fully sheathed.

Table 8.3: Monotonic and initial cyclic interstory drifts at yield, capacity and failure

	Wall Specimens								
	no tie-down anchors (OSB)			anchors at end of wall only <sup>(1)</sup> (Plywood)			maximum amount of tie-down anchors (OSB)		
	A	D	E	A <sup>(2)</sup>	D	E	A <sup>(2)</sup>	D	E
Monotonic									
$\Delta_{\text{yield}}$ (in)	0.4	0.6	0.5	0.6	0.6	0.9	0.4	0.7	0.7
$\Delta_{\text{Fpeak}}$ (in)	1.2	2.0	1.2	2.3	1.9	2.6	1.6	2.0	2.2
$\Delta_{\text{failure}}$ (in)	1.6	3.3	2.3	4.0	4.0	4.9	3.7	3.8	3.2
SPD									
$\Delta_{\text{yield}}$ (in)	0.4	0.6	0.4	0.4	0.6	0.4	0.4	0.6	0.5
$\Delta_{\text{Fpeak}}$ (in)	1.1	1.3	1.2	1.2	1.5	1.2	1.2	1.3	1.2
$\Delta_{\text{failure}}$ (in)	1.3	2.2	2.0	1.9	1.9	2.0	1.9	1.7	1.8

<sup>(1)</sup> These specimens had OSB sheathing

<sup>(2)</sup> These specimens had plywood sheathing (Johnson 1997)

<sup>(3)</sup> Wall A has the same anchorage requirements for the anchors at the end of wall only and maximum amount of tie-down anchors due to being fully sheathed.

## 8.3 Effect of Corner Framing

### 8.3.1 Capacity

Initial capacities of wall configuration A (fully-sheathed, 40ft long) and the two corner wall structures are presented in Table 8.4. Since the walls have different lengths, comparisons can only be made on a unit-shear basis. Unit shear is the average shear force resisted by a one foot long, eight foot high, fully-sheathed segment. Consequently the unit shear figures listed in Table 8.4 were simply obtained by dividing  $F_{\text{peak}}$  by wall length, excluding the length of the corner segments. This equation does not account for the effects of wall length on unit shear. In other words, the assumption was made that

unit shear remains constant and uniformly distributed with changing wall length, and the data reflect the observed unit shears.

The values from Table 8.4 are depicted in Figure 8.4, which illustrates the effect of corner framing on unit shear. Walls with 4 foot corners show somewhat higher ultimate unit shear values than walls without corners or overturning restraint. This indicates that the interaction of two mutually perpendicular walls provides some restraint against overturning forces, and in turn increases shear capacity. However, the average ultimate unit shear obtained from walls with 2 foot corners is somewhat lower than the unit shear for walls without overturning restraint. This is partly attributed to the difference in length between the specimens. In addition, the high variation of the values obtained from the walls with 2 foot corner framing and the small sample size may also contribute to the observed difference. It is interesting to note that the tested average unit shear was 689 lbs. with a standard deviation of only 49 lbs..

Table 8.4: Cyclic capacities and unit shear values of walls with corner framing and long straight walls with and without tie-down anchors

	Wall Specimen			
	12 ft Walls with corner framing		40 ft walls no corner framing	
	2 ft corner <sup>(1)</sup>	4 ft corner <sup>(1)</sup>	no overturning restraint <sup>(2)</sup>	overturning restraint <sup>(1)</sup>
Capacity				
Initial SPD (kips)	7.6	8.5	26.7	30.0
Unit shear	634	708	668	746

<sup>(1)</sup> Average values out of two specimens

<sup>(2)</sup> Values obtained from one specimen only

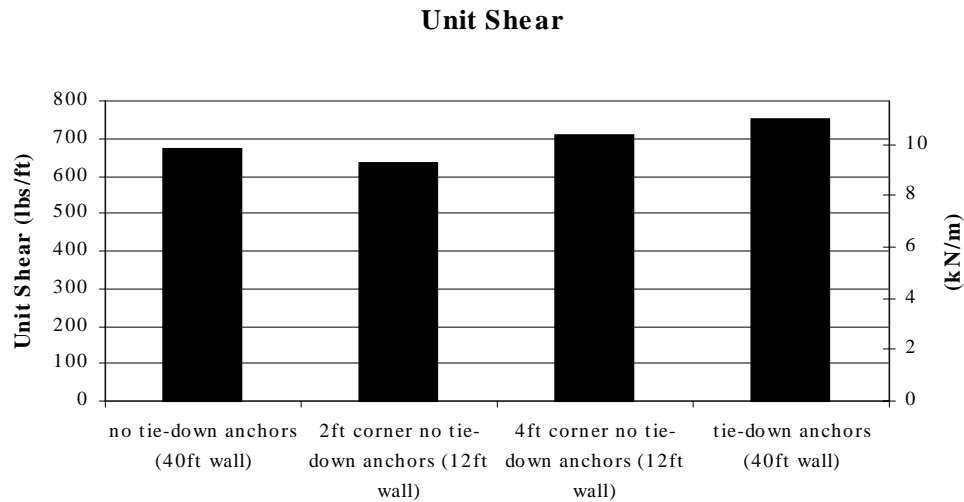


Figure 8.4: Unit shear at ultimate capacity of walls with no tie-down anchors, tie-down anchors at the end and 2ft and 4ft corner segments, respectively

### 8.3.2 Equivalent Energy Elastic Plastic Parameters

According to a parametric study conducted by White (1995) initial stiffness increases linearly as wall length increases, all other parameters held constant. If this is true,  $F_{yield}$  is close to being linearly correlated to wall length as well since capacity is also proportional to wall length. Therefore, elastic stiffness and yield load, as presented in Table 8.5, are based on unit length. There is hardly any difference between the yield loads of each wall configuration. According to the information given, corner segments have no influence on yield load. If wall length is considered, the elastic stiffness values of both corner walls listed in Table 8.5 exceed the elastic stiffness of Wall A without tie-down anchors by approximately 100 percent. Corner framing significantly increased elastic stiffness, forcing the wall to distort out of its plane during the test. However, further testing must evaluate whether the influence of corners on wall response diminishes with increasing wall length.

Ductility, as defined in Chapter 5, is somewhat influenced by wall length but definitely not linearly. It stands to question whether it is correct to compare the ductility

obtained for a 40 feet long wall with the ductility of a 12 feet long wall with corner segments attached. The walls with corner framing show a significantly higher ductility than Wall A without tie-down anchors (Table 8.5), but does that really mean that the corner walls were more ductile? If ductility is considered as the ability to undergo large deformations until failure when comparing walls with the same height this is hard to believe in view of the little racking and early failure that occurred in the corner walls during cyclic tests. Ductility should always be considered together with other performance indicators. It is not a “stand-alone” property value that evaluates shear wall performance. However, ductility remains an important comparison parameter to determine factors of safety for seismic design.

Table 8.5: Equivalent energy elastic-plastic curve parameters

	Wall Specimen		
	2ft corners average	4ft corners average	40ft Wall No anchors
$F_{yield}$			
Initial SPD (kips/ft)	0.6	0.7	0.6
Stabilized SPD (kips/ft)	0.5	0.5	0.5
Stabilized/Initial	0.82	0.83	0.83
Elastic Stiffness			
Initial SPD (kips/(in   ft))	3.1	3.0	1.5
Stabilized SPD (kips/(in   ft))	3.5	3.3	1.5
Stabilized/Initial	1.12	1.11	0.99
Ductility			
Initial SPD ductility	6.2	6.2	2.7
Stabilized SPD ductility	7.5	8.2	4.1
Stabilized/Initial	1.21	1.32	1.51

## 8.4 Summary

The effect of the two testing procedures on wall performance can be summarized as follows:

- 1) Ultimate capacities reached in SPD tests were up to 23 percent lower for walls restrained against uplift when compared to monotonic test results. However, for walls with no tie-down anchors, ultimate capacities obtained from SPD testing were up to 8 percent higher than capacities recorded during monotonic testing.
- 2) The difference between monotonic and SPD capacity increased with increasing overturning restraint. In other words, the increase in ultimate capacity and stiffness with increasing amount of tie-down anchors is less pronounced for SPD tested walls.
- 3) Cyclic elastic stiffness was typically higher than monotonic elastic stiffness for walls without restraint
- 4) In general, monotonically tested walls sustained higher loads beyond capacity than walls subjected to SPD loading. Ductility ratios for all cyclic conditions ranged from 2.7 to 7.3. This indicates that wood shear walls can sustain fairly high ductility demands in all anchorage conditions; however, the amount of energy dissipated differed significantly.

According to the findings of this preliminary investigation, during SPD tests, the main effects of corner framing when compared to straight walls were:

- 1) Corner framing generally provides a hold-down effect that increases wall capacity when compared to straight walls without overturning restraint and no perpendicular walls attached.
- 2) Elastic stiffness increased by approximately 100% compared to walls without tie-down anchors when corner framing was attached.
- 3) The hold-down capacity provided by corner framing is sufficient to develop unit shears slightly less than, but comparable to, straight walls with tie-down devices.

## Chapter 9

# Summary, Conclusions, and Recommendations

### 9.1 Summary

The primary objective of this study was to quantify the effects of overturning restraint on the performance of light-frame shear walls. Sixteen full-scale wall specimens, with and without window and door openings, were tested using monotonic (one-directional) and sequential phased displacement procedures. Anchorage conditions were a) not restrained against uplift (the bottom plate was bolted to the foundation), b) restrained against uplift forces according to the perforated shear wall method design using tie-down anchors, c) restrained by the maximum amount of tie-down anchors as common in engineered design, and d) restrained by transverse corner framing attached at each wall end. Data analysis included the determination of performance indicators such as capacity, yield strength, elastic and cyclic stiffness, ductility, and energy dissipation characteristics. Data of tension bolts located at the extreme ends of each specimen were analyzed and, together with the measurements that monitored sheathing rotation and translation, the overall wall behavior was discussed.

### 9.2 Conclusions

#### 9.2.1 Overturning Restraint

In summary, varying overturning restraint influences shear wall performance as listed below:

- The amount of overturning restraint is positively correlated with ultimate capacity and elastic stiffness. The magnitude of influence depends on the amount of openings in the wall. The greater the openings, the higher the increase in capacity and stiffness when overturning restraint is increased from zero to maximum. Overturning restraint

in the form of tie-down anchors applied according to traditional engineered design help utilize overall material strength most efficiently.

- Without overturning restraints, shear walls exhibit a pronounced rigid body rotation arising from uplift and separation along the bottom plate. The main failure mode is sheathing and stud separation from the bottom plate when overturning restraint is omitted. With increasing restraint the failure mode shifts to nail fatigue when tested cyclically and nails tearing through the sheathing material during monotonic testing.
- Damage experienced by the walls during cyclic tests (stabilized versus initial response) is fairly uniform regardless of the type of overturning restraint and amount of openings present. This indicates that strength degradation of light-frame timber shear walls is mainly a function of the behavior of the nailed sheathing-to-stud connection. This information will be helpful when establishing building code regulations regarding the required earthquake resistance for light-frame shear walls.
- Corner framing significantly enhances wall performance and generally provides a hold-down effect that increases capacity and doubles elastic stiffness when compared to straight walls without overturning restraints. Thus, the performance improvements of mechanical tie-down anchors may not be justified depending on design loads magnitude, construction costs, and design criteria.

### **9.2.2 Testing Procedures**

In light of the fact that the majority of past research conducted on light-frame shear walls employed monotonic testing procedures, an established link between monotonic and reversed cyclic protocol would allow data from previous tests to be used for modern high-wind and earthquake design. However, a cyclic testing procedure should always be the preferred testing method, for it gives essential information about energy dissipation and stiffness degradation. The following observations regarding the effect of the monotonic and sequential phased displacement procedures, with respect to hold-down condition, were made:

- Results of the cyclically tested walls, employing the Sequential Phased Displacement Procedure, were significantly affected by nail fatigue. With mechanical tie-down anchors applied, cyclic ultimate capacities were significantly lower than monotonic peak loads. The discrepancy increased with increasing overturning restraint, which resulted in a more uniform load distribution and increased nail fatigue. In general, monotonically tested walls sustained higher loads at displacements beyond capacity than walls subjected to reversed cyclic loading.
- Cyclically tested wall specimens ultimately resisted higher loads compared to specimens tested monotonically when overturning restraints were omitted. Cyclic elastic stiffness was higher than monotonic elastic stiffness for walls not restrained against uplift, and failure modes observed during either testing procedure were more alike. Nail fatigue was less pronounced.

Some additional conclusions about reversed cyclic performance are:

- Cyclic stiffness is not influenced by anchorage condition. Cyclic stiffness degrades exponentially and approaches zero at failure.
- Within the elastic range, equivalent viscous damping ratio averaged 8.2 percent (Std. Dev. = 2.7%) for all wall configurations. Between the elastic range and failure, linear peak potential and hysteretic energy tend toward the same value and the equivalent viscous damping ratio ranges between 10 and 16 percent.
- Gypsum wall board sheathing was observed to get damaged quickly during reversed cyclic tests.

### **9.2.3 Perforated Shear Wall Design Method**

The perforated shear wall design approach predicts conservative shear strength ratios even for walls not restrained against uplift forces, independent of the testing protocol used. It was found that Equation 4.6 developed by Sugiyama (1994), provided

closer predictions of shear strength ratios at capacity for all anchorage and testing conditions.

#### **9.2.4 Other Conclusions and Observations**

- Ductility should not be considered as a stand-alone measure to evaluate shear wall performance. Ductility values showed no apparent trend when compared among anchorage conditions.
- Walls with corner segments attached, showed no apparent racking of the sheathing. The walls responded mainly through rigid body rotation until complete separation from the bottom plate occurred. No nail fatigue was observed, and there were no signs of damage at joints between drywall panels.
- Wood shear walls can sustain fairly high ductility demands in all anchorage conditions; however, the amount of energy dissipated differs significantly among anchorage conditions.

## **9.2 Recommendations for Future Research**

It is of the essence that a internationally standardized, cyclic testing procedure along with a uniform format of property definitions and a constant notation and nomenclature be developed in the near future to facilitate comparisons between test results.

In light of the important findings on the effect of corner framing, testing should be expanded and an engineered approach for conventionally-framed wood walls without tie-down devices should be developed. More tests are needed combining gravity loads and corner framing effects while confirming a perforated shear wall approach. Future tests should also investigate the effect of corner framing on varying shear wall length.

Additional research is needed to quantify the effect of interconnections between light-frame shear walls and ceiling and floor diaphragms. The effects of non-rigid foundations should also be investigated in order to quantify the response of shear walls in upper levels of buildings.

## Bibliography

- [1] Almsaker, T., 1995. "Diaphragm and Shear Walls." *Timber Engineering Step 1*, , pp B13/1-7. Centrum Hout, The Netherlands.
- [2] American Forest and Paper Association, 1991. *National Design Specifications for Wood Construction*. Washington, D.C.
- [3] American Forest & Paper Association (AF&PA), 1995, *Wood Frame Construction Manual for One- and Two- Family Dwellings - SBC High Wind Edition*. American Forest and Paper Association, Washington, D.C.
- [4] American Plywood Association, 1997. *Design Capacities of APA Performance-rated Structural-use Panles*. No. N375, Tacoma, Washington
- [5] American Plywood Association, 1994. *Northridge, California Earthquake*. APA Report T94-5, Tacoma, Washington
- [6] ASTM 1997. *Annual Book of ASTM Standards*. American Society of Testing and Materials, Philadelphia, PA.
- [7] Aune, P. and Patton-Mallory, M., 1986. "Lateral Load-Bearing Capacity of Nailed Joints Based on the Yield Theory – Theoretical Development and Experimental Verification." US Department of Agriculture, Forest Products Laboratory, Research Papers FPL 469 & 470.
- [8] Ceccotti, A. 1995. "Timber Connections under Seismic Actions." *Timber Engineering Step 1*. Centrum Hout, Almere. Netherlands.
- [9] Chopra, A.K., 1995. *Dynamics of Structures: Theory and Applications to Earthquake Engineering*. Prentice Hall, Englewood Cliffs, NJ.
- [10] Dean, J.A., 1988. "The Ductility of Nailed Sheathing Joints in Timber Framed Shearwalls." Report CE 88/14, Civil Engineering Department, University of Canterbury, Christchurch, New Zealand.
- [11] Diekmann, E.F., 1994. "Design and Code Issues in the Design of Diaphragms and Shearwalls," *Analysis, Design and Testing of Timber Structures Under Seismic*

- Loads, Proceedings of a Research Needs Workshop*, University of California, Forest Products Laboratory, Richmond, CA, pp. 9-20.
- [12] Diekmann, E.F., 1989. "Wood Shearwalls for Engineers," *Proceedings of the Second Pacific Timber Engineering Conference 1989*, Vol. 2, pp263-267.
- [13] Dolan, J.D., 1989. *The Dynamic Response of Timber Shear Walls*, thesis submitted in partial fulfillment of the Doctor of Philosophy Degree at the University of British Columbia, Vancouver, British Columbia.
- [14] Dolan, J.D., 1993. "Proposed Test Method For Dynamic Properties of Connections Assembled with Mechanical Fasteners." Paper prepared for presentation at 26<sup>th</sup> Meeting of CIB W18 in Athens, Georgia, USA.
- [15] Dolan, J.D. and Johnson, A.C., 1996 a. "Monotonic Tests of Long Shear Walls with Openings." Virginia Polytechnic Institute and State University Timber Engineering Report TE-1996-001.
- [16] Dolan, J.D. and Johnson, A.C. 1996 b. "Cyclic Tests of Long Shear Walls with Openings." Virginia Polytechnic Institute and State University Timber Engineering Report TE-1996-002.
- [17] Dolan, J.D. and Madsen, B., 1992a. "monotonic and Cyclic Nail Connection Tests." *Canadian Journal of Civil Engineering* 19:97-104.
- [18] Dowrick, D.J., 1986. "Hysteresis Loops for Timber Structures," *Bulletin of the New Zealand National Society of Earthquake Engineering*, 19(20): 143-152.
- [19] Easley, J.T., 1977. "Strength and Stiffness of Corrugated Metal Shear Diaphragms," *Journal of the Structural Division, Proceedings of the American Society of Civil Engineers*, Vol. 103, No. ST7, pp. 169-180.
- [20] Easley, J.T., Foomani, M., and Dodds, R.H., 1982. "Formulas for Wood Shear Walls," *Journal of the Structural Division, Proceedings of the American Society of Civil Engineers*, Vol. 108, No. ST11, pp. 2460-2478.
- [21] Falk, R.H. and Itani, R.Y., 1989. "Finite Element Modeling of Wood Diaphragms," *Journal of Structural Engineering*, Vol. 115, No. 3, pp 543-559.
- [22] Foliente, G.C., 1997. "Modeling and Analysis of Timber Structures Under Seismic Loads: State-of-the-Art," *Earthquake Performance and Safety of Timber Structures*, Forest Products Society publication, pp. 55-73.

- [23] Foliente, G.C., 1996. "Issues in Seismic Performance Testing and Evaluation of Timber structural Systems," *Proceedings of the 1996 International Wood Engineering Conference, New Orleans*, Vol. 1, pp. 29-36.
- [24] Foliente, G.C. and Zacher E.G., 1994. "Performance Tests of Timber Structural Systems Under Seismic Loads," *Analysis, Design and Testing of Timber Structures Under Seismic Loads*, Proceedings of a research needs workshop, University of California, Forest Products Laboratory, Richmond, CA, pp. 21-86.
- [25] Foschi, R.O., 1977. "Analysis of Wood Diaphragms and Trusses: Part I: Diaphragms," *Canadian Journal of Civil Engineering*, Vol. 4, No. 3, pp. 345-352.
- [26] Foschi, R.O., 1980. "Summary on Racking Tests Conducted on Waferboard Sheathing." TECO Project 80-37 Report, Washington, D.C..
- [27] Foschi, R.O., 1982. "Load/Slip Results for Nailed Connections using Waferboard Panels." *Supplementary Report A*, Report to the Canadian Waferboard Association by Forintek Canada Corp., Vancouver, British Columbia.
- [28] Foschi, R.O. and Filiatrault, A., 1990. "Performance Evaluation of the 3M Scotch Grip Wood Adhesive 5230 for the Static and Dynamic Design of Timber Shear Walls and Diaphragms." *Final Report Prepared for 3M Corporation*, 43 pp.
- [29] Ge, Y., 1991. *Response of Wood-Frame Houses to Lateral Loads*, thesis submitted in partial fulfillment of the Masters of Science Degree at the University of Missouri-Columbia.
- [30] Griffiths, D.R., 1984. "Determining the Racking Resistance of Timber Framed Walls," *Proceedings of the Pacific Timber Engineering Conference, Auckland, New Zealand, Vol. I, Timber Construction*. Institution of Professional Engineers, Wellington, New Zealand, pp. 504-512.
- [31] Gupto, A.K. and Kuo, G.P., 1985. "Behavior of Wood-Frame Shear Walls," *Journal of Structural Engineering*, Vol. 111, No. 8, pp. 1722-1733.
- [32] Gupto, A.K. and Kuo, G.P., 1987. "Wood-Framed Shear Walls with Uplifting," *Journal of Structural Engineering*, Vol. 113, No. 2, pp. 241-259.
- [33] Hilson, B.O., Whale, L.R.J. and Smith, I., 1990. "Characteristic Properties of Nailed and Bolted Joints under Short-Term Lateral Load." Part 5 – Appraisal of current design data in BS5268:Part 2:1984 Structural Use of Timber. *J. Inst. Wood Science*. 11(6) 208-212.

- [34] Itani, R.Y., and Cheung, C.K., 1984. "Nonlinear Analysis of Sheathed Wood Diaphragms," *Journal of Structural Engineering*, Vol. 110, No. 9, pp. 2137-2147.
- [35] Itani, R.Y., Tuomi, R.L., and McCutcheon, W.J., 1982, "Methodology to Evaluate Racking Resistance of Nailed Walls," *Forest Products Journal*, Vol. 32, No. 1, pp. 30-36.
- [36] Johansen, K.W., 1949, "Theory of Timber Connections." International Association of Bridge and Structural Engineering. Publication no. 9:249-262. Bern.
- [37] Johnson, A.C., 1997. *Monotonic and Cyclic Performance of Long Shear Walls with Openings*, thesis submitted in partial fulfillment of the Masters of Science Degree at Virginia Polytechnic Institute and State University, Blacksburg, Virginia.
- [38] Larsen, H.J., 1973, "The Yield Load of Bolted and Nailed Joints," Proceedings 5<sup>th</sup> IUFRO Conference Pretoria, 1973, pp. 646-654.
- [39] Lowe, P.G. and Edwards, M.R., 1984, "Aspects of Ductility in Nailed Timber Connections." Proceedings Pacific Timber Engineering Conference, Auckland, New Zealand, 2:622-630.
- [40] McCutcheon, W.J., 1985. "Racking Deformations in Wood Shear Walls," *Journal of Structural Engineering*, Vol. 111, No. 2, pp. 257-269.
- [41] Möller, T., 1951, "En ny metod för beräkning av spikförband. Report No 117, Chalmers University of Technology, Sweden
- [42] Patton-Mallory, M., Gutkowski, R.M., and Soltis, L.A., 1984. "Racking Performance of Light-Frame Walls Sheathed on Two Sides," *Research Paper FPL 448*, U.S. Department of Agriculture, Forest Service, Forest Products Laboratory, Madison, WI, 16 p.
- [43] Patton-Mallory, M., McCutcheon, W.J., 1987. "Predicting Racking Performance of Walls Sheathed on Both Sides," *Forest Products Journal*, Vol. 37, No. 9, pp. 27-32.
- [44] Patton-Mallory, M., Wolfe, R.W., Soltis, L.A., and Gutkowski, R.M., 1985. "Light Frame Shear Wall Length and Opening Effects," *Journal of Structural Engineering*, Vol. 111, No. 10, pp. 2227-2239.

- [45] Polensek, A., 1988. "Effects of Testing Variables on Damping and Stiffness of Nailed Wood-to-Sheathing Joints," *ASTM Journal of Testing and Evaluation*, 16(5): 474-480.
- [46] Porter, M.L., 1987. "Sequential Phased Displacement (SPD) Procedure for TCCMAR Testing." Proceedings of the Third Meeting of the Joint Technical Coordinating Committee on Masonry Research, U.S. - Japan Coordinated Earthquake Research Program, Tomamu, Japan.
- [47] Price, E.W. and Gromala, D.S., 1980. "Racking Strength of Walls Sheathed with Structural Flakeboards Made From Southern Species," *Forest Products Journal*, Vol. 30, No. 12, pp 19-23.
- [48] Reardon, G.F. 1980. "Recommendations for the Testing of Roofs and Walls to Resist Wind Forces." Technical Report no. 5. Cyclone Testing Station, James Cook Structural Testing Station, Queensland.
- [49] Robertson, A., 1980. Discussion of "Racking Strength of Light-Frame Nailed Walls" by Tuomi, R.L. and McCutcheon, W.J., *Journal of Structural Engineering*, Vol. 106, No. 9, pp. 1981-1985.
- [50] Skaggs, T.D. and Rose, J.D., 1996. "Cyclic Load Testing of Wood Structural Panel Shear Walls," *Proceedings of the 1996 International Wood Engineering Conference New Orleans*, Vol. 2, pp. 195-200.
- [51] *Standard Building Code*, 1994, Southern Building Code Congress International, Birmingham, AL..
- [52] Stewart, W.G., 1987. *The Seismic Design of Plywood Sheathed Shearwalls*, thesis submitted in partial fulfillment of the Doctor of Philosophy Degree at the University of Canterbury, New Zealand.
- [53] Sugiyama, H., 1981. "The Evaluation of Shear Strength of Plywood Sheathed Walls with Openings." *Mokuzai Kogyo (Wood Industry)*. 36-7, 1981.
- [54] Sugiyama, H., and Matsumoto, T., 1994. "Empirical equations for the estimation of Racking Strength of a Plywood Sheathed Shear Wall with Openings." *Mokuzai Gakkaishi*, Vol. 39, No. 8, pp. 924-929
- [55] Thurston, S.J., 1984. "In-Plane Cyclic Shear Tests on Ply-Sheathed Bracing Walls." Central Laboratories, MWD, Wellington, Report 5-24/2, 155pp.
- [56] Tissel, J.R. and Rose, J.D., 1988. "Plywood and Shear Walls in Mobile Homes." Res. Rept. 151. American Plywood Association, Tacoma, Washington.

- [57] Tuomi, R.L. and McCutcheon, W.J., 1977. "Predicting Racking Strength of Light-Frame Walls," Preprint for ASCE Annual Convention, San Francisco, California.
- [58] Van Vlack, L.H., 1967. *Elements of Materials Science*. Addison-Wesley Publishing Company. Reading, Massachusetts.
- [59] White, M.W., 1995. *Parametric Study of Timber Shear Walls*. dissertation submitted in partial fulfillment of the Doctor of Philosophy Degree at Virginia Polytechnic Institute and State University, Blacksburg, Virginia.
- [60] White, M.W., and Dolan, J.D., 1995, "Nonlinear Shear-Wall Analysis," *Journal of Structural Engineering*, Vol. 121, No. 11, pp 1629-1635.
- [61] Wolfe, R.W., 1983. *Research Paper FPL 439 - Contribution of Gypsum Wallboard to Racking Resistance of Light-Frame Walls*, United States Department of Agriculture, Forest Products Laboratory.
- [62] Yasumara, M. and Sugiyama, H., 1983. "Rigidity and Strength of Plywood-Sheathed Wall Panels Under Reversed Cyclic Loading", *Transaction of the Architectural Institute of Japan* 338(April): 88-98.
- [63] Yasumara, M. and Sugiyama, H., 1984. "Shear Properties of Plywood-Sheathed Wall Panels with Opening", *Transaction of the Architectural Institute of Japan* 338(April): 88-98.

## **Appendix**

Initial and stabilized cyclic data of each wall specimen are presented in Tables A1 through A 20. Following each table pair, two figures are presented that depict the load-interstory drift history and initial hysteresis loops along with a bar graph showing potential and hysteretic energies per initial cycle, respectively. For clarity, the initial loops were each plotted separately next to each other. Note that one rectangle of the mesh represents 1000 lbs. and 1 inch.

Table A.1: Initial cyclic data of Wall A (no anchors,  $r = 1.0$ )

<b>Phase</b>	<b>Int. Drift</b> (in.)	<b>Load</b> (lbs.)	<b>Avg. <math>k_c</math></b> (lbs./in.)	<b><math>U_1</math></b> (lbs.-in.)	<b><math>W_d</math></b> (lbs.-in.)	<b>EVDR</b> (rad <sup>-1</sup> )
<b>1</b>	0.02	1739	77942	31	15	0.08
	-0.02	-1363				
<b>2</b>	0.05	2787	76941	120	65	0.09
	-0.03	-3216				
<b>3</b>	0.08	4049	73103	274	156	0.09
	-0.05	-4881				
<b>4</b>	0.10	5204	58381	499	317	0.10
	-0.07	-6681				
<b>5</b>	0.24	12428	50878	3192	2409	0.12
	-0.23	-14871				
<b>6</b>	0.33	16080	43357	5614	4333	0.12
	-0.34	-17718				
<b>7</b>	0.50	21746	36131	11294	9910	0.14
	-0.52	-22498				
<b>8</b>	0.67	24566	29422	17553	15135	0.14
	-0.72	-25775				
<b>9</b>	0.87	25641	24661	23505	20359	0.14
	-0.92	-26930				
<b>10</b>	1.05	25909	19480	28850	24280	0.13
	-1.11	-27413				
<b>11</b>	1.24	23036	14695	31828	27218	0.14
	-1.32	-26742				
<b>12</b>	1.38	19195	10019	29632	29894	0.16
	-1.45	-22525				
<b>13</b>	1.63	16698	7322	27799	23602	0.14
	-1.71	-16671				
<b>14</b>	1.84	13878	4070	25757	27185	0.17
	-1.91	-13582				
<b>15</b>	2.05	9581	2915	17502	17581	0.16
	-2.10	-7298				

Table A.2: Stabilized cyclic data of Wall A (no anchors,  $r = 1.0$ )

<b>Phase</b>	<b>Int. Drift</b> (in.)	<b>Load</b> (lbs.)	<b>Avg. <math>k_c</math></b> (lbs./in.)	<b><math>U_1</math></b> (lbs.-in.)	<b><math>W_d</math></b> (lbs.-in.)	<b>EVDR</b> (rad <sup>-1</sup> )
<b>1</b>	0.02	1739	85202	37	19	0.08
	-0.02	-1632				
<b>2</b>	0.06	2975	78653	136	94	0.11
	-0.03	-3512				
<b>3</b>	0.08	4049	77863	275	157	0.09
	-0.05	-4881				
<b>4</b>	0.10	5123	73871	472	270	0.09
	-0.07	-6439				
<b>5</b>	0.24	12025	55175	3091	2001	0.10
	-0.24	-14093				
<b>6</b>	0.32	15221	47900	5159	3795	0.12
	-0.33	-16214				
<b>7</b>	0.49	18954	38094	9891	7556	0.12
	-0.53	-19840				
<b>8</b>	0.67	20995	30811	15104	11405	0.12
	-0.73	-22122				
<b>9</b>	0.87	21720	24873	20105	15131	0.12
	-0.93	-22982				
<b>10</b>	1.06	20001	19867	23588	18230	0.12
	-1.12	-23277				
<b>11</b>	1.25	17799	14884	24390	23397	0.15
	-1.31	-20296				
<b>12</b>	1.42	15328	10495	22486	18534	0.13
	-1.51	-15382				
<b>13</b>	1.64	12267	7330	20628	21193	0.16
	-1.72	-12320				
<b>14</b>	1.83	8560	4073	14216	16008	0.18
	-1.92	-6654				
<b>15</b>	2.04	6788	2839	12217	10844	0.14
	-2.12	-4989				

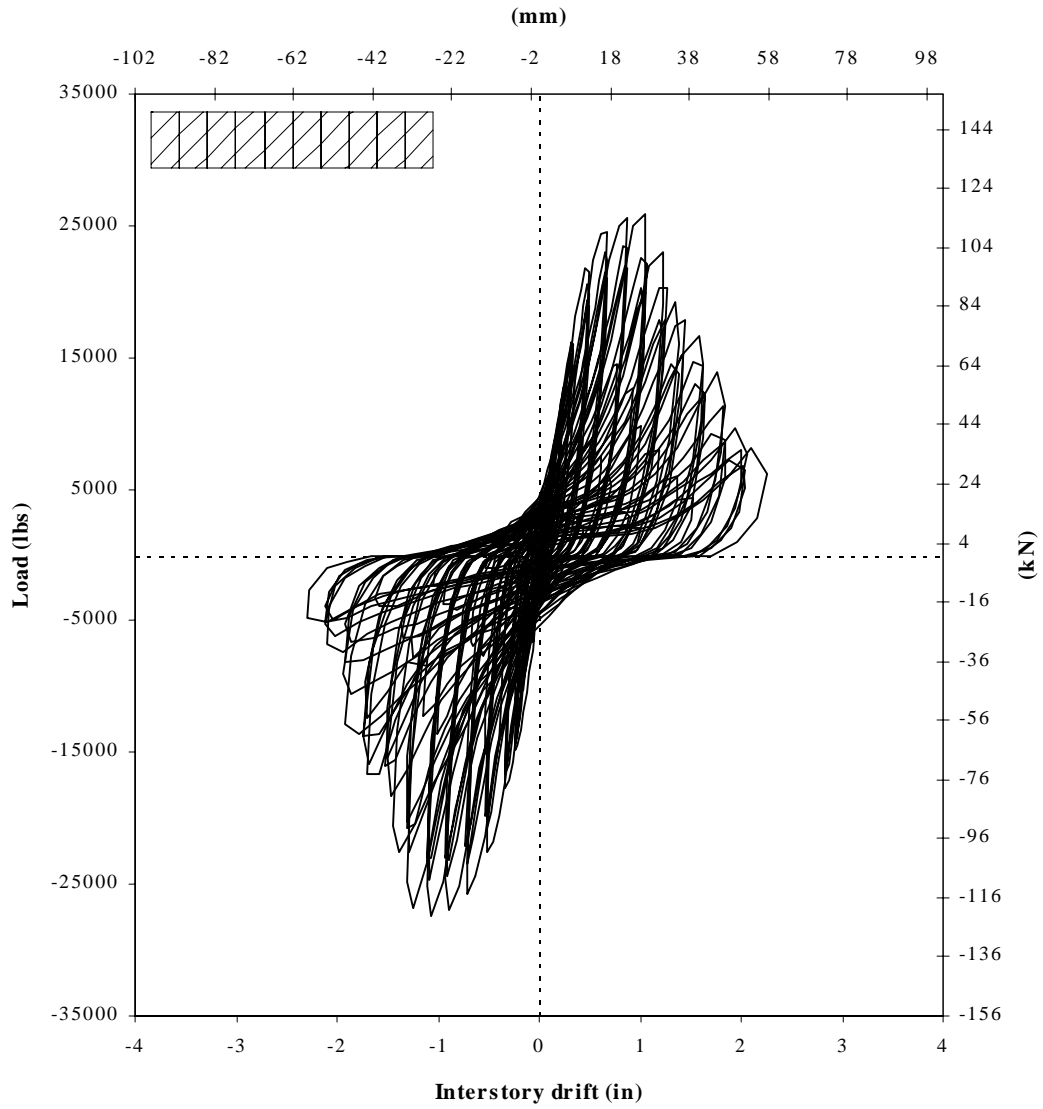


Figure A.1: Hysteresis loops of Wall A (no anchors)

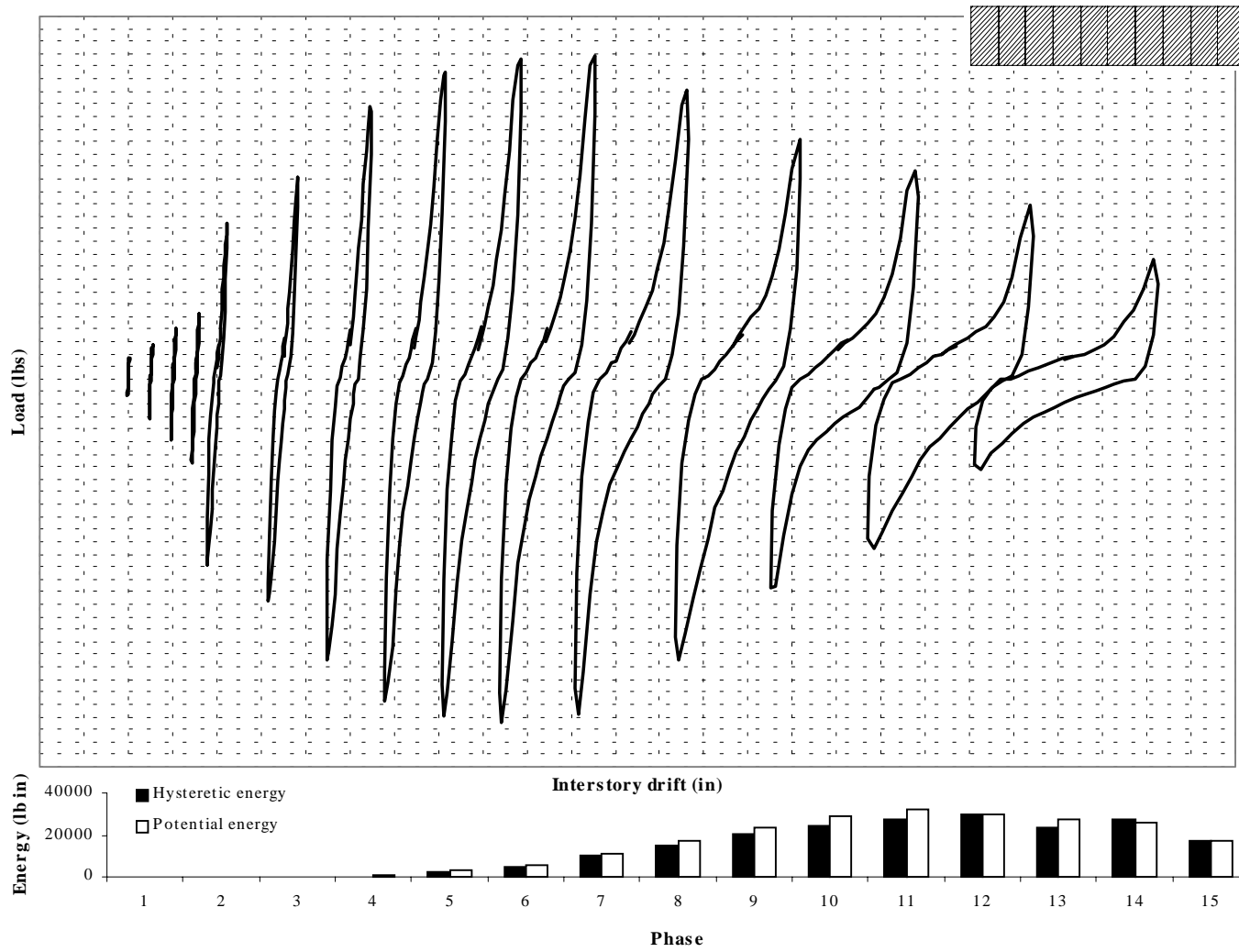


Figure A.2: Initial hysteresis loops of Wall A (no anchors) together with hyst. and pot. energy for comparison

Table A.3: Initial cyclic data of Wall D (no anchors,  $r = 0.48$ )

Phase	Int. Drift (in.)	Load (lbs.)	Avg. $k_c$ (lbs./in.)	$U_1$ (lbs.-in.)	$W_d$ (lbs.-in.)	EVDR (rad <sup>-1</sup> )
1	0.02	853	26442	11	4	0.06
	-0.02	-155				
2	0.04	1524	23514	53	28	0.08
	-0.05	-853				
3	0.07	2035	23459	121	75	0.10
	-0.07	-1336				
4	0.10	2491	21802	218	149	0.11
	-0.10	-1873				
5	0.29	5123	15920	1298	1108	0.14
	-0.28	-3968				
6	0.39	6117	14286	2158	1665	0.12
	-0.39	-4989				
7	0.58	7782	12225	4151	3388	0.13
	-0.58	-6466				
8	0.77	8775	10639	6379	4993	0.12
	-0.77	-7701				
9	0.97	9608	9523	9054	6862	0.12
	-0.98	-8963				
10	1.16	10091	8459	11500	8462	0.12
	-1.17	-9635				
11	1.35	10306	7512	13520	10080	0.12
	-1.34	-9850				
12	1.48	9823	6423	14375	10448	0.12
	-1.51	-9393				
13	1.73	9608	5529	16933	12695	0.12
	-1.77	-9742				
14	1.95	8802	4583	17636	13409	0.12
	-1.98	-9178				
15	2.15	8131	3809	17818	13563	0.12
	-2.17	-8346				
16	2.35	7567	3191	17751	14706	0.13
	-2.37	-7486				
17	2.55	6815	2677	17415	16157	0.15
	-2.55	-6842				
18	2.75	5848	2050	15482	14837	0.15
	-2.75	-5418				
19	2.81	3780	1283	10131	9227	0.14
	-2.81	-3431				
20	3.10	3538	1082	10126	9261	0.15
	-3.01	-3082				
21	3.22	2625	687	7367	8866	0.19
	-3.35	-1873				
22	3.49	558	147	974	3370	0.55
	-3.56	0				
23	3.46	396	57	1635	2464	0.24
	-3.76	-504				

Table A.4: Stabilized cyclic data of Wall D (no anchors,  $r = 0.48$ )

Phase	Int. Drift (in.)	Load (lbs.)	Avg. $k_c$ (lbs./in.)	$U_1$ (lbs.-in.)	$W_d$ (lbs.-in.)	EVDR (rad <sup>-1</sup> )
1	0.02	880	25695	12	4	0.05
	-0.02	-208				
2	0.05	1551	24310	56	30	0.08
	-0.05	-853				
3	0.07	2061	23455	121	70	0.09
	-0.07	-1309				
4	0.10	2518	21727	211	139	0.11
	-0.10	-1766				
5	0.29	4908	14955	1270	925	0.12
	-0.30	-3807				
6	0.39	5687	13145	1997	1430	0.11
	-0.39	-4559				
7	0.58	6949	10872	3687	2644	0.11
	-0.59	-5714				
8	0.77	7782	9387	5654	4049	0.11
	-0.78	-6788				
9	0.97	8426	8294	7892	5566	0.11
	-0.98	-7755				
10	1.16	8722	7302	9942	6979	0.11
	-1.17	-8319				
11	1.35	8883	6380	11813	8361	0.11
	-1.37	-8480				
12	1.53	8534	5515	13207	9503	0.11
	-1.56	-8534				
13	1.75	8023	4588	14125	10397	0.12
	-1.75	-8077				
14	1.95	7325	3789	14423	10891	0.12
	-1.96	-7459				
15	2.13	6734	3099	14286	11325	0.13
	-2.16	-6573				
16	2.34	6063	2524	13928	11602	0.13
	-2.36	-5794				
17	2.54	5177	2040	13271	11435	0.14
	-2.56	-5230				
18	2.74	3968	1323	10047	9236	0.15
	-2.77	-3324				
19	2.90	3565	1135	9652	8538	0.14
	-2.94	-3055				
20	3.04	2787	852	8094	7641	0.15
	-3.13	-2464				
21	3.33	1148	195	2173	3986	0.29
	-3.35	-155				
22	3.54	772	127	1591	2726	0.27
	-3.53	-128				

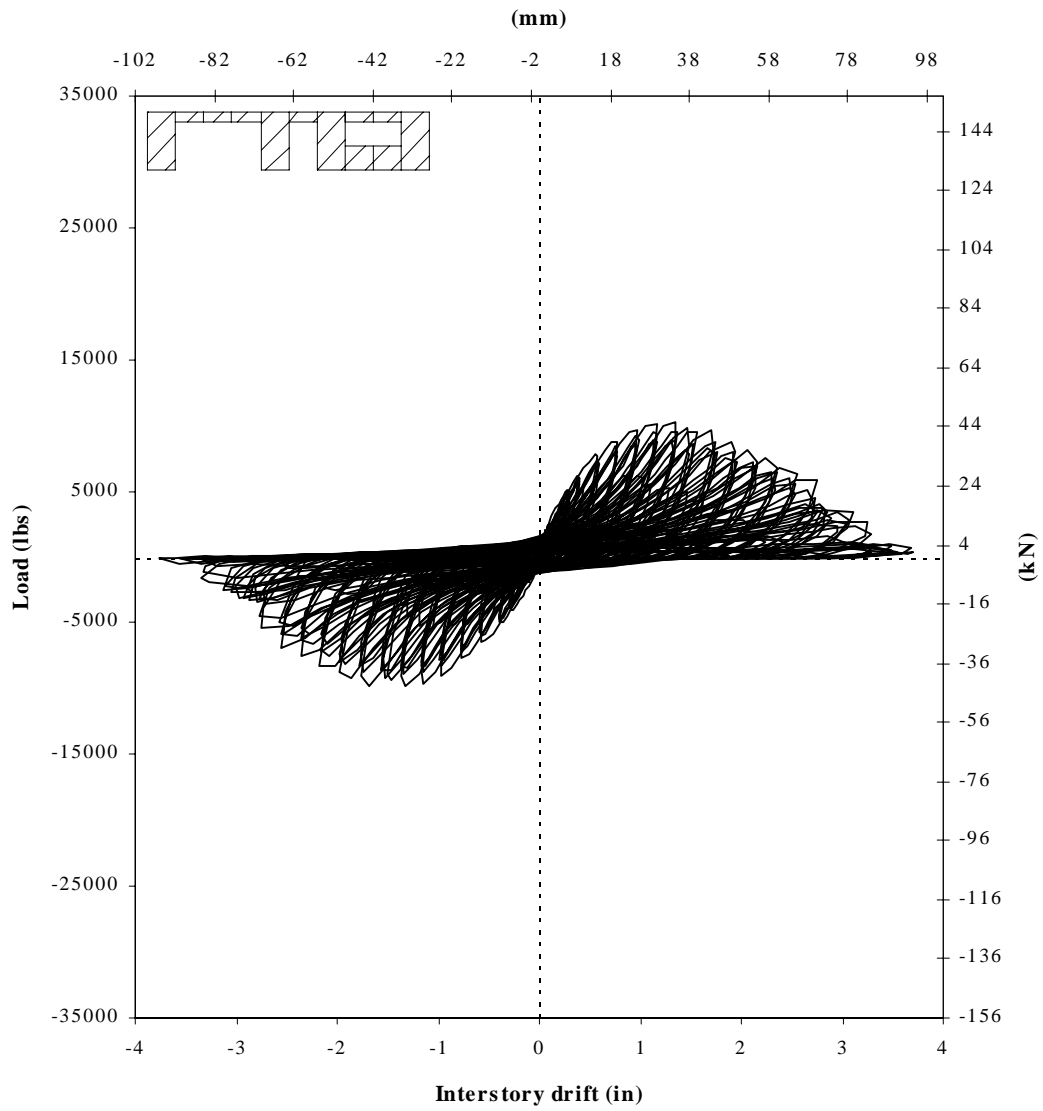


Figure A.3: Hysteresis loops of Wall D (no anchors)

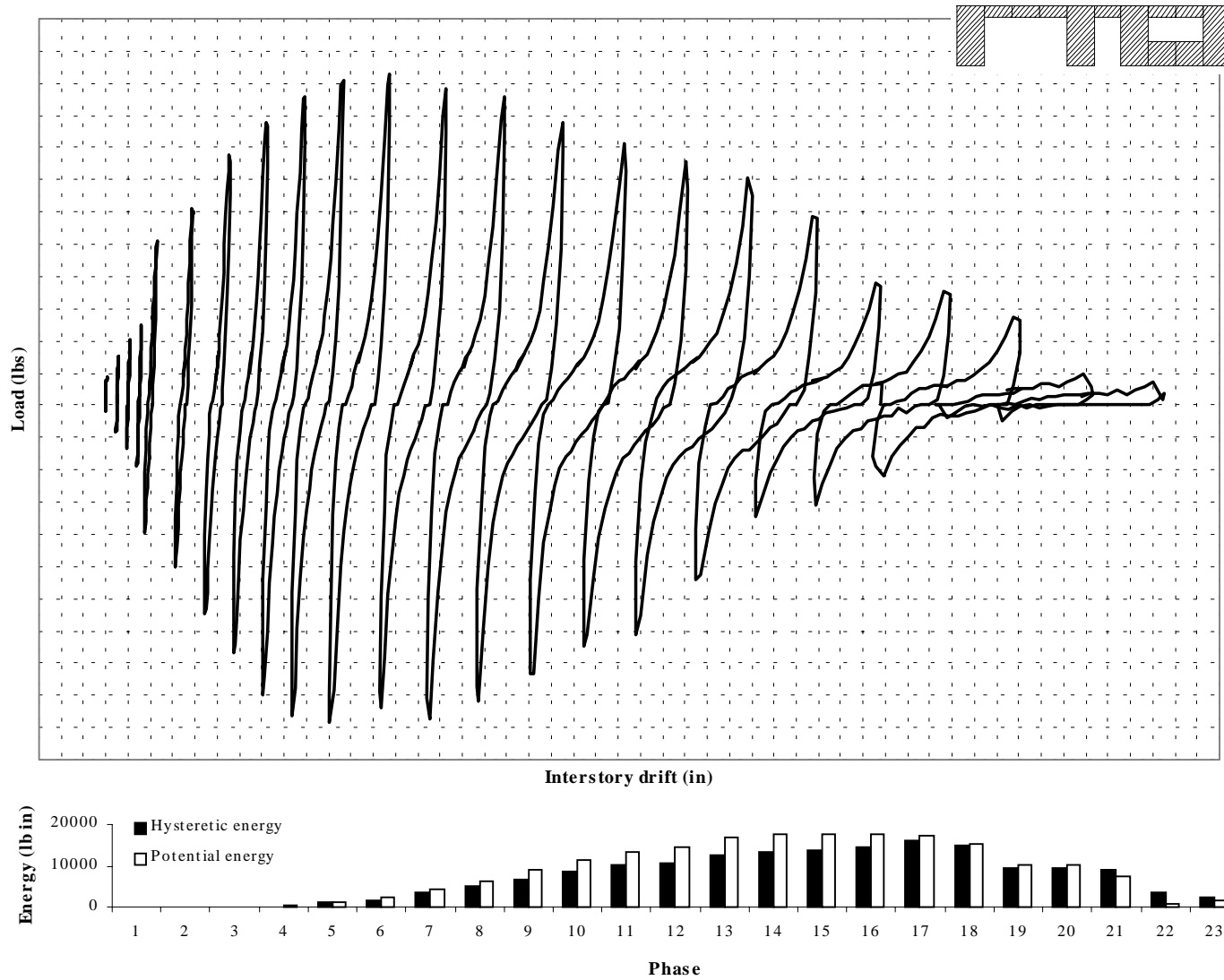


Figure A.4: Initial hysteresis loops of Wall D (no anchors) together with hyst. and pot. energy for comparison

Table A.5: Initial cyclic data of Wall E (no anchors,  $r = 0.30$ )

Phase	Int. Drift (in.)	Load (lbs.)	Avg. $k_c$ (lbs./in.)	$U_1$ (lbs.-in.)	$W_d$ (lbs.-in.)	EVDR (rad <sup>-1</sup> )
1	0.02	692	18846	7	5	0.11
	-0.02	-47				
2	0.04	1041	17408	32	29	0.15
	-0.05	-450				
3	0.07	1390	15675	80	72	0.14
	-0.07	-853				
4	0.10	1632	14022	141	133	0.15
	-0.10	-1175				
5	0.29	2787	9215	763	871	0.18
	-0.29	-2518				
6	0.39	3270	8087	1247	1211	0.15
	-0.40	-3082				
7	0.58	4156	6879	2320	2347	0.16
	-0.59	-3834				
8	0.77	4613	5669	3412	3339	0.16
	-0.79	-4183				
9	0.96	4908	4792	4571	4331	0.15
	-0.99	-4452				
10	1.15	5069	4138	5507	5092	0.15
	-1.16	-4478				
11	1.34	5069	3415	6305	5605	0.14
	-1.38	-4210				
12	1.48	4801	2957	6664	5663	0.14
	-1.53	-4076				
13	1.73	4586	2478	7617	6897	0.14
	-1.78	-4102				
14	1.94	4452	2045	7857	7690	0.16
	-1.98	-3565				
15	2.15	3189	1499	7018	6600	0.15
	-2.18	-3297				
16	2.35	3377	1340	7462	6457	0.14
	-2.37	-2948				
17	2.55	1471	566	3686	5334	0.23
	-2.56	-1417				
18	2.75	853	329	2637	2739	0.17
	-2.75	-1068				
19	3.02	611	296	2105	2346	0.18
	-2.61	-907				

Table A.6: Stabilized cyclic data of Wall E (no anchors,  $r = 0.30$ )

Phase	Int. Drift (in.)	Load (lbs.)	Avg. $k_c$ (lbs./in.)	$U_1$ (lbs.-in.)	$W_d$ (lbs.-in.)	EVDR (rad <sup>-1</sup> )
1	0.02	692	17856	9	6	0.10
	-0.03	-101				
2	0.04	1068	17064	34	27	0.13
	-0.05	-450				
3	0.07	1363	15645	79	70	0.14
	-0.08	-853				
4	0.10	1578	13301	132	127	0.15
	-0.10	-1068				
5	0.29	2599	8295	716	712	0.16
	-0.30	-2276				
6	0.39	3028	7389	1134	1064	0.15
	-0.40	-2760				
7	0.58	3673	5988	2044	1881	0.15
	-0.59	-3324				
8	0.76	4022	4921	2967	2705	0.15
	-0.79	-3619				
9	0.97	4237	4101	3918	3539	0.14
	-0.99	-3780				
10	1.15	4371	3460	4707	4127	0.14
	-1.18	-3700				
11	1.35	4317	2974	5512	4649	0.13
	-1.38	-3780				
12	1.52	4183	2512	5977	5303	0.14
	-1.57	-3565				
13	1.74	4022	2055	6326	6199	0.16
	-1.77	-3189				
14	1.93	3538	1635	6223	5541	0.14
	-1.98	-2840				
15	2.13	2948	1270	5881	5449	0.15
	-2.18	-2518				
16	2.34	2437	943	5238	5817	0.18
	-2.38	-2008				
17	2.54	450	306	1946	2322	0.19
	-2.57	-1068				
18	2.96	584	276	2094	2012	0.15
	-2.56	-960				

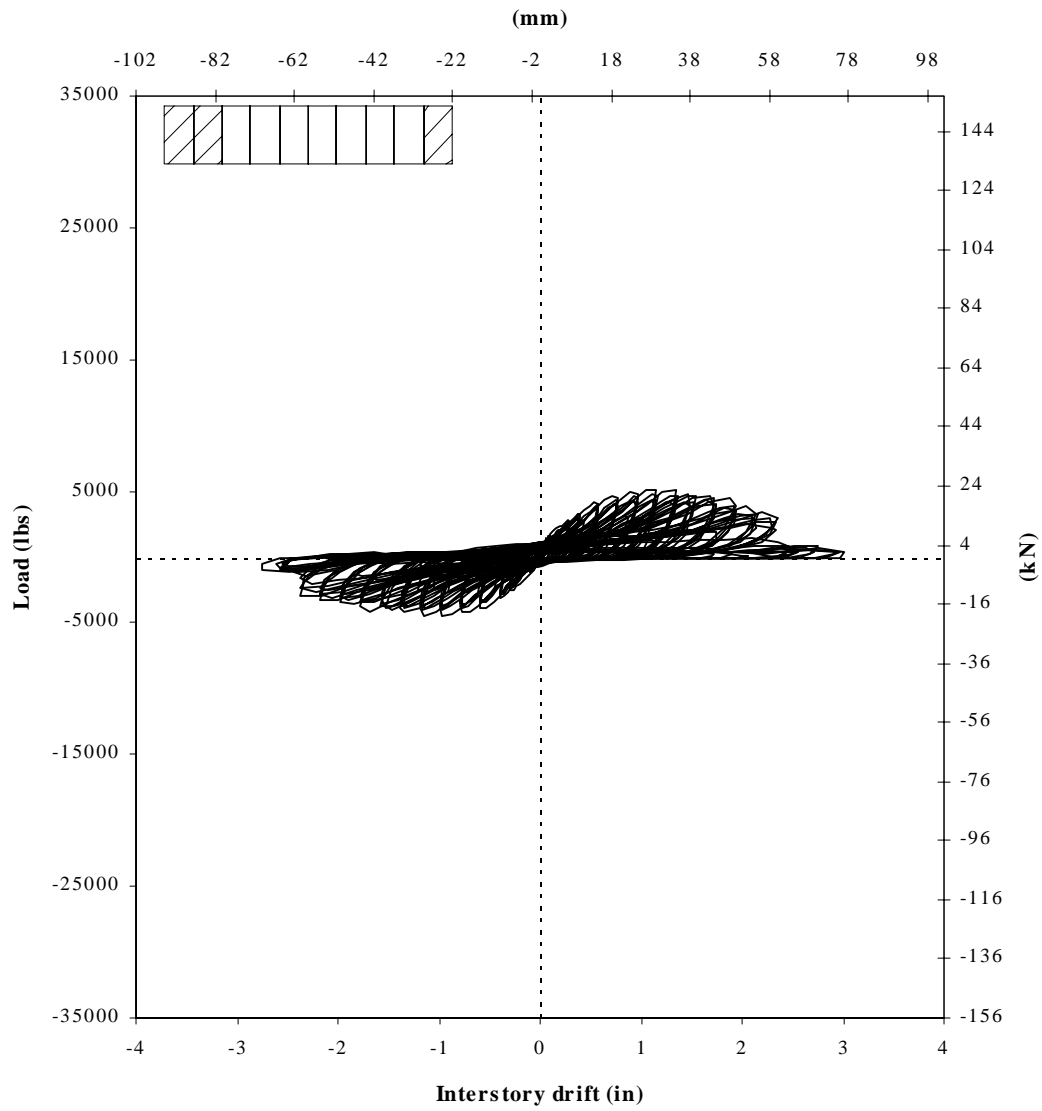


Figure A.5: Hysteresis loops of Wall E (no anchors)

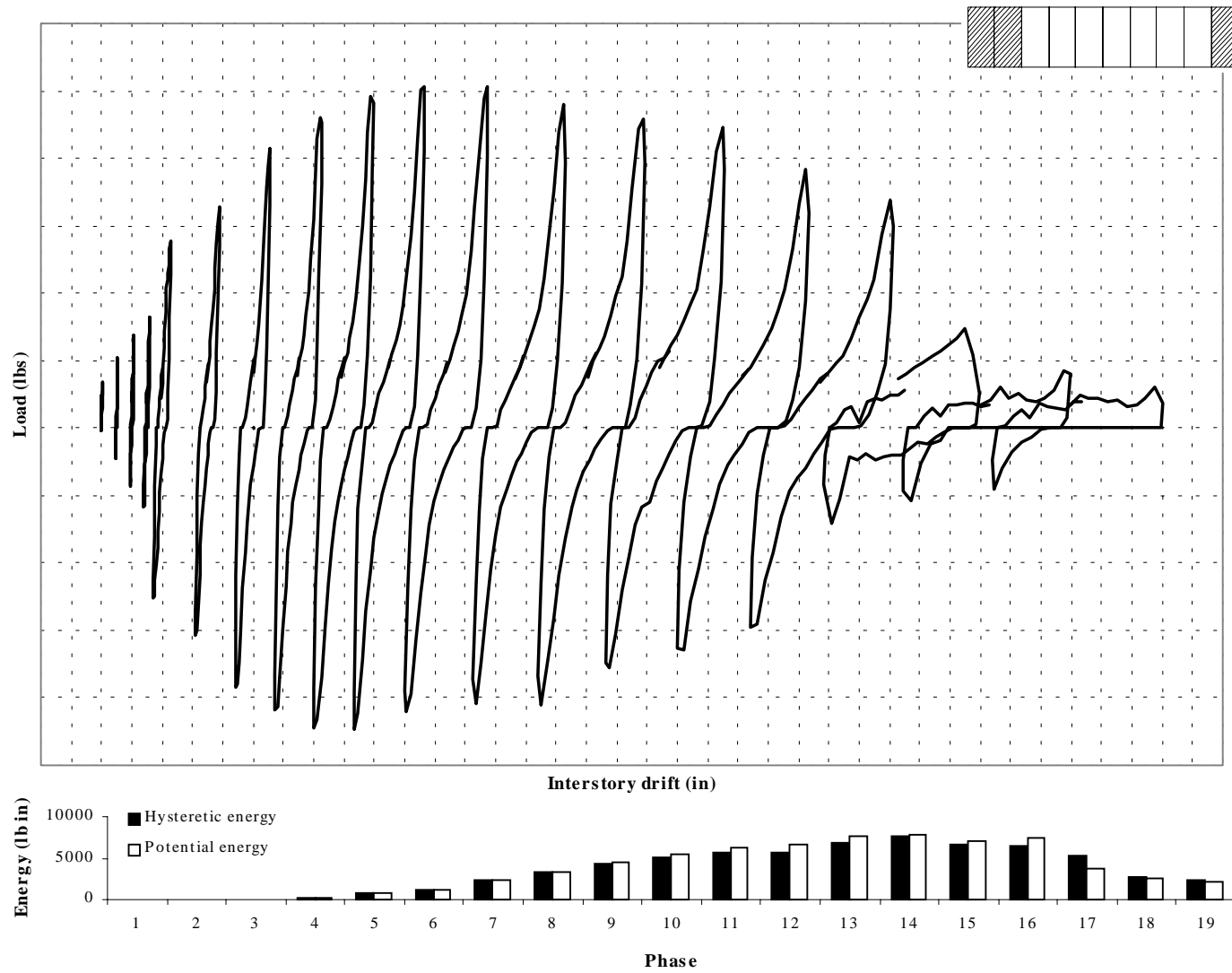


Figure A.6: Initial hysteresis loops of Wall E (no anchors) together with hyst. and pot. energy for comparison

Table A.7: Initial cyclic data of Wall A (max. anchors,  $r = 1.0$ )

Phase	Int. Drift (in.)	Load (lbs.)	Avg. $k_c$ (lbs./in.)	$U_1$ (lbs.-in.)	$W_d$ (lbs.-in.)	EVDR (rad <sup>-1</sup> )
1	0.02	1659	118783	46	22	0.08
	-0.02	-2985				
2	0.05	3369	101138	177	101	0.09
	-0.04	-5061				
3	0.07	5440	90709	417	220	0.08
	-0.06	-6831				
4	0.10	7529	81696	787	452	0.09
	-0.09	-8480				
5	0.29	15806	60966	3963	3247	0.13
	-0.22	-15049				
6	0.40	18140	50524	6235	4585	0.12
	-0.31	-17052				
7	0.57	23017	42495	11507	9006	0.12
	-0.48	-21046				
8	0.72	25743	36102	16910	12994	0.12
	-0.65	-23616				
9	0.92	27625	30028	23271	17868	0.12
	-0.84	-25200				
10	1.10	28570	25784	29138	21943	0.12
	-1.02	-26213				
11	1.27	28901	22558	34101	25989	0.12
	-1.19	-26543				
12	1.43	27682	19102	36945	26095	0.11
	-1.35	-25426				
13	1.68	28068	16411	44554	32926	0.12
	-1.61	-26000				
14	1.90	26540	13764	47464	34474	0.12
	-1.81	-24566				
15	2.10	22515	10441	44425	32986	0.12
	-2.02	-20551				
16	2.32	16601	7219	37487	26482	0.11
	-2.24	-16295				
17	2.52	14590	5617	34589	23451	0.11
	-2.44	-13284				
18	2.72	12852	4563	33163	21961	0.11
	-2.67	-11751				
19	2.82	11045	3697	28592	17992	0.10
	-2.74	-9517				
20	3.12	11380	3369	30994	19364	0.10
	-2.93	-9047				
22	3.29	10123	2633	30703	19529	0.10
	-3.25	-8622				
23	3.55	9302	2590	30202	17955	0.09
	-3.46	-7892				
24	3.77	8450	2258	29260	16726	0.09
	-3.66	-7279				
25	4.80	7757	1803	28593	16607	0.09
	-3.08	-6476				

Table A.8: Stabilized cyclic data of Wall A (max. anchors,  $r = 1.0$ )

Phase	Int. Drift (in.)	Load (lbs.)	Avg. $k_c$ (lbs./in.)	$U_1$ (lbs.-in.)	$W_d$ (lbs.-in.)	EVDR (rad <sup>-1</sup> )
1	0.02	2008	89749	54	24	0.07
	-0.02	-3069				
2	0.05	3616	81142	187	95	0.08
	-0.04	-5042				
3	0.07	5679	75627	437	217	0.08
	-0.07	-6842				
4	0.10	7551	60854	747	395	0.08
	-0.09	-7991				
5	0.31	14726	53252	3889	2628	0.11
	-0.23	-13714				
6	0.40	16896	46513	5754	3843	0.11
	-0.30	-15497				
7	0.56	20557	38048	10258	6670	0.10
	-0.47	-18806				
8	0.72	22600	31450	14895	9455	0.10
	-0.65	-20627				
9	0.92	24000	26103	20223	13239	0.10
	-0.84	-21910				
10	1.10	24660	22212	25035	16815	0.11
	-1.02	-22474				
11	1.30	24744	18802	29841	20440	0.11
	-1.22	-22606				
12	1.48	24459	16254	34085	23649	0.11
	-1.42	-22606				
13	1.71	22139	13047	36177	26423	0.12
	-1.62	-21298				
14	1.91	21051	10771	37638	26837	0.11
	-1.82	-19206				
15	2.13	15511	7310	31804	22089	0.11
	-2.04	-14979				
16	2.34	13454	5647	29838	20072	0.11
	-2.26	-12503				
17	2.53	12186	4624	29041	18828	0.10
	-2.48	-10988				
18	2.76	11101	3763	27876	17919	0.10
	-2.68	-9380				
19	2.90	10604	3403	28132	17348	0.10
	-2.84	-8963				
20	3.05	9224	2647	26320	16727	0.10
	-3.04	-8064				
21	3.36	8861	2578	26725	15791	0.09
	-3.27	-7255				
22	3.58	7943	2065	25880	14858	0.09
	-3.46	-6742				
23	4.51	7435	1935	25605	16650	0.10
	-2.88	-6141				
24	4.81	7121	1715	27230	14634	0.09
	-3.25	-6216				

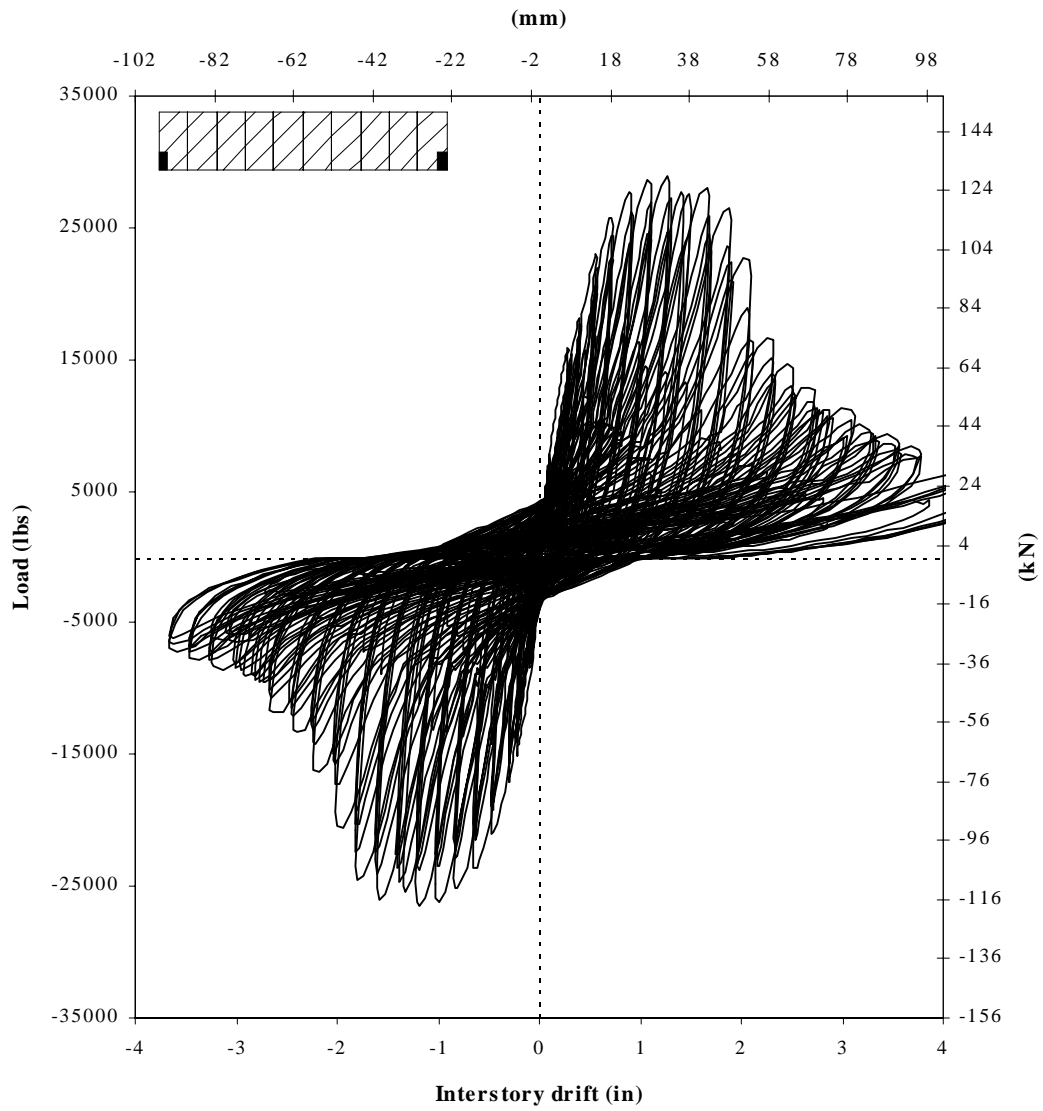


Figure A.7: Hysteresis loops of Wall A (max. anchors)

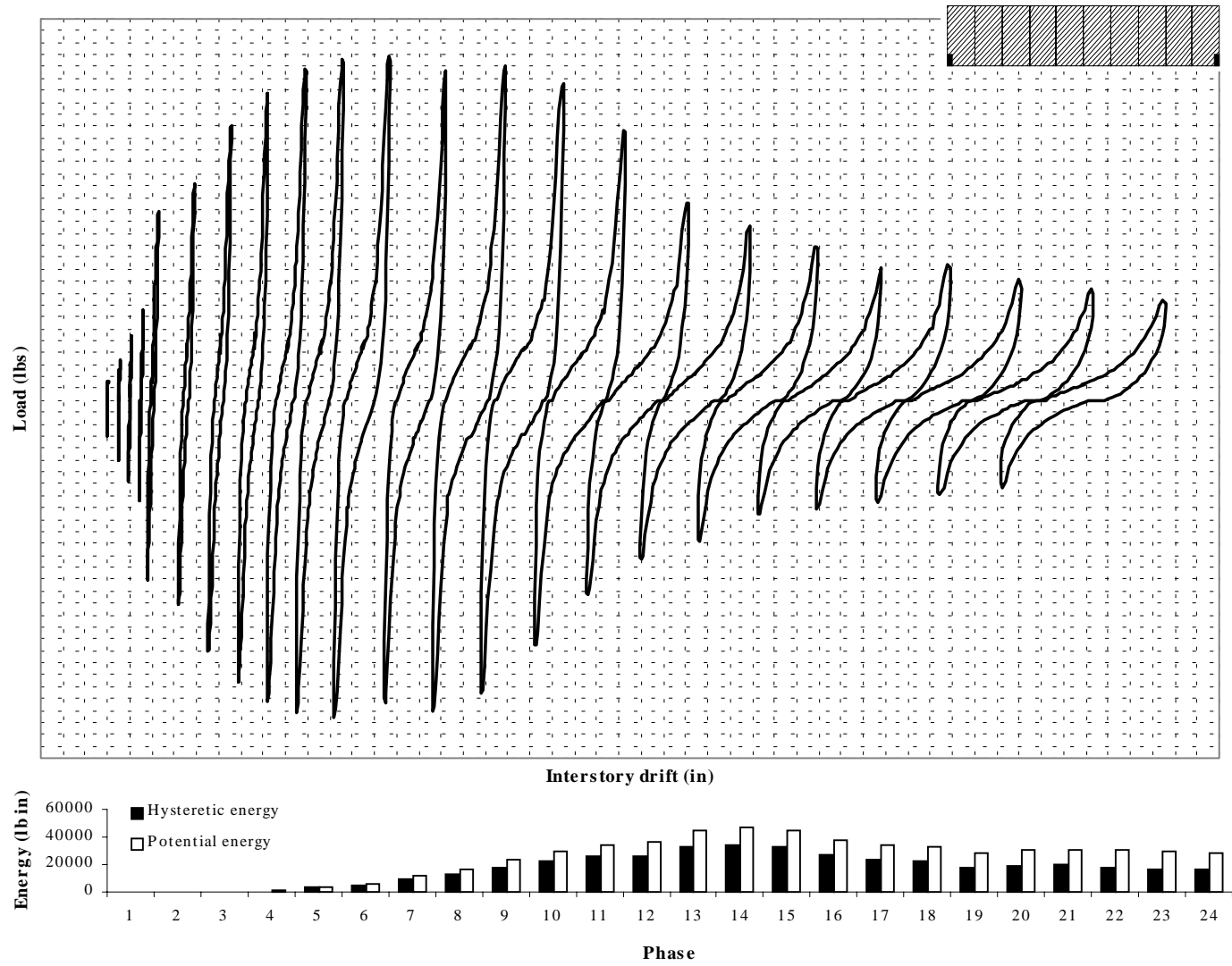


Figure A.8: Initial hysteresis loops of Wall A (max. anchors) together with hyst. and pot. energy for comparison

Table A.9: Initial cyclic data of Wall D (max. anchors,  $r = 0.48$ )

Phase	Int. Drift (in.)	Load (lbs.)	Avg. $k_c$ (lbs./in.)	$U_1$ (lbs.-in.)	$W_d$ (lbs.-in.)	EVDR (rad <sup>-1</sup> )
1	0.02	1497	34138	17	9	0.08
	-0.02	-20				
2	0.05	2088	32200	70	39	0.09
	-0.04	-907				
3	0.07	2652	29516	154	90	0.09
	-0.07	-1605				
4	0.10	3216	27656	286	170	0.09
	-0.10	-2411				
5	0.29	6170	21095	1727	1219	0.11
	-0.29	-5902				
6	0.38	7352	18955	2863	1769	0.10
	-0.39	-7379				
7	0.57	9286	16464	5531	3811	0.11
	-0.59	-9796				
8	0.74	10897	14679	8665	5706	0.10
	-0.79	-11649				
9	0.92	12052	12938	12119	7951	0.10
	-1.01	-12965				
10	1.08	12589	11412	15182	9760	0.10
	-1.22	-13690				
11	1.26	12992	9982	18042	11468	0.10
	-1.43	-13797				
12	1.38	12616	8775	19115	11664	0.10
	-1.57	-13233				
13	1.63	12750	7663	22873	14837	0.10
	-1.82	-13690				
14	1.85	11461	6011	22516	15092	0.11
	-2.02	-11783				
15	2.06	7755	3775	17310	12241	0.11
	-2.22	-8399				
16	2.26	6788	3093	16924	11092	0.10
	-2.41	-7674				
17	2.45	5848	2549	16344	10684	0.10
	-2.60	-7057				
18	2.65	5230	2129	15852	10180	0.10
	-2.79	-6385				
19	2.72	4129	1752	13681	8876	0.10
	-2.85	-5660				
20	3.01	4237	1609	14811	9427	0.10
	-3.05	-5526				
21	3.16	4049	1435	15543	9664	0.10
	-3.39	-5392				
22	3.40	3592	1174	14532	9087	0.10
	-3.61	-4666				
23	3.62	2867	1000	14000	8807	0.10
	-3.82	-4613				
24	3.83	2572	865	13505	8415	0.10
	-4.02	-4264				

Table A.10: Stabilized cyclic data of Wall D (max. anchors,  $r = 0.48$ )

Phase	Int. Drift (in.)	Load (lbs.)	Avg. $k_c$ (lbs./in.)	$U_1$ (lbs.-in.)	$W_d$ (lbs.-in.)	EVDR (rad <sup>-1</sup> )
1	0.02	1471	28568	17	8	0.07
	-0.02	-47				
2	0.05	2088	27267	74	38	0.08
	-0.04	-933				
3	0.07	2625	22230	152	86	0.09
	-0.07	-1632				
4	0.10	3109	21631	265	151	0.09
	-0.10	-2276				
5	0.28	5875	18303	1654	934	0.09
	-0.30	-5526				
6	0.38	6788	16015	2620	1457	0.09
	-0.40	-6707				
7	0.56	8507	13997	5023	2773	0.09
	-0.60	-8829				
8	0.73	9688	12209	7756	4303	0.09
	-0.81	-10413				
9	0.90	10440	10577	10544	5966	0.09
	-1.03	-11353				
10	1.08	10924	9213	13125	7532	0.09
	-1.23	-11729				
11	1.26	11273	8036	15575	9067	0.09
	-1.43	-11837				
12	1.43	11165	6897	17795	10597	0.09
	-1.62	-12079				
13	1.66	10494	4950	18752	11559	0.10
	-1.81	-11139				
14	1.85	6922	3583	14633	11045	0.12
	-2.01	-8184				
15	2.04	6305	2604	13547	8973	0.11
	-2.21	-6439				
16	2.24	5150	2140	12886	8591	0.11
	-2.41	-5902				
17	2.44	4478	1805	12475	8310	0.11
	-2.61	-5365				
18	2.65	4129	1625	12698	8402	0.11
	-2.82	-5123				
19	2.81	4022	1522	14006	8605	0.10
	-2.98	-5606				
20	2.95	3431	1344	13282	7977	0.10
	-3.18	-5177				
21	3.24	3431	1054	12809	7967	0.10
	-3.40	-4264				
22	3.45	2948	944	12587	7645	0.10
	-3.59	-4183				
23	3.64	2625	854	11994	7362	0.10
	-3.77	-3834				

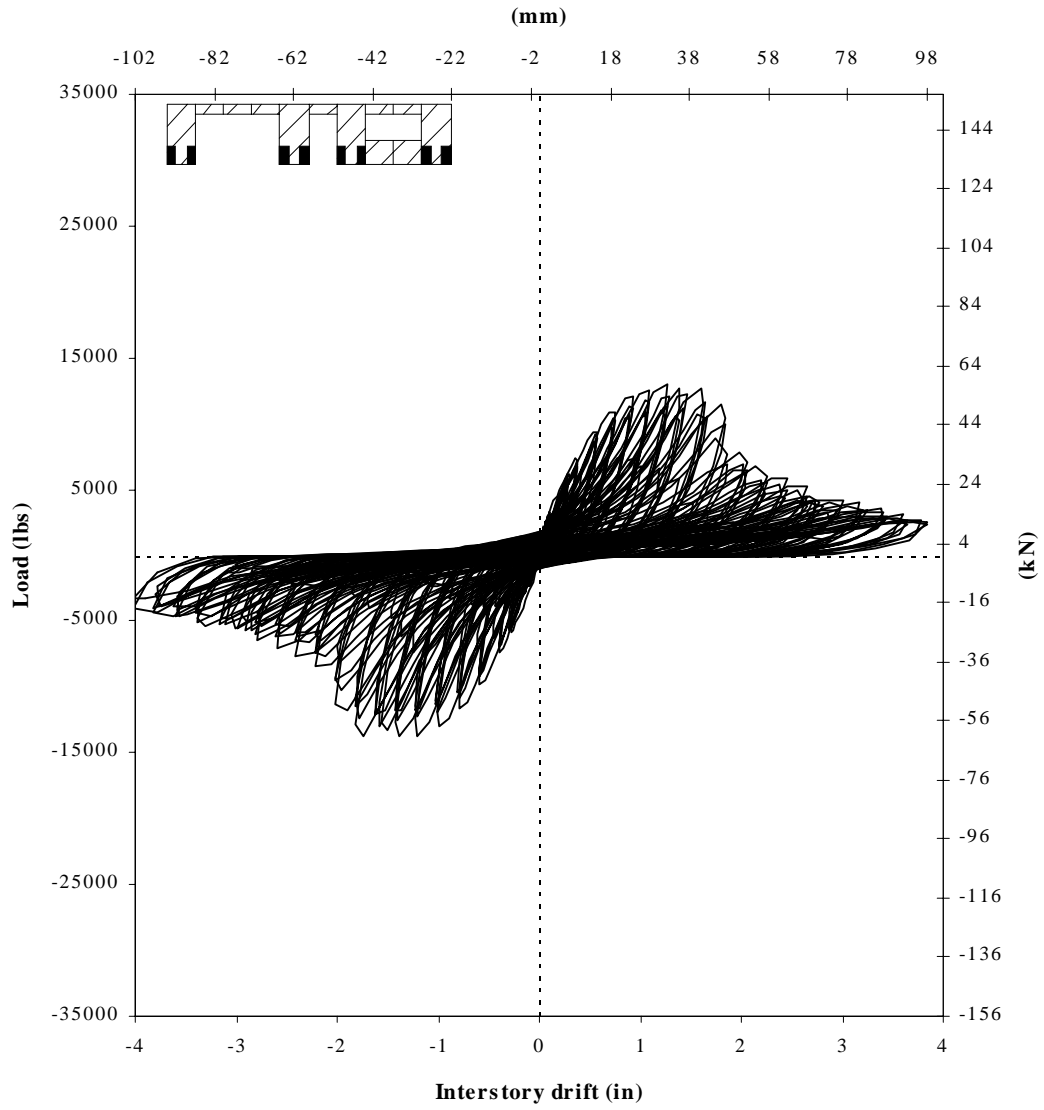


Figure A.9: Hysteresis loops of Wall D (max anchors)

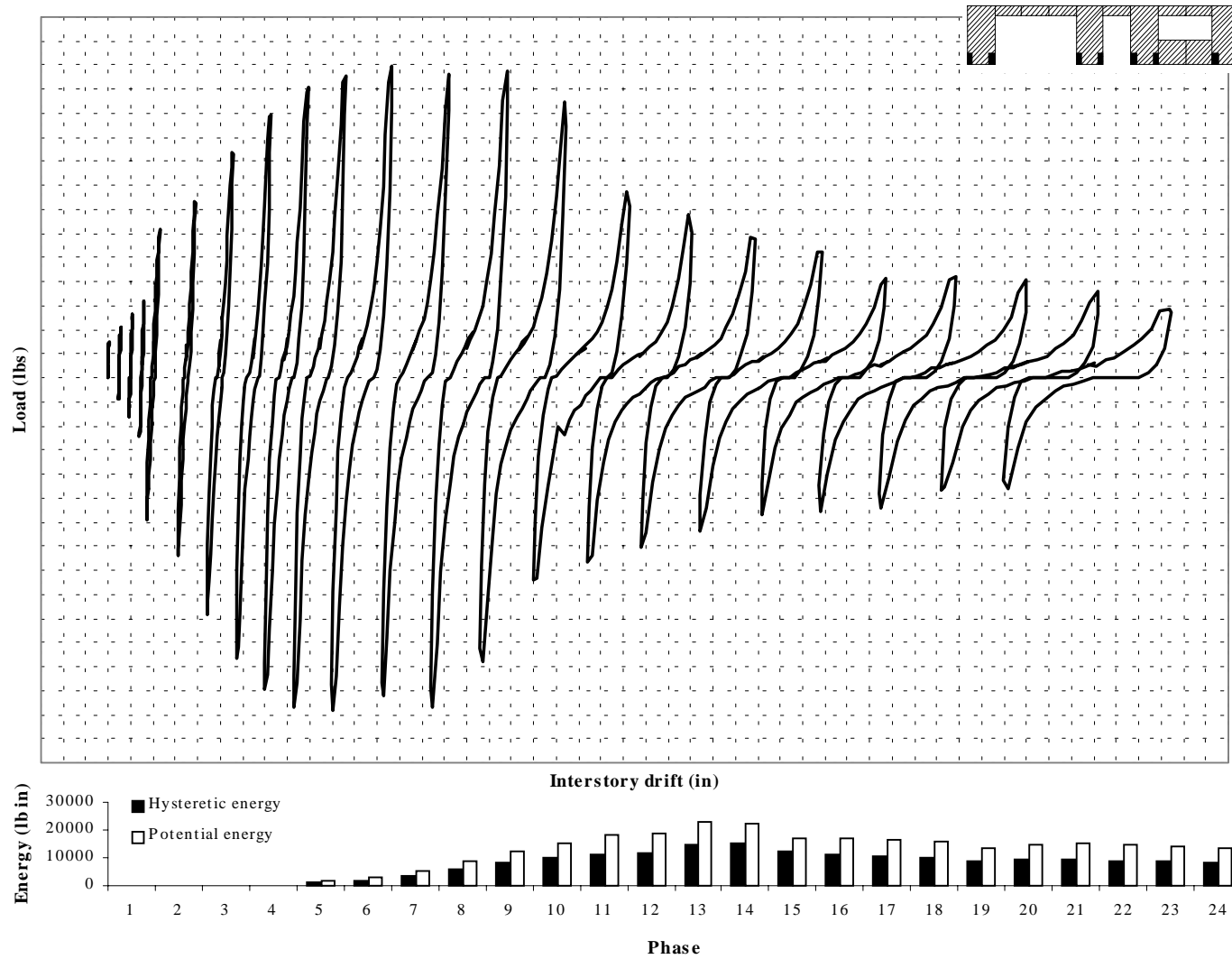


Figure A.10: Initial hysteresis loops of Wall D (max. anchors) together with hyst. and pot. energy for comparison

Table A.11: Initial cyclic data of Wall E (max. anchors,  $r = 0.30$ )

Phase	Int. Drift (in.)	Load (lbs.)	Avg. $k_c$ (lbs./in.)	$U_1$ (lbs.-in.)	$W_d$ (lbs.-in.)	EVDR (rad <sup>-1</sup> )
1	0.02	799	26902	11	3	0.05
	-0.02	-289				
2	0.04	1444	25765	54	30	0.09
	-0.05	-907				
3	0.07	1927	23760	116	76	0.10
	-0.07	-1390				
4	0.10	2384	21635	218	145	0.11
	-0.10	-1954				
5	0.28	4532	15290	1234	1046	0.13
	-0.29	-4156				
6	0.38	5445	13531	2033	1492	0.12
	-0.39	-5042				
7	0.56	7057	11705	3860	3029	0.12
	-0.58	-6385				
8	0.76	7970	9944	5820	4432	0.12
	-0.78	-7245				
9	0.96	8480	8427	7897	5956	0.12
	-0.98	-7835				
10	1.16	8695	7165	9659	7128	0.12
	-1.17	-7943				
11	1.30	8775	6238	11064	8261	0.12
	-1.37	-7835				
12	1.50	8184	5192	11704	8101	0.11
	-1.51	-7406				
13	1.74	8292	4436	13604	9800	0.11
	-1.76	-7245				
14	1.96	6278	2913	11155	8399	0.12
	-1.95	-5123				
15	2.16	5579	2378	11038	7370	0.11
	-2.15	-4666				
16	2.35	5230	2009	11091	7078	0.10
	-2.35	-4210				
17	2.53	4666	1518	9752	6529	0.11
	-2.54	-3028				
18	2.73	4156	1313	9830	6206	0.10
	-2.75	-3028				
19	2.81	3538	1101	8703	5367	0.10
	-2.82	-2652				
20	3.11	3780	1039	9791	5894	0.10
	-3.01	-2599				
21	3.29	3861	974	10622	6464	0.10
	-3.33	-2572				
22	3.54	3700	822	10278	5666	0.09
	-3.53	-2115				
23	3.74	3189	663	9253	5100	0.09
	-3.72	-1766				
24	3.94	2840	566	8723	5089	0.09
	-3.89	-1605				

Table A.12: Stabilized cyclic data of Wall E (max. anchors,  $r = 0.30$ )

Phase	Int. Drift (in.)	Load (lbs.)	Avg. $k_c$ (lbs./in.)	$U_1$ (lbs.-in.)	$W_d$ (lbs.-in.)	EVDR (rad <sup>-1</sup> )
1	0.02	880	27632	13	7	0.09
	-0.03	-289				
2	0.04	1471	25783	54	31	0.09
	-0.05	-880				
3	0.07	1927	23373	120	73	0.10
	-0.07	-1417				
4	0.10	2357	20845	207	132	0.10
	-0.10	-1793				
5	0.29	4290	14196	1178	781	0.11
	-0.29	-3888				
6	0.38	5042	12572	1854	1186	0.10
	-0.39	-4613				
7	0.57	6305	10387	3461	2210	0.10
	-0.58	-5687				
8	0.76	7003	8704	5107	3294	0.10
	-0.77	-6331				
9	0.96	7352	7295	6774	86634	2.04
	-0.97	-6707				
10	1.15	7459	6123	8194	5479	0.11
	-1.16	-6707				
11	1.35	7406	5107	9383	6359	0.11
	-1.36	-6439				
12	1.53	7164	4370	10420	7110	0.11
	-1.56	-6331				
13	1.76	6278	3177	9894	7026	0.11
	-1.77	-4935				
14	1.97	4881	2238	8644	5870	0.11
	-1.96	-3914				
15	2.17	4559	1926	9029	5791	0.10
	-2.16	-3780				
16	2.37	4317	1619	9015	5639	0.10
	-2.35	-3324				
17	2.56	3861	1272	8269	5225	0.10
	-2.54	-2625				
18	2.76	3646	1139	8557	5310	0.10
	-2.72	-2599				
19	2.90	3673	1080	9030	5382	0.09
	-2.89	-2572				
20	3.02	3297	875	8125	5020	0.10
	-3.09	-2035				
21	3.30	3163	728	7982	4833	0.10
	-3.33	-1659				
22	3.53	2572	584	7272	4408	0.10
	-3.53	-1551				
23	3.74	2357	525	7148	4253	0.09
	-3.73	-1471				
24	3.94	2518	512	8417	4482	0.08
	-4.10	-1685				

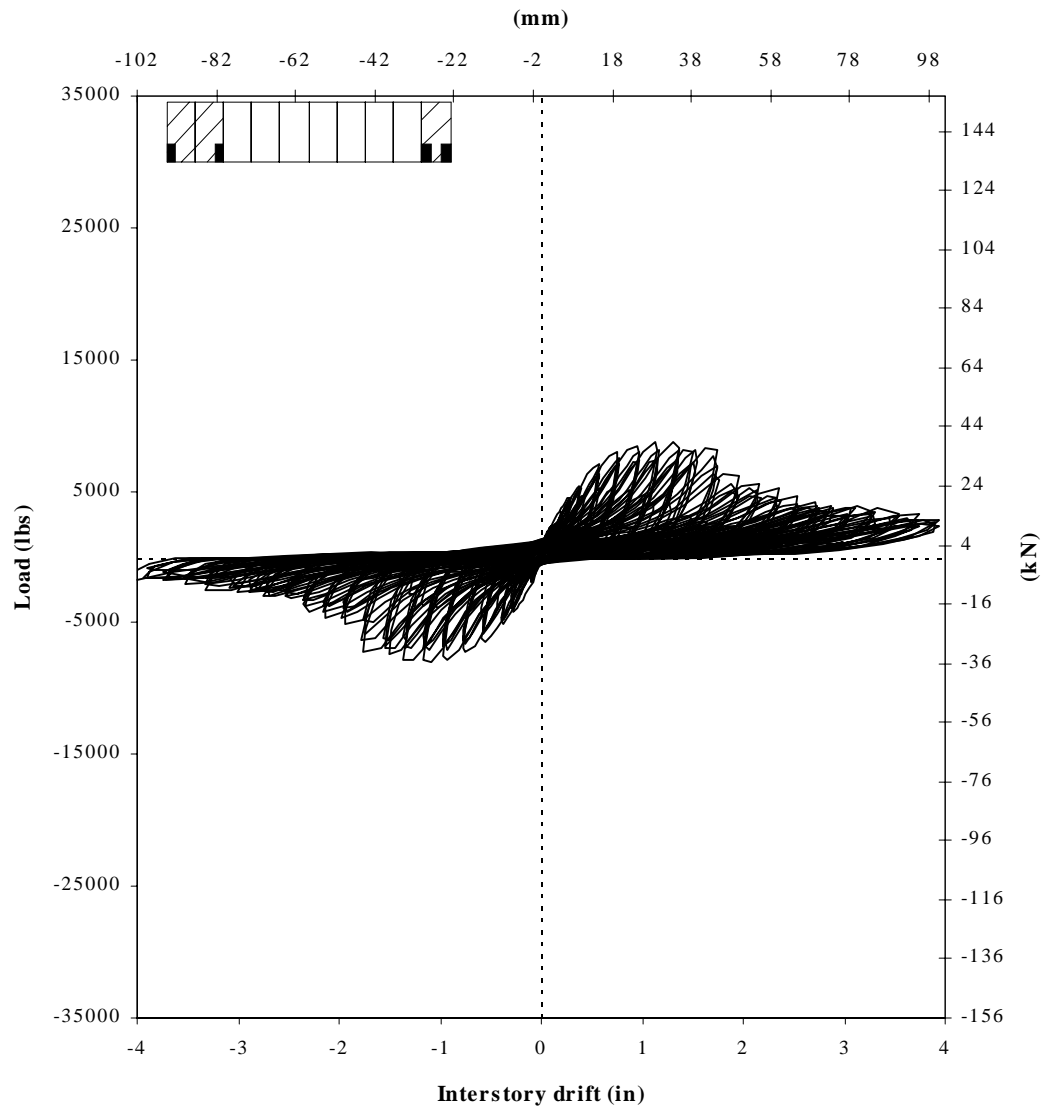


Figure A.11: Hysteresis loops of Wall E (max. anchors)

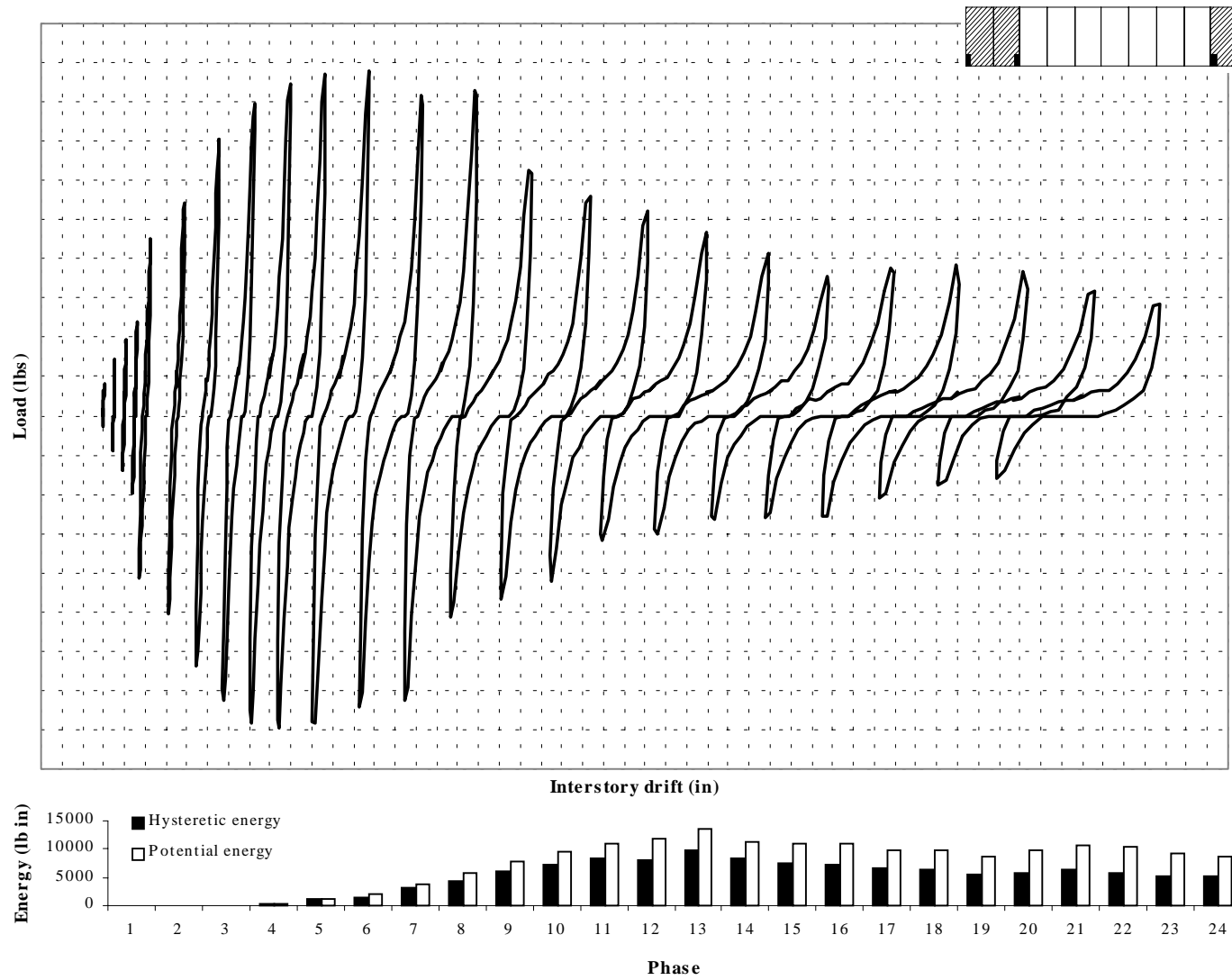


Figure A.12: Initial hysteresis loops of Wall E (max. anchors) together with hyst. and pot. energy for comparison

Table A.13: Initial cyclic data of Wall 2.1 (2 ft corner segments)

<b>Phase</b>	<b>Int. Drift</b> (in.)	<b>Load</b> (lbs.)	<b>Avg. <math>k_c</math></b> (lbs./in.)	<b><math>U_1</math></b> (lbs.-in.)	<b><math>W_d</math></b> (lbs.-in.)	<b>EVDR</b> (rad <sup>-1</sup> )
<b>1</b>	0.02	695	56714	20	3	0.02
	-0.02	-1420				
<b>2</b>	0.04	1688	54437	62	16	0.04
	-0.03	-1876				
<b>3</b>	0.06	2172	51950	98	27	0.04
	-0.03	-2198				
<b>4</b>	0.07	2655	46685	158	44	0.04
	-0.05	-2709				
<b>5</b>	0.19	5260	30494	915	641	0.11
	-0.16	-5260				
<b>6</b>	0.27	6173	24003	1599	1196	0.12
	-0.24	-6200				
<b>7</b>	0.44	7462	17630	3175	2886	0.14
	-0.41	-7489				
<b>8</b>	0.61	7972	13482	4829	4112	0.14
	-0.59	-8160				
<b>9</b>	0.80	8187	10473	6528	7842	0.19
	-0.78	-8348				
<b>10</b>	0.97	7570	8141	7650	6509	0.14
	-0.96	-8214				
<b>11</b>	1.17	5018	5349	7312	6992	0.15
	-1.17	-7489				
<b>12</b>	1.34	2709	3433	5955	5541	0.15
	-1.31	-6334				
<b>13</b>	1.66	1554	1143	2310	6629	0.46
	-1.23	-1661				

Table A.14: Stabilized cyclic data of Wall 2.1 (2 ft corner segments)

<b>Phase</b>	<b>Int. Drift</b> (in.)	<b>Load</b> (lbs.)	<b>Avg. <math>k_c</math></b> (lbs./in.)	<b><math>U_1</math></b> (lbs.-in.)	<b><math>W_d</math></b> (lbs.-in.)	<b>EVDR</b> (rad <sup>-1</sup> )
<b>1</b>	0.02	990	56280	26	7	0.04
	-0.02	-1393				
<b>2</b>	0.04	1715	55416	60	18	0.05
	-0.03	-1876				
<b>3</b>	0.05	2198	53017	96	26	0.04
	-0.03	-2198				
<b>4</b>	0.07	2548	48928	141	40	0.05
	-0.04	-2601				
<b>5</b>	0.19	4750	27835	838	475	0.09
	-0.16	-4884				
<b>6</b>	0.27	5555	22045	1426	893	0.10
	-0.24	-5636				
<b>7</b>	0.44	6254	14945	2733	1884	0.11
	-0.41	-6522				
<b>8</b>	0.63	6630	11114	4137	2890	0.11
	-0.59	-6925				
<b>9</b>	0.80	6442	8459	5302	3871	0.12
	-0.79	-6952				
<b>10</b>	0.99	4562	5651	5461	4451	0.13
	-0.98	-6549				
<b>11</b>	1.21	2709	3580	5085	4453	0.14
	-1.18	-5824				
<b>12</b>	1.44	1581	2149	4200	5232	0.20
	-1.38	-4427				

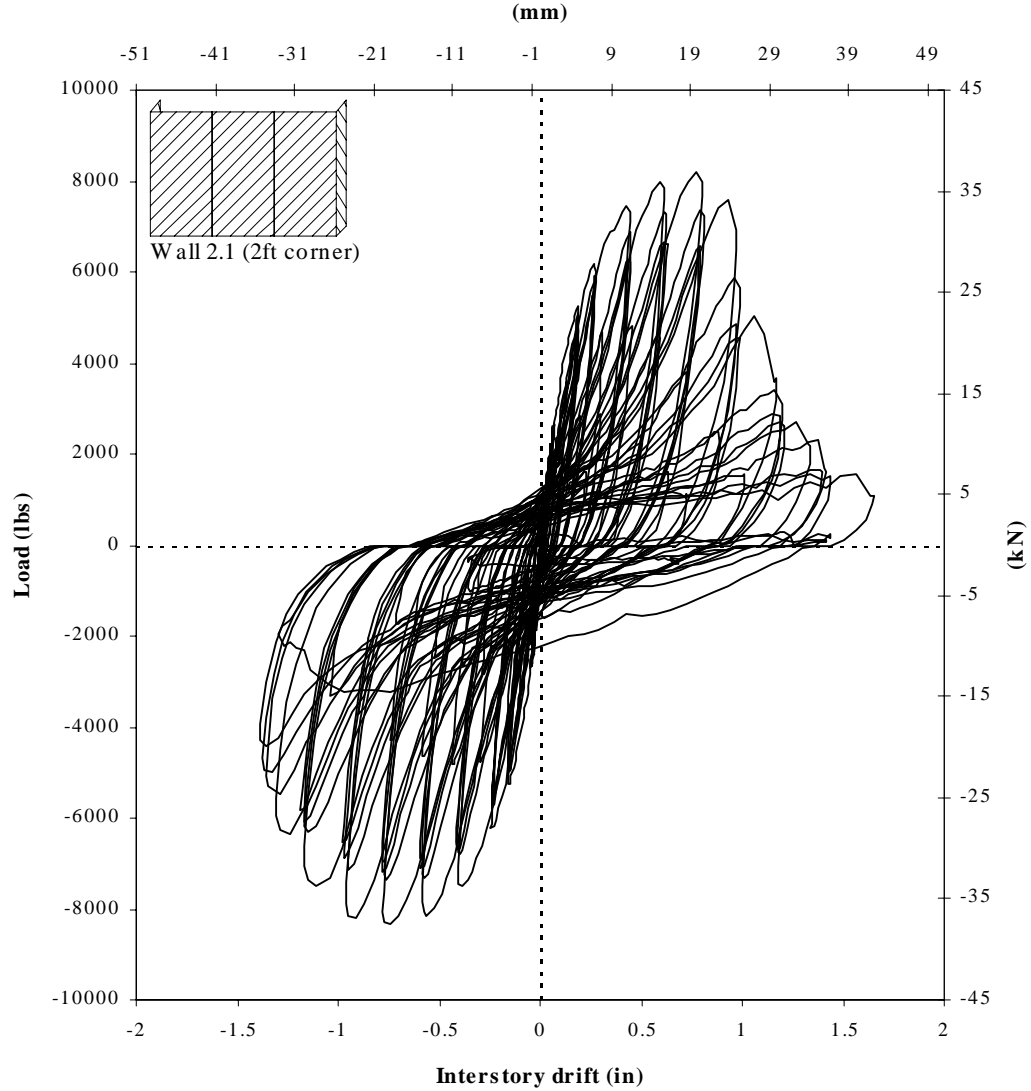


Figure A.13: Hysteresis loops of Wall 2.1 (2 ft corner segments)

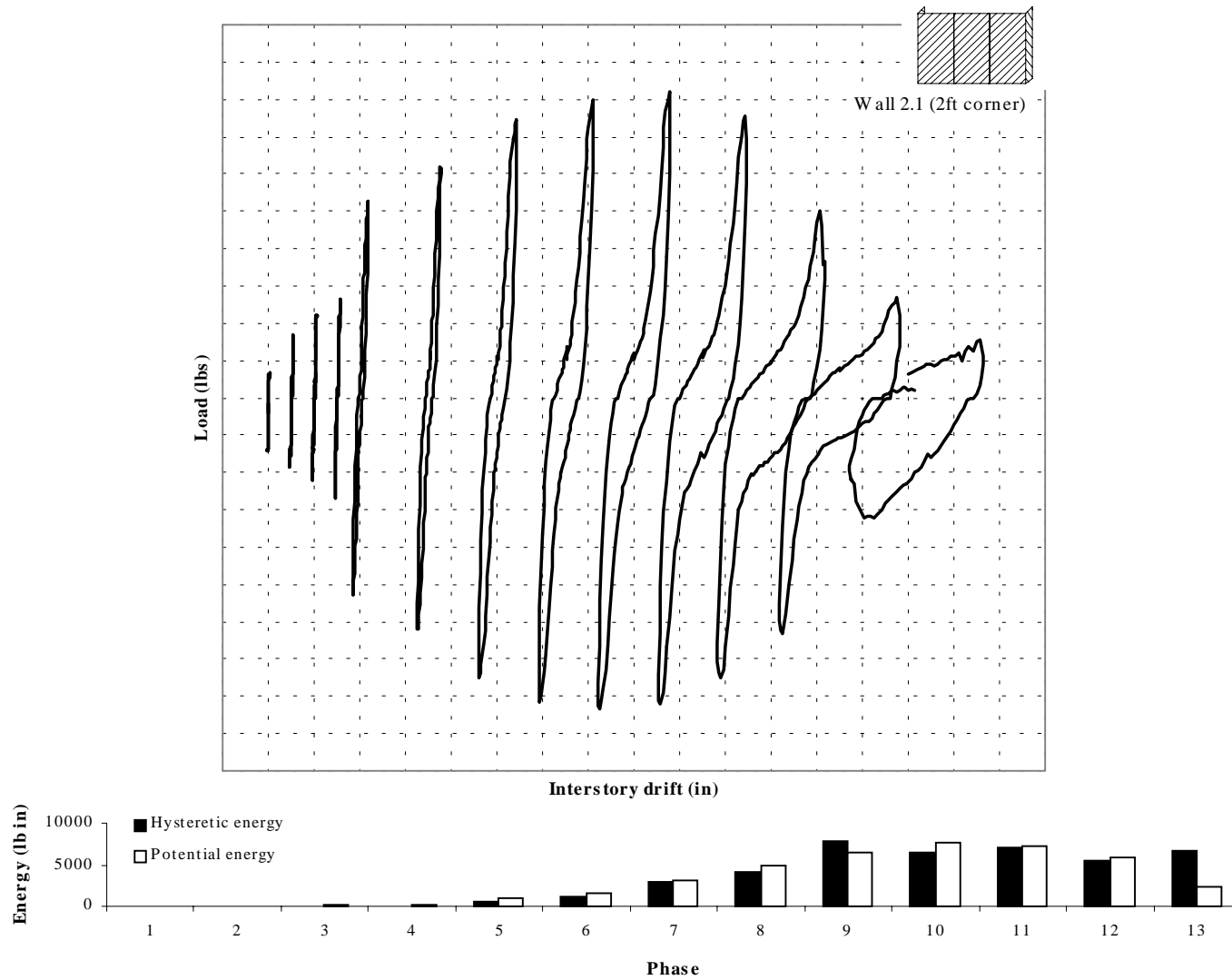


Figure A.14: Initial hysteresis loops of Wall 2.1 (2 ft corner segments) together with hyst. and pot. energy for comparison

Table A.15: Initial cyclic data of Wall 2.2 (2 ft corner segments)

<b>Phase</b>	<b>Int. Drift</b> (in.)	<b>Load</b> (lbs.)	<b>Avg. <math>k_c</math></b> (lbs./in.)	<b><math>U_1</math></b> (lbs.-in.)	<b><math>W_d</math></b> (lbs.-in.)	<b>EVDR</b> (rad <sup>-1</sup> )
<b>1</b>	0.02 -0.02	1232 -1017	51660	25	10	0.07
<b>2</b>	0.04 -0.04	2064 -1849	45964	83	50	0.10
<b>3</b>	0.07 -0.07	2682 -2521	38047	178	123	0.11
<b>4</b>	0.10 -0.10	3165 -3192	32699	309	222	0.11
<b>5</b>	0.24 -0.23	5233 -5126	22220	1209	1131	0.15
<b>6</b>	0.33 -0.31	5690 -5824	17904	1852	1459	0.13
<b>7</b>	0.49 -0.47	6549 -6898	13946	3243	2957	0.15
<b>8</b>	0.68 -0.66	6683 -7167	10351	4634	4276	0.15
<b>9</b>	0.87 -0.88	6388 -6979	7641	5846	5655	0.15
<b>10</b>	1.05 -1.08	5367 -6092	5367	6118	6304	0.16
<b>11</b>	1.25 -1.30	3461 -4884	3260	5341	6338	0.19
<b>12</b>	1.47 -1.43	1500 -3487	1730	3596	5155	0.23

Table A.16: Stabilized cyclic data of Wall 2.1 (2 ft corner segments)

<b>Phase</b>	<b>Int. Drift</b> (in.)	<b>Load</b> (lbs.)	<b>Avg. <math>k_c</math></b> (lbs./in.)	<b><math>U_1</math></b> (lbs.-in.)	<b><math>W_d</math></b> (lbs.-in.)	<b>EVDR</b> (rad <sup>-1</sup> )
<b>1</b>	0.02	1285	52420	26	11	0.07
	-0.02	-1044				
<b>2</b>	0.05	2064	44478	86	53	0.10
	-0.04	-1849				
<b>3</b>	0.07	2628	36969	178	115	0.10
	-0.07	-2494				
<b>4</b>	0.09	3031	32367	287	203	0.11
	-0.10	-3058				
<b>5</b>	0.25	4669	19465	1173	858	0.12
	-0.24	-4884				
<b>6</b>	0.34	5045	16074	1664	1196	0.11
	-0.31	-5287				
<b>7</b>	0.52	5421	11350	2789	2145	0.12
	-0.48	-5824				
<b>8</b>	0.70	5260	8065	3846	3360	0.14
	-0.68	-5878				
<b>9</b>	0.88	4777	5717	4453	4239	0.15
	-0.89	-5314				
<b>10</b>	1.06	3246	3508	4168	4705	0.18
	-1.11	-4401				
<b>11</b>	1.33	1554	1878	3240	4624	0.23
	-1.31	-3380				

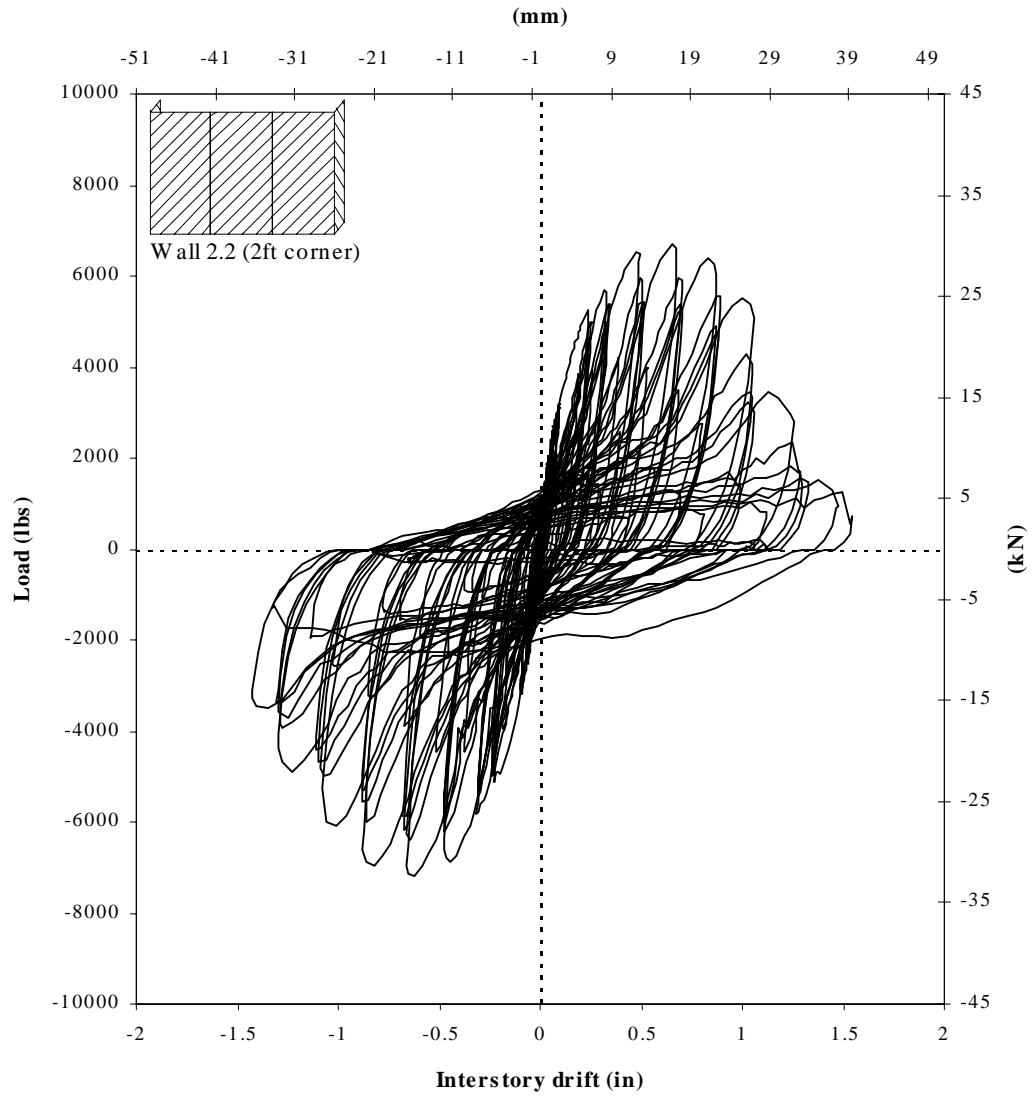


Figure A.15: Hysteresis loops of Wall 2.2 (2 ft corner segments)

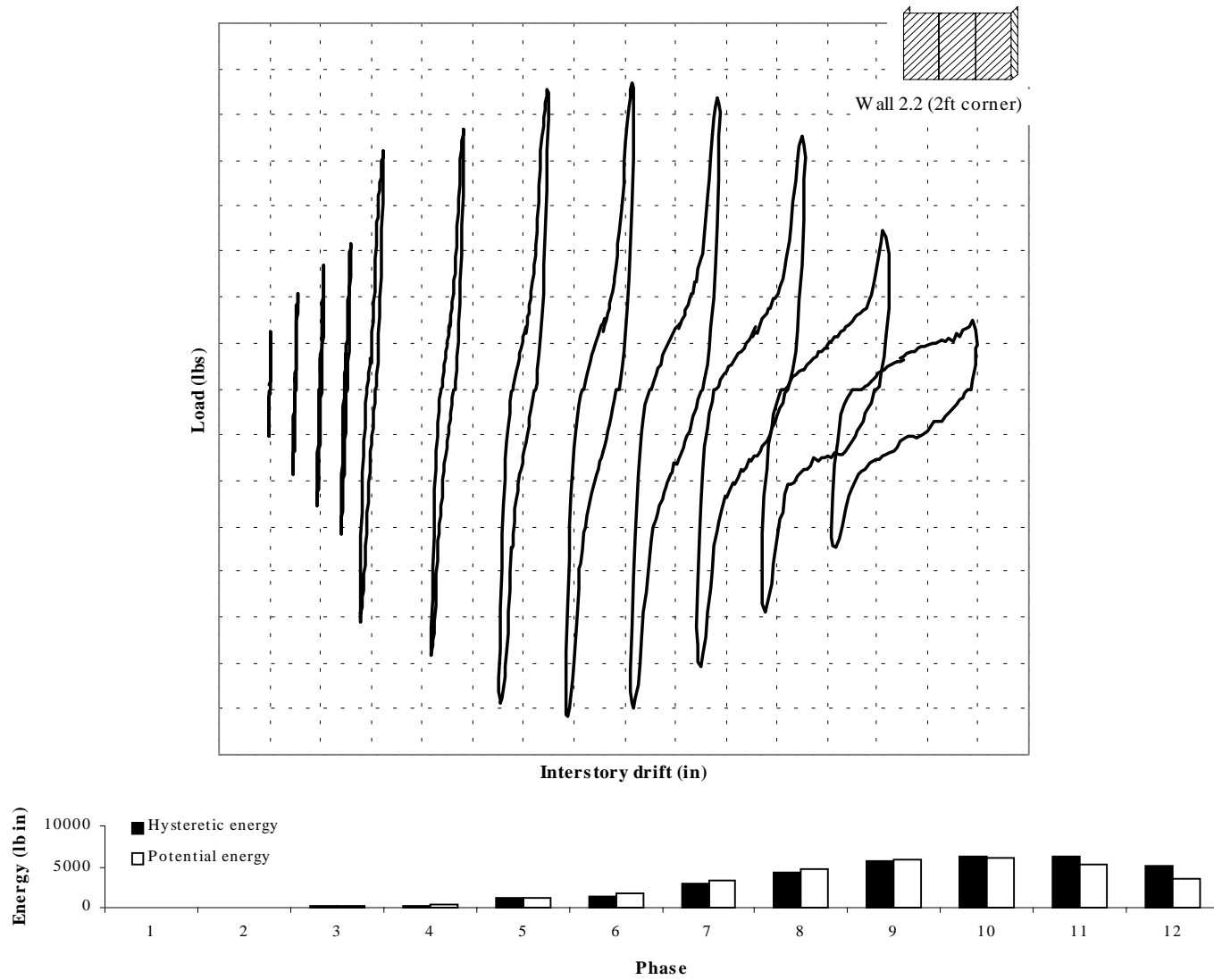


Figure A.16: Initial hysteresis loops of Wall 2.2 (2 ft corner segments) together with hyst. and pot. energy for comparison

Table A.17: Initial cyclic data of Wall 4.1 (4 ft corner segments)

<b>Phase</b>	<b>Int. Drift (in.)</b>	<b>Load (lbs.)</b>	<b>Avg. <math>k_c</math> (lbs./in.)</b>	<b><math>U_1</math> (lbs.-in.)</b>	<b><math>W_d</math> (lbs.-in.)</b>	<b>EVDR (rad<sup>-1</sup>)</b>
<b>1</b>	0.02 -0.02	1527 -695	49131	25	15	0.10
<b>2</b>	0.04 -0.05	2037 -1554	41344	79	54	0.11
<b>3</b>	0.05 -0.07	2548 -2145	38296	146	87	0.09
<b>4</b>	0.07 -0.09	2950 -2601	35859	219	143	0.10
<b>5</b>	0.18 -0.22	5287 -4938	26283	1004	723	0.11
<b>6</b>	0.25 -0.30	6146 -6012	22397	1664	1105	0.11
<b>7</b>	0.40 -0.45	7462 -7596	17661	3222	2483	0.12
<b>8</b>	0.56 -0.63	8080 -8429	13886	4921	3842	0.12
<b>9</b>	0.75 -0.83	8053 -8832	10729	6661	5337	0.13
<b>10</b>	0.91 -1.03	7462 -8885	8388	7994	6190	0.12
<b>11</b>	1.09 -1.23	6818 -8590	6639	8972	6880	0.12
<b>12</b>	1.22 -1.36	5690 -8348	5403	9146	6523	0.11
<b>13</b>	1.45 -1.60	5260 -8214	4386	10373	7853	0.12
<b>14</b>	1.65 -1.79	4213 -6925	3214	9665	8407	0.14

Table A.18: Stabilized cyclic data of Wall 4.1 (4 ft corner segments)

<b>Phase</b>	<b>Int. Drift</b> (in.)	<b>Load</b> (lbs.)	<b>Avg. <math>k_c</math></b> (lbs./in.)	<b><math>U_1</math></b> (lbs.-in.)	<b><math>W_d</math></b> (lbs.-in.)	<b>EVDR</b> (rad <sup>-1</sup> )
<b>1</b>	0.02 -0.03	1608 -802	47687	30	17	0.09
<b>2</b>	0.04 -0.05	2091 -1527	41930	79	49	0.10
<b>3</b>	0.05 -0.07	2521 -2145	39943	140	96	0.11
<b>4</b>	0.06 -0.09	2843 -2548	36161	207	132	0.10
<b>5</b>	0.17 -0.22	4803 -4723	24529	937	532	0.09
<b>6</b>	0.25 -0.30	5529 -5555	20640	1500	874	0.09
<b>7</b>	0.40 -0.46	6468 -6791	15486	2849	1417	0.08
<b>8</b>	0.57 -0.63	6737 -7328	11672	4246	2691	0.10
<b>9</b>	0.75 -0.84	6415 -7596	8762	5619	3837	0.11
<b>10</b>	0.92 -1.04	5878 -7596	6869	6632	4579	0.11
<b>11</b>	1.10 -1.22	5126 -7408	5366	7340	5119	0.11
<b>12</b>	1.27 -1.42	4615 -7355	4417 3293	8134	5758	0.11
<b>13</b>	1.47 -1.60	3863 -6334		7907	6279	0.13

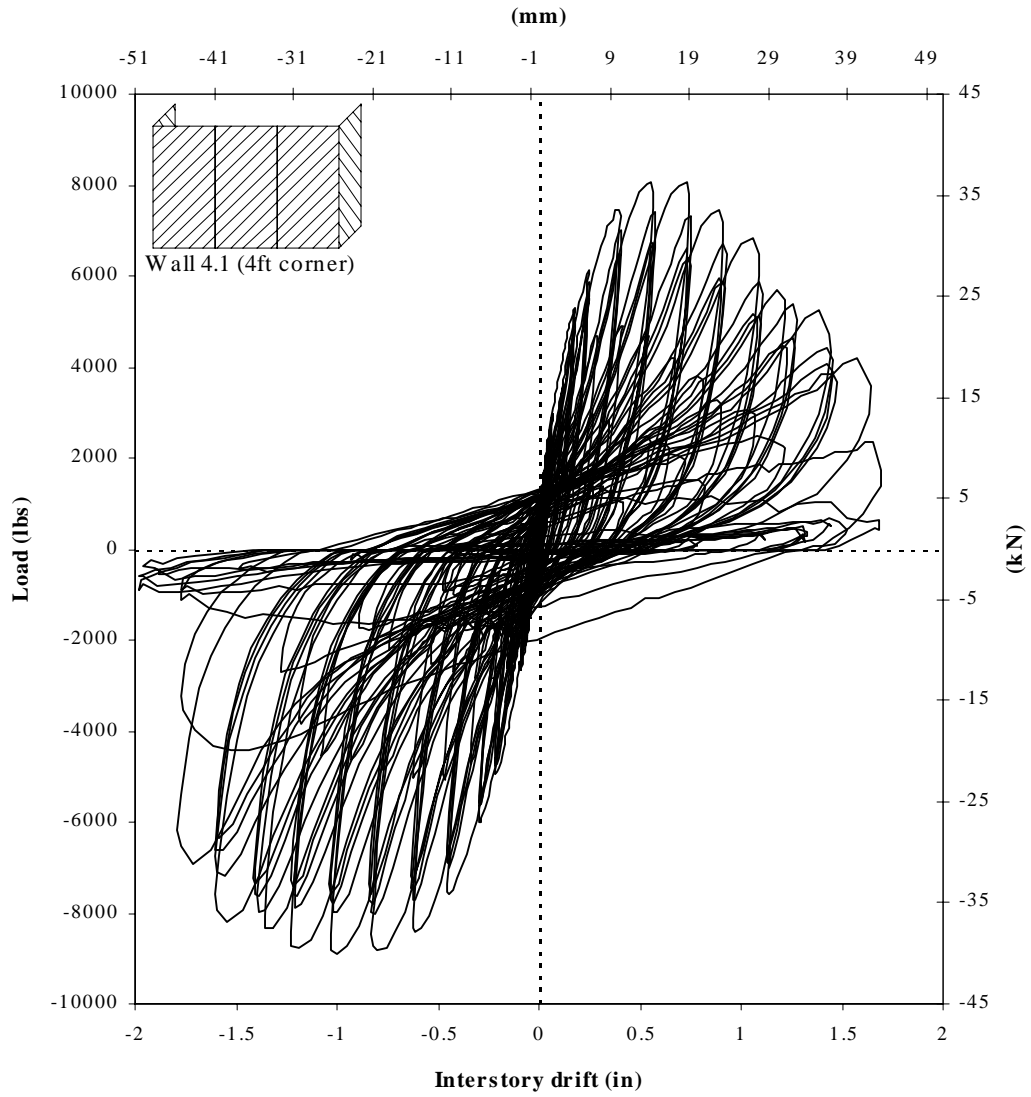


Figure A.17: Hysteresis loops of Wall 4.1 (4 ft corner segments)

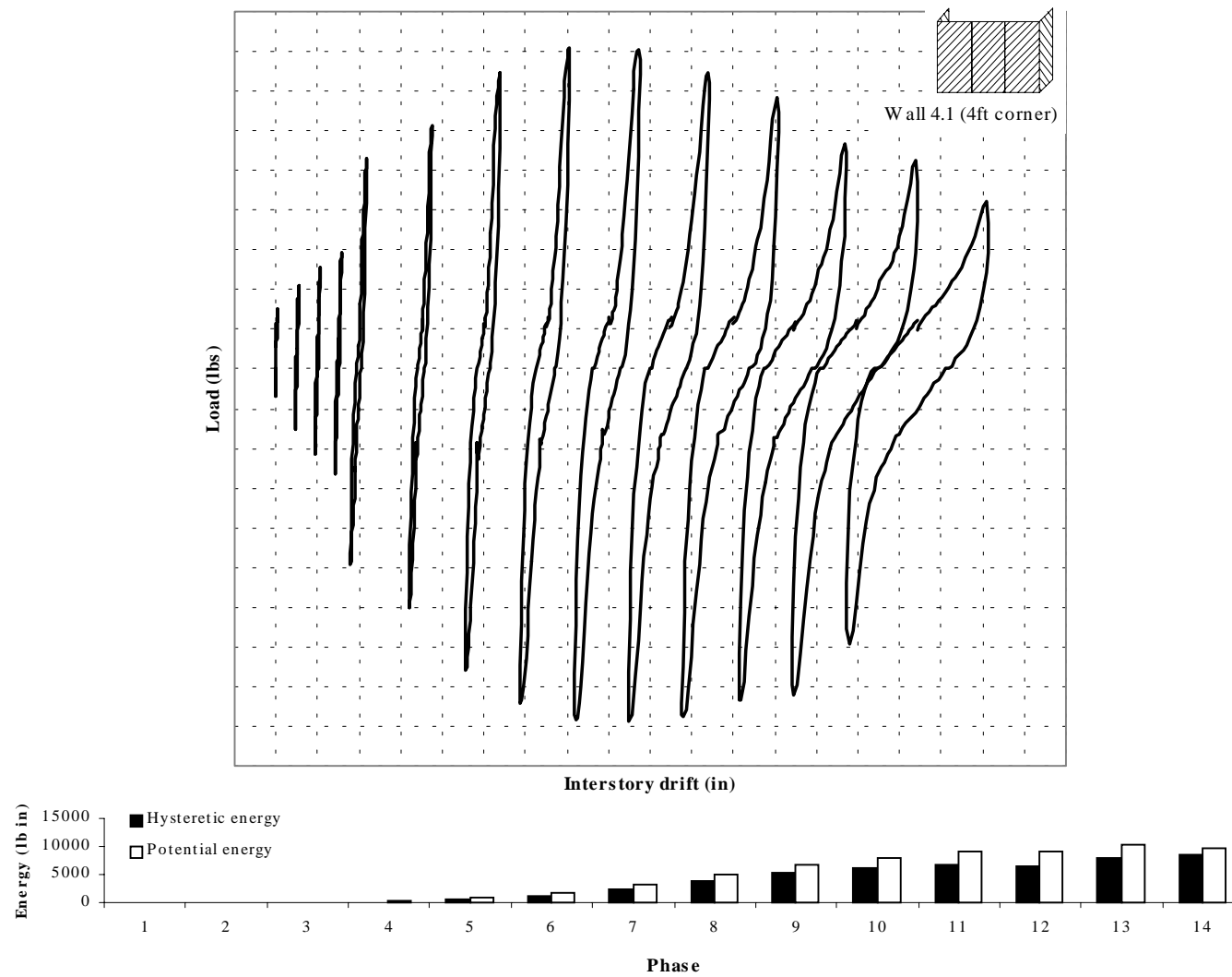


Figure A.18: Initial hysteresis loops of Wall 4.1 (4 ft corner segments) together with hyst. and pot. energy for comparison

Table A.19: Initial cyclic data of Wall 4.2 (4 ft corner segments)

<b>Phase</b>	<b>Int. Drift</b> (in.)	<b>Load</b> (lbs.)	<b>Avg. <math>k_c</math></b> (lbs./in.)	<b><math>U_1</math></b> (lbs.-in.)	<b><math>W_d</math></b> (lbs.-in.)	<b>EVDR</b> (rad <sup>-1</sup> )
<b>1</b>	0.04	1957	52918	67	22	0.05
	-0.04	-1796				
<b>2</b>	0.05	2413	48529	122	40	0.05
	-0.05	-2440				
<b>3</b>	0.05	2601	47551	170	51	0.05
	-0.07	-3004				
<b>4</b>	0.14	4884	32013	880	560	0.10
	-0.19	-5609				
<b>5</b>	0.21	5770	25836	1528	978	0.10
	-0.28	-6683				
<b>6</b>	0.36	7301	19388	3051	2386	0.12
	-0.43	-8026				
<b>7</b>	0.52	7999	14787	4707	3822	0.13
	-0.60	-8644				
<b>8</b>	0.70	8214	11382	6430	5200	0.13
	-0.80	-8859				
<b>9</b>	0.87	8187	9084	7937	6193	0.12
	-1.00	-8751				
<b>10</b>	1.03	8026	7347	9150	7022	0.12
	-1.21	-8321				
<b>11</b>	1.13	7274	6009	9177	6676	0.12
	-1.35	-7516				
<b>12</b>	1.33	6979	4881	10287	7776	0.12
	-1.58	-7140				
<b>13</b>	1.47	6200	3713	9456	7766	0.13
	-1.74	-5609				
<b>14</b>	1.55	4965	2574	7579	7273	0.15
	-1.96	-3810				

Table A.20: Stabilized cyclic data of Wall 4.2 (4 ft corner segments)

<b>Phase</b>	<b>Int. Drift</b> (in.)	<b>Load</b> (lbs.)	<b>Avg. <math>k_c</math></b> (lbs./in.)	<b><math>U_1</math></b> (lbs.-in.)	<b><math>W_d</math></b> (lbs.-in.)	<b>EVDR</b> (rad <sup>-1</sup> )
<b>1</b>	0.02 -0.02	1393 -990	55843	25	8	0.05
<b>2</b>	0.03 -0.04	1930 -1849	54393	66	14	0.03
<b>3</b>	0.04 -0.05	2360 -2413	51860	111	32	0.05
<b>4</b>	0.05 -0.07	2494 -2870	47998	155	37	0.04
<b>5</b>	0.14 -0.20	4508 -5314	29972	830	416	0.08
<b>6</b>	0.21 -0.27	5287 -6092	23790	1387	772	0.09
<b>7</b>	0.36 -0.43	6280 -7032	16892	2647	1652	0.10
<b>8</b>	0.52 -0.61	6710 -7408	12535	3997	2704	0.11
<b>9</b>	0.70 -0.81	6791 -7489	9502	5395	3765	0.11
<b>10</b>	0.86 -1.01	6710 -7167	7448	6508	4665	0.11
<b>11</b>	1.02 -1.22	6442 -6683	5901	7358	5355	0.12
<b>12</b>	1.16 -1.40	6119 -6415	4937 3435	8024	5765	0.11
<b>13</b>	1.32 -1.60	5529 -5367	3034	7947	6157	0.12
<b>14</b>	1.30 -1.81	4562 -3407		6037	5774	0.15

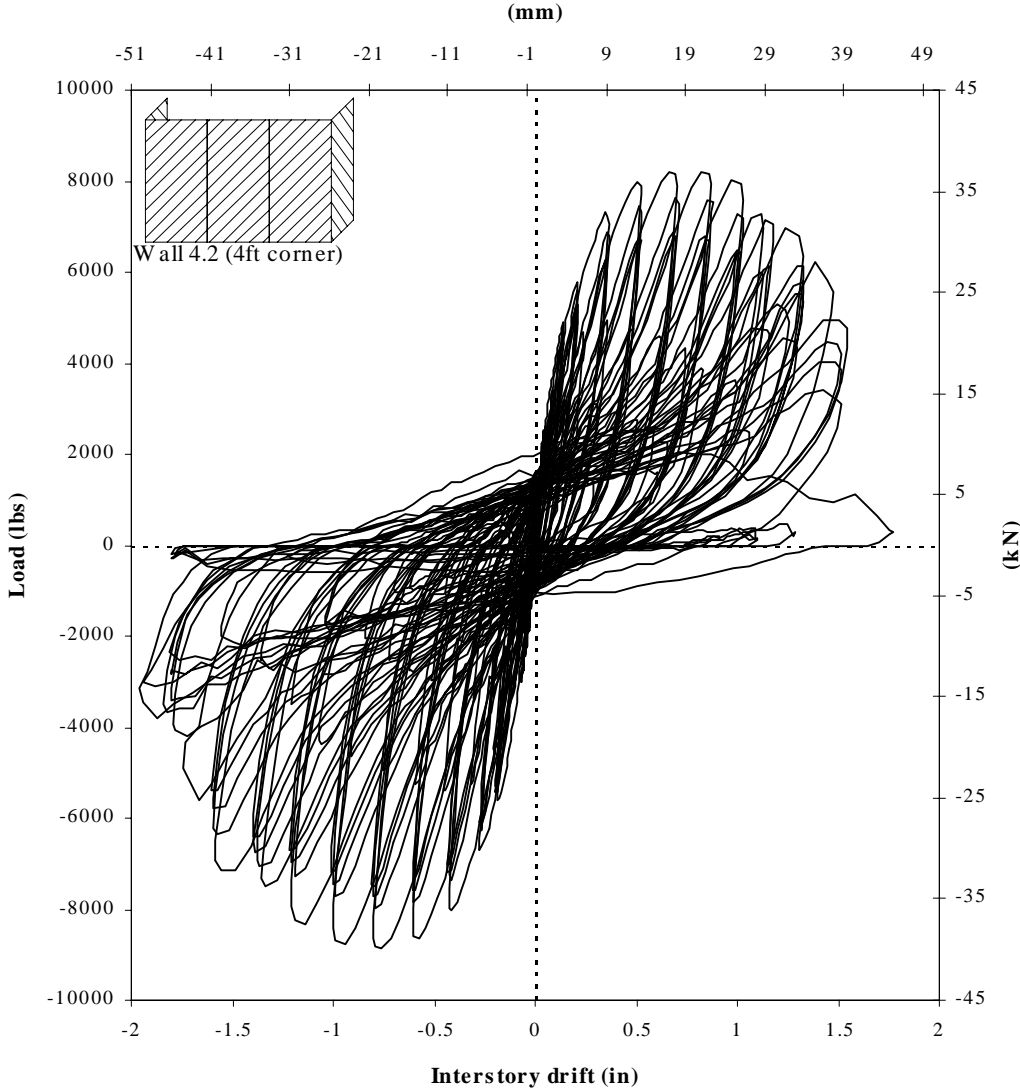


Figure A.19: Hysteresis loops of Wall 4.2 (4 ft corner segments)

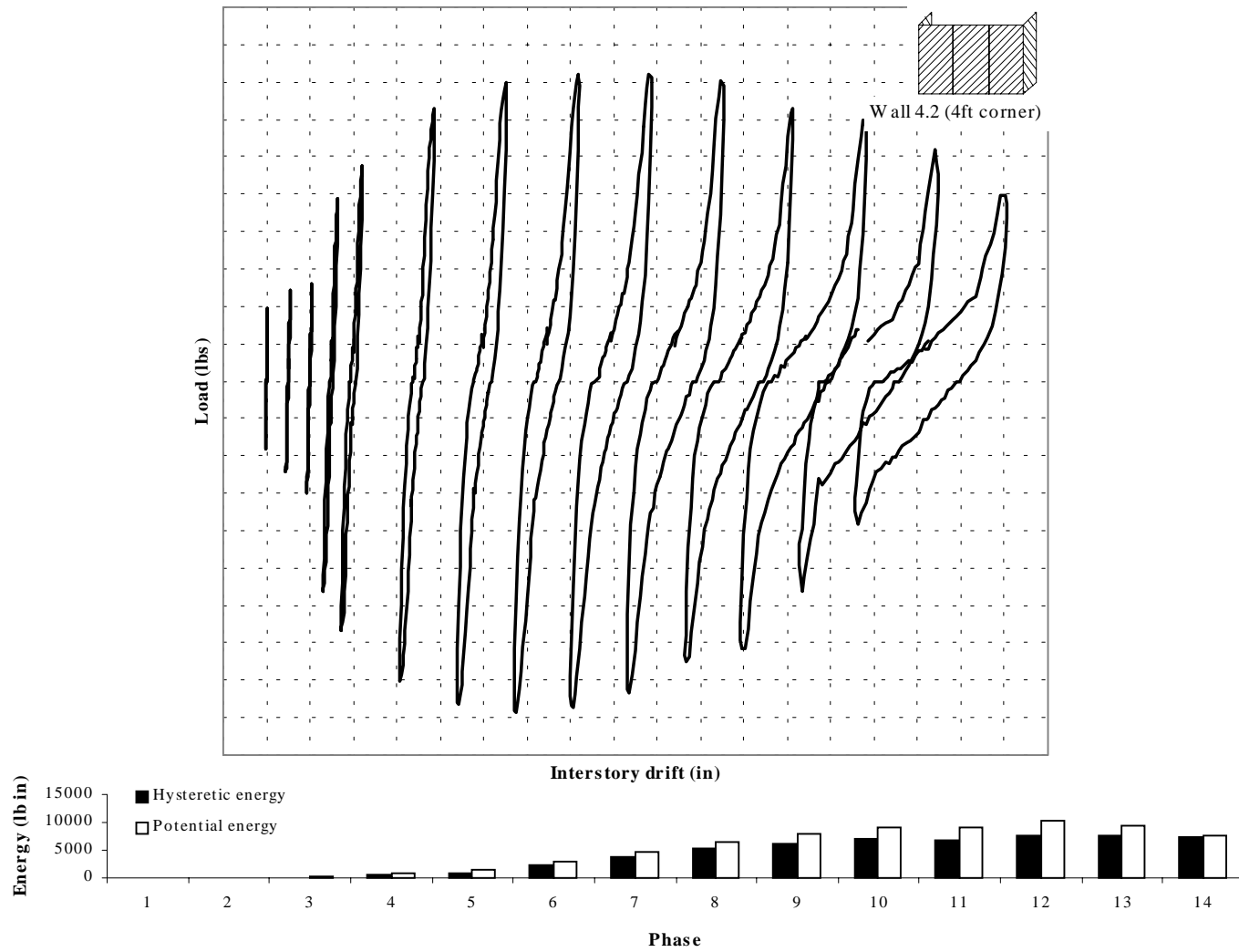


Figure A.20: Initial hysteresis loops of Wall 4.2 (4 ft corner segments) together with hyst. and pot. energy for comparison

## **Vita**

*(December, 1997)*

The author, Christian Peter Heine, was born on April 17, 1972 in Stuttgart, Germany. He graduated with honors from Besigheim High School in 1991. Upon graduation, he began an apprenticeship to become a licensed Joiner/Furniture-maker and graduated as best student in 1993. He then started his study in Wood Technology at Rosenheim University, Germany where he was awarded a Carl Duisberg Society Fellowship. Christian participated in the Carl Duisberg International Program and came to the United States to complete an internship at the Applied Radiant Energy Cooperation in Lynchburg, Virginia.

Christian entered the graduate Wood Science Program at Virginia Polytechnic Institute and State University in Summer 1996. Upon graduation, he will continue graduate work at Virginia Tech and pursue his Ph.D.